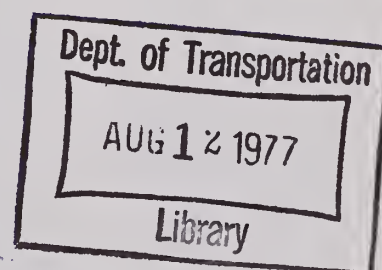


TE  
662  
.A3  
no.  
FHWA-  
RD-  
77-57

Report No. FHWA-RD-77-57

# **INVESTIGATION OF THE EFFECTIVENESS OF EXISTING BRIDGE DESIGN METHODOLOGY IN PROVIDING ADEQUATE STRUCTURAL RESISTANCE TO SEISMIC DISTURBANCES.**

**Phase V: Correlative Investigations on Theoretical and  
Experimental Dynamic Behavior of a Model Bridge Structure**



**July 1976**

**Final Report**

This document is available to the public  
through the National Technical Information  
Service, Springfield, Virginia 22161

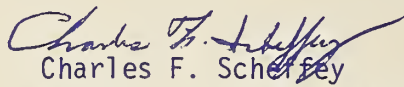
**Prepared for**

**FEDERAL HIGHWAY ADMINISTRATION  
Offices of Research & Development  
Washington, D.C. 20590**

## FOREWORD

This report is the fourth in a series to result from research being conducted at the University of California, Berkeley, for the Federal Highway Administration (FHWA), Office of Research, under Contract DOT-FH-11-7798. The report will be of interest to structural researchers concerned with earthquake resistant design of highway bridges. It outlines correlations between analytical and experimental seismic response of a highway bridge modeled to incorporate features of typical high curved highway structures.

Copies of the report are being distributed by FHWA transmittal memorandum. Additional copies may be obtained from the National Technical Information Service, 5285 Port Royal Road, Springfield, Virginia 22161.



Charles F. Scherrey  
Director, Office of Research  
Federal Highway Administration

## DISCLAIMER NOTICE

This document is disseminated under the sponsorship of the Department of Transportation in the interest of information exchange. The United States Government assumes no liability for its contents or use thereof.

The contents of this report reflect the view of the authors, who are responsible for the facts and the accuracy of the data presented herein. The contents do not necessarily reflect the official views or policy of the Department of Transportation.

This report does not constitute a standard, specification, or regulation.

1. Report No. FHWA-RD-77-57	2. Government Accession No.	3. Recipient's Catalog No.	
4. Title and Subtitle An Investigation of the Effectiveness of Existing Bridge Design Methodology in Providing Adequate Structural Resistance to Seismic Disturbances. Phase V Correlative Investigations on Theoretical and Experimental Dynamic Behavior of a Model Bridge Structure.		5. Report Date July 1976	
		6. Performing Organization Code	
7. Author(s) Kazuhiko Kawashima and Joseph Penzien		8. Performing Organization Report No. EERC-76-29	
9. Performing Organization Name and Address University of California Campus Research Office 118 California Hall Berkeley, California 94720		10. Work Unit No. (TRIS)	
12. Sponsoring Agency Name and Address Office of Research and Development Federal Highway Administration U.S. Department of Transportation Washington, D.C. 20590		11. Contract or Grant No. DOT-FH-11-7798	
		13. Type of Report and Period Covered Phase V Final Report	
15. Supplementary Notes FHWA Contract Manager: James D. Cooper, HRS-11		14. Sponsoring Agency Code	
16. Abstract <p>This report is one in a series to result from the investigation, "An Investigation of the Effectiveness of Existing Bridge Design Methodology in Providing Adequate Structural Resistance to Seismic Disturbances," sponsored by the U. S. Department of Transportation, Federal Highway Administration. Descriptions are given of the correlations between analytical and experimental seismic responses of a model bridge structure which was constructed to have the same features as the typical full-scale high curved highway bridge structure.</p> <p>Modifications of the previously reported mathematical procedures for simulating the nonlinear behavior of expansion joints are presented. These include subdividing the time interval of integration and applying an equilibrium correction at the end of each interval and each subinterval.</p> <p>Correlations of displacement response of the bridge model carried out for three different excitations are described. Parameter studies conducted to assist in the interpretation of correlation results are presented and the characteristics of the dynamic behavior of the bridge model are discussed.</p> <p>Finally, based on the correlation results presented, general conclusions are deduced and summarized.</p>			
17. Key Words Earthquake, Bridges, Seismic Analysis, Structural Analysis, Dynamic Behavior		18. Distribution Statement No restrictions. This document is available through the National Technical Information Service, Springfield, Virginia 22161	
19. Security Classif. (of this report) Unclassified	20. Security Classif. (of this page) Unclassified	21. No. of Pages 228	22. Price

## ACKNOWLEDGMENT

The authors wish to express their sincere thanks and appreciation to Dr. D. Williams, Mr. S. Howe and Professor W. G. Godden for providing the experimental test data of the bridge model structure studied in the investigation and to Dr. W. S. Tseng, Bechtel Power Corporation, San Francisco, for his assistance in modifying the computer programs and his encouragement throughout the study. Special thanks are also extended to the Public Works Research Institute, Ministry of Construction, Government of Japan, for allowing the senior author to work at Earthquake Engineering Research Center, University of California, Berkeley, during the period of the investigation reported herein.



## TABLE OF CONTENTS

	<u>Page</u>
ABSTRACT . . . . .	i
ACKNOWLEDGMENT . . . . .	ii
LIST OF TABLES . . . . .	v
LIST OF FIGURES . . . . .	vi
 I. INTRODUCTION . . . . .	 1
A. STATEMENT OF PROBLEM . . . . .	1
B. OBJECTIVES AND SCOPE . . . . .	3
 II. ANALYTICAL MODEL OF EXPANSION JOINTS . . . . .	 6
A. PIECEWISE LINEAR EXPANSION JOINT STIFFNESS . . . . .	6
B. COLLISIONS . . . . .	11
C. COULOMB FRICTION FORCE . . . . .	13
 III. DYNAMIC ANALYSIS PROCEDURE . . . . .	 21
A. INCREMENTAL EQUATION OF MOTION . . . . .	21
B. STEP-BY-STEP INTEGRATION . . . . .	23
C. ACCURACY OF SOLUTION . . . . .	25
D. SUBDIVISION OF TIME INTERVAL . . . . .	26
E. EQUILIBRIUM ITERATION . . . . .	27
 IV. EXPERIMENTAL MODEL STUDY AND TEST RESULTS . . . . .	 33
A. EXPERIMENTAL MODEL . . . . .	33
B. TEST PROCEDURES AND TEST RESULTS . . . . .	36
 V. FORMULATION OF A BASIC ANALYTICAL MODEL . . . . .	 79
A. IDEALIZATION OF EXPERIMENTAL MODEL . . . . .	79
B. BASIC ANALYTICAL MODEL . . . . .	79

	<u>Page</u>
VI. ANALYTICAL PREDICTION OF SEISMIC RESPONSES . . . . .	89
A. LOW INTENSITY SEISMIC EXCITATION (TEST H1) . . . . .	89
B. HIGH INTENSITY SEISMIC EXCITATION (TEST HV2) . . . . .	94
C. HIGH INTENSITY SEISMIC EXCITATION (TEST H3). . . . .	99
VII. DISCUSSION OF CORRELATION RESULTS . . . . .	136
A. JOINT RESTRAINER TIE BARS . . . . .	136
B. COLLISIONS . . . . .	137
C. COULOMB FRICTION FORCE . . . . .	137
D. VERTICAL EXCITATION . . . . .	138
E. IMPACT SPRING STIFFNESS . . . . .	139
VIII. CONCLUSIONS . . . . .	145
BIBLIOGRAPHY . . . . .	147
APPENDIX	
A. LONGITUDINAL COLLINEAR COLLISION OF TWO RODS . . . . .	A-1
B. FREE VIBRATION OF A SINGLE SPRING-MASS SYSTEM WITH COULOMB FRICTION . . . . .	B-1
C. COMPUTER LISTING OF NEABS . . . . .	C-1

LIST OF TABLES

	<u>Page</u>
TABLE 4.1    PRINCIPAL FEATURES OF SEISMIC EXCITATION IN SERIES IV . . . . .	49
TABLE 5.1    STIFFNESS PROPERTIES AND BOUNDARY CONDITIONS OF EXPERIMENTAL MODEL . . . . .	84
TABLE 5.2    EFFECTS OF EXPANSION JOINT CONSTRAINTS ON CALCULATED LOW FREQUENCY CHARACTERISTICS OF BRIDGE MODEL . . . . .	86
TABLE A.1    EFFECTS OF VARIOUS PARAMETERS ON PREDICTED RESPONSE OF COLLIDING RODS . . . . .	A-8

## LIST OF FIGURES

	<u>Page</u>
FIG. 2.1 IDEALIZED EXPANSION JOINT . . . . .	18
FIG. 2.2 COORDINATE SYSTEM FOR EXPANSION JOINT . . . . .	19
FIG. 2.3 RIGID-PLASTIC HYSTERETIC MODEL FOR COULOMB FRICTION . .	20
FIG. 2.4 ELASTOPLASTIC HYSTERETIC MODEL FOR COULOMB FRICTION . .	20
FIG. 4.1 EXPERIMENTAL MODEL BRIDGE STRUCTURE . . . . .	50
FIG. 4.2 MEASUREMENTS OF RESPONSE DISPLACEMENT . . . . .	51
FIG. 4.3 EXPANSION JOINT OF BRIDGE MODEL . . . . .	52
FIG. 4.4.1 ESTIMATED FORCE VS. RELATIVE DISPLACEMENT RELATION OF EXPANSION JOINT; EFFECT OF RUBBER PAD AND SLIPPAGES . . . . .	53
FIG. 4.4.2 ESTIMATED FORCE VS. RELATIVE DISPLACEMENT RELATION OF EXPANSION JOINT; EFFECT OF TIE BARS AND COLLISIONS . . . . .	54
FIG. 4.5 TYPICAL FORCE VS. DEFORMATION RELATION OF TIE BAR . . .	55
FIG. 4.6 TYPICAL FORCE VS. DEFORMATION RELATION OF RUBBER PAD . . . . .	56
FIG. 4.7 STATIC LOAD-DEFORMATION TEST FOR SIDE SUBASSEMBLAGE . .	57
FIG. 4.8 RESONANT CURVE OF BRIDGE MODEL IN TRANSVERSE EXCITATION . . . . .	58
FIG. 4.9 ACCELERATION RESPONSE SPECTRUM OF TABLE MOTION (TESTS H1, H3 AND HV2). . . . .	59
FIG. 4.10 RELATION BETWEEN MAXIMUM HORIZONTAL TABLE ACCELERATION AND MAXIMUM HORIZONTAL RESPONSE AT CENTER OF BRIDGE MODEL . . . . .	60
FIG. 4.11 HORIZONTAL TABLE ACCELERATION TIME HISTORY; TEST H1 . . . . .	61
FIG. 4.12.1 MEASURED RESPONSE OF SIDE GIRDER NO. 1; LONGITUDINAL (X) DIRECTION; TEST H1 . . . . .	62
FIG. 4.12.2 MEASURED RESPONSE OF SIDE GIRDER NO. 1; TRANSVERSE (Y) DIRECTION; TEST H1 . . . . .	62
FIG. 4.12.3 MEASURED RESPONSE OF CENTER GIRDER; TRANSVERSE (Y) DIRECTION; TEST H1 . . . . .	63



	<u>Page</u>
FIG. 4.12.4 MEASURED RESPONSE OF SIDE GIRDER NO. 2; LONGITUDINAL (X) DIRECTION; TEST H1 . . . . .	63
FIG. 4.12.5 MEASURED RESPONSE OF SIDE GIRDER NO. 2; TRANSVERSE (Y) DIRECTION; TEST H1 . . . . .	64
FIG. 4.12.6 MEASURED RESPONSE OF EXPANSION JOINT NO. 1; INNER SIDE; TEST H1 . . . . .	64
FIG. 4.12.7 MEASURED RESPONSE OF EXPANSION JOINT NO. 1; OUTER SIDE; TEST H1 . . . . .	65
FIG. 4.12.8 MEASURED RESPONSE OF EXPANSION JOINT NO. 2; INNER SIDE; TEST H1 . . . . .	65
FIG. 4.12.9 MEASURED RESPONSE OF EXPANSION JOINT NO. 2; OUTER SIDE; TEST H1 . . . . .	66
FIG. 4.13 HORIZONTAL TABLE ACCELERATION TIME HISTORY; TEST H2 . . . . .	67
FIG. 4.14.1 MEASURED RESPONSE OF SIDE GIRDER NO. 1; LONGITUDINAL (X) DIRECTION; TEST H2 . . . . .	68
FIG. 4.14.2 MEASURED RESPONSE OF SIDE GIRDER NO. 1; TRANSVERSE (Y) DIRECTION; TEST H2 . . . . .	68
FIG. 4.14.3 MEASURED RESPONSE OF CENTER GIRDER; TRANSVERSE (Y) DIRECTION; TEST H2 . . . . .	69
FIG. 4.14.4 MEASURED RESPONSE OF SIDE GIRDER NO. 2; LONGITUDINAL (X) DIRECTION; TEST H2 . . . . .	69
FIG. 4.14.5 MEASURED RESPONSE OF SIDE GIRDER NO. 2; TRANSVERSE (Y) DIRECTION; TEST H2 . . . . .	70
FIG. 4.14.6 MEASURED RESPONSE OF EXPANSION JOINT NO. 1; INNER SIDE; TEST H2 . . . . .	70
FIG. 4.14.7 MEASURED RESPONSE OF EXPANSION JOINT NO. 1; OUTER SIDE; TEST H2 . . . . .	71
FIG. 4.14.8 MEASURED RESPONSE OF EXPANSION JOINT NO. 2; INNER SIDE; TEST H2 . . . . .	71
FIG. 4.14.9 MEASURED RESPONSE OF EXPANSION JOINT NO. 2; OUTER SIDE; TEST H2 . . . . .	72
FIG. 4.15.1 HORIZONTAL TABLE ACCELERATION TIME HISTORY; TEST HV2 . . . . .	73
FIG. 4.15.2 VERTICAL TABLE ACCELERATION TIME HISTORY; TEST HV2 . . . . .	73

	<u>Page</u>
FIG. 4.16.1 MEASURED RESPONSE OF SIDE GIRDER NO. 1; LONGITUDINAL (X) DIRECTION; TEST HV2 . . . . .	74
FIG. 4.16.2 MEASURED RESPONSE OF SIDE GIRDER NO. 1; TRANSVERSE (Y) DIRECTION; TEST HV2 . . . . .	74
FIG. 4.16.3 MEASURED RESPONSE OF CENTER GIRDER; TRANSVERSE (Y) DIRECTION; TEST HV2 . . . . .	75
FIG. 4.16.4 MEASURED RESPONSE OF SIDE GIRDER NO. 2; LONGITUDINAL (X) DIRECTION; TEST HV2 . . . . .	75
FIG. 4.16.5 MEASURED RESPONSE OF SIDE GIRDER NO. 2; TRANSVERSE (Y) DIRECTION; TEST HV2 . . . . .	76
FIG. 4.16.6 MEASURED RESPONSE OF EXPANSION JOINT NO. 1; INNER SIDE; TEST HV2 . . . . .	76
FIG. 4.16.7 MEASURED RESPONSE OF EXPANSION JOINT NO. 1; OUTER SIDE; TEST HV2 . . . . .	77
FIG. 4.16.8 MEASURED RESPONSE OF EXPANSION JOINT NO. 2; INNER SIDE; TEST HV2 . . . . .	77
FIG. 4.16.9 MEASURED RESPONSE OF EXPANSION JOINT NO. 2; OUTER SIDE; TEST HV2 . . . . .	78
FIG. 5.1 ANALYTICAL MODEL OF BRIDGE MODEL . . . . .	87
FIG. 5.2.1 CALCULATED LOWEST VIBRATION MODE; LONGITUDINAL (X) DIRECTION . . . . .	87
FIG. 5.2.2 CALCULATED LOWEST VIBRATION MODE; TRANSVERSE (Y) DIRECTION . . . . .	88
FIG. 5.2.3 CALCULATED LOWEST VIBRATION MODE; VERTICAL (Z) DIRECTION . . . . .	88
FIG. 6.1.1 LINEAR CORRELATION FOR TEST H1; SIDE GIRDER NO. 1; LONGITUDINAL (X) DIRECTION . . . . .	101
FIG. 6.1.2 LINEAR CORRELATION FOR TEST H1; SIDE GIRDER NO. 1; TRANSVERSE (Y) DIRECTION . . . . .	101
FIG. 6.1.3 LINEAR CORRELATION FOR TEST H1; CENTER GIRDER; TRANSVERSE (Y) DIRECTION . . . . .	102
FIG. 6.1.4 LINEAR CORRELATION FOR TEST H1; SIDE GIRDER NO. 2; LONGITUDINAL (X) DIRECTION . . . . .	102
FIG. 6.1.5 LINEAR CORRELATION FOR TEST H1; SIDE GIRDER NO. 2; TRANSVERSE (Y) DIRECTION . . . . .	103

	<u>Page</u>
FIG. 6.1.6 LINEAR CORRELATION FOR TEST H1; EXPANSION JOINT NO. 1; INNER SIDE . . . . .	103
FIG. 6.1.7 LINEAR CORRELATION FOR TEST H1; EXPANSION JOINT NO. 1; OUTER SIDE . . . . .	104
FIG. 6.1.8 LINEAR CORRELATION FOR TEST H1; EXPANSION JOINT NO. 2; INNER SIDE . . . . .	104
FIG. 6.1.9 LINEAR CORRELATION FOR TEST H1; EXPANSION JOINT NO. 2; OUTER SIDE . . . . .	105
FIG. 6.2.1 NONLINEAR CORRELATION FOR TEST H1; SIDE GIRDER NO. 1; LONGITUDINAL (X) DIRECTION . . . . .	106
FIG. 6.2.2 NONLINEAR CORRELATION FOR TEST H1; SIDE GIRDER NO. 1; TRANSVERSE (Y) DIRECTION . . . . .	106
FIG. 6.2.3 NONLINEAR CORRELATION FOR TEST H1; CENTER GIRDER; TRANSVERSE (Y) DIRECTION . . . . .	107
FIG. 6.2.4 NONLINEAR CORRELATION FOR TEST H1; SIDE GIRDER NO. 2; LONGITUDINAL (X) DIRECTION . . . . .	107
FIG. 6.2.5 NONLINEAR CORRELATION FOR TEST H1; SIDE GIRDER NO. 2; TRANSVERSE (Y) DIRECTION . . . . .	108
FIG. 6.2.6 NONLINEAR CORRELATION FOR TEST H1; EXPANSION JOINT NO. 1; INNER SIDE . . . . .	108
FIG. 6.2.7 NONLINEAR CORRELATION FOR TEST H1; EXPANSION JOINT NO. 1; OUTER SIDE . . . . .	109
FIG. 6.2.8 NONLINEAR CORRELATION FOR TEST H2; EXPANSION JOINT NO. 2; INNER SIDE . . . . .	109
FIG. 6.2.9 NONLINEAR CORRELATION FOR TEST H1; EXPANSION JOINT NO. 2; OUTER SIDE . . . . .	110
FIG. 6.3.1 PREDICTED TIE BAR FORCE FOR TEST H2; EXPANSION JOINT NO. 1 . . . . .	111
FIG. 6.3.2 PREDICTED TIE BAR FORCE FOR TEST H1; EXPANSION JOINT NO. 2 . . . . .	111
FIG. 6.4.1 LINEAR CORRELATION FOR TEST HV2; SIDE GIRDER NO. 1; LONGITUDINAL (X) DIRECTION . . . . .	112
FIG. 6.4.2 LINEAR CORRELATION FOR TEST HV2; SIDE GIRDER NO. 1; TRANSVERSE (Y) DIRECTION . . . . .	112
FIG. 6.4.3 LINEAR CORRELATION FOR TEST HV2; CENTER GIRDER; TRANSVERSE (Y) DIRECTION . . . . .	113

	<u>Page</u>
FIG. 6.4.4 LINEAR CORRELATION FOR TEST HV2; SIDE GIRDER NO. 2; LONGITUDINAL (X) DIRECTION . . . . .	113
FIG. 6.4.5 LINEAR CORRELATION FOR TEST HV2; SIDE GIRDER NO. 2; TRANSVERSE (Y) DIRECTION . . . . .	114
FIG. 6.4.6 LINEAR CORRELATION FOR TEST HV2; EXPANSION JOINT NO. 1; INNER SIDE . . . . .	114
FIG. 6.4.7 LINEAR CORRELATION FOR TEST HV2; EXPANSION JOINT NO. 1; OUTER SIDE . . . . .	115
FIG. 6.4.8 LINEAR CORRELATION FOR TEST HV2; EXPANSION JOINT NO. 2; INNER SIDE . . . . .	115
FIG. 6.4.9 LINEAR CORRELATION FOR TEST HV2; EXPANSION JOINT NO. 2; OUTER SIDE . . . . .	116
FIG. 6.5.1 NONLINEAR CORRELATION FOR TEST HV2; SIDE GIRDER NO. 1; LONGITUDINAL (X) DIRECTION . . . . .	117
FIG. 6.5.2 NONLINEAR CORRELATION FOR TEST HV2; SIDE GIRDER NO. 1; TRANSVERSE (Y) DIRECTION . . . . .	117
FIG. 6.5.3 NONLINEAR CORRELATION FOR TEST HV2; CENTER GIRDER; TRANSVERSE (Y) DIRECTION . . . . .	118
FIG. 6.5.4 NONLINEAR CORRELATION FOR TEST HV2; SIDE GIRDER NO. 2; LONGITUDINAL (X) DIRECTION . . . . .	118
FIG. 6.5.5 NONLINEAR CORRELATION FOR TEST HV2; SIDE GIRDER NO. 2; TRANSVERSE (Y) DIRECTION . . . . .	119
FIG. 6.5.6 NONLINEAR CORRELATION FOR TEST HV2; EXPANSION JOINT NO. 1; INNER SIDE . . . . .	119
FIG. 6.5.7 NONLINEAR CORRELATION FOR TEST HV2; EXPANSION JOINT NO. 1; OUTER SIDE . . . . .	120
FIG. 6.5.8 NONLINEAR CORRELATION FOR TEST HV2; EXPANSION JOINT NO. 2; INNER SIDE . . . . .	120
FIG. 6.5.9 NONLINEAR CORRELATION FOR TEST HV2; EXPANSION JOINT NO. 2; OUTER SIDE . . . . .	121
FIG. 6.6.1 PREDICTED TIE BAR FORCE AND YIELD LENGTH FOR TEST HV2; EXPANSION JOINT NO. 1 . . . . .	122
FIG. 6.6.2 PREDICTED TIE BAR FORCE AND YIELD LENGTH FOR TEST HV2; EXPANSION JOINT NO. 2 . . . . .	122
FIG. 6.7.1 PREDICTED CONTACT FORCE FOR TEST HV2; EXPANSION JOINT NO. 1 . . . . .	123



	<u>Page</u>
FIG. 6.7.2 PREDICTED CONTACT FORCE FOR TEST HV2; EXPANSION JOINT NO. 2 . . . . .	123
FIG. 6.8.1 LINEAR CORRELATION FOR TEST H3; SIDE GIRDER NO. 1; LONGITUDINAL (X) DIRECTION . . . . .	124
FIG. 6.8.2 LINEAR CORRELATION FOR TEST H3; SIDE GIRDER NO. 1; TRANSVERSE (Y) DIRECTION . . . . .	124
FIG. 6.8.3 LINEAR CORRELATION FOR TEST H3; CENTER GIRDER; TRANSVERSE (Y) DIRECTION . . . . .	125
FIG. 6.8.4 LINEAR CORRELATION FOR TEST H3; SIDE GIRDER NO. 2; LONGITUDINAL (X) DIRECTION . . . . .	125
FIG. 6.8.5 LINEAR CORRELATION FOR TEST H3; SIDE GIRDER NO. 2; TRANSVERSE (Y) DIRECTION . . . . .	126
FIG. 6.8.6 LINEAR CORRELATION FOR TEST H3; EXPANSION JOINT NO. 1; INNER SIDE . . . . .	126
FIG. 6.8.7 LINEAR CORRELATION FOR TEST H3; EXPANSION JOINT NO. 1; OUTER SIDE . . . . .	127
FIG. 6.8.8 LINEAR CORRELATION FOR TEST H3; EXPANSION JOINT NO. 2; INNER SIDE . . . . .	127
FIG. 6.8.9 LINEAR CORRELATION FOR TEST H3; EXPANSION JOINT NO. 2; OUTER SIDE . . . . .	128
FIG. 6.9.1 NONLINEAR CORRELATION FOR TEST H3; SIDE GIRDER NO. 1; LONGITUDINAL (X) DIRECTION . . . . .	129
FIG. 6.9.2 NONLINEAR CORRELATION FOR TEST H3; SIDE GIRDER NO. 1; TRANSVERSE (Y) DIRECTION . . . . .	129
FIG. 6.9.3 NONLINEAR CORRELATION FOR TEST H3; CENTER GIRDER; TRANSVERSE (Y) DIRECTION . . . . .	130
FIG. 6.9.4 NONLINEAR CORRELATION FOR TEST H3; SIDE GIRDER NO. 2; LONGITUDINAL (X) DIRECTION . . . . .	130
FIG. 6.9.5 NONLINEAR CORRELATION FOR TEST H3; SIDE GIRDER NO. 2; TRANSVERSE (Y) DIRECTION . . . . .	131
FIG. 6.9.6 NONLINEAR CORRELATION FOR TEST H3; EXPANSION JOINT NO. 1; INNER SIDE . . . . .	131
FIG. 6.9.7 NONLINEAR CORRELATION FOR TEST H3; EXPANSION JOINT NO. 1; OUTER SIDE . . . . .	132
FIG. 6.9.8 NONLINEAR CORRELATION FOR TEST H3; EXPANSION JOINT NO. 2; INNER SIDE . . . . .	132

	<u>Page</u>
FIG. 6.9.9 NONLINEAR CORRELATION FOR TEST H3; EXPANSION JOINT NO. 2; OUTER SIDE . . . . .	133
FIG. 6.10.1 PREDICTED TIE BAR FORCE AND YIELD LENGTH FOR TEST H3; EXPANSION JOINT NO. 1 . . . . .	134
FIG. 6.10.2 PREDICTED TIE BAR FORCE AND YIELD LENGTH FOR TEST H3; EXPANSION JOINT NO. 2 . . . . .	134
FIG. 6.11.1 PREDICTED CONTACT FORCE FOR TEST H3; EXPANSION JOINT NO. 1 . . . . .	135
FIG. 6.11.2 PREDICTED CONTACT FORCE FOR TEST H3; EXPANSION JOINT NO. 2 . . . . .	135
FIG. 7.1.1 EFFECT OF LONGITUDINAL RESTRAINER TIE BARS ON RESPONSE OF CENTER GIRDER; TEST HV2 . . . . .	140
FIG. 7.1.2 EFFECT OF LONGITUDINAL RESTRAINER TIE BARS ON RELATIVE RESPONSE OF EXPANSION JOINT NO. 2 (OUTER SIDE); TEST HV2 . . . . .	140
FIG. 7.2.1 EFFECT OF COLLISIONS ON RESPONSE OF CENTER GIRDER; TEST HV2 . . . . .	141
FIG. 7.2.2 EFFECT OF COLLISIONS ON RELATIVE RESPONSE OF EXPANSION JOINT NO. 2 (OUTER SIDE); TEST HV2 . . . . .	141
FIG. 7.3.1 EFFECT OF COULOMB FRICTION ON RESPONSE OF CENTER GIRDER; TEST HV2 . . . . .	142
FIG. 7.3.2 EFFECT OF COULOMB FRICTION ON RELATIVE RESPONSE OF EXPANSION JOINT NO. 2 (OUTER SIDE); TEST HV2 . . . . .	142
FIG. 7.4.1 EFFECT OF VERTICAL EXCITATION ON RESPONSE OF CENTER GIRDER; TEST HV2 . . . . .	143
FIG. 7.4.2 EFFECT OF VERTICAL EXCITATION ON RELATIVE RESPONSE OF EXPANSION JOINT NO. 2 (OUTER SIDE); TEST HV2 . . . . .	143
FIG. 7.5.1 EFFECT OF IMPACT SPRING STIFFNESS ON RESPONSE OF CENTER GIRDER; TEST HV2 . . . . .	144
FIG. 7.5.2 EFFECT OF IMPACT SPRING STIFFNESS ON RELATIVE RESPONSE OF EXPANSION JOINT NO. 2 (OUTER SIDE); TEST HV2 . . . . .	144
FIG. A.1 LONGITUDINAL COLINEAR COLLISION OF TWO RODS . . . . .	A-9
FIG. A.2 ANALYTICAL MODEL FOR COLLISION OF RODS . . . . .	A-10
FIG. A.3 EXACT SOLUTION OF RELATIVE DISPLACEMENT AND RELATIVE VELOCITY . . . . .	A-11

	<u>Page</u>
FIG. A.4.1 EFFECT OF IMPACT SPRING STIFFNESS ON RELATIVE RESPONSE OF RODS ( $k_I = 10, 10^2$ and $10^3$ ) . . . . .	A-12
FIG. A.4.2 EFFECT OF IMPACT SPRING STIFFNESS ON RELATIVE RESPONSE OF RODS ( $k_I = 10^4$ and $10^5$ ) . . . . .	A-13
FIG. A.5 EFFECT OF TIME INTERVAL ON RELATIVE RESPONSE OF RODS . . . . .	A-14
FIG. A.6 EFFECT OF ELEMENT NUMBER ON RELATIVE RESPONSE OF RODS . . . . .	A-15
FIG. A.7 PREDICTED PARTICLE VELOCITY AND STRESS OF RODS . . . .	A-16
FIG. B.1 FREE VIBRATION OF A BLOCK WITH COULOMB FRICTION . . . .	B-6
FIG. B.2 FREE VIBRATION RESPONSE OF A BLOCK WITH COULOMB FRICTION . . . . .	B-7
FIG. B.3 EFFECT OF MAGNITUDE OF $u^e$ ON FREE VIBRATION RESPONSE OF A BLOCK . . . . .	B-8
FIG. B.4 EFFECT OF TIME INTERVAL ON FREE VIBRATION RESPONSE OF A BLOCK . . . . .	B-9

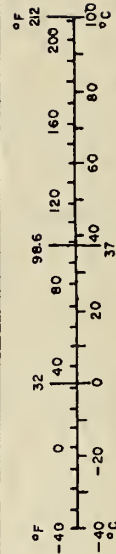
# METRIC CONVERSION FACTORS

## Approximate Conversions to Metric Measures

Symbol	When You Know	Multiply by	To Find	Symbol
<b>LENGTH</b>				
in	inches	2.5	centimeters	cm
ft	feet	30	centimeters	cm
yd	yards	0.9	meters	m
mi	miles	1.6	kilometers	km
<b>AREA</b>				
in <sup>2</sup>	square inches	6.5	square centimeters	cm <sup>2</sup>
ft <sup>2</sup>	square feet	0.09	square meters	m <sup>2</sup>
yd <sup>2</sup>	square yards	0.8	square meters	m <sup>2</sup>
mi <sup>2</sup>	square miles	2.6	square kilometers	km <sup>2</sup>
	acres	0.4	hectares	ha
<b>MASS (weight)</b>				
oz	ounces	28	grams	g
lb	pounds	0.45	kilograms	kg
	short tons	0.9	tonnes	t
	(2000 lb)			
<b>VOLUME</b>				
tsp	teaspoons	5	milliliters	ml
Tbsp	tablespoons	15	milliliters	ml
fl oz	fluid ounces	30	milliliters	ml
c	cups	0.24	liters	l
pt	pints	0.47	liters	l
qt	quarts	0.95	liters	l
gal	gallons	3.8	liters	l
ft <sup>3</sup>	cubic feet	0.03	cubic meters	m <sup>3</sup>
yd <sup>3</sup>	cubic yards	0.76	cubic meters	m <sup>3</sup>
<b>TEMPERATURE (exact)</b>				
°F	Fahrenheit temperature	5/9 (after subtracting 32)	Celsius temperature	°C

## Approximate Conversions from Metric Measures

When You Know	Multiply by	To Find	Symbol
<b>LENGTH</b>			
millimeters	0.04	inches	in
centimeters	0.4	inches	in
meters	3.3	feet	ft
kilometers	1.1	yards	yd
	0.6	miles	mi
<b>AREA</b>			
square centimeters	0.16	square inches	in <sup>2</sup>
square meters	1.2	square yards	yd <sup>2</sup>
square kilometers	0.4	square miles	mi <sup>2</sup>
hectares (10,000 m <sup>2</sup> )	2.5	acres	
<b>MASS (weight)</b>			
grams	0.035	ounces	oz
kilograms	2.2	pounds	lb
tonnes (1000 kg)	1.1	short tons	
<b>VOLUME</b>			
milliliters	0.03	fluid ounces	fl oz
liters	2.1	pints	pt
liters	1.06	quarts	qt
liters	0.26	gallons	gal
cubic meters	35	cubic feet	ft <sup>3</sup>
cubic meters	1.3	cubic yards	yd <sup>3</sup>
<b>TEMPERATURE (exact)</b>			
Celsius temperature	9/5 (then add 32)	Fahrenheit temperature	°F



\*1 in ± 2.54 (exactly). For other exact conversions and more detailed tables, see NBS Misc. Publ. 286, Units of Weights and Measures, Price \$2.25, SD Catalog No. C13.10/286.



## I. INTRODUCTION

### A. STATEMENT OF THE PROBLEM

In the past, numerous highway bridges have suffered extensive damages due to strong motion earthquake [1]\*. The older bridges, consisting of single or multiple simple truss or girder spans supported on massive piers and abutments, were particularly vulnerable to the action of strong ground motions. Seismic damages were most commonly caused by foundation failures resulting from excessive ground deformation and/or loss of stability and bearing capacity of the foundation soils. As a direct result, the substructures often tilted, settled, slid, or even overturned; thus severe cracking or complete failure was often experienced. These large support displacements also caused relative shifting of and damage to the superstructures, induced failures within the bearing supports, and even caused spans to fall off their supports. It is significant to note that very little damage occurred to these older structures as a direct result of structural vibration effects.

Certain types of modern highway bridges may, on the other hand, be quite susceptible to damage from strong ground vibration effects. This fact became very evident during the San Fernando earthquake of February 9, 1971, when numerous reinforced concrete highway bridges which were designed by the traditional elastic approach; i.e., by the equivalent static seismic coefficient method similar to that previously adopted for buildings, suffered severe damages. Because of this experience, it was immediately apparent that the seismic requirements used were inadequate and that the design methodology should be critically examined. Action was quickly taken following the earthquake to correct certain design

---

\*Numbers in brackets refer to bibliography numbers.

deficiencies; however, the basic static approach to design still remains in effect.

Recognizing the urgent need for both theoretical and experimental research related directly to seismic effects on bridge structures, an investigation entitled "An Investigation Of The Effectiveness of Existing Bridge Design Methodology in Providing Adequate Structural Resistance to Seismic Disturbances" was initiated in 1971 within the Earthquake Engineering Research Center, University of California, Berkeley, under the sponsorship of the U.S. Department of Transportation, Federal Highway Administration. This investigation consists of the following six phases:

- (1) A thorough review of the world's literature on seismic effects on highway bridge structure including damages to bridges during the San Fernando earthquake of February 9, 1971.
- (2) An analytical investigation of the dynamic response of long, multiple-span, highway overcrossings of the type which suffered heavy damages during the 1971 San Fernando earthquake.
- (3) An analytical investigation of the dynamic response of short, single and multiple span highway overcrossings of the type which suffered heavy damages during the 1971 San Fernando earthquake.
- (4) Detailed model experiments on a shaking table to provide dynamic response data similar to prototype behavior which can be used to verify the validity of theoretical response predictions.
- (5) Correlation of dynamic response data obtained from shaking table experiments with theoretical response and modification of analytical procedures as found necessary.

- (6) Preparation of recommendations for changes in seismic design specifications and methodology as necessary to provide adequate protection of reinforced concrete highway bridges against future earthquakes.

Final reports covering Phases 1, 2, and 3 have been published [1,2,6] and the final report covering Phase 4 is now nearing completion. The present final report covers Phase 5 and the final report on Phase 6 will be completed during summer and fall of 1977.

#### B. OBJECTIVES AND SCOPE

The primary objectives of the investigation in Phase 5 are to correlate the dynamic responses of the experimental model measured during shaking table tests conducted in Phase 4 with the corresponding responses determined using the analytical model and numerical procedures developed in Phase 2.

To achieve these objectives, the analytical model and numerical procedures defined and developed in Phase 2 have been re-examined for use in predicting the seismic response of the experimental model structure. Modifications of the analytical model simulating nonlinear dynamic behavior of expansion joints and the analytical procedure for numerical integration of equations of motion have been found necessary. These changes have been incorporated into the nonlinear response analysis computer program NEABS.

Experimental test results obtained in Phase 4 were reviewed to select suitable excitation tests for correlation purposes. Since it was found that the model structure is more susceptible to damage when the excitation is oriented in the transverse direction, test results obtained under transverse and under simultaneous transverse and vertical excitations were used for correlation purposes.



Correlation of the measured experimental displacement response with the corresponding response predicted by linear and nonlinear analyses has been performed for three types of seismic excitation (Series IV excitation tests), namely, (1) low intensity excitation in the transverse direction, (2) high intensity excitation in the transverse direction, and (3) high intensity excitation in both the transverse and vertical directions. The linear response analysis computer program BSAP and the nonlinear response analysis computer program NEABS as revised have been used for these correlations.

Finally, a parameter study of the dynamic response was conducted using the nonlinear analytical model and analysis procedures.

Chapter II of this report describes the modifications introduced into the nonlinear analytical model of expansion joints which allow proper simulations of the impact phenomenon, slippage with Coulomb type friction, and separation under the action of elastoplastic joint restrainer tie bars acting in tension only. Chapter III describes certain modification to the analytical procedures including an equilibrium correction introduced through iteration and subdivision of time intervals into a specified number of equal sub-intervals. Chapter IV describes the experimental model and test results which were used to formulate the analytical model used in the correlation study. Chapter V describes the procedure used to formulate a basic analytical model which reproduces the observed dynamic characteristics of the experimental model under the initial low intensity excitations. Chapter VI presents the correlation results for the three seismic excitations having various intensities of table motion. Chapter VII gives a discussion of the correlation results and Chapter VIII summarizes the conclusions drawn from the investigation.



Finally, numerical results obtained from the parameter studies of impact and Coulomb friction are presented in order to show the applicability of the analytical model and numerical procedures defined in Chapters II and III.

## II. ANALYTICAL MODEL OF EXPANSION JOINTS

A nonlinear analytical model for simulating the dynamic behavior of expansion joints was formulated by Tseng and Penzien [2,4]. It includes relative translational and rotational degrees of freedom, elastoplastic joint restrainer tie bars acting in tension, impact, and Coulomb type friction with slippage. Although the original analytical model of expansion joints was basically correct, certain modifications were needed to make it fully reproduce the characteristics of the model bridge structure. The modifications introduced into the original analytical model and into the nonlinear analysis computer program NEABS [2] were the following:

- (1) The impact spring was modified in such a way that it approximates elastic collisions.
- (2) The Coulomb type friction force was approximated by an elastoplastic hysteretic model.

The subsequent discussion in this chapter concentrates on the above modifications to the analytical model of the expansion joints with some mention of the basic equations needed to characterize their nonlinear behavior.

### A. PIECEWISE LINEAR EXPANSION JOINT STIFFNESS [2,4]

The force vs. displacement relation of the idealized expansion joint as shown in Fig. 2.1 can be characterized using an expansion joint coordinate system as defined in Fig. 2.2, i.e.,

$$\Delta \bar{S} = \bar{k}_t^{EJ} \Delta \bar{r} \quad (1)$$

where

$$\Delta \bar{S} = \begin{Bmatrix} \Delta \bar{S}_I \\ \Delta \bar{S}_J \end{Bmatrix}, \quad \Delta \bar{S}_K = \begin{Bmatrix} \Delta S_{Ax} \\ \Delta S_y \\ \Delta S_{Az} \\ \Delta S_{Bx} \\ \Delta M_s \\ \Delta S_{Bz} \end{Bmatrix}_K \quad (K = I, J) \quad (2)$$

$$\Delta \bar{r} = \begin{Bmatrix} \Delta \bar{r}_I \\ \Delta \bar{r}_J \end{Bmatrix}, \quad \Delta \bar{r}_K = \begin{Bmatrix} \Delta r_{Ax} \\ \Delta r_y \\ \Delta r_{Az} \\ \Delta r_{Bx} \\ \Delta \theta_s \\ \Delta r_{Bz} \end{Bmatrix}_K \quad (K = I, J) \quad (3)$$

Matrix  $\bar{k}_t^{EJ}$  is a tangent stiffness matrix at time  $t$  which relates the expansion joint force increment  $\Delta \bar{S}$  with the expansion joint displacement increment  $\Delta \bar{r}$ .

The expansion joint coordinate system can be related to the local nodal coordinate system defined by

$$\bar{r} = \begin{Bmatrix} \bar{r}_I \\ \bar{r}_J \end{Bmatrix}, \quad \bar{r}_K = \begin{Bmatrix} r_x \\ r_y \\ r_z \\ \theta_x \\ \theta_y \\ \theta_z \end{Bmatrix}_K \quad (K = I, J) \quad (4)$$

$$\underline{s} = \begin{Bmatrix} \underline{s}_I \\ \underline{s}_J \end{Bmatrix}, \quad \underline{s}_K = \begin{Bmatrix} s_x \\ s_y \\ s_z \\ M_x \\ M_y \\ M_z \end{Bmatrix}_K \quad (K = I, J) \quad (5)$$

through the transformations

$$\underline{r} = \begin{Bmatrix} \underline{r}_I \\ \underline{r}_J \end{Bmatrix} = \begin{bmatrix} \underline{a} & 0 \\ 0 & \underline{a} \end{bmatrix} \begin{Bmatrix} \underline{r}_I \\ \underline{r}_J \end{Bmatrix} \equiv \underline{A} \underline{r} \quad (6)$$

and

$$\underline{s} = \begin{Bmatrix} \underline{s}_I \\ \underline{s}_J \end{Bmatrix} = \begin{bmatrix} \underline{a}^T & 0 \\ 0 & \underline{a}^T \end{bmatrix} \begin{Bmatrix} \underline{s}_I \\ \underline{s}_J \end{Bmatrix} \equiv \underline{A}^T \underline{s} \quad (7)$$

where matrix  $\underline{a}$  is given by

$$\underline{a} = \begin{bmatrix} 1 & 0 & 0 & 0 & 0 & d/2 \\ 0 & 1 & 0 & 0 & 0 & 0 \\ 0 & 0 & 1 & -d/2 & d/2 \cdot \tan\psi & 0 \\ 1 & 0 & 0 & 0 & 0 & -d/2 \\ 0 & 0 & 0 & 0 & 1/\cos\psi & 0 \\ 0 & 0 & 1 & d/2 & -d/2 \cdot \tan\psi & 0 \end{bmatrix} \quad (8)$$

in which  $\psi$  represents the skew angle of the deck.

It is convenient to define the stiffness coefficients of  $\underline{k}_t^{EJ}$  in terms of the relative expansion joint displacements  $\underline{u}$  defined by



$$\bar{u} = \begin{Bmatrix} u_{Ax} \\ u_y \\ u_{Az} \\ u_{Bx} \\ u_s \\ u_{Bz} \end{Bmatrix} \equiv \begin{Bmatrix} r_{Ax} \\ r_y \\ r_{Az} \\ r_{Bx} \\ \theta_s \\ r_{Bz} \end{Bmatrix}_J - \begin{Bmatrix} r_{Ax} \\ r_y \\ r_{Az} \\ r_{Bx} \\ \theta_s \\ r_{Bz} \end{Bmatrix}_I = \bar{r}_J - \bar{r}_I \quad (9)$$

and the corresponding expansion joint force  $\bar{F}$  defined by

$$\bar{F} = \begin{Bmatrix} F_{Ax} \\ F_y \\ F_{Az} \\ F_{Bx} \\ M_s \\ F_{Bz} \end{Bmatrix} = \begin{Bmatrix} S_{Ax} \\ S_y \\ S_{Az} \\ S_{Bx} \\ M_s \\ S_{Bz} \end{Bmatrix}_J = \bar{S}_J - \bar{S}_I \quad (10)$$

Thus, the idealized expansion joint can be characterized by a stiffness matrix  $\bar{k}$  relating  $\Delta\bar{F}$  to  $\Delta\bar{u}$ , i.e.,

$$\Delta\bar{F} = \bar{k} \Delta\bar{u} \quad (11)$$

Using Eqs. (9) and (10), the stiffness matrix  $\bar{k}_t^{EJ}$  can be expressed as

$$\bar{k}_t^{EJ} = \begin{bmatrix} \bar{k} & -\bar{k} \\ -\bar{k} & \bar{k} \end{bmatrix} \quad (12)$$

The stiffness matrix  $\bar{k}_t^{EJ}$  must be transformed to the local nodal coordinate system using Eqs. (6) and (7). This transformation results in the relation

$$\underline{\Delta S} = \underline{k}_{-t}^{EJ} \underline{\Delta r} \quad , \quad \underline{k}_{-t}^{EJ} = \underline{A}^T \underline{\bar{k}}_{-t}^{EJ} \underline{A} \quad (13)$$

Matrix  $\underline{k}_{-t}^{EJ}$  is the stiffness matrix which relates the vector of local nodal force increments  $\underline{\Delta S}$  to the vector of local nodal displacement increments  $\underline{\Delta r}$  at time  $t$ , and which, after local to global coordinate transformation, can be used to assemble the total stiffness matrix  $\underline{K}_{-t}$  for the complete structural system.

Stiffness matrix  $\underline{\bar{k}}$  defined in Eq. (11) represents contributions from two sources. One contribution is a stiffness matrix  $\underline{\bar{k}}_1$  of the idealized joint without collisions and another contribution is matrix  $\underline{\bar{k}}_2$  that represents the effect of collisions, i.e.,

$$\underline{\bar{k}} = \underline{\bar{k}}_1 + \underline{\bar{k}}_2 \quad (14)$$

The stiffness coefficients of  $\underline{\bar{k}}_1$  can be written in the form

$$\underline{\bar{k}}_1 = \begin{bmatrix} k_{AA} & 0 & 0 & k_{AB} & 0 & 0 \\ 0 & k_S & 0 & 0 & 0 & 0 \\ 0 & 0 & k_V & 0 & 0 & 0 \\ k_{AB} & 0 & 0 & k_{BB} & 0 & 0 \\ 0 & 0 & 0 & 0 & 0 & 0 \\ 0 & 0 & 0 & 0 & 0 & k_V \end{bmatrix} \quad (15)$$

where  $k_S$  is the elastic stiffness of the spring which resists the relative transverse displacement,  $k_V$  is the elastic stiffness of the springs which resists the relative vertical displacement at points A and B, and

$$\begin{aligned}
k_{AA} &= \sum_{i=1}^{N_T} k_{Ti} \left( \frac{1}{2} - \frac{y_i}{d} \right)^2 \\
k_{BB} &= \sum_{i=1}^{N_T} k_{Ti} \left( \frac{1}{2} + \frac{y_i}{d} \right)^2 \\
k_{AB} &= \sum_{i=1}^{N_T} k_{Ti} \left( \frac{1}{2} - \frac{y_i}{d} \right) \left( \frac{1}{2} + \frac{y_i}{d} \right)
\end{aligned} \tag{16}$$

in which  $N_T$  is the number of tie bars and  $k_{Ti}$  is the instantaneous stiffness of the  $i$ th tie bar at time  $t$ .

The stiffness coefficients of  $\bar{k}_2$  is described in the following paragraph.

#### B. COLLISIONS

Longitudinal collisions are defined to take place at points A and B when the relative displacement between the two end diaphragms close the joint gap  $\Delta_G$  with a nonzero relative velocity. At the instant collision takes place, the longitudinal impact springs having large stiffness  $k_I$  which are attached to one end diaphragm leaving a small gap  $\Delta_G$  with the other end diaphragm start to resist the motion. A collision is completed when rebound occurs and the relative displacement between the two diaphragms becomes equal to the joint gap  $\Delta_G$ .

The contact forces acting at points A and B can be written as

$$\begin{aligned}
P_{AI} &= k_I < u_{Ax} + \Delta_G > (u_{Ax} + \Delta_G) \\
P_{BI} &= k_I < u_{Bx} + \Delta_G > (u_{Bx} + \Delta_G)
\end{aligned} \tag{17}$$

where

$$\begin{aligned}
< u_{Ax} + \Delta_G > &= \begin{cases} 1 & u_{Ax} + \Delta_G < 0 \\ 0 & u_{Ax} + \Delta_G \geq 0 \end{cases} \\
< u_{Bx} + \Delta_G > &= \begin{cases} 1 & u_{Bx} + \Delta_G < 0 \\ 0 & u_{Bx} + \Delta_G \geq 0 \end{cases}
\end{aligned} \tag{18}$$

If it is assumed that  $(u_{Ax} + \Delta_G)$  and  $(u_{Bx} + \Delta_G)$  do not change sign during a time interval  $\Delta t$ , the change of contact force during a time interval can be expressed as

$$\begin{aligned}
\Delta P_{AI} &= k_I < u_{Ax} + \Delta_G > \Delta u_{Ax} \\
\Delta P_{BI} &= k_I < u_{Bx} + \Delta_G > \Delta u_{Bx}
\end{aligned} \tag{19}$$

Let  $\Delta \bar{F}^I$  represent the incremental contact force vector in the relative expansion joint coordinate system during a time interval  $\Delta t$  as defined by

$$\Delta \bar{F}^I = \begin{Bmatrix} \Delta P_{AI} \\ 0 \\ 0 \\ \Delta P_{BI} \\ 0 \\ 0 \end{Bmatrix} \tag{20}$$

Then,  $\Delta \bar{F}^I$  can be expressed as

$$\Delta \bar{F}^I = \bar{k}_2 \Delta \bar{u} \tag{21}$$

in which



$$\bar{k}_2 = \begin{bmatrix} k_I < u_{Ax} + \Delta_G > & 0 & 0 & 0 & 0 & 0 \\ 0 & 0 & 0 & 0 & 0 & 0 \\ 0 & 0 & 0 & 0 & 0 & 0 \\ 0 & 0 & 0 & k_I < u_{Bx} + \Delta_G > & 0 & 0 \\ 0 & 0 & 0 & 0 & 0 & 0 \\ 0 & 0 & 0 & 0 & 0 & 0 \end{bmatrix} \quad (22)$$

### C. COULOMB FRICTION FORCES

Coulomb friction forces are developed at contact points A and B when the expansion joint undergoes longitudinal relative displacement and when the vertical contact forces are compressive. The friction at each point A and B always acts in the direction opposite to the relative velocity as a pair of self equilibrating forces. When the expansion joint does not undergo longitudinal relative displacement, each friction force can have a magnitude anywhere between its maximum and minimum values. The magnitude of a friction force depends on the magnitude of other forces acting on the expansion joint. Such characteristics can be represented by a rigid-plastic hysteretic force-relative displacement model as shown in Fig. 2.3. It should be noted here that the model of the Coulomb friction force represented in Fig. 2.3 is mathematically the same as the model of a rigid-plastic restoring force. Plastic deformations in the latter model correspond to slippages in the former model. In order to avoid numerical instability caused by a sudden change in the Coulomb friction force at zero relative velocity, the force is modeled by the elastoplastic hysteretic force-relative displacement model shown in Fig. 2.4. If the slope of OA in Fig. 2.4 is taken large enough, then both models of Figs. 2.3 and 2.4 are practically the same.

According to the assumption described, the Coulomb friction forces acting at points A and B at time t can be expressed as

$$C_{Ax} = \begin{cases} -\nu < F_{Az} > |F_{Az}| & \text{for } u_{Ax} \leq u_{Ax}^S - u_{Ax}^E \\ k^C < F_{Az} > (u_{Ax} - u_{Ax}^S) & \text{for } u_{Ax}^S - u_{Ax}^E < u_{Ax} < u_{Ax}^S + u_{Ax}^E \\ \nu < F_{Az} > |F_{Az}| & \text{for } u_{Ax} \geq u_{Ax}^S + u_{Ax}^E \end{cases} \quad (23)$$

$$C_{Bx} = \begin{cases} -\nu < F_{Bz} > |F_{Bz}| & \text{for } u_{Bx} \leq u_{Bx}^S - u_{Bx}^E \\ k^C < F_{Bz} > (u_{Bx} - u_{Bx}^S) & \text{for } u_{Bx}^S - u_{Bx}^E < u_{Bx} < u_{Bx}^S + u_{Bx}^E \\ \nu < F_{Bz} > |F_{Bz}| & \text{for } u_{Bx} \geq u_{Bx}^S + u_{Bx}^E \end{cases}$$

where  $\nu$  is a constant coefficient of Coulomb friction,  $u_{Ax}^S$  and  $u_{Bx}^S$  are the current slippages at points A and B, respectively, and  $u_{Ax}^E$  and  $u_{Bx}^E$  are the elastic deformations at points A and B, respectively, as given by

$$u_{Ax}^E = \nu |F_{Az}| / k_C, \quad u_{Bx}^E = \nu |F_{Bz}| / k_C \quad (24)$$

where

$$< F_{Az} > = \begin{cases} 1 & F_{Az} < 0 \\ 0 & F_{Az} \geq 0 \end{cases} \quad (25)$$

$$< F_{Bz} > = \begin{cases} 1 & F_{Bz} < 0 \\ 0 & F_{Bz} \geq 0 \end{cases}$$

If it is assumed that the vertical compressive contact forces  $F_{Az}$  and  $F_{Bz}$  are constant and deformations  $(u_{Ax} - u_{Ax}^S + u_{Ax}^E)$  and  $(u_{Bx} - u_{Bx}^S + u_{Bx}^E)$

do not change signs during a time interval  $\Delta t$ , then the changes of Coulomb friction force during the time interval can be expressed as

$$\Delta C_{Ax} = \begin{cases} k^C < F_{Az} > \Delta u_{Ax} & \text{for } u_{Ax}^S - u_{Ax}^E < u_{Ax} < u_{Ax}^S + u_{Ax}^E \\ 0 & \text{for } u_{Ax} \leq u_{Ax}^S - u_{Ax}^E \text{ or } \\ & u_{Ax} \geq u_{Ax}^S + u_{Ax}^E \end{cases} \quad (26)$$

$$\Delta C_{Bx} = \begin{cases} k^C < F_{Bz} > \Delta u_{Bx} & \text{for } u_{Bx}^S - u_{Bx}^E < u_{Bx} < u_{Bx}^S + u_{Bx}^E \\ 0 & \text{for } u_{Bx} \leq u_{Bx}^S - u_{Bx}^E \text{ or } \\ & u_{Bx} \geq u_{Bx}^S + u_{Bx}^E \end{cases}$$

Let  $\Delta \bar{P}^C$  represent the incremental Coulomb friction force vector in the expansion joint coordinate system during the time interval  $\Delta t$ ; then,  $\Delta \bar{P}^C$  can be expressed as

$$\Delta \bar{P}^C = \begin{Bmatrix} \Delta \bar{P}_{-I}^C \\ \Delta \bar{P}_{-J}^C \end{Bmatrix}, \quad \Delta \bar{P}_{-I}^C = \begin{Bmatrix} -\Delta C_{Ax} \\ 0 \\ 0 \\ -\Delta C_{Bx} \\ 0 \\ 0 \end{Bmatrix}, \quad \Delta \bar{P}_{-J}^C = \begin{Bmatrix} \Delta C_{Ax} \\ 0 \\ 0 \\ \Delta C_{Bx} \\ 0 \\ 0 \end{Bmatrix} \quad (27)$$

Thus  $\Delta \bar{P}^C$  can be related to the vector of incremental expansion joint displacement  $\Delta \bar{r}$  by a matrix  $\bar{k}_t^C$  in the form

$$\Delta \bar{P}^C = \bar{k}_t^C \Delta \bar{r} \quad (28)$$

where  $\bar{k}_t^C$  is a function of  $\bar{r}$  at time  $t$ .

From Eqs. (9) and (10),  $\bar{k}_t^C$  can be written in the form

$$\bar{k}_t^C = \begin{bmatrix} \bar{k}_3 & -\bar{k}_3 \\ -\bar{k}_3 & \bar{k}_3 \end{bmatrix} \quad (29)$$

in which  $\bar{k}_3$  is a matrix defined in the relative expansion joint coordinate system which relates the change of Coulomb friction force vector during a time interval  $\Delta t$  to the change of relative expansion joint displacement  $\Delta \bar{u}$ . From Eqs. (26) and (27),  $\bar{k}_3$  can be written as

$$\bar{k}_3 = \begin{bmatrix} k_A^C & 0 & 0 & 0 & 0 & 0 \\ 0 & 0 & 0 & 0 & 0 & 0 \\ 0 & 0 & 0 & 0 & 0 & 0 \\ 0 & 0 & 0 & k_B^C & 0 & 0 \\ 0 & 0 & 0 & 0 & 0 & 0 \\ 0 & 0 & 0 & 0 & 0 & 0 \end{bmatrix} \quad (30)$$

where

$$k_A^C = \begin{cases} k^C < F_{Az} > & \text{for } u_{Ax}^S - u_{Ax}^E < u_{Ax} < u_{Ax}^S + u_{Ax}^E \\ 0 & \text{for } u_{Ax} \leq u_{Ax}^S - u_{Ax}^E \text{ or } u_{Ax} \geq u_{Ax}^S + u_{Ax}^E \end{cases} \quad (31)$$

$$k_B^C = \begin{cases} k^C < F_{Bz} > & \text{for } u_{Bx}^S - u_{Bx}^E < u_{Bx} < u_{Bx}^S + u_{Bx}^E \\ 0 & \text{for } u_{Bx} \leq u_{Bx}^S - u_{Bx}^E \text{ or } u_{Bx} \geq u_{Bx}^S + u_{Bx}^E \end{cases}$$



Finally, the matrix  $\bar{k}_{-t}^C$  must be transformed to the local coordinate system using Eqs. (6) and (7). This transformation results in the relation

$$\Delta \underline{P}^C = \underline{k}_{-t}^C \Delta \underline{r} \quad , \quad \underline{k}_{-t}^C = \underline{A}^T \bar{k}_{-t}^C \underline{A} \quad (32)$$

Matrix  $\underline{k}_{-t}^C$  relates the vector of local nodal Coulomb friction force increment  $\Delta \underline{P}^C$  to the vector of local nodal displacement increment  $\Delta \underline{r}$ . After local to global coordinate transformation, it can be used to assemble the total stiffness matrix  $\underline{K}_{-t}$  together with the stiffness matrix  $\underline{k}_{-t}^{EJ}$  defined in Eq. (13).

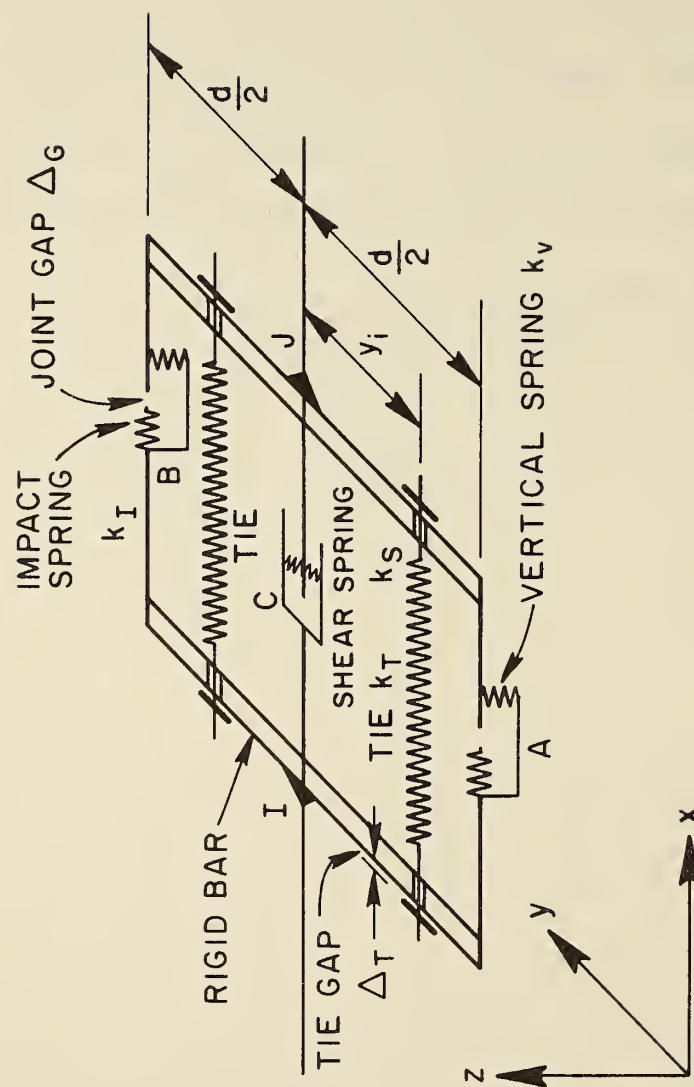
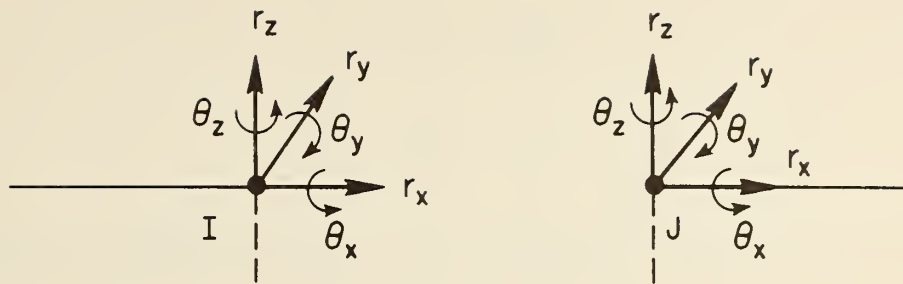
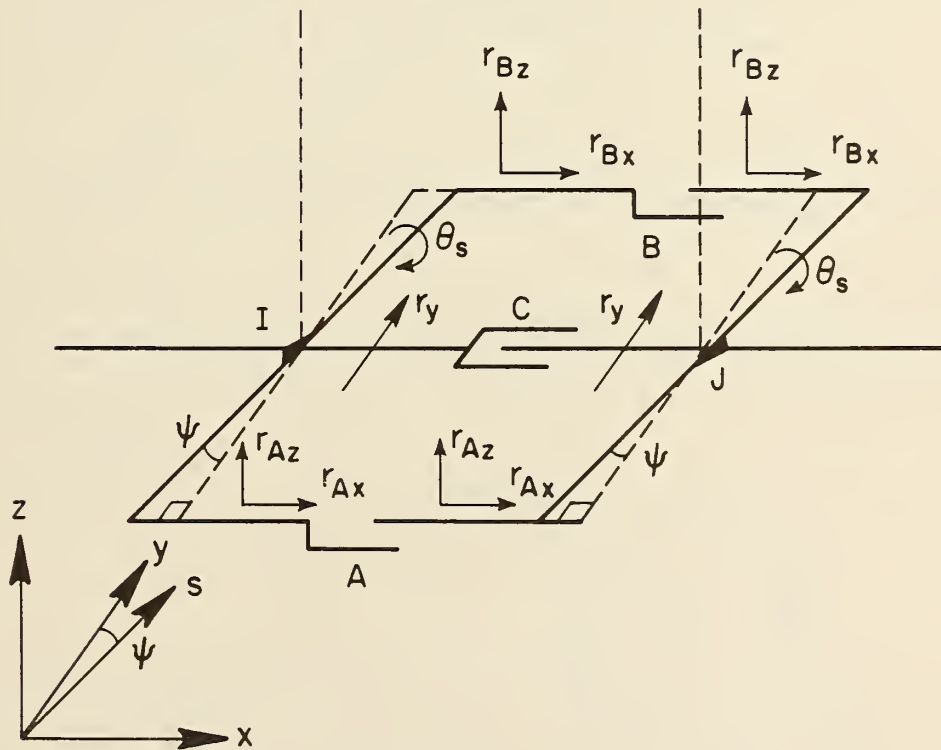


FIG. 2.1 IDEALIZED EXPANSION JOINT [2]



LOCAL NODAL COORDINATE SYSTEM  $\underline{r}$



EXPANSION JOINT COORDINATE SYSTEM  $\bar{r}$

FIG. 2.2 COORDINATE SYSTEM FOR EXPANSION JOINT [2]

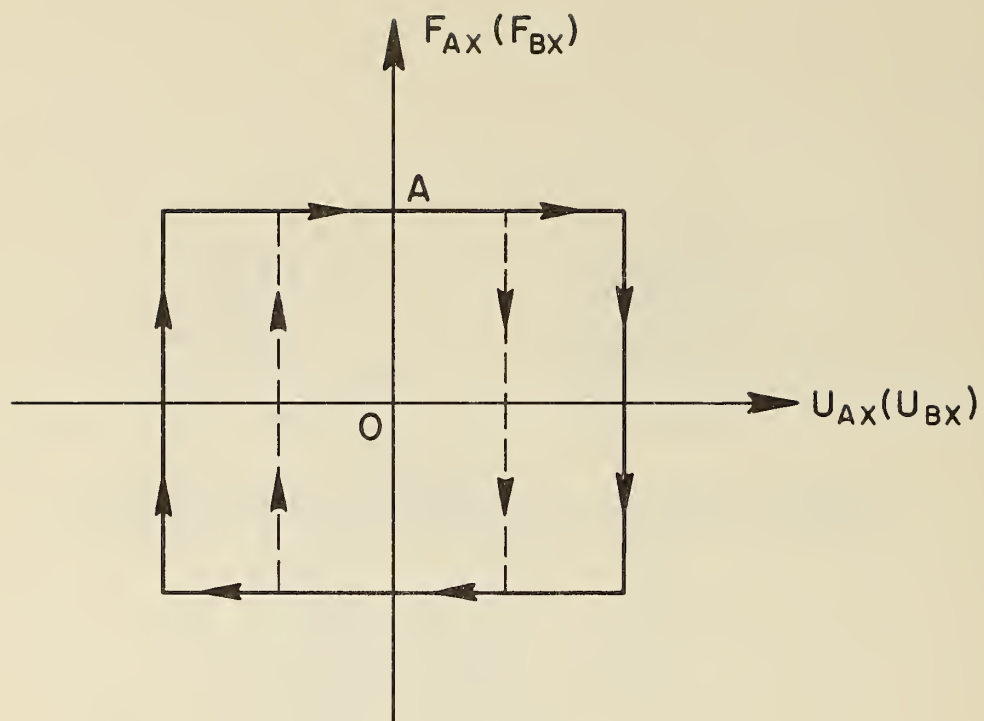


FIG. 2.3 RIGID-PLASTIC HYSTERETIC MODEL FOR COULOMB FRICTION

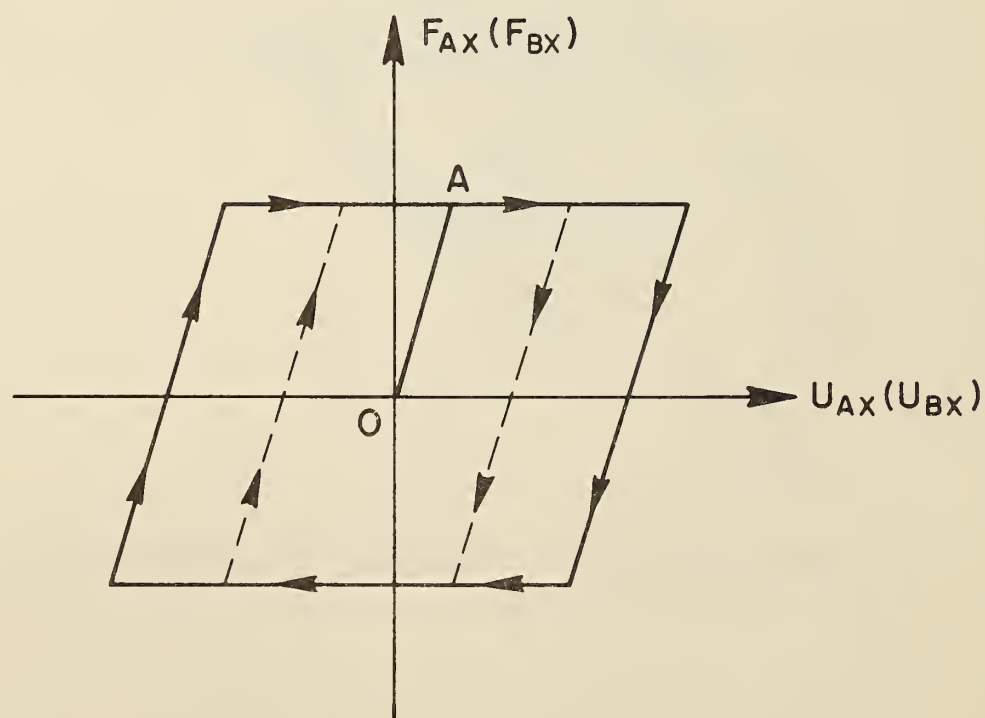


FIG. 2.4 ELASTOPLASTIC HYSTERETIC MODEL FOR COULOMB FRICTION



### III. DYNAMIC ANALYSIS PROCEDURE

#### A. INCREMENTAL EQUATION OF MOTION

The equation of motion for an  $n$  degree of freedom system representing dynamic equilibrium at time  $t$  can be expressed as

$$\underline{F}_t^I + \underline{F}_t^D + \underline{F}_t^S = \underline{R}_t \quad (33)$$

where,  $\underline{F}_t^I$ ,  $\underline{F}_t^D$ ,  $\underline{F}_t^S$  and  $\underline{R}_t$  are the nodal inertia force vector, nodal damping force vector, nodal restoring force vector and nodal external force vector at time  $t$ , respectively. When the structure is nonlinear, Eq. (33) is written for time  $t + \Delta t$  in the form

$$\left( \underline{F}_t^I + \Delta \underline{F}_t^I \right) + \left( \underline{F}_t^D + \Delta \underline{F}_t^D \right) + \left( \underline{F}_t^S + \Delta \underline{F}_t^S \right) = \underline{R}_{t+\Delta t} \quad (34)$$

where,  $\Delta \underline{F}_t^I$ ,  $\Delta \underline{F}_t^D$  and  $\Delta \underline{F}_t^S$  are the changes of the nodal inertia forces, nodal damping forces and nodal restoring forces during a time interval  $\Delta t$ , respectively. These changes of the forces are assumed to be given by

$$\Delta \underline{F}_t^I = \underline{M} \Delta \ddot{\underline{u}}_t; \Delta \underline{F}_t^D = \underline{C} \Delta \dot{\underline{u}}_t; \Delta \underline{F}_t^S = \underline{K}_t \Delta \underline{u}_t \quad (35)$$

where,  $\underline{M}$ ,  $\underline{C}$  and  $\underline{K}_t$  represent the constant mass matrix, constant viscous damping matrix and tangent stiffness matrix at time  $t$ , respectively. Vectors  $\Delta \ddot{\underline{u}}_t$ ,  $\Delta \dot{\underline{u}}_t$  and  $\Delta \underline{u}_t$  are the changes of nodal accelerations, nodal velocities and nodal displacements during time interval  $\Delta t$  as defined by

$$\begin{aligned}
\Delta \ddot{u}_{-t} &= \ddot{u}_{-t+\Delta t} - \ddot{u}_{-t} \\
\Delta \dot{u}_{-t} &= \dot{u}_{-t+\Delta t} - \dot{u}_{-t} \\
\Delta u_{-t} &= u_{-t+\Delta t} - u_{-t}
\end{aligned} \tag{36}$$

Substituting Eq. (35) into Eq. (34), one can obtain the equation of motion in incremental form as

$$\underline{M} \Delta \ddot{u}_{-t} + \underline{C} \Delta \dot{u}_{-t} + \underline{K}_{-t} \Delta u_{-t} = \underline{R}_{-t+\Delta t} - \underline{M} \ddot{u}_{-t} - \underline{C} \dot{u}_{-t} - \underline{F}_{-t}^S \tag{37}$$

The nodal external force vector  $\underline{R}_{-t+\Delta t}$  is assumed to be derived from two types of loading [2]; an applied dynamic force  $\underline{P}_{-t+\Delta t}$  and an inertia force due to ground motion  $\ddot{u}_{-g}(t+\Delta t)$ , i.e.,

$$\underline{R}_{-t+\Delta t} = \underline{P}_{-t+\Delta t} - \underline{M} \underline{B} \ddot{u}_{-g}(t+\Delta t) \tag{38}$$

in which  $\underline{B}$  is a matrix of ground motion influence coefficients.

The tangent stiffness matrix  $\underline{K}_{-t}$  consists of time independent coefficients  $\underline{K}_{-t}^L$  which are assembled before excitation based on the initial stress stage and time-dependent coefficients  $\underline{K}_{-t}^N$  which change in each time internal, i.e.,

$$\underline{K}_{-t} = \underline{K}_{-t}^L + \underline{K}_{-t}^N \tag{39}$$

where

$$\begin{aligned}
\underline{K}_{-t}^L &= \sum_{j=1}^{LEL} \underline{k}_{-t}(j) + \sum_{j=1}^{NEL} \underline{k}_{-t}(j) \\
\underline{K}_{-t}^N &= \sum_{j=1}^{NEL} \underline{k}_{-t}^N(j), \quad \underline{k}_{-t}^N(j) = \underline{k}_{-t}(j) - \underline{k}_{-t}(j)
\end{aligned} \tag{40}$$

in which LEL and NEL represent numbers of linear and nonlinear elements in the system. Matrices  $\underline{k}_{(j)}$  and  $\underline{k}_{-t(j)}$  represent time independent stiffness coefficients for the jth linear or nonlinear element and time dependent stiffness coefficients for the jth nonlinear element, respectively. From Eq. (39),  $\underline{F}_{-t}^S$  can be written as

$$\underline{F}_{-t}^S = \underline{F}_{-t}^{SL} + \underline{F}_{-t}^{SN} = \underline{K}_{-t}^L \underline{u}_{-t} + \sum_{j=1}^{NEL} \underline{f}_{-t(j)}^{SN} \quad (41)$$

in which  $\underline{f}_{-t(j)}^{SN}$  represents time dependent nodal restoring forces for the jth nonlinear element. It is desirable to calculate  $\underline{f}_{-t(j)}^{SN}$  ( $j \in NEL$ ) directly from current element deformations in order to avoid accumulating errors during the numerical computation [16].

The damping matrix is assumed to be of the form

$$\underline{C} = \alpha \underline{M} + \beta \underline{K}^L \quad (42)$$

showing one part proportional to the mass distribution and the other part proportional to the initial stiffness distribution before excitation.

#### B. STEP-BY-STEP INTEGRATION

Newmark's generalized acceleration method assumes the following approximations for the nodal velocities and displacements [12]

$$\begin{aligned} \dot{\underline{u}}_{-t+\Delta t} &= \dot{\underline{u}}_{-t} + \left[ (1 - \delta) \ddot{\underline{u}}_{-t} + \delta \ddot{\underline{u}}_{-t+\Delta t} \right] \Delta t \\ \underline{u}_{-t+\Delta t} &= \underline{u}_{-t} + \dot{\underline{u}}_{-t} \Delta t + \left[ \left( \frac{1}{2} - \sigma \right) \ddot{\underline{u}}_{-t} + \sigma \ddot{\underline{u}}_{-t+\Delta t} \right] \Delta t^2 \end{aligned} \quad (43)$$

where parameters  $\delta$  and  $\sigma$  can be chosen to give the required integration stability and accuracy. When  $\delta = 1/2$  and  $\sigma = 1/6$ , the approximations correspond to the linear acceleration method and when

$\delta = 1/2$  and  $\sigma = 1/4$ , they correspond to the constant acceleration method.

Using Eq. (36), the approximations given by Eq. (43) can be expressed in the incremental form

$$\begin{aligned}\Delta \ddot{u}_{-t} &= c_1 \Delta u_{-t} - c_2 \dot{u}_{-t} - c_3 \ddot{u}_{-t} \\ \Delta \dot{u}_{-t} &= c_4 \Delta u_{-t} - c_5 \dot{u}_{-t} - c_6 \ddot{u}_{-t}\end{aligned}\tag{44}$$

where

$$\begin{aligned}c_1 &= \frac{1}{\sigma \Delta t^2}, \quad c_2 = \frac{1}{\sigma \Delta t}, \quad c_3 = \frac{1}{2\sigma} \\ c_4 &= \frac{\delta}{\sigma \Delta t}, \quad c_5 = \frac{\delta}{\sigma}, \quad c_6 = \left( \frac{\delta}{2\sigma} - 1 \right) \Delta t\end{aligned}\tag{45}$$

Substituting Eqs. (41) and (44) into Eq. (37), one can obtain

$$\begin{aligned}\left[ c_1 \underline{M} + c_4 \underline{C} + \underline{K}_{-t} \right] \Delta u_{-t} &= \underline{R}_{-t+\Delta t} - \underline{M} \ddot{u}_{-t} - \underline{C} \dot{u}_{-t} - \underline{K}^L u_{-t} - \underline{F}_{-t}^{NS} \\ &+ \underline{M} \left[ c_2 \dot{u}_{-t} + c_3 \ddot{u}_{-t} \right] + \underline{C} \left[ c_5 \dot{u}_{-t} + c_6 \ddot{u}_{-t} \right]\end{aligned}\tag{46}$$

Using Eq. (42), i.e.,  $\underline{C} = \alpha \underline{M} + \beta \underline{K}^L$ , and introducing the following normalized constants.

$$\begin{aligned}c_7 &= c_1 + \alpha c_4, & c_8 &= \beta c_4, & c_9 &= c_2 + \alpha c_5 - \alpha \\ c_{10} &= 1 - c_3 - \alpha c_6, & c_{11} &= \beta(c_5 - 1), & c_{12} &= \beta c_6\end{aligned}\tag{47}$$

Eq. (46) can be written in the form

$$\bar{\underline{K}}_{-t} \Delta u_{-t} = \Delta \bar{\underline{R}}_{-t}\tag{48}$$



where

$$\begin{aligned}\bar{K}_{-t} &= K_{-t} + C_7 \underline{M} + C_8 K_{-t}^L \\ \Delta \bar{R}_{-t} &= R_{-t+\Delta t} - \underline{M} [C_{10} \ddot{u}_{-t} - C_9 \dot{u}_{-t}] - K_{-t}^L [u_{-t} - C_{11} \dot{u}_{-t} - C_{12} \ddot{u}_{-t}] - F_{-t}^{NS} \quad (49)\end{aligned}$$

Equation (49) can be solved for  $\Delta u_{-t}$  at each time step and the nodal accelerations, velocities and displacements at time  $t + \Delta t$  can be determined from Eqs. (36) and (44) giving

$$\begin{aligned}\ddot{u}_{-t+\Delta t} &= \ddot{u}_{-t} + C_1 \Delta u_{-t} - C_2 \dot{u}_{-t} - C_3 \ddot{u}_{-t} \\ \dot{u}_{-t+\Delta t} &= \dot{u}_{-t} + C_4 \Delta u_{-t} - C_5 \dot{u}_{-t} - C_6 \ddot{u}_{-t} \\ u_{-t+\Delta t} &= u_{-t} + \Delta u_{-t}\end{aligned} \quad (50)$$

### C. ACCURACY OF SOLUTION

Equation (48) is an approximate form of the actual equation of motion to be solved at each time step since it was derived from approximations of the instantaneous linearized stiffness relations between the incremental forces and the incremental displacements. Depending on the nonlinearity of the equation and the magnitude of time interval  $\Delta t$ , the incremental linearization may introduce an instability in the overall solution. A measurement of how well the dynamic equilibrium at time  $t + \Delta t$  is being satisfied by the approximate solution of Eq. (48) may be expressed by the residual or unbalanced forces  $\delta R_{-t+\Delta t}$ . The correctness of solution using Eq. (48) may then be given by comparing the ratio of the Euclidean norm of the residual forces and the external forces  $\Delta_p$  with a specified tolerance  $\Delta_{ps}$  using the relation

$$\Delta_p = \frac{||\delta_{R_{-t+\Delta t}}||}{||R_{-t+\Delta t}|| + ||R_{-t+\Delta t} - \delta_{R_{-t+\Delta t}}||} \leq \Delta_{ps} \quad (51)$$

where

$$\delta_{R_{-t+\Delta t}} = R_{-t+\Delta t} - \frac{M}{-} \ddot{u}_{-t+\Delta t} - \frac{C}{-} \dot{u}_{-t+\Delta t} - \frac{K^L}{-} u_{-t+\Delta t} - F_{-t+\Delta t}^{NS} \quad (52)$$

When the accuracy of solution is unsatisfactory, it may be improved by using smaller time intervals or by applying an equilibrium correction through an iteration process.

#### D. SUBDIVISION OF TIME INTERVAL

Although sufficient accuracy of solution can be maintained using small time intervals throughout the period of dynamic response, the computational effort may be excessive. Therefore, it is more efficient to use the smaller intervals only during those intervals of time when they are actually needed and to use longer intervals during the remaining part of the response. When the solution at time  $t$  satisfies dynamic equilibrium with the specified accuracy but the solution at time  $t + \Delta t$  does not, one can return to the solution at time  $t$  and use smaller equidistant sub-intervals between times  $t$  and  $t + \Delta t$ . The accuracy of solution thus obtained by the smaller time intervals can be checked using Eq. (51) at the end of each of the smaller time intervals.

As seen from Eq. (44), the nodal accelerations, nodal velocities and nodal displacements at time  $t + \Delta t$  can be reversed to the solution at time  $t$  using the relations

$$\begin{aligned} \ddot{u}_t &= C_{14} \Delta u_t - C_{15} \dot{u}_{-t+\Delta t} - C_{16} \ddot{u}_{-t+\Delta t} \\ \dot{u}_t &= C_{17} \Delta u_t - C_{18} \dot{u}_{-t+\Delta t} - C_{19} \ddot{u}_{-t+\Delta t} \\ u_t &= u_{-t+\Delta t} - \Delta u_t \end{aligned} \quad (53)$$

where

$$\begin{aligned}
 c_{13} &= \frac{1}{\delta - \sigma - 1/2} , & c_{14} &= \frac{c_{13}}{\Delta t^2} , & c_{15} &= \frac{c_{13}}{\Delta t} \\
 c_{16} &= c_{13}(\sigma - \delta) , & c_{17} &= \frac{c_{13}(\delta - 1)}{\Delta t} , & c_{18} &= c_{13}(\sigma - 1/2) \\
 c_{19} &= c_{13} \left( \frac{\delta}{2} - \sigma \right) \Delta t
 \end{aligned} \tag{54}$$

#### E. EQUILIBRIUM ITERATION

The equation of motion for the  $i$ th equilibrium iteration at time  $t$  is expressed as

$$\underline{M} \delta \ddot{\underline{u}}_t^{(i)} + \underline{C} \delta \dot{\underline{u}}_t^{(i)} + \underline{K}_t^{(i)} \delta \underline{u}_t^{(i)} = \delta \underline{R}_t^{(i)} \tag{55}$$

where,  $\underline{M}$  and  $\underline{C}$  are the constant mass and damping matrices, respectively,  $\underline{K}_t^{(i)}$  is the tangent stiffness matrix at time  $t$  for the  $i$ th iteration,  $\delta \ddot{\underline{u}}_t^{(i)}$ ,  $\delta \dot{\underline{u}}_t^{(i)}$ , and  $\delta \underline{u}_t^{(i)}$  are the corrective nodal accelerations, nodal velocities and nodal displacements, respectively, for the  $i$ th iteration as defined by

$$\begin{aligned}
 \delta \ddot{\underline{u}}_t^{(i)} &= \ddot{\underline{u}}_t^{(i+1)} - \ddot{\underline{u}}_t^{(i)} \\
 \delta \dot{\underline{u}}_t^{(i)} &= \dot{\underline{u}}_t^{(i+1)} - \dot{\underline{u}}_t^{(i)} \\
 \delta \underline{u}_t^{(i)} &= \underline{u}_t^{(i+1)} - \underline{u}_t^{(i)}
 \end{aligned} \tag{56}$$

and where  $\delta \underline{R}_t^{(i)}$  representing the nodal residual forces for the  $i$ th iteration is given by

$$\delta \underline{R}_t^{(i)} = \underline{R}_t - \underline{M} \ddot{\underline{u}}_t^{(i)} - \underline{C} \dot{\underline{u}}_t^{(i)} - \underline{K}_t^L \underline{u}_t^{(i)} - \underline{F}_t^{NS(i)} \tag{57}$$

From the integration scheme of Eq. (44), the corrective accelerations and velocities of Eq. (56) can be written as [22]

$$\begin{aligned}\ddot{\underline{u}}_{-t}^{(i)} &= C_1 \delta \underline{u}_{-t}^{(i)} \\ \dot{\underline{u}}_{-t}^{(i)} &= C_4 \delta \underline{u}_{-t}^{(i)}\end{aligned}\tag{58}$$

Substituting Eqs. (57) and (58) into Eq. (55), one obtains

$$\bar{\underline{K}}_{-t}^{(i)} \delta \underline{u}_{-t}^{(i)} = \delta \bar{\underline{R}}_{-t}^{(i)}\tag{59}$$

where

$$\begin{aligned}\bar{\underline{K}}_{-t}^{(i)} &= \underline{K}_{-t}^{(i)} + C_7 \underline{M} + C_8 \underline{K}_{-t}^L \\ \delta \bar{\underline{R}}_{-t}^{(i)} &= \underline{R}_{-t} - \underline{M} [\ddot{\underline{u}}_{-t}^{(i)} + \alpha \dot{\underline{u}}_{-t}^{(i)}] - \underline{K}_{-t}^L [\underline{u}_{-t}^{(i)} + \beta \dot{\underline{u}}_{-t}^{(i)}] - \underline{F}_{-t}^{NS(i)}\end{aligned}\tag{60}$$

Equation (59) can be solved for the  $i$ th corrective displacements  $\delta \underline{u}_{-t}^{(i)}$  and then the corrected nodal accelerations, nodal velocities and nodal displacements can be calculated using Eqs. (56) and (58), i.e.,

$$\begin{aligned}\ddot{\underline{u}}_{-t}^{(i+1)} &= \ddot{\underline{u}}_{-t}^{(i)} + C_1 \delta \underline{u}_{-t}^{(i)} \\ \dot{\underline{u}}_{-t}^{(i+1)} &= \dot{\underline{u}}_{-t}^{(i)} + C_4 \delta \underline{u}_{-t}^{(i)} \\ \underline{u}_{-t}^{(i+1)} &= \underline{u}_{-t}^{(i)} + \delta \underline{u}_{-t}^{(i)}\end{aligned}\tag{61}$$

If convergence occurs, the iteration can be continued until the dynamic equilibrium of the motion is satisfied within the specified accuracy. The convergence of equilibrium iteration may be expressed by comparing the ratio of the Euclidean norm of the corrective displacement to the total displacement  $\Delta_{\underline{u}}^I$  with a specified tolerance  $\Delta_{\underline{u}s}^I$  in the form



$$\Delta_u^I \equiv \frac{||\delta \underline{u}_t^{(i)}||}{||\underline{u}_t^{(i)}|| + ||\underline{u}_t^{(i+1)}||} \leq \Delta_{us}^I \quad (62)$$

or by comparing the ratio of the Euclidean norm of the residual forces to the total external forces  $\Delta_p^I$  with a specified tolerance  $\Delta_{ps}^I$  in the form

$$\Delta_p^I \equiv \frac{||\delta \underline{R}_t^{(i)}||}{||\underline{R}_t|| + ||\underline{R}_t - \delta \underline{R}_t^{(i)}||} \leq \Delta_{ps}^I \quad (63)$$

The step-by-step integration algorithm used herein for non-linear systems including the equilibrium iteration and the subdivision of time intervals may be summarized as follows:

(1) Initial Calculations

- (a) Form the initial stiffness matrix  $\underline{K}^L$  and the mass matrix  $\underline{M}$  for the system.
- (b) Solve for the initial displacement and calculate the element forces due to static loads.
- (c) Set up the dynamic load and ground excitation time history.
- (d) Set initial conditions  $\ddot{\underline{u}}_0 = \dot{\underline{u}}_0 = \underline{u}_0 = \underline{0}$ ,  $f_0^{NS}(j) = 0$  for  $j \in \text{NEL}$ ,  $\underline{K}_0 = \underline{K}^L$ .
- (e) Calculate the step-by-step integration constants  $C_i$  ( $i = 1, 2, \dots, 12$ ) and subdivision control constants  $C_i$  ( $i = 13, 14, \dots, 19$ ).

(2) For Each Time Increment  $\Delta t$

- (f) Form the effective dynamic stiffness matrix  $\bar{\mathbf{K}}_{-t}$  and the effective dynamic load vector  $\Delta \bar{\mathbf{R}}_{-t}$ .
- (g) Solve for the displacement increment  $\Delta \mathbf{u}_{-t}$ .
- (h) Compute current accelerations, velocities and displacements  $\ddot{\mathbf{u}}_{-t+\Delta t}$ ,  $\dot{\mathbf{u}}_{-t+\Delta t}$ ,  $\mathbf{u}_{-t+\Delta t}$ .
- (i) Calculate current element forces, check nonlinearity conditions, and compute the new element tangent stiffness matrix  $\mathbf{k}_{-t(j)}^N$  for  $j \in \text{NEL}$ ; determine the inelastic deformation vectors, and current inelastic element nodal restoring force vectors  $\mathbf{f}_{-t(j)}^{\text{SN}}$  for  $j \in \text{NEL}$ .
- (j) Compute residual force vector  $\delta \mathbf{R}_{-t+\Delta t}$  and check the accuracy of solution;
- i) if calculated responses are sufficiently accurate, skip to (k).
  - ii) if subdivision of time interval is needed, go to (3) after reversing the current inelastic element deformations from time  $t + \Delta t$  to time  $t$ .
  - iii) if equilibrium iteration is needed, go to (4).
- (k) Repeat steps (f) through (j) for the next time increment.
- (3) Subdivision of Time Interval
- (l) Backspace accelerations, velocities and displacements from time  $t + \Delta t$  to time  $t$ , and calculate element tangent stiffness matrices and inelastic element nodal restoring forces at time  $t$ .
- (m) Calculate the dynamic load at time  $\hat{t} = t + i \Delta \hat{t}$  for  $i = 1, 2, \dots, n$  in which  $\Delta \hat{t} = \Delta t/n$  and  $n$  is a specified number of time interval.

- (n) Form the effective dynamic stiffness matrix  $\bar{\mathbf{K}}_{-t-\Delta t}^{\wedge}$  and the effective dynamic load vector  $\Delta \bar{\mathbf{R}}_{-t-\Delta t}^{\wedge}$ .
- (o) Solve for the displacement increment  $\Delta \mathbf{u}_{-t-\Delta t}^{\wedge}$ .
- (p) Compute current accelerations, velocities and displacements  $\ddot{\mathbf{u}}_t^{\wedge}, \dot{\mathbf{u}}_t^{\wedge}, \mathbf{u}_t^{\wedge}$ .
- (q) Calculate current element forces, check nonlinearity conditions, and compute new element tangent stiffness matrices  $\mathbf{k}_{-t}^N(j)$  for  $j \in \text{NEL}$ ; determine the inelastic deformation vectors, and current inelastic element nodal restoring force vector  $\mathbf{f}_{-t}^{\text{SN}}(j)$  for  $j \in \text{NEL}$ .
- (r) Compute residual force vector  $\delta \mathbf{R}_{-t}^{\wedge}$  and check the accuracy of solution;
- i) if calculated responses are sufficiently accurate, skip to (s).
  - ii) if equilibrium iteration is needed, go to (4).
- (s) Repeat steps (m) through (r) for next sub-time increment ( $i = 1, 2, \dots, n$ ). If  $i=n$ , then go back to (k).
- (4) Equilibrium Iteration
- (t) Form the effective dynamic stiffness matrix  $\bar{\mathbf{K}}_{-t+\Delta t}^{(i)}$  and solve for the corrective displacement vector  $\delta \mathbf{u}_{-t+\Delta t}^{(i)}$ .
- (u) Compute the  $i+1^{\text{th}}$  corrected accelerations, velocities and displacements  $\ddot{\mathbf{u}}_{-t+\Delta t}^{(i+1)}, \dot{\mathbf{u}}_{-t+\Delta t}^{(i+1)}, \mathbf{u}_{-t+\Delta t}^{(i+1)}$ .
- (v) Calculate current element forces, check nonlinearity conditions, and compute element tangent stiffness matrices; determine the inelastic deformation vectors, and current element nodal restoring force vectors.

- (w) Compute residual force vector  $\delta R_{-t+\Delta t}^{(i+1)}$  and check the accuracy of solution;
- i) if corrected responses are sufficiently accurate, go back to (k).
  - ii) if convergence occurs and corrected responses are not yet sufficiently accurate, repeat steps (t) through (w).

#### IV. EXPERIMENTAL MODEL STUDY AND TEST RESULTS

The purpose of this chapter is to present the characteristics of the model bridge structure, test procedures and test results obtained in the Series IV excitation test program including the results of a number of preliminary component tests used in formulating the analytical model and in interpreting the correlation results of seismic responses with analytical predictions. Detailed information on the experimental phase of the overall program are given in references [23] and [24].

##### A. EXPERIMENTAL MODEL [23,24]

The bridge model was originally based on a symmetrical simplified version of the east half of the 5/14 South Connector Overcrossing that suffered severe structural damages during the San Fernando earthquake in 1971. It was designed with the aim of providing the primary features of high curved highway bridge structures, namely, deck curvature, expansion joints, and long columns.

Based on size and performance of the shaking table at the University of California, Berkeley [27], scales of the model were established as follows;

$$\begin{aligned} L_r &= 30 \\ F_r &= L_r^2 = 900 \\ T_r &= \sqrt{L_r} \approx 1/5.5 \end{aligned} \tag{64}$$

in which  $L_r$ ,  $F_r$  and  $T_r$  represent the geometric, force and time scale factors. In order to bring the inertia forces including gravitational forces into the force scale factor  $F_r$ , substantial amount of lead weights were placed on the model. The total weight including the lead



weights was approximately 8.5 kips which corresponds to approximately 8.5% of the weight of the shaking table.

The bridge model structure adopted was composed of three sub-assemblages as shown in Fig. 4.1; a center girder/column system and two side girder/column/abutment systems which were essentially independent of each other having different dynamic characteristics. These sub-assemblages were tied together by two expansion joints placed in symmetrical positions.

Seismic responses of displacement relative to the shaking table were measured by LVDT at three points of the model as shown in Fig. 4.2, i.e. at the end of side girder No. 1, center of the center girder and end of side girder No. 2. Two horizontal components, namely the longitudinal (X) component and the transverse (Y) component, were measured at each point. In addition to these displacements, relative movements between the two end diaphragms (opening and closing of joint gap) of each expansion joint at both the inner and outer sides were measured. Thus in all, 10 responses of displacement (6 relative to the shaking table and 4 across the expansion joints) were recorded during the periods of seismic excitation. However since the response at the center of the center girder in the longitudinal (X) direction was very small due to the direction of excitation, it was finally disregarded, leaving 9 responses of displacement to be used for the correlation study.

The model was made as a component system allowing repeated experimental data to be derived from one basic model as damaged components were either repaired or replaced. The properties of each component are described as follows:

1. Superstructure - The superstructure of the model consisted of

one center girder and two side girders. They were constructed with a rectangular cross section 8.5 inches in width and 2 1/2 inches in thickness. This section was overdesigned by a factor of approximately 2 to insure that the superstructure would behave elastically during all tests [23]. A high strength (8000 psi.) shrinkage resistant, microconcrete was used in constructing the girders to avoid shrinkage cracks which would adversely affect the stiffness and damping characteristics.

2. Columns - Two types of columns having different sections were used in the model; i.e. two weak columns (COL-1B and 2B) having a section 2 1/2 x 1 1/2 inches which supported the center girder and two strong columns (COL-1A and 2A) having a section 2 1/2 x 4 inches which supported the side girders. All columns were constructed using 4500 psi. strength normal Portland cement microconcrete and four #2 (2/8 inch) annealed reinforcing bars having a yield strength of approximately 50 ksi.

The bottoms of the columns were clamped to a base steel frame which was designed with sufficiently high stiffness that essentially full fixity was provided at the base of each column. The top of the columns were attached to the girders.

3. Expansion Joints - Expansion joint element consisted of a hinge seat, a transverse shear key, a rubber pad, a vertical restrainer and a pair of longitudinal joint restrainer tie bars as shown in Fig. 4.3.

The hinge seat and the shear key were constructed of concrete having the same properties as those of the concrete used for the superstructure and they were heavily reinforced to provide high resistance to shear forces and bending moments. The section of the hinge seat was 8.5 inches in width and 0.5 inches in length. The shear key having a

section 2.5 inches in width, 0.5 inches in length, and 1.5 inches in height was designed to prevent transverse relative motion between the girders.

A 1/16 inch thickness rubber pad was placed over the entire hinge seat simulating the prototype elastomeric bearing pad.

A pair of vertical stoppers was provided at each expansion joint to prevent up-lift of the girders from the hinge seats.

A pair of longitudinal joint restrainer bars 5 1/2 inches in length and 1/8 of an inch in diameter was used to tie together the superstructure. They were made of annealed mild steels having yield and ultimate strengths (strain) of approximately 650 lbs. (0.2%) and 750 lbs. (20%), respectively. The restrainer tie bars were mounted on each side of the superstructure parallel to the bridge axis. They were designed to resist only opening of the joint gaps when the relative movement exceeded the initial gap  $\Delta_T$ .

4. Abutments - The abutments were constructed as steel frames to support the outer ends of the side girders. They were originally designed to provide full fixity to the ends of the girders except for allowing rotational freedom around the transverse horizontal (y) axis. However, due to lack of stiffness of the steel cover plate at the abutment, some rotational freedom around the vertical (z) axis was also provided.

## B. TEST PROCEDURES AND TEST RESULTS

1. Stiffness Properties of Components - A number of preliminary tests were performed on the components of the model to determine their stiffness properties and their boundary conditions. The test results



obtained are used subsequently in formulating the analytical model of the complete structure.

Columns - Flexural rigidities of columns were determined from the results of static load-deflection tests. The measured load vs. deflection relations were linear up to those levels later produced during the high intensity seismic excitations. The measured flexural rigidities were confirmed by comparing the resulting calculated lowest natural frequencies of the free standing columns with their experimental values, Other column rigidities such as those in the longitudinal and torsional directions were calculated using the known sectional and material properties.

Superstructure - The flexural rigidities of the girders around their strong axes were determined from static load vs. deflection tests, The load vs. deflection relations were linear up to those levels developed during high intensity seismic excitations. The flexural rigidities of the girders around their weak axes, however, could not be determined in the same way since twisting associated with the deck curvature was coupled with bending. Therefore, these rigidities were determined from free vibration tests of the side subassemblage as described in the subsequent paragraph. The longitudinal and torsional rigidities were calculated from their sectional and material properties.

Expansion Joint - The expansion joint is the most complicated component in the entire bridge model. This complexity results from the combined actions of the rubber pad, shear key and tie bars associated with slippages and collisions which take place between girders.

Figure 4.4 shows the force vs. relative displacement relation of the expansion joint in which plus relative displacement corresponds to

an opening of the joint gap and minus relative displacement corresponds closing of the joint gap. When the expansion joint undergoes an increasing relative movement in the positive direction, the rubber pad first deforms under shear action providing resistance to the motion. Then, slippage takes place when the applied force reaches the maximum friction force which can be developed on the contact plane of the expansion joint (Fig. 4.4.1). It should be noted here that the difference between dynamic and static frictions is disregarded in this force vs. displacement relation. When the positive relative movement reaches the tie gap  $\Delta_T$ , the pair of tie bars begin resisting further opening of the joint gap. This resistance builds up linearly with joint separation until the yield strength of the tie bars is reached; then, yielding under constant force takes place (Fig. 4.4.2). When the expansion joint undergoes a relative movement in the negative direction, the rubber pad deforms and resists the motion in the same manner described above for the positive direction. However the tie bars do not resist motion in this direction. If the expansion joint undergoes further negative relative motion reaching the value of the seat gap  $\Delta_G$ , collision takes place between the girders.

Although the expansion joints have such complex characteristics, a direct measurement of their constraint at the expansion joint was not performed because of difficulties involved in such an experimental test. Therefore the experimental data obtained to formulate the analytical model of the expansion joint were certain element properties.

The stiffness and strength of the tie bar were measured after they were made by annealing mild steel [23]. One typical stress vs. strain relation is displayed in Fig. 4.5. A longitudinal stiffness of



$6.47 \times 10^4$  lbs/inch and a yield (ultimate) strength of 650 lbs (750 lbs) were determined from the test results.

Preliminary tests were performed on the rubber pad to determine its shearing stiffness [25]. To accomplish this, a specimen of the rubber pad was sandwiched between two steel plates which were then displaced so that pure shear deformation was produced in the pad. The specimen used for this test was 1 inch long and 1/2 inch wide. The test was performed with a changing frequency of cyclic shear load and contact force. Some typical results of the shear force vs. deformation are shown in Fig. 4.6. From the results, it is apparent that the rubber pad has a slight hysteretic type behavior with the average stiffness being significantly affected by contact pressure but less affected by frequency in the range 0-5 Hz. Assuming the stress-strain relation of the rubber pad can be modeled by a linear elastic spring with stiffness proportional to both the contact force and the size of specimen, the effective stiffness of the pad  $k_x^R$  was found to be

$$k_x^R = 22800 \text{ lbs/inch} \quad (65)$$

A preliminary tests was also performed to determine the friction coefficient [25]. One of the expansion joint components was subjected to an increasing static force in its longitudinal direction while under compressive contact pressure. The maximum frictional resisting force was measured when slippage first occurred. Then, the friction coefficient was obtained by dividing the measured maximum resisting force by the contact pressure. However, due to large variations in the measured data, the test results could only suggest that the friction coefficient was within the range

$$0.3 < \nu^{EJ} < 0.6$$

(66)

Therefore considering the condition of the contact plane, the friction coefficient was taken as 0.4 for the analytical study. The effect of this assumed value on dynamic response is discussed in Chapter VII.

Finally, combining the measured and estimated data for the expansion joint, its force vs. relative displacement relation was established as shown in Fig. 4.4. Since the vertical contact force at the expansion joint in the bridge model is estimated to be approximately 380 lbs, a friction force of approximately  $0.4 \times 380$  lbs in the longitudinal direction can be developed. Under this force the rubber pad can deform approximately 0.01 inch ( $0.4 \times 380 / 22,800$ ) before slippages take place. The maximum elastic elongation of the tie bar is approximately 0.01 inch ( $650 / 64,700$ ) and the maximum total tie bar force (2 bars) is approximately  $2 \times 650$  lbs.

2. Static and Dynamic Tests for Side Subassemblage - After one side subassemblage composed of the side girder, column and abutment was fabricated, both a free vibration test and a static load-deflection test were conducted [25]. These test results provided valuable information in determining stiffness properties of the components and also in formulating an analytical model.

The side subassemblage was first excited manually in both horizontal and vertical directions. Since the frequencies decreased slightly with amplitude of vibration, the frequencies corresponding to those amplitudes developed during high intensity seismic excitations were estimated through extrapolation to give

$$F_H^S \approx 5.8 \text{ Hz} \quad \text{horizontal vibration}$$

(67)

$$F_V^S \approx 9.5 \text{ Hz} \quad \text{vertical vibration}$$

The side subassembly was then subjected to an increasing static load up to 400 lbs in the horizontal radial direction and the resulting load vs. deflection relation was measured.

From the test results, the flexural rigidity of the side girder around its weak axis was calculated from the measured natural frequency of vertical vibration. Since the boundary condition of the side girder in that direction was well defined, the flexural rigidity thus determined was considered to be sufficiently reliable.

The natural frequencies of the side subassembly were then calculated based on the known stiffness properties and boundary conditions and they were compared with the measured results. From these comparisons it was found that the calculated natural frequency in the horizontal direction was approximately 25% higher than the measured result. Because of this discrepancy, the boundary condition of the experimental model was re-examined and it was found that significant flexibility existed in the abutment allowing a rotation to develop around the vertical (z) axis [25]. The abutment steel cover was not sufficiently stiff to provide full fixity to the side girder in that direction. Some flexibility for the rotational component was then introduced into the analytical model so that the calculated natural frequency would match the measured value.

Finally, a static load was applied to the corrected analytical model described above and its static load vs. deflection relation was compared with the measured relations. As shown in Fig. 4.7, both relations are in good agreement.



Based on the good agreement finally achieved in the static load vs. deflection relation, it was felt that the stiffness properties and boundary conditions of the side subassemblage had been determined with sufficient accuracy to be used in formulating the analytical model of the whole bridge model.

3. Small Amplitude Dynamic Properties of the Model - Free vibration tests and forced harmonic excitation tests were conducted to determine the small amplitude dynamic characteristics of the complete model. The free vibration tests were initiated by hand and it was found that the first vibration mode consisted of longitudinal motion of the center girder/column subassemblage combined with antisymmetrical motion of the side subassemblages [23]. The natural frequency of this mode was found to be

$$F_L \approx 5 \text{ Hz} \quad (68)$$

The second free vibration mode was found to be essentially a symmetric rigid body motion of the superstructure in a horizontal plane. The natural frequency of this mode could not be clearly obtained however since the first free vibrations mode was always excited making it difficult to measure the second mode frequency. This difficulty was encountered even when the test was performed by displacing the structure into essentially a second mode shape and suddenly releasing it by fracturing the tensioned cables attached at three symmetrical points of the model [23]. It should be noted that to excite a particular mode, the excitation should be applied so that a maximum of energy is transferred to this mode with a minimum of energy transferred to its neighboring modes [33]. As described above, the vibration shape of the

side subassemblage were similar for both the first and the second modes; thus increasing the difficulty of manually exciting either mode without the other being presented. Furthermore, the second natural frequency is close to the first natural frequency; thus, causing additional difficulty in distinguishing the higher mode from the lower mode.

Forced harmonic excitation tests were conducted by sweeping the frequency of table input motion from 5.5 Hz to 7.5 Hz for transverse vibration and from 8 Hz to 10 Hz for vertical vibration. The table acceleration amplitude was held constant over both frequency ranges. From these tests, it was found that the transverse vibration mode was essentially the same as that observed from the free vibration test and the vertical vibration mode produced vertical motions primarily in the side girders. Resonant curves of response amplitude are shown in Fig. 4.8 for the transverse vibration. The natural frequency and damping ratio determined from this test were

$$\left. \begin{array}{l} F_T \approx 6.6 \text{ Hz} \\ \xi \approx 6\% \text{ of critical} \end{array} \right\} \text{ transverse vibration} \quad (69)$$

For vertical vibrations, the amplitudes could not be easily measured so that only the natural frequency was measured, i.e.,

$$F_V \approx 9 \sim 10 \text{ Hz} \quad \text{vertical vibration} \quad (70)$$

4. Seismic Behavior of the Model - The model was subjected to six different earthquake excitations in the Series IV test program. Three of these excitations designated as Tests H1, H2, and H3 consisted of horizontal motion only while the other three excitations designated as Tests HV1, HV2, and HV3 consisted of both horizontal and vertical motions.



The horizontal excitation was prescribed by an artificially generated accelerogram previously defined for post earthquake studies of the Olive View Hospital [28]. The vertical excitation was also prescribed by an artificially generated accelerogram [24]. The peak vertical excitation was chosen to be approximately one half the peak horizontal excitation. Both vertical and horizontal excitations were scaled in time  $1/5.5$  so as to satisfy the time scale factor  $T_r$ . The acceleration response spectra for the motions measured on the shaking table during Tests H1, H3, and HV2 are shown in Fig. 4.9. It is observed that although there are some discrepancies in the amplification factors, the maximum response spectral values occurred at approximately 10 Hz for both the horizontal and vertical motions.

Peak table accelerations, maximum horizontal response of center girder, initial tie gaps, and observed damages for the six excitation tests are summarized in Table 4.1. The superstructure and the abutments suffered no visible structural damages throughout this series of tests. The columns suffered no damage except for one weak column that suffered a slight hair crack at its base. The shear keys of the expansion joints, especially at expansion joint No. 2, suffered severe spalling of concrete during Tests H3 and HV3 requiring that they be replaced after these particular tests. The tie gaps were set at almost zero values before Tests H1 and HV1; however, for the other tests, the initial tie gaps were controlled by the previously accumulated elongations of the tie bars. Collisions occurred in the expansion joints during Test H3, HV1, HV2 and HV3. Sometimes during high intensity excitations, impact at one joint would immediately cause impact to occur at the other joint. Thus, multiple collisions were observed between the center girder and the two side girders. The sounds produced by the impacts were quite severe in intensity.

The relation between peak horizontal table acceleration and maximum horizontal displacement at the deck center is plotted in Fig. 4.10. From this relation, it is observed that the maximum response of the model increases almost linearly with peak table acceleration in the lower intensity range; however, a scatter of maximum response values is observed in the higher intensity range, i.e. for Tests H3, HV2 and HV3. Although Tests H3 and HV2 were conducted using almost the same intensity of horizontal table accelerations, namely 0.5G, the maximum response for Test H3 is approximately 50% larger than that produced in Test HV2. Certainly the presence of the vertical excitation in Test HV2 cannot be credited with this 50% difference. The same discrepancy is observed when comparing the results obtained in Tests HV2 and HV3. Test HV3 followed immediately after the Test HV2 and used almost the same intensities of table motion. To explain this discrepancy, it is necessary to recall that a shear key in expansion joint No. 2 which was undamaged after Test HV2 suffered severe spalling failure during Tests H3 and HV3. Thus, it is believed that failure of the shear key allowed large transverse relative motions to take place between the girders at the expansion joint, which, in turn, resulted in a significant increase in overall response of the complete bridge model. It is of interest to speculate why the shear key failed during Tests H3 and HV3 but did not in the previous Test HV2. The initial and boundary conditions for the superstructure, columns and abutments are the same for all three tests; however, the initial tie gaps were different. For Test HV2 the initial tie gaps were small since little yielding of the tie bars had taken place during Test HV1. Due to yielding of the tie bars which occurred during the previous tests, the initial gaps were reasonably large for Tests H3

and HV3. It should be noted that when superstructure motion takes place in the outward direction, only the tie bars resist the motions at the expansion joints. Hence the large initial tie gaps in Tests H3 and HV3 allowed the model to build up large transverse oscillations before the tie bars became effective. These large oscillations were sufficient to cause failure of the shear key.

Based on the above considerations of model response, three tests were chosen among the six conducted for correlation purposes, namely, Tests H1, H3 and HV2. Test H1 represents a typical response for low intensity excitation. No yielding of tie bars or collisions of girders took place in this test. Tests H3 and HV2 on the other hand represent typical response for high intensity excitations. Yielding of the tie bars and multiple collision did take place in these tests. In addition, a failure of the shear key is believed to have taken during Test H3.

Test H1 - The model was subjected to low intensity excitation with a peak acceleration of 0.11G in the transverse (Y) horizontal direction. The table acceleration and the measured responses of displacement are displayed in Figs. 4.11 and 4.12, respectively.

During this test, collisions of the girders did not occur since the relative response displacements at the expansion joints remained below the initial joint gap of approximately 0.05 inch. The joint restrainer tie bars however resisted the joint separations. It was found by inspection following the test that yielding of the tie bars had not taken place. Since the tie bars resisted only joint separation, the displacement response was small in the outward direction but large for the inward direction. While some non-symmetrical model response was observed, the major response was primarily in a symmetrical mode. This type of response



should be expected due to the symmetry conditions of model and seismic loading.

Test H3 - During this test, the model was subjected to high intensity excitation having a peak acceleration of 0.5G in transverse (Y) horizontal direction. The table acceleration and the measured responses of displacement are displayed in Figs 4.13 and 4.14, respectively.

Multiple collisions of the girders together with yieldings of the joint restrainer tie bars took place at the expansion joints. Furthermore, spalling failure of the transverse shear key took place at expansion joint No. 2. Like Test H1, the responses of displacement, especially at the expansion joints, were somewhat unsymmetrical. However they were of a type opposite to that developed in Test H1, i.e. the motions were large in the outward direction and small in the inward direction. This type of response was caused by closure of the joints during inward motion causing stiff arch action to take place between abutments while motion in the outward direction was resisted mainly by the more flexible tie bars. The maximum opening at expansion joint No. 2 equal to approximately 0.35 inch exceeded that of expansion joint No. 1 by a factor of approximately 2. Hence adding the maximum closure (initial joint gap) of approximately 0.05 inch to the maximum opening, the total relative displacement of the joint was approximately 0.4 inch which corresponds to 4/5 of the hinge seat length. This implies that the center girder was supported on only a 0.1 inch hinge seat at the expansion joint. The damages of the rubber pad observed after this test were undoubtedly caused by this severe relative motion.

It was observed from the measured response that substantial drift, especially at expansion joint No. 2, took place during the excitation.

Once this drift developed, the subsequent responses did not return to their original values but simply vibrated the new drifted positions. It should be noted that although the spalling failure of the transverse shear key allowed a large relative transverse movement to take place between the girders, it had essentially nothing to do with the observed drift in response. Most likely this drift was caused by a combination of concrete fractures in the shear key and tearing of the rubber pad in the joint. Obviously, such drift could not be predicted analytically.

Test HV2 - During this test, the model was subjected simultaneously to high intensity horizontal and vertical excitations having peak accelerations of 0.47G and 0.27G, respectively. The table accelerations and the measured responses of displacement are displayed in Figs. 4.15 and 4.16, respectively. The general features of this test are similar to those of Test H3 except that failure of the shear key did not take place. Therefore, the overall response of the model was more symmetrical than the response of Test H3 and drifts in response did not develop.

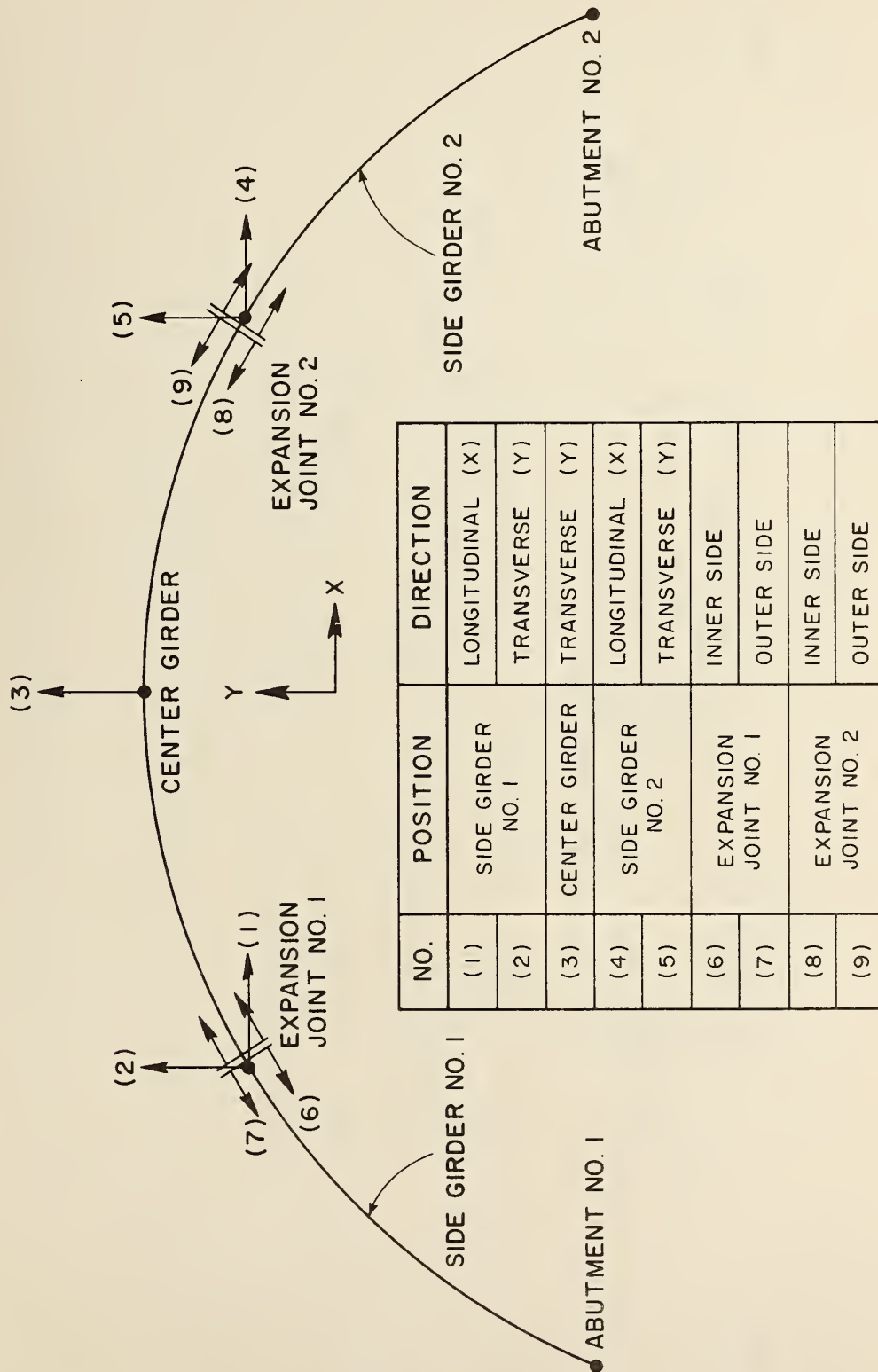


TABLE 4.1 PRINCIPAL FEATURES OF SEISMIC EXCITATIONS IN SERIES IV TEST

	Peak Table Input Acceleration [G]		Maximum Horizontal Response of Center Girder [inch]	Measured Initial Tie Gap $\Delta_T$ [inch]	Observed Features			
	Horizontal	Vertical			Yield of Tie Bars	Collisions	Failure of Shear Key	Permanent Drift of Response
TEST H1	0.11	—	-0.06	set to 0 for both EJs	NO	NO	NO	NO
TEST H2	0.28	—	0.13	0 for both EJs	YES	NO	NO	NO
TEST H3	0.50	—	0.40	0.03 for EJ1 0.04 for EJ2	YES	YES	YES	YES
TEST HV1	0.31	0.16	0.16	set to 0 for both EJs	YES	YES	NO	NO
TEST HV2	0.47	0.27	0.27	0.01 for EJ1 0.02 for EJ2	YES	YES	NO	NO
TEST HV3	0.46	0.25	0.42	0.07 for EJ1 0.17 for EJ2	YES	YES	YES	YES



FIG. 4.1 EXPERIMENTAL MODEL BRIDGE STRUCTURE



ARROW ( → ) INDICATES POSITIVE DIRECTION OF RESPONSE

FIG. 4.2 MEASUREMENTS OF RESPONSE DISPLACEMENT

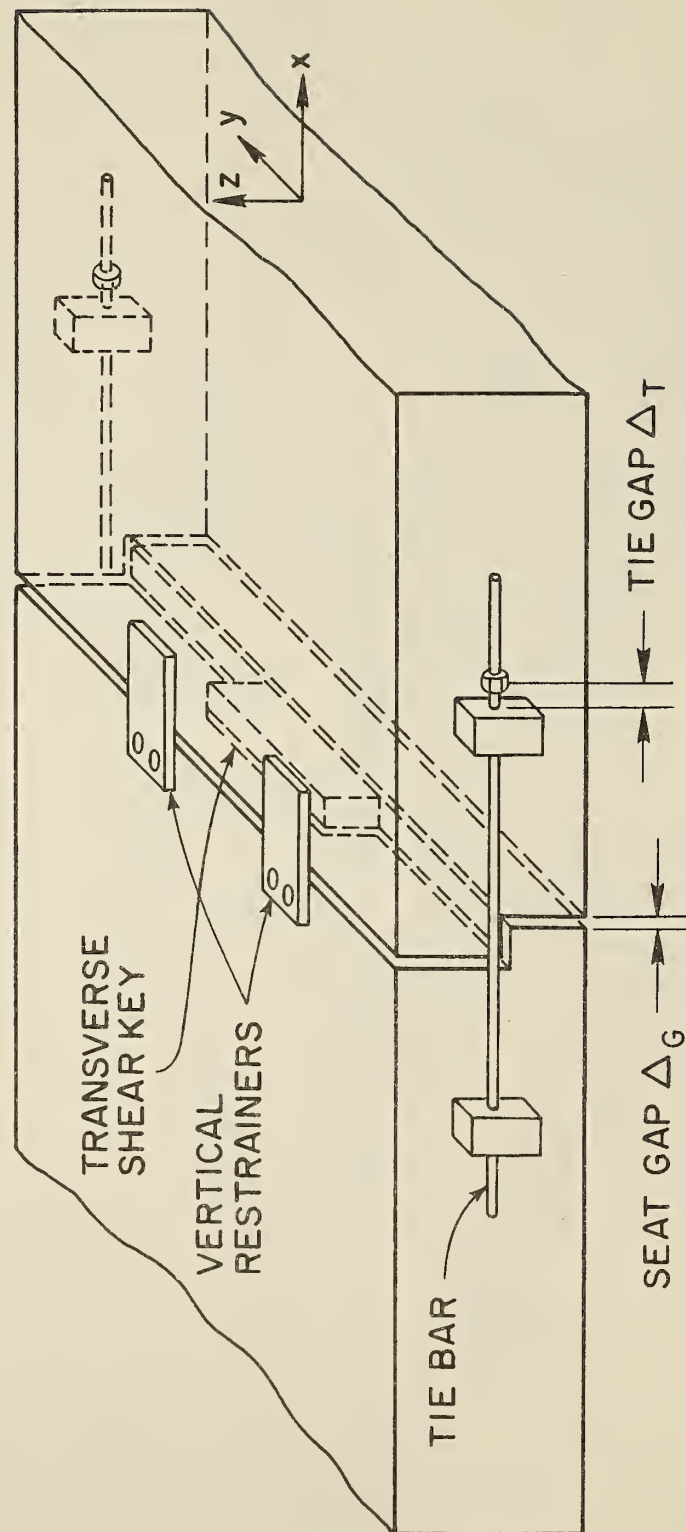


FIG. 4.3 EXPANSION JOINT OF BRIDGE MODEL



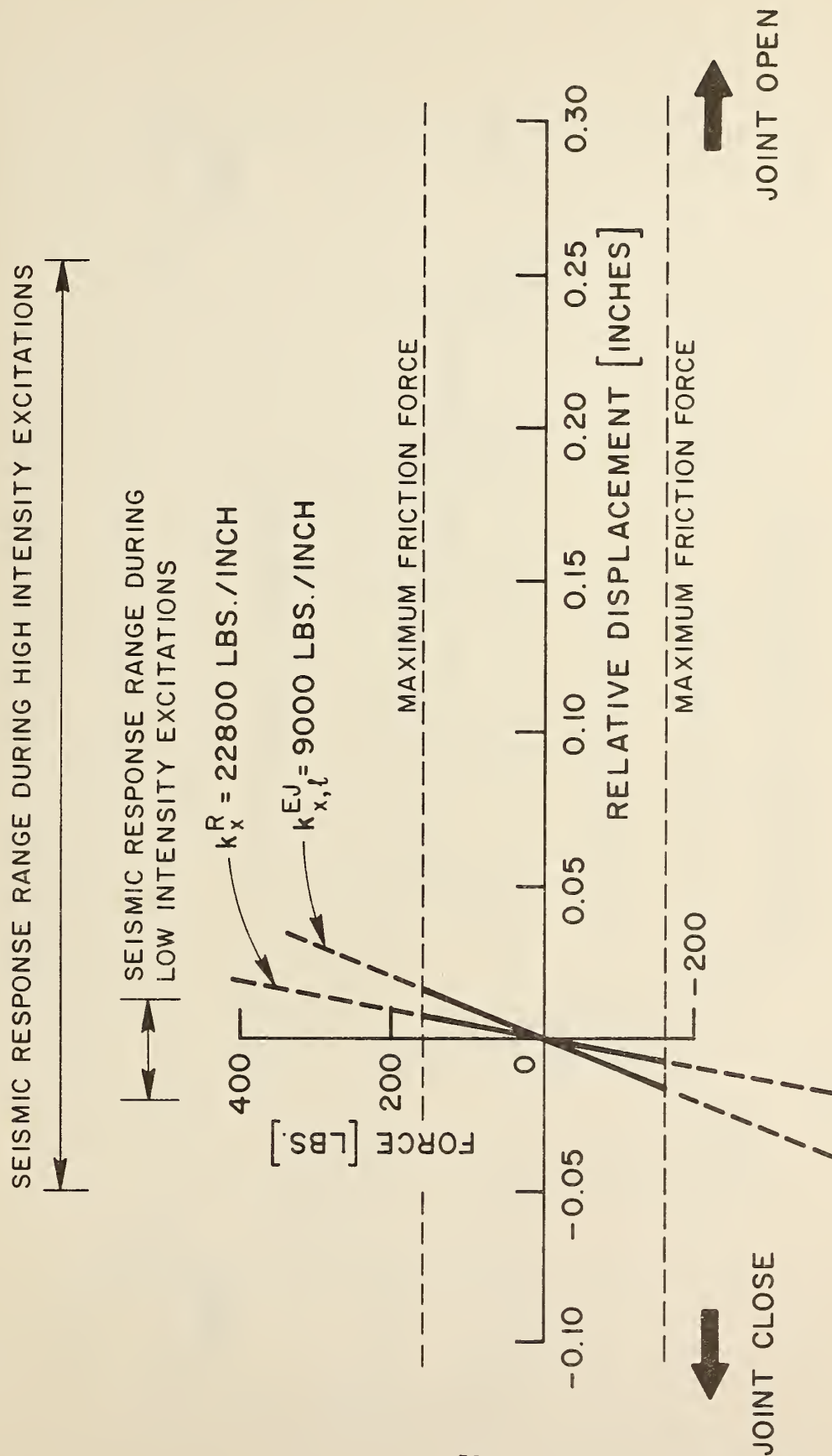


FIG. 4.4.1.1 ESTIMATED FORCE VS. RELATIVE DISPLACEMENT RELATION OF EXPANSION JOINT; EFFECT OF RUBBER PAD AND SLIPPAGES



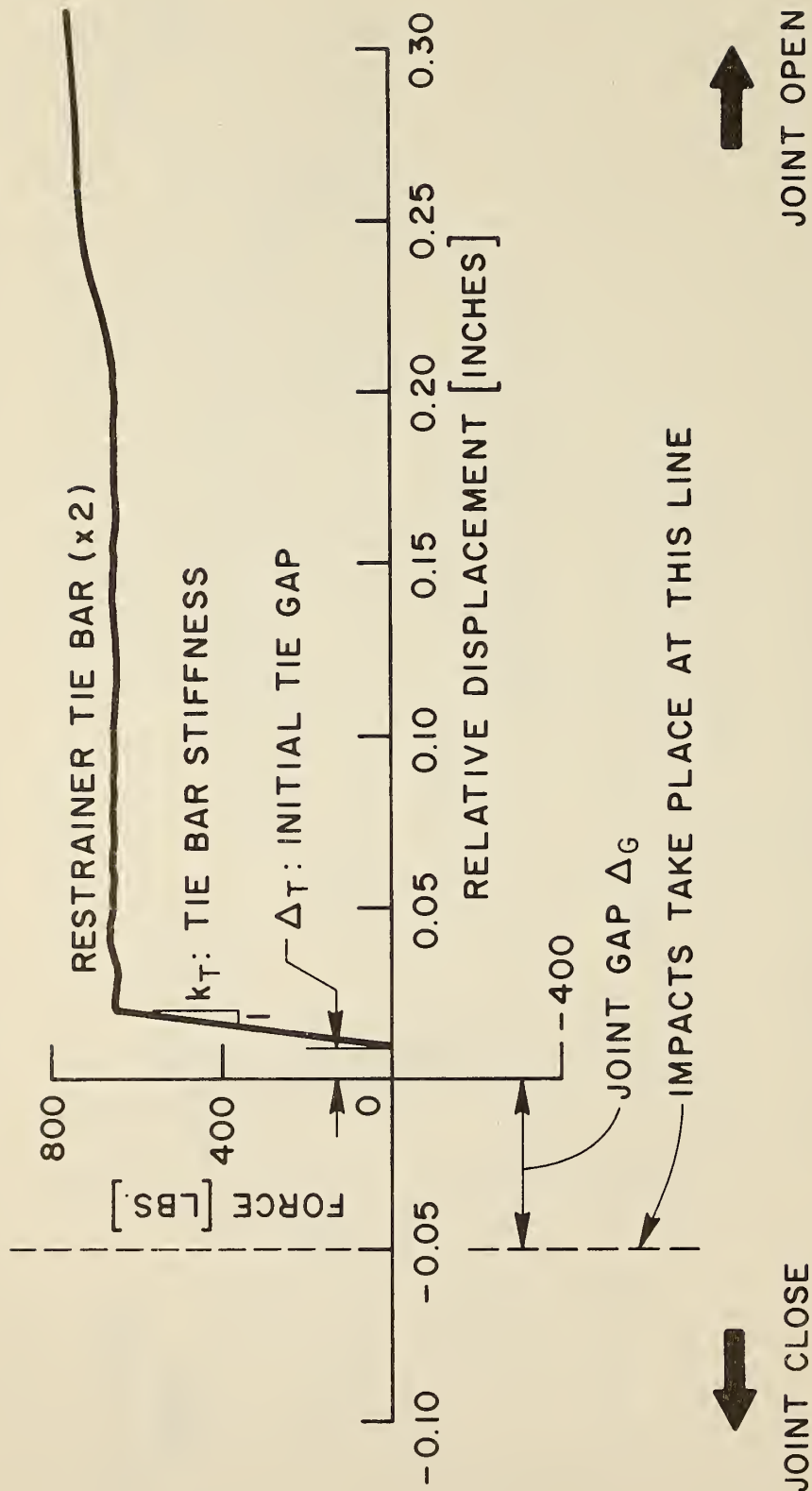


FIG. 4.4.2 ESTIMATED FORCE VS. RELATIVE DISPLACEMENT RELATION OF EXPANSION JOINT; EFFECT OF TIE BARS AND COLLISIONS

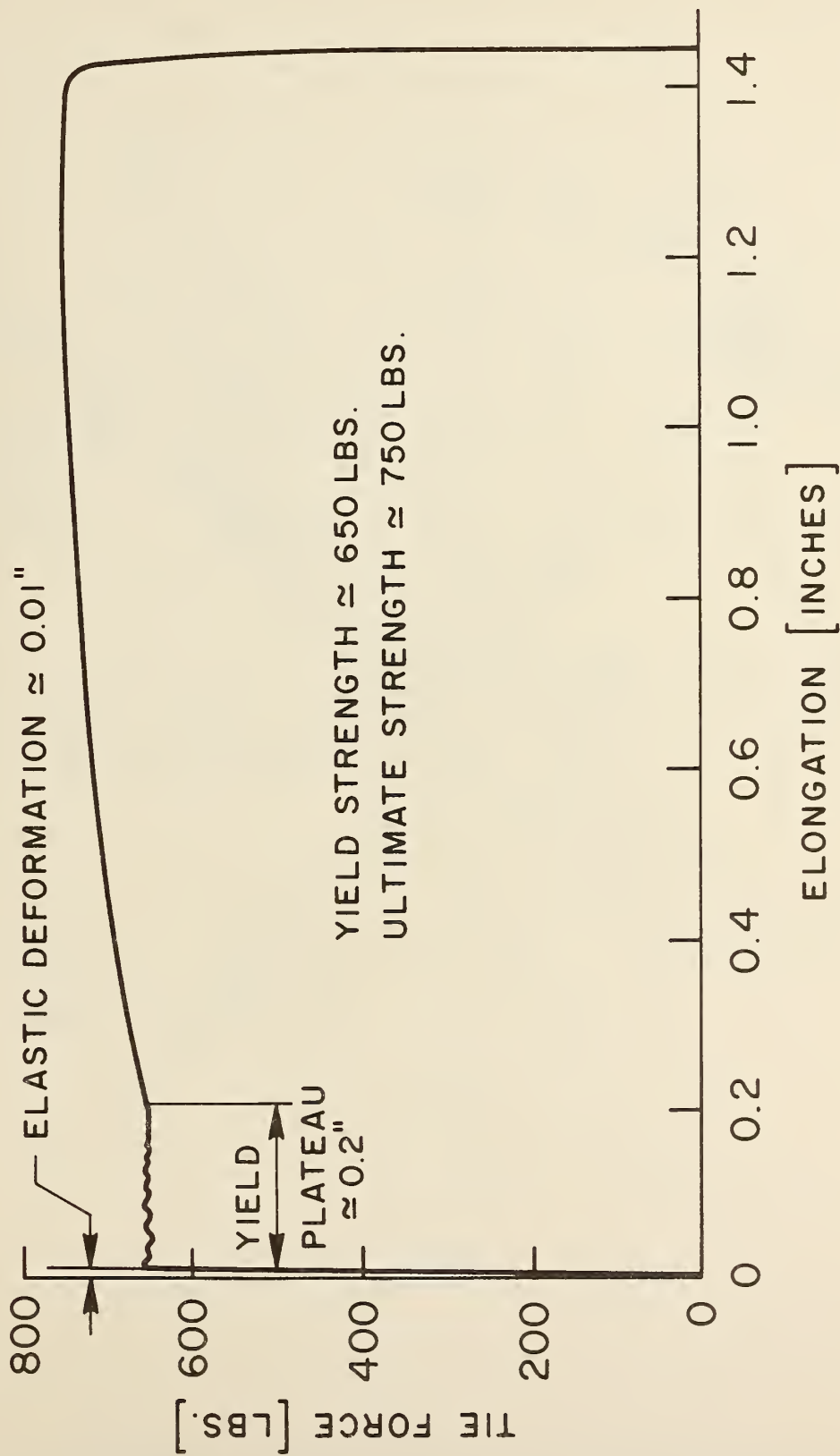


FIG. 4.5 TYPICAL FORCE VS. DEFORMATION RELATION OF TIE BAR [25]

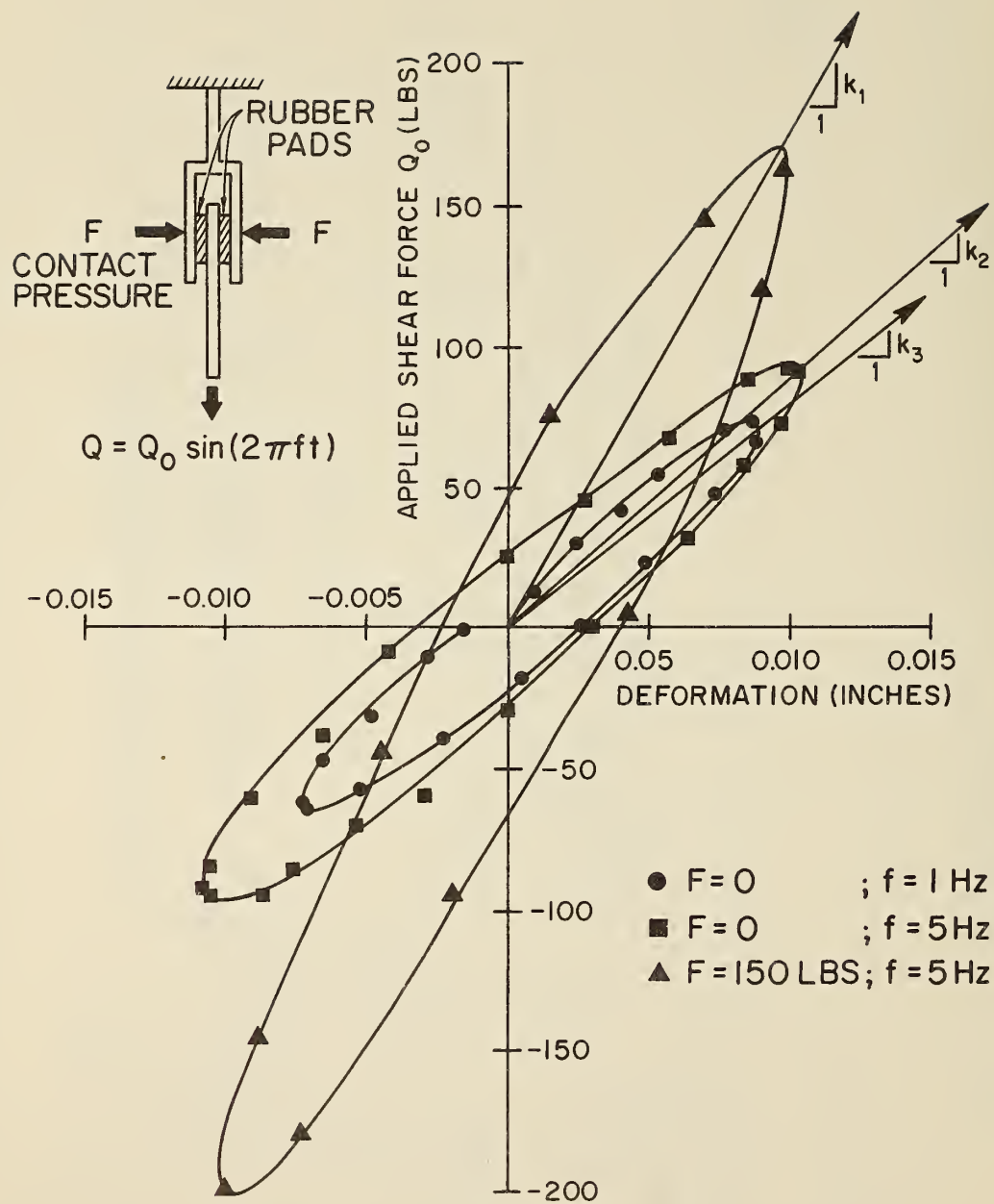


FIG. 4.6 TYPICAL FORCE VS. DEFORMATION RELATION OF RUBBER PAD [25]

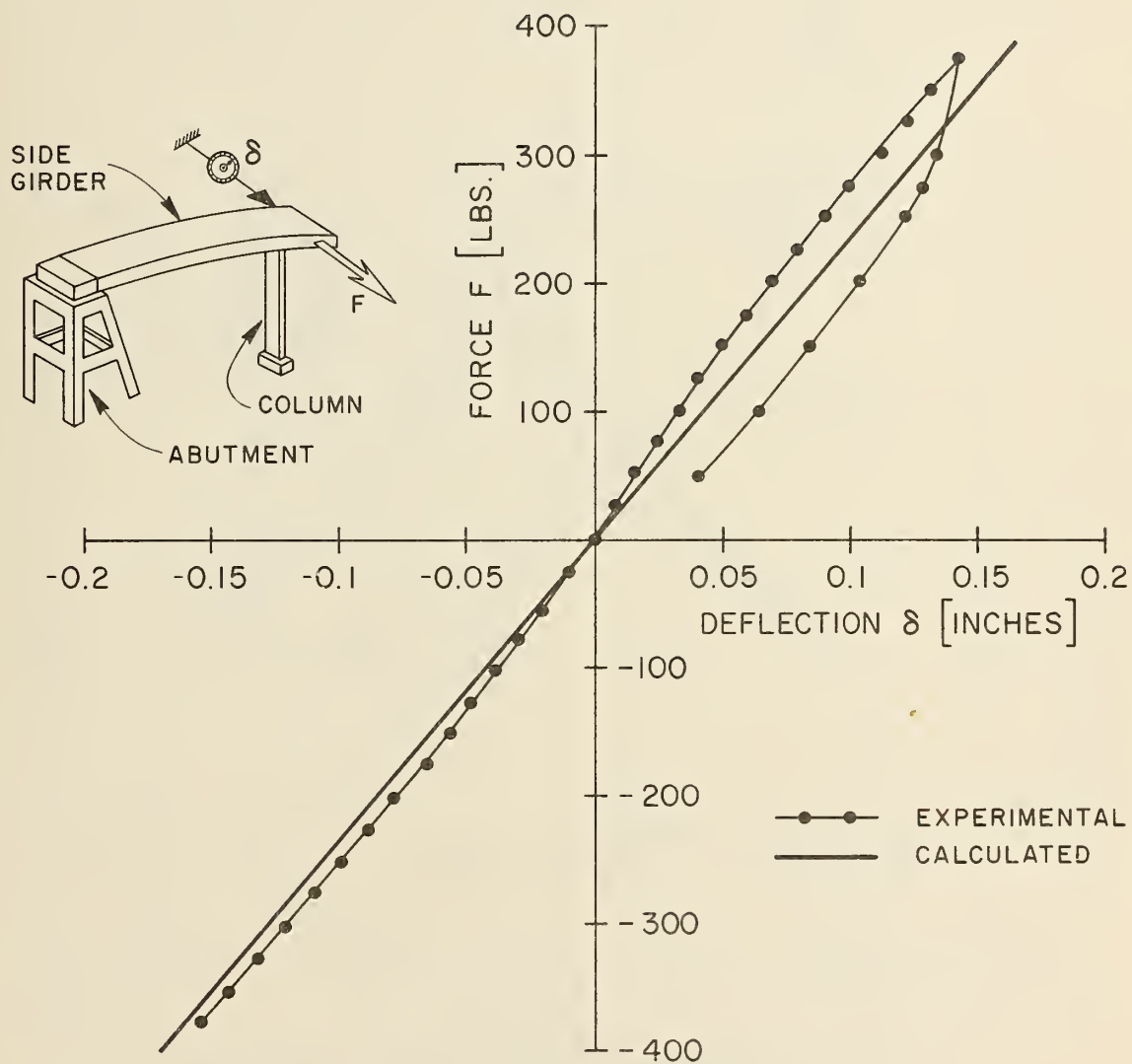


FIG. 4.7 STATIC LOAD-DEFORMATION TEST FOR SIDE SUBASSEMBLY [25]

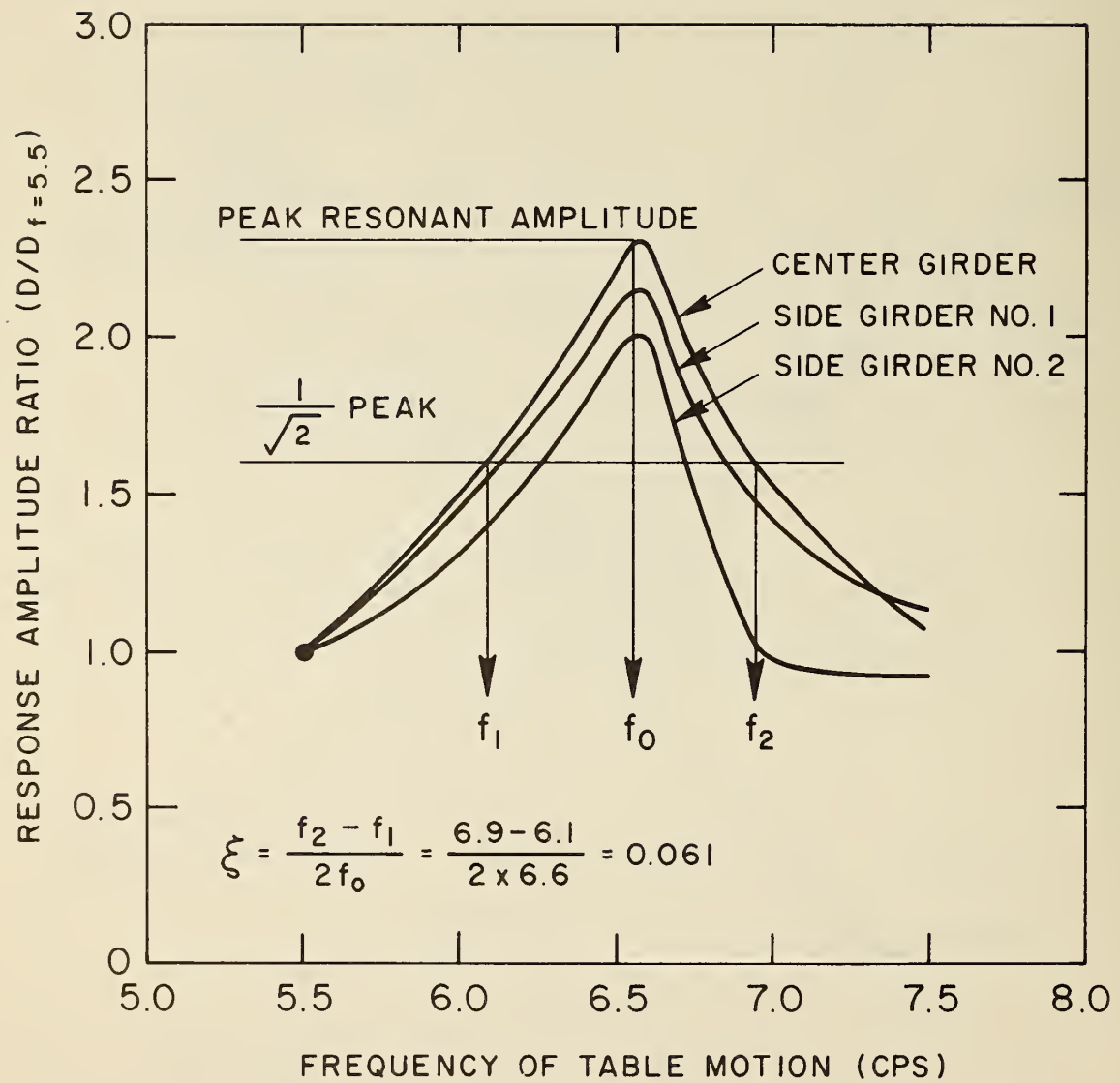


FIG. 4.8 RESONANT CURVE OF BRIDGE MODEL IN TRANSVERSE EXCITATION



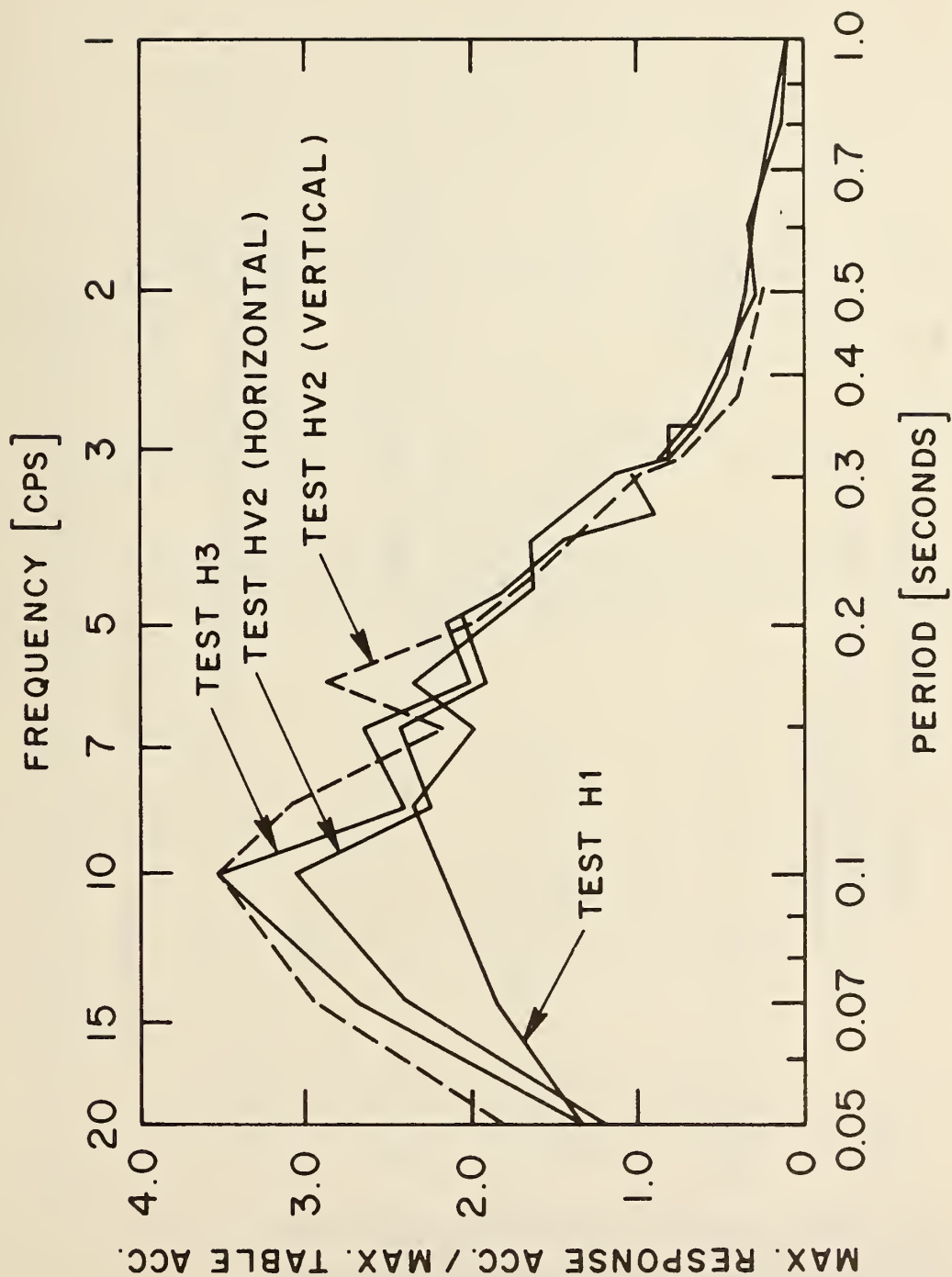


FIG. 4.9 ACCELERATION RESPONSE SPECTRUM OF TABLE MOTIONS  
(TESTS H1, H3 AND HV2)

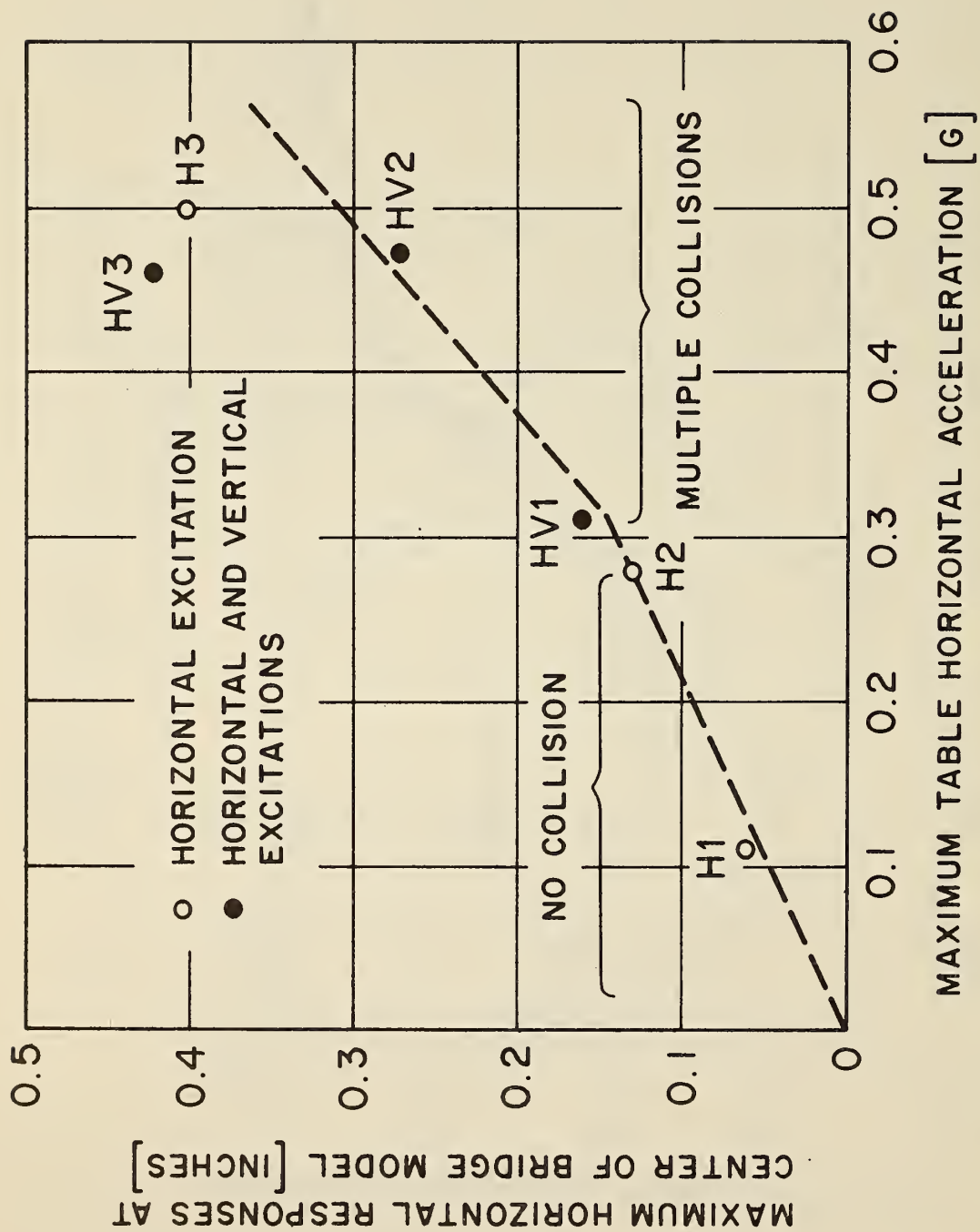


FIG. 4.10 RELATION BETWEEN MAXIMUM HORIZONTAL TABLE ACCELERATION AND MAXIMUM HORIZONTAL RESPONSE AT CENTER OF BRIDGE MODEL

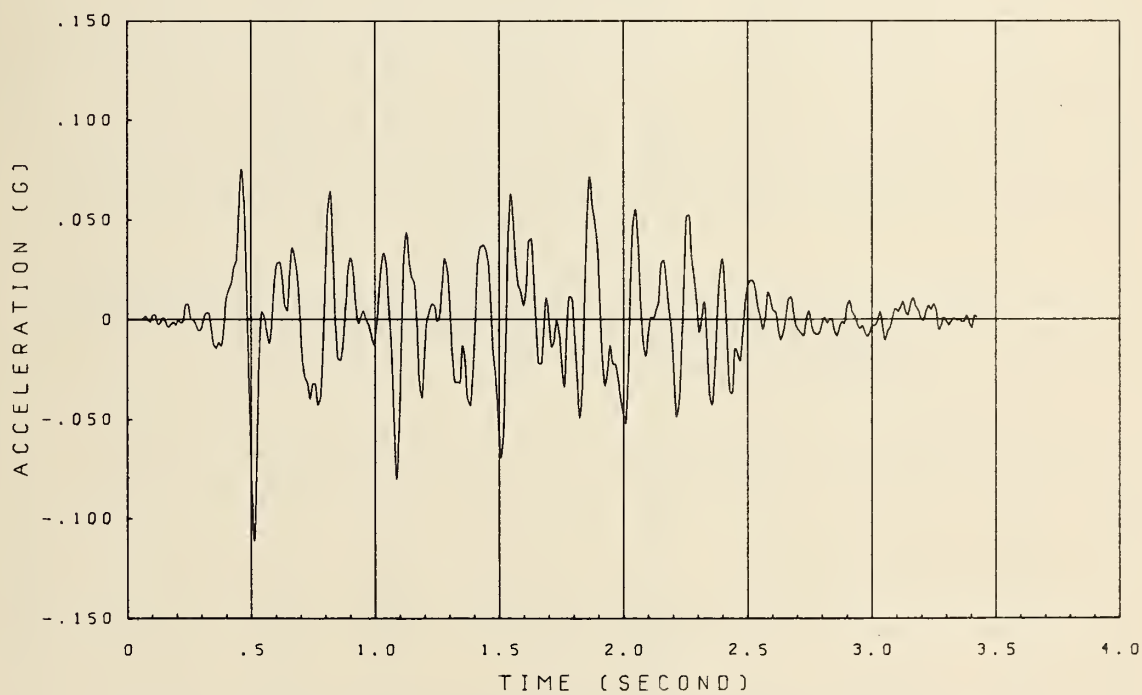


FIG. 4.11 HORIZONTAL TABLE ACCELERATION TIME HISTORY; TEST H1

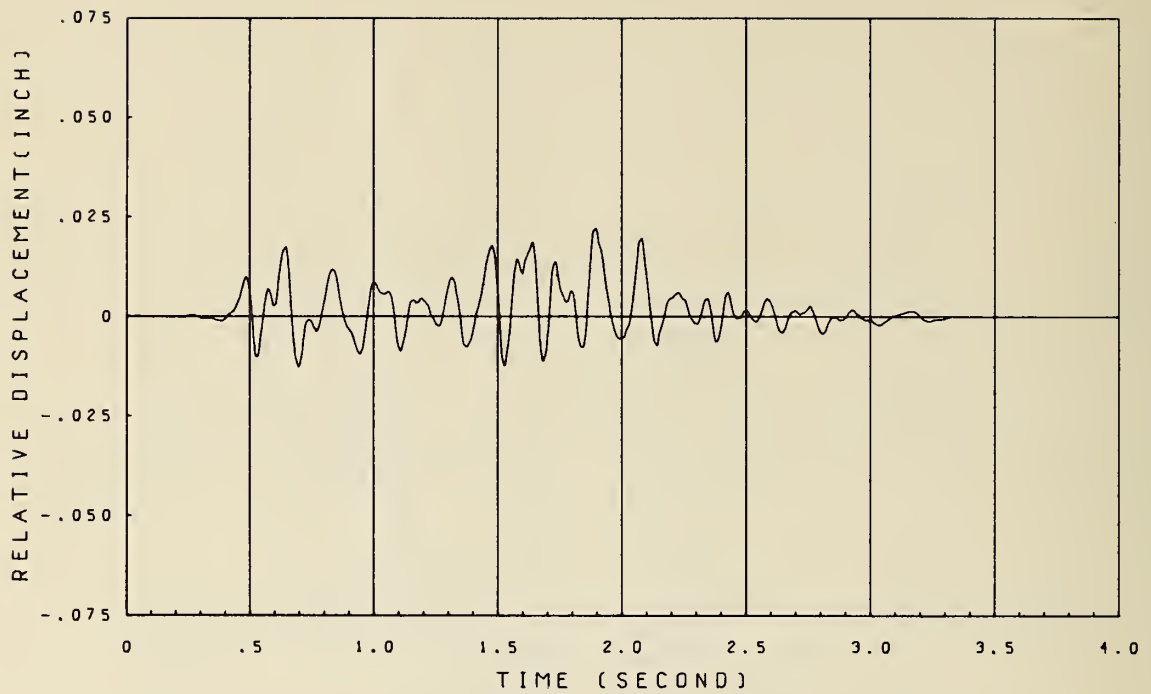


FIG. 4.12.1 MEASURED RESPONSE OF SIDE GIRDER NO. 1; LONGITUDINAL (X) DIRECTION; TEST H1

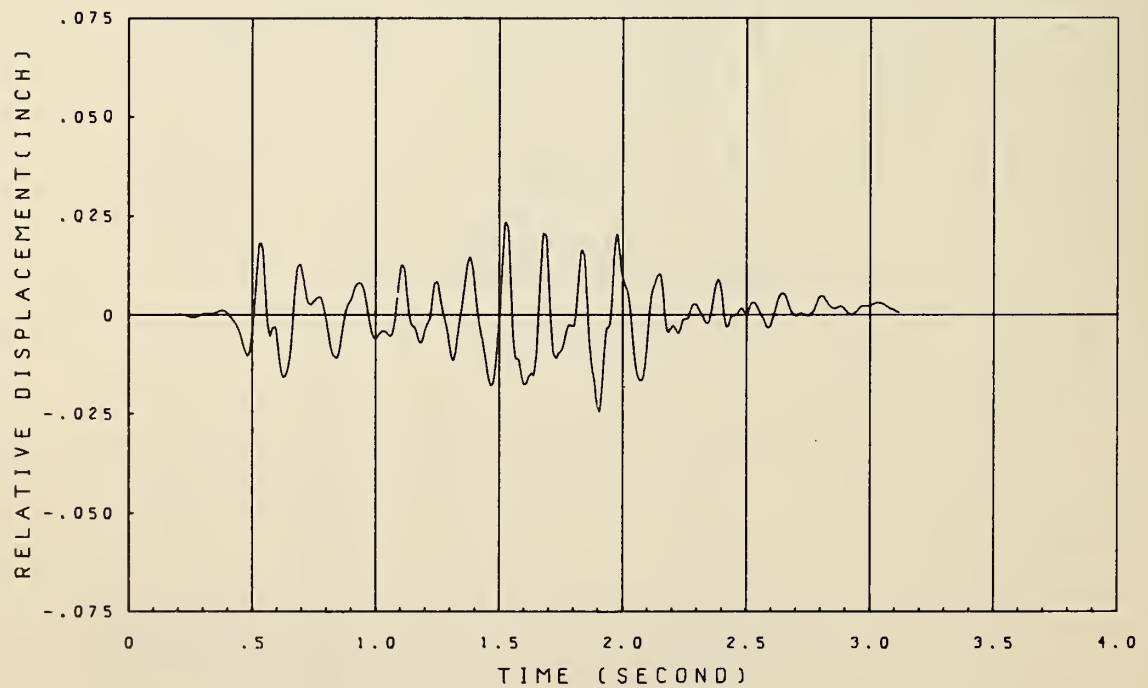


FIG. 4.12.2 MEASURED RESPONSE OF SIDE GIRDER NO. 1; TRANSVERSE (Y) DIRECTION; TEST H1



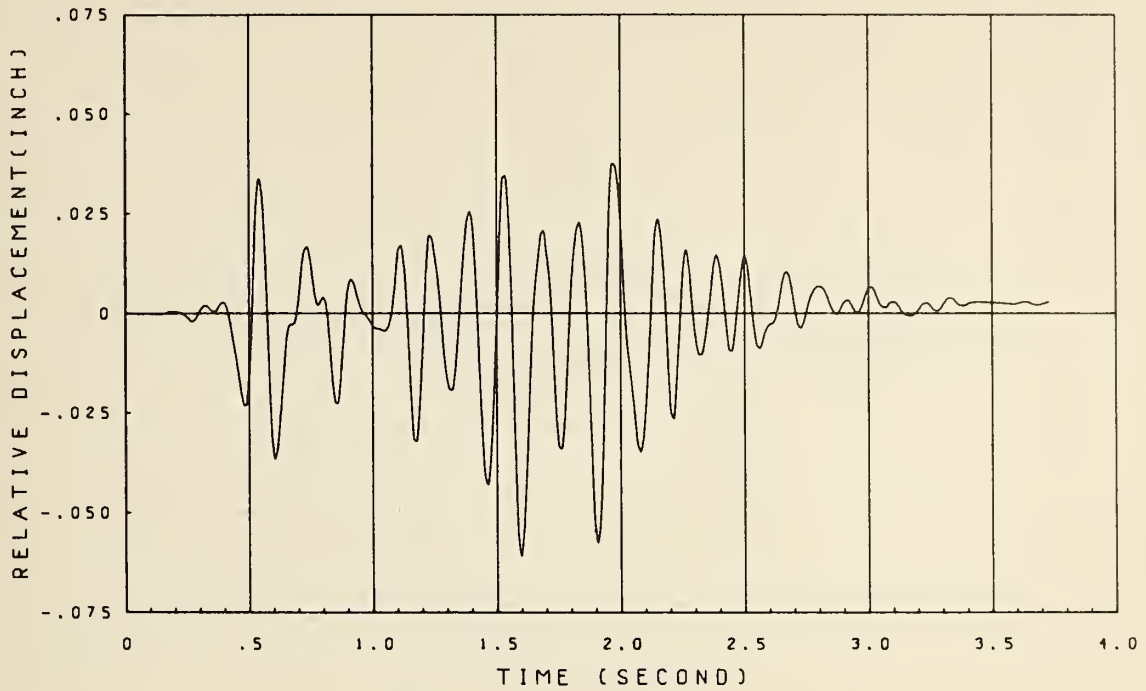


FIG. 4.12.3 MEASURED RESPONSE OF CENTER GIRDER; TRANSVERSE (Y) DIRECTION; TEST H1

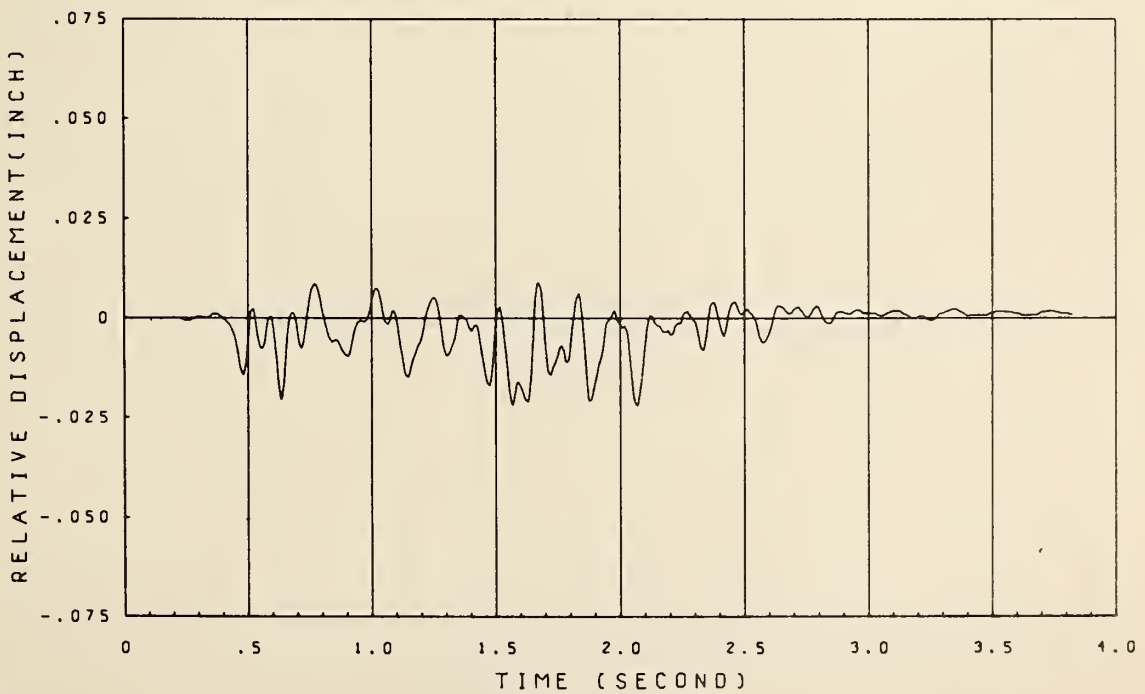


FIG. 4.12.4 MEASURED RESPONSE OF SIDE GIRDER NO. 2; LONGITUDINAL (X) DIRECTION; TEST H1

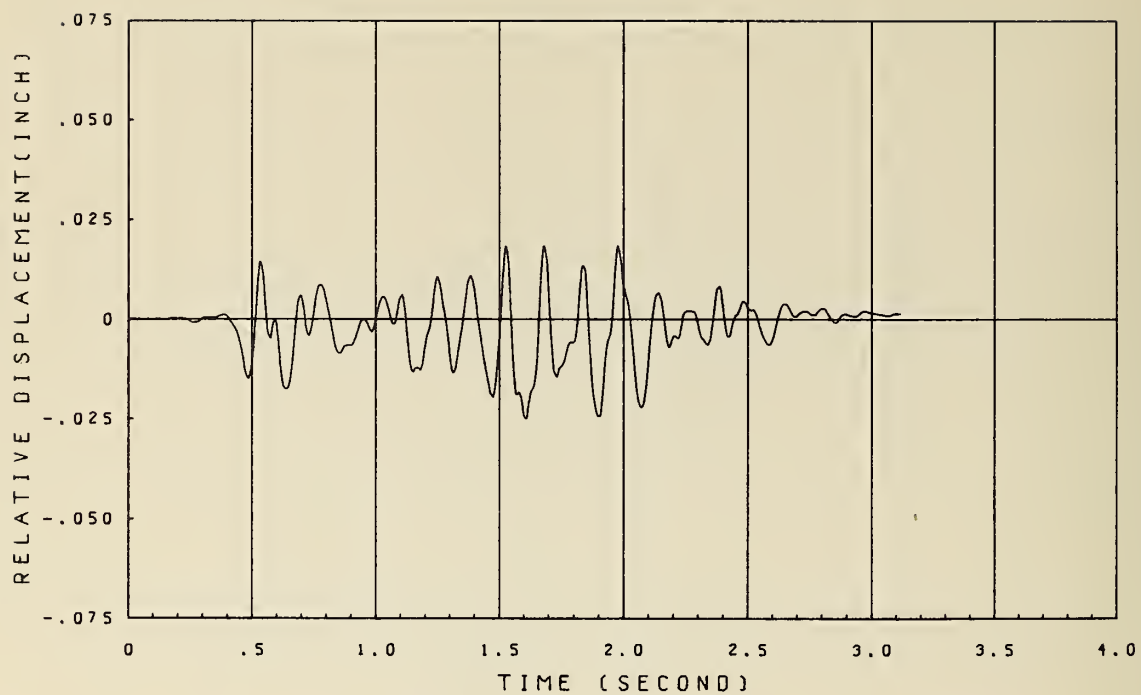


FIG. 4.12.5 MEASURED RESPONSE OF SIDE GIRDER NO. 2; TRANSVERSE (Y) DIRECTION; TEST H1

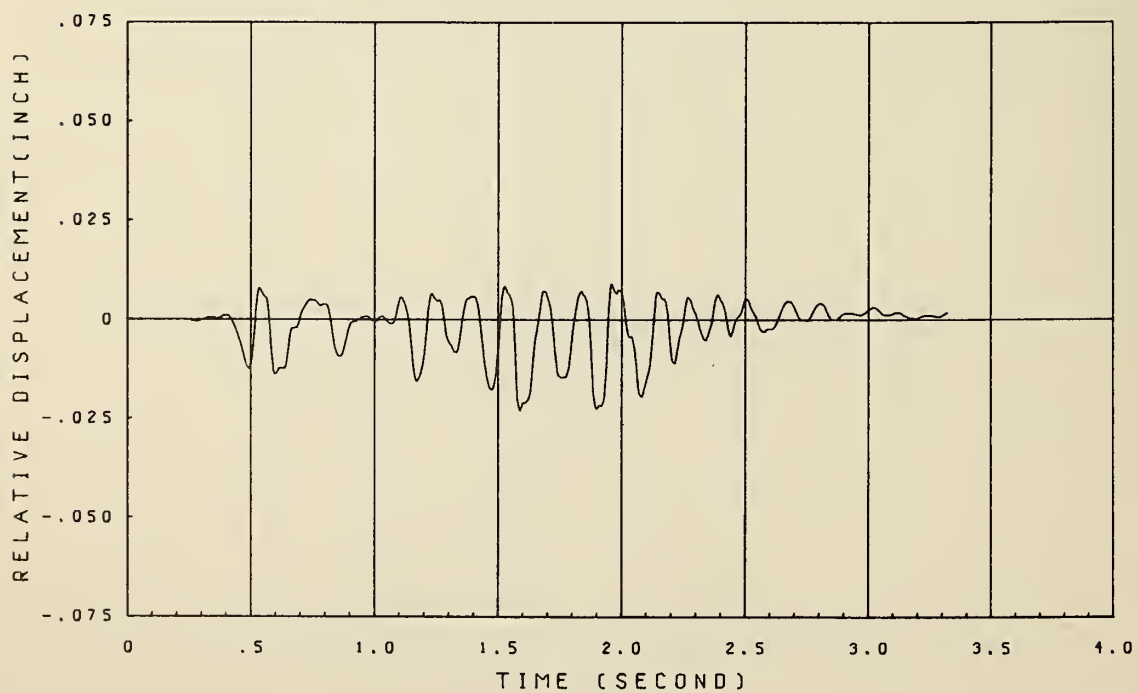


FIG. 4.12.6 MEASURED RESPONSE OF EXPANSION JOINT NO. 1; INNER SIDE; TEST H1

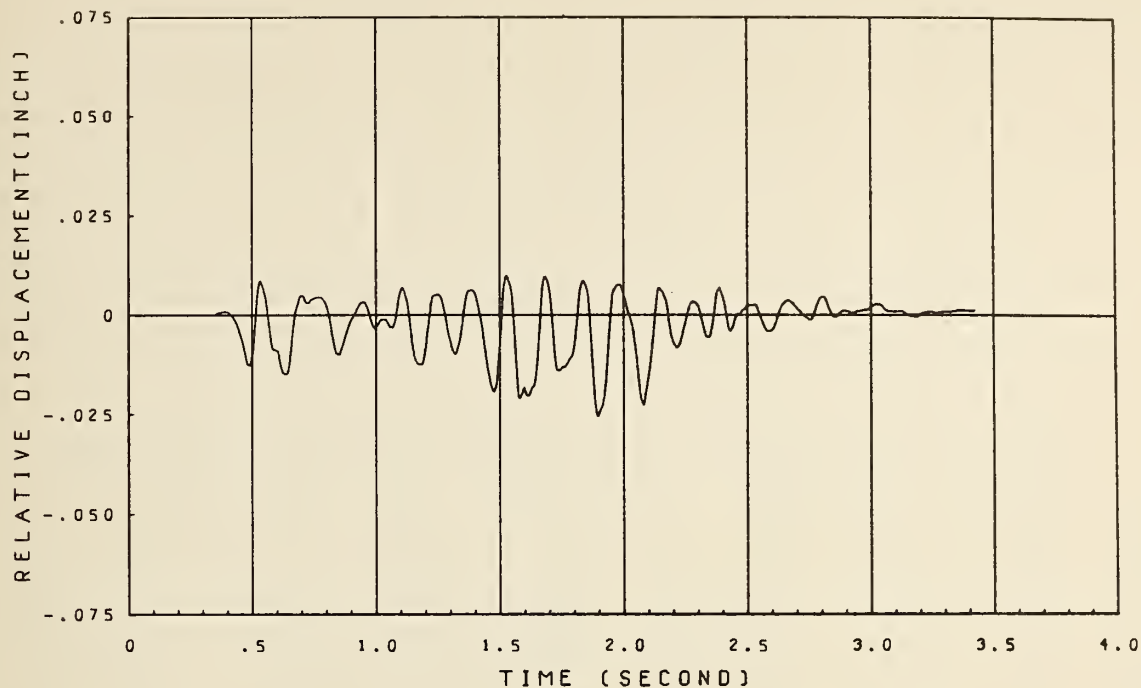


FIG. 4.12.7 MEASURED RESPONSE OF EXPANSION JOINT NO. 1; OUTER SIDE;  
TEST H1

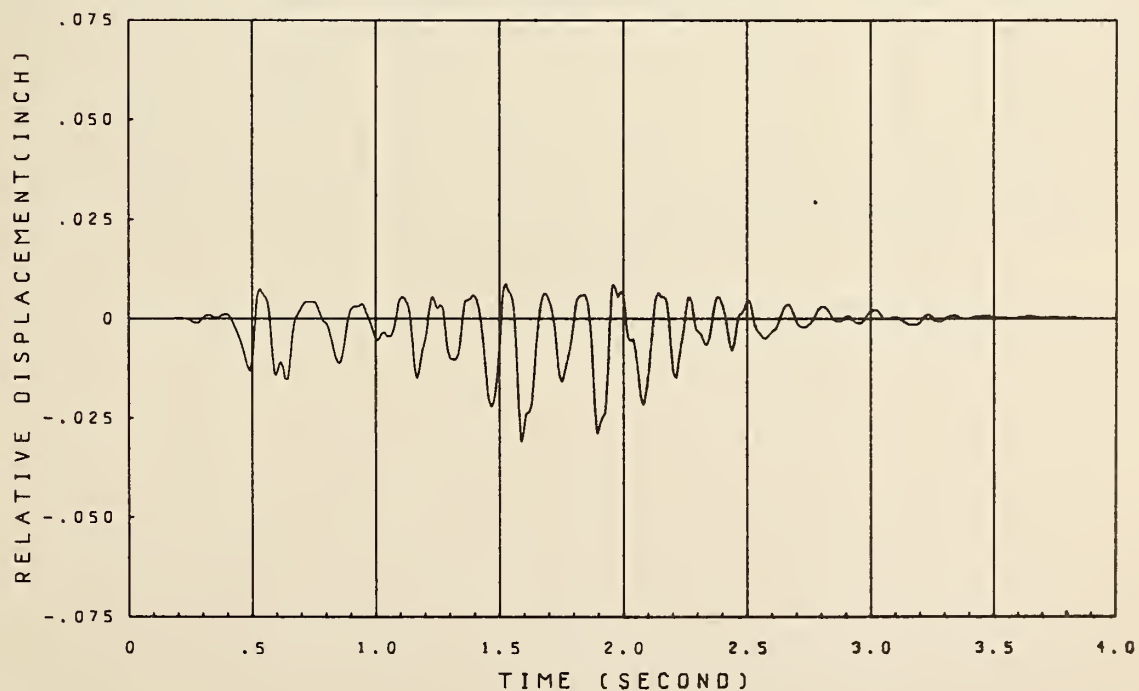


FIG. 4.12.8 MEASURED RESPONSE OF EXPANSION JOINT NO. 2; INNER SIDE;  
TEST H1

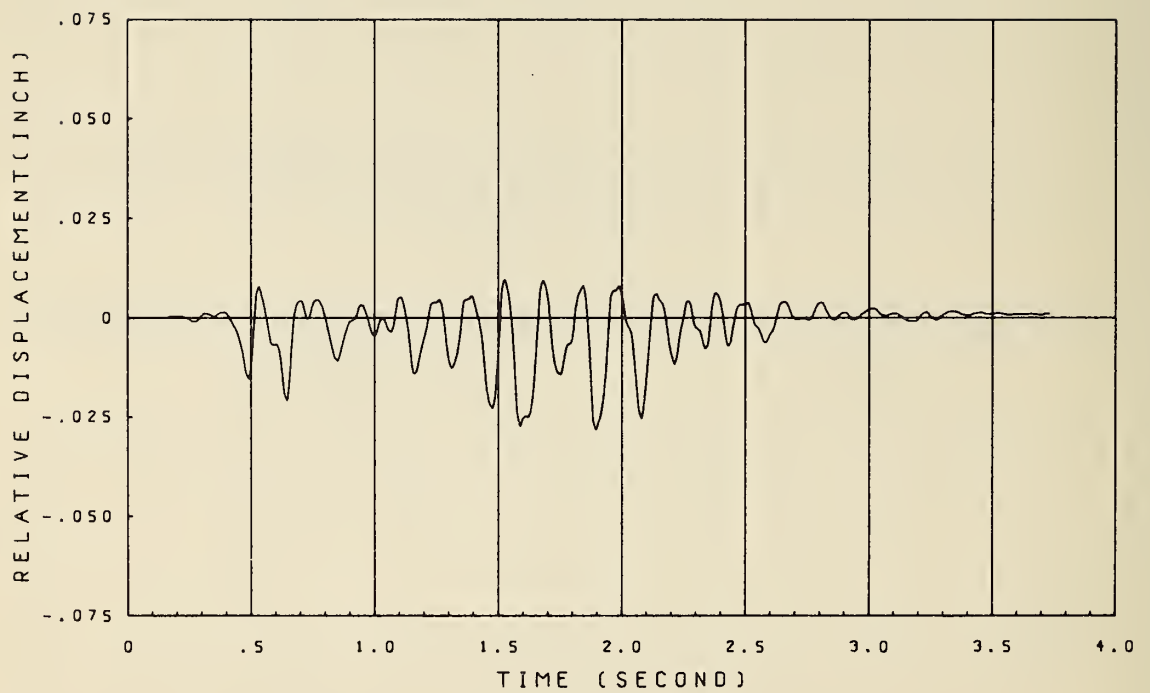


FIG. 4.12.9 MEASURED RESPONSE OF EXPANSION JOINT NO. 2; OUTER SIDE;  
TEST H1



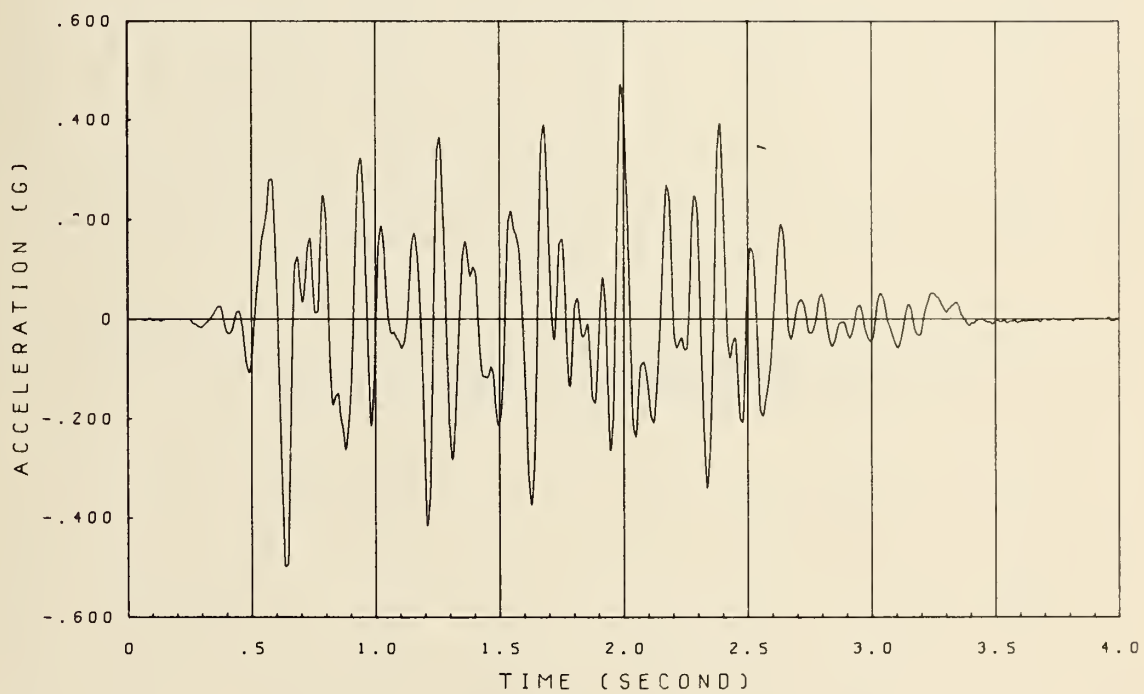


FIG. 4.13 HORIZONTAL TABLE ACCELERATION TIME HISTORY; TEST H2

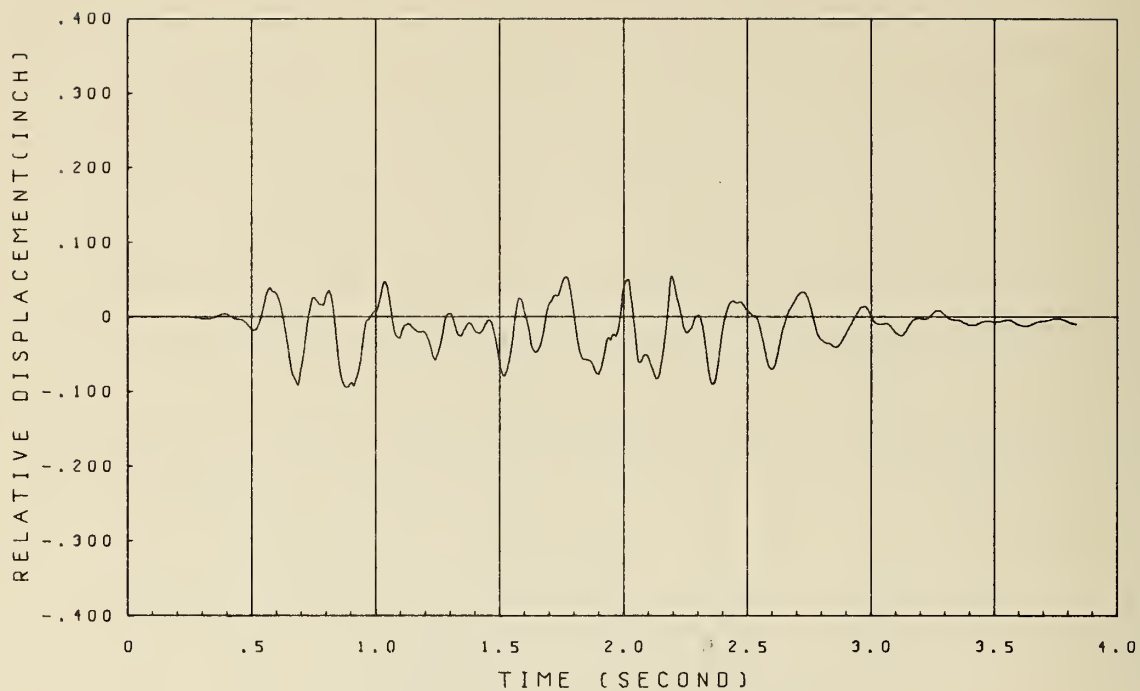


FIG. 4.14.1 MEASURED RESPONSE OF SIDE GIRDER NO. 1; LONGITUDINAL (X) DIRECTION; TEST H2

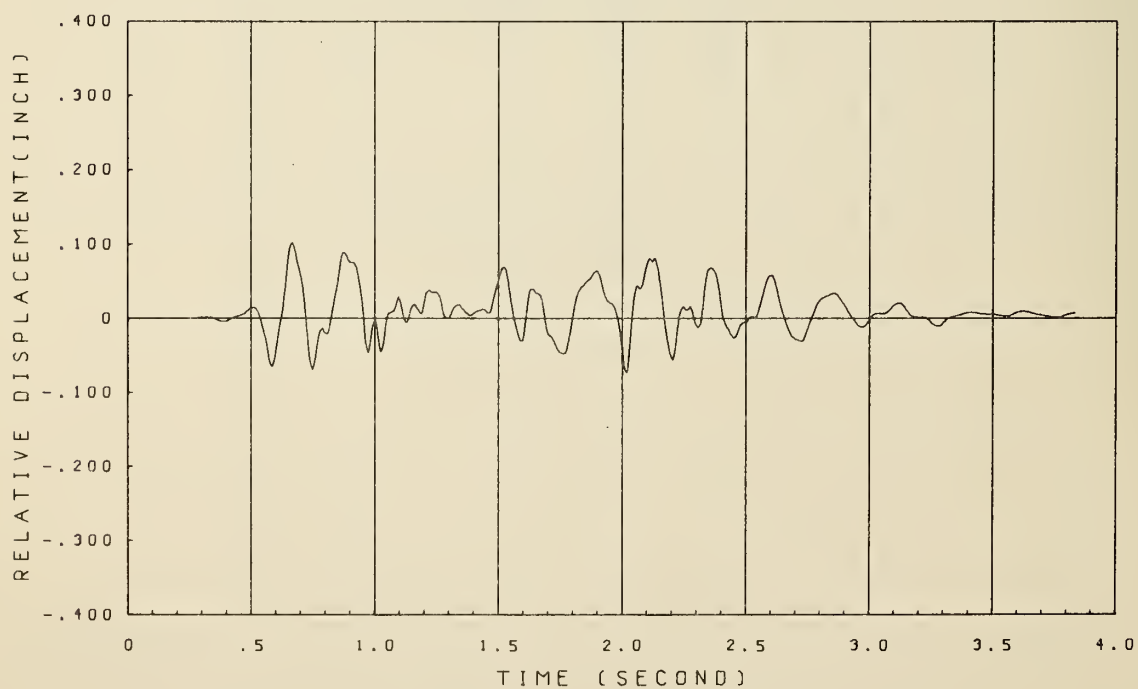


FIG. 4.14.2 MEASURED RESPONSE OF SIDE GIRDER NO. 1; TRANSVERSE (Y) DIRECTION; TEST H2

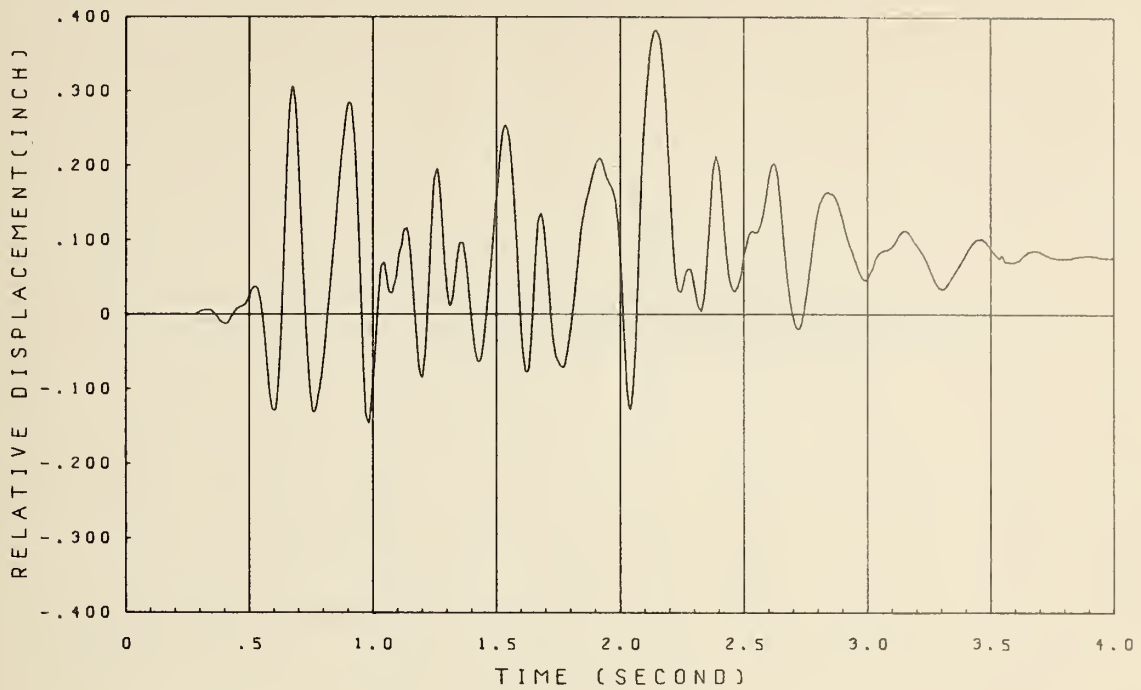


FIG. 4.14.3 MEASURED RESPONSE OF CENTER GIRDER; TRANSVERSE (Y) DIRECTION; TEST H2

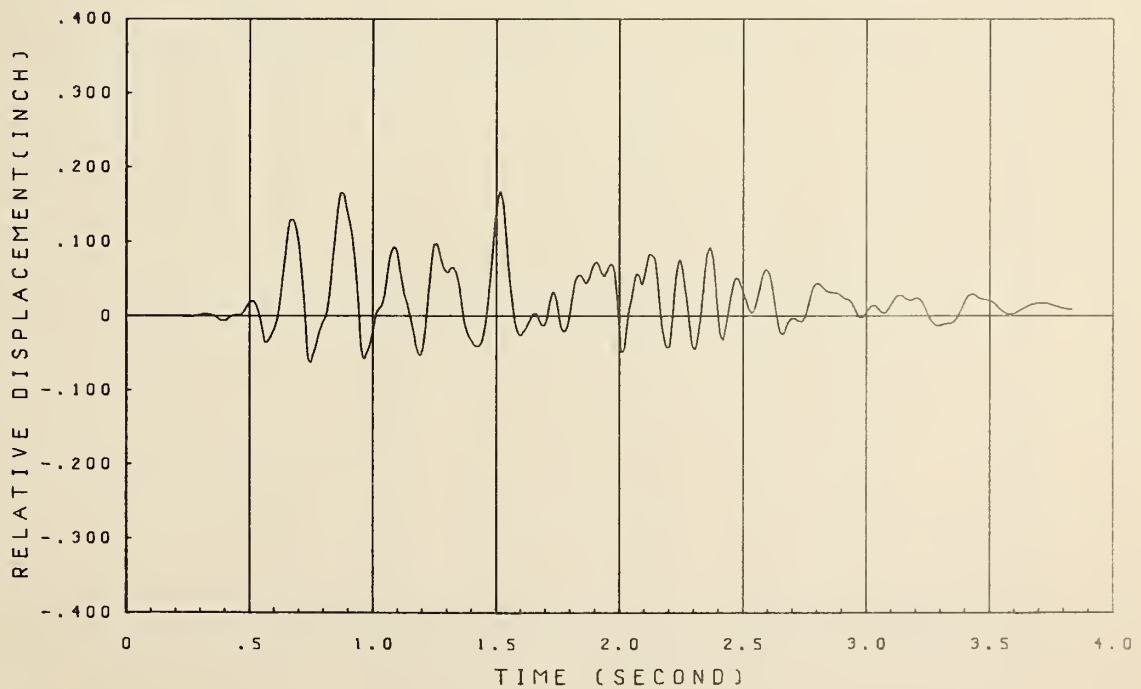


FIG. 4.14.4 MEASURED RESPONSE OF SIDE GIRDER NO. 2; LONGITUDINAL (X) DIRECTION; TEST H2

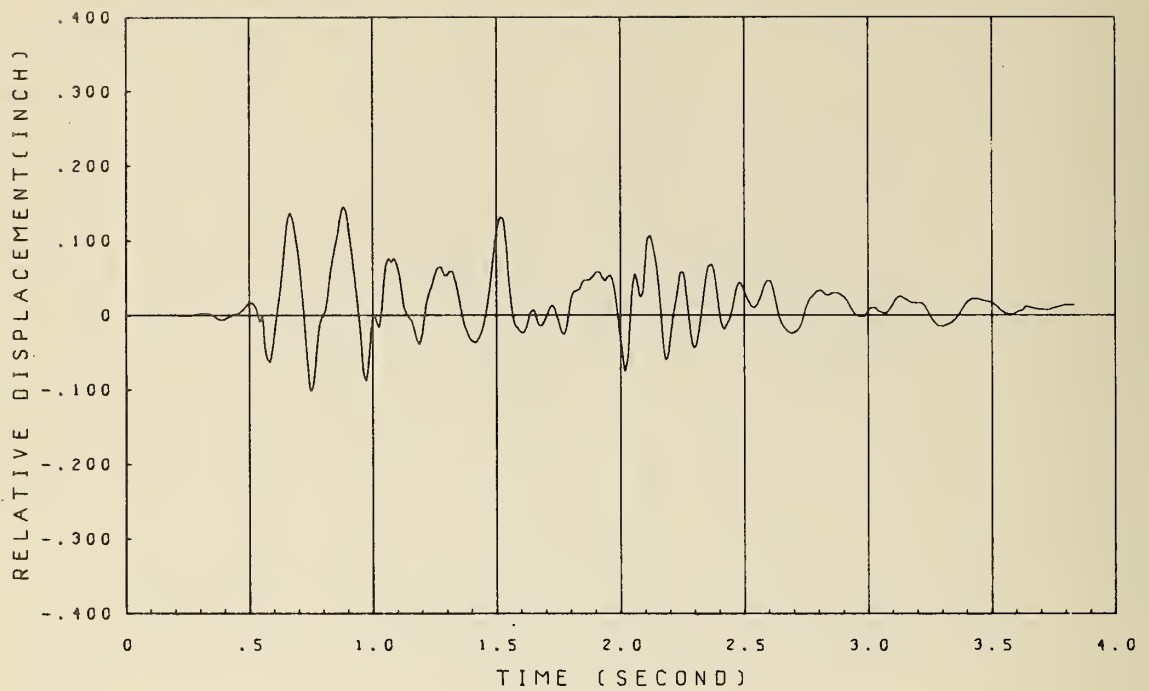


FIG. 4.14.5 MEASURED RESPONSE OF SIDE GIRDER NO. 2; TRANSVERSE (Y) DIRECTION; TEST H2

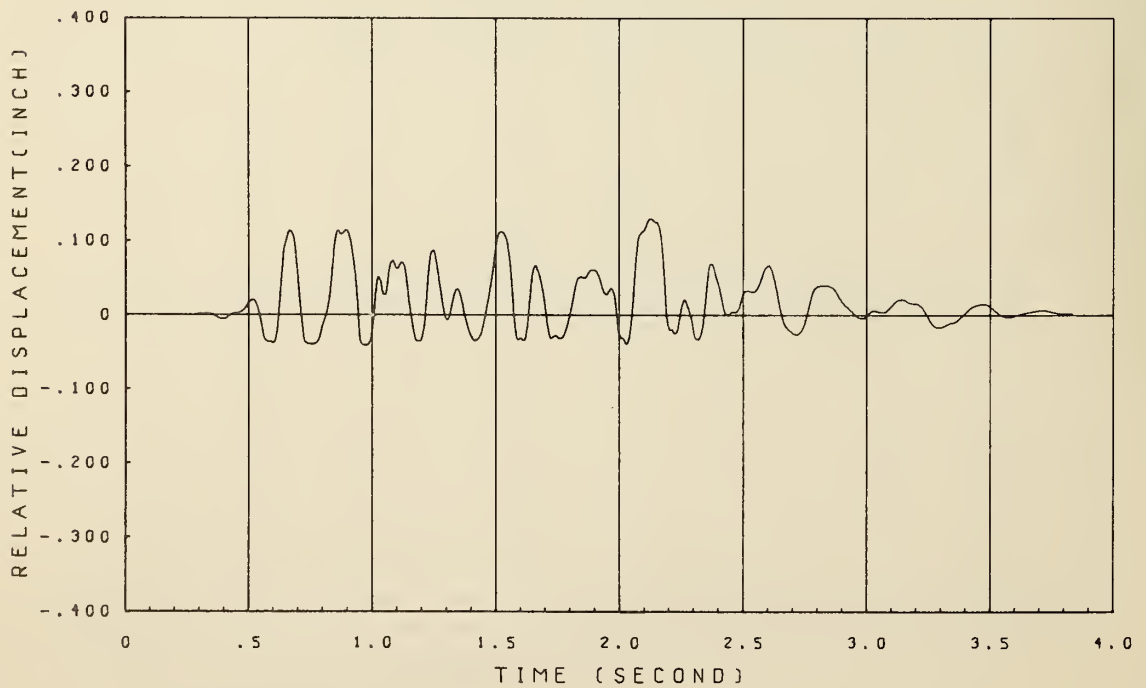


FIG. 4.14.6 MEASURED RESPONSE OF EXPANSION JOINT NO. 1; INNER SIDE; TEST H2

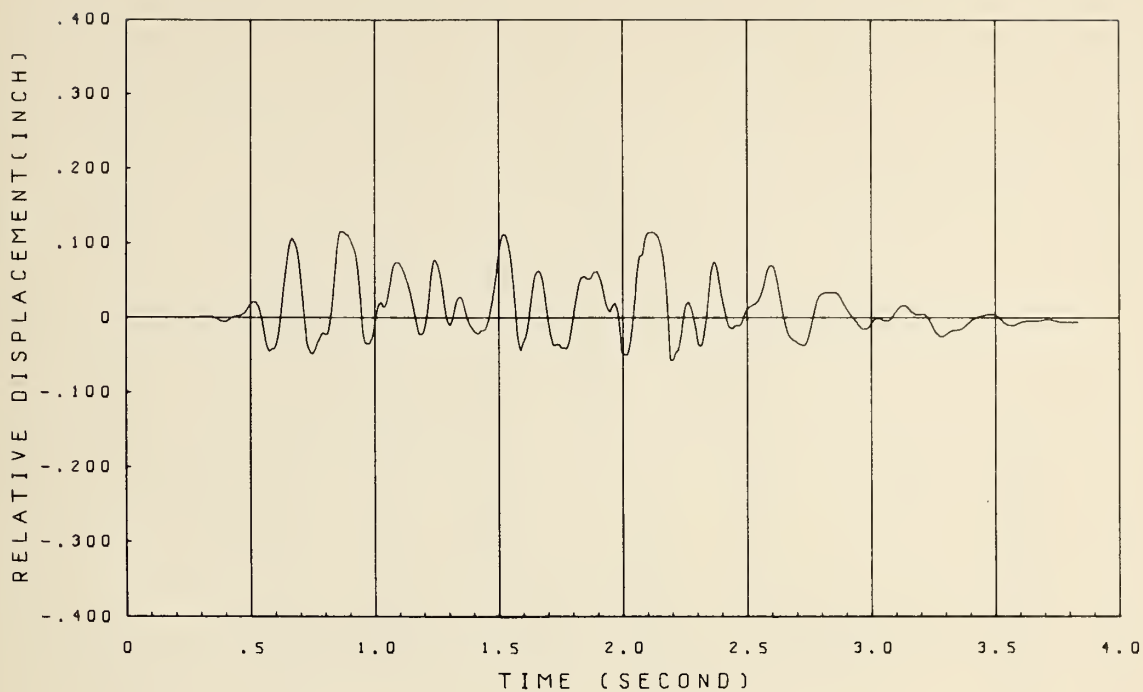


FIG. 4.14.7 MEASURED RESPONSE OF EXPANSION JOINT NO. 1; OUTER SIDE;  
TEST H2

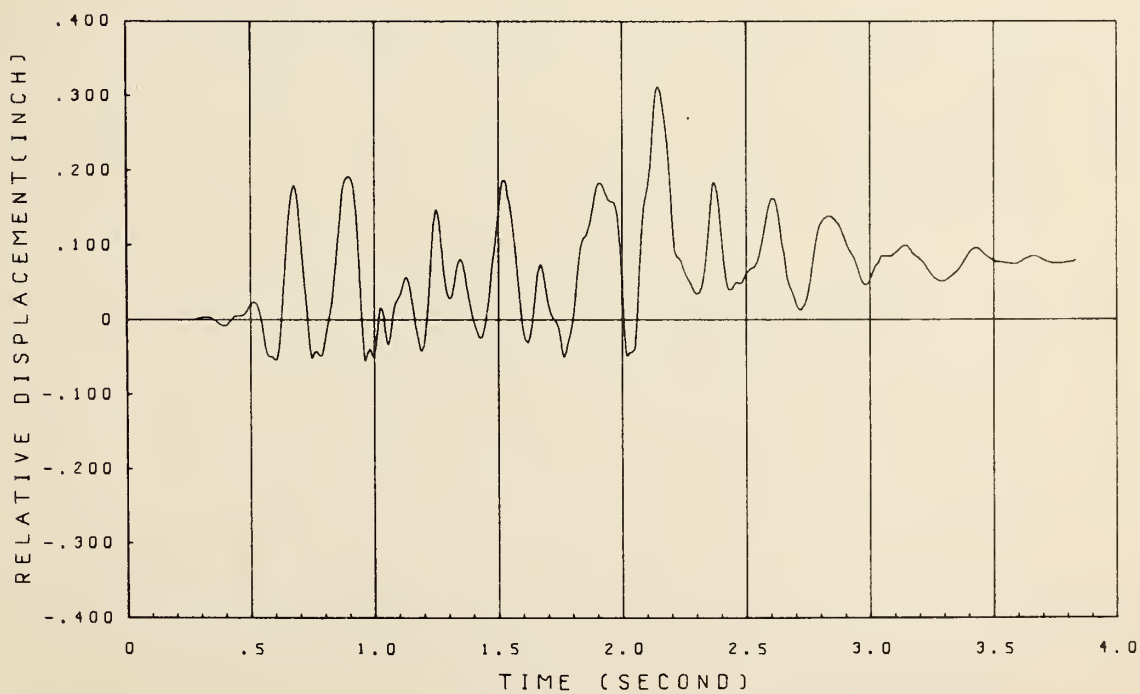


FIG. 4.14.8 MEASURED RESPONSE OF EXPANSION JOINT NO. 2; INNER SIDE;  
TEST H2



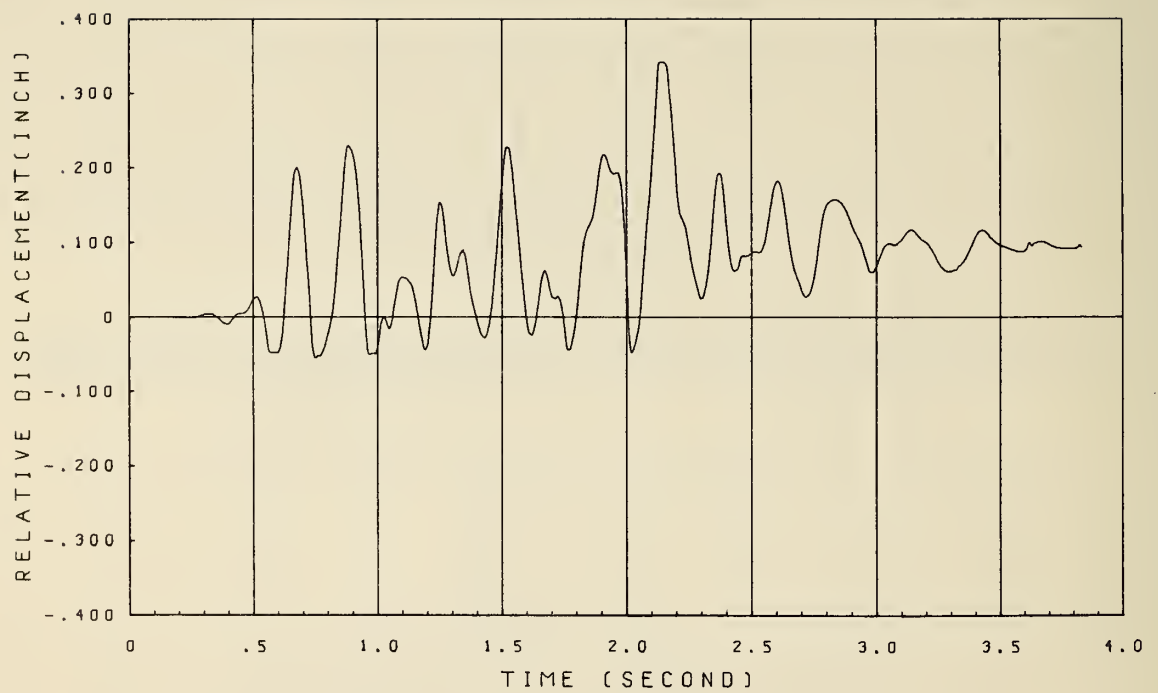


FIG. 4.14.9 MEASURED RESPONSE OF EXPANSION JOINT NO. 2; OUTER SIDE;  
TEST H2

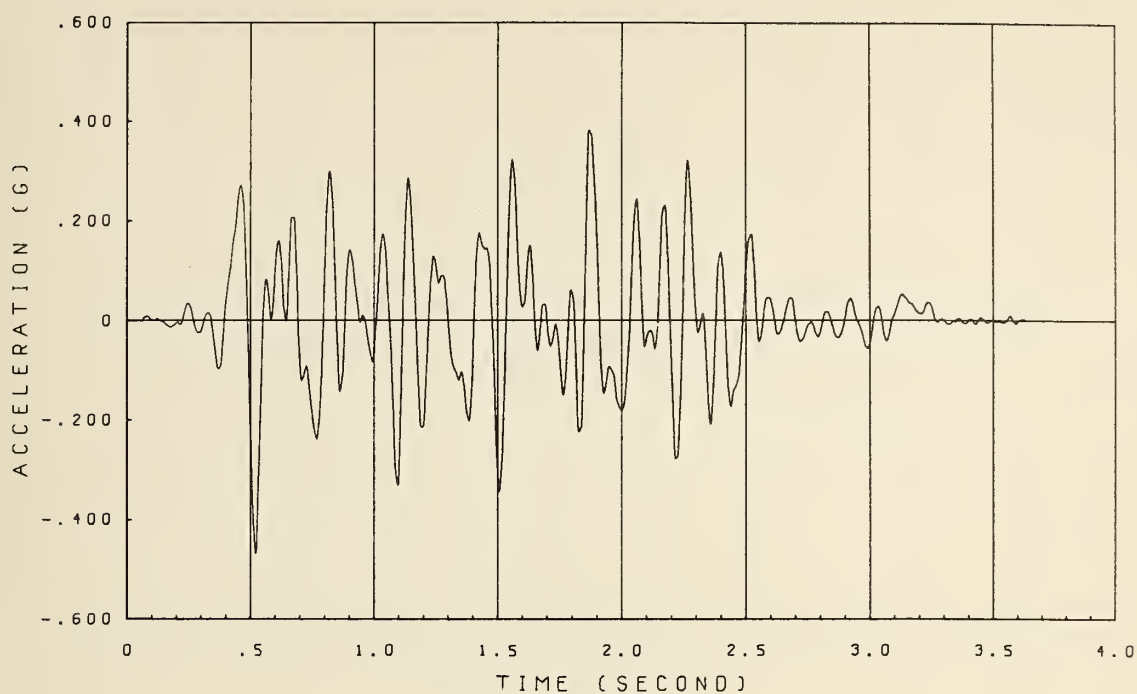


FIG. 4.15.1 HORIZONTAL TABLE ACCELERATION TIME HISTORY; TEST HV2

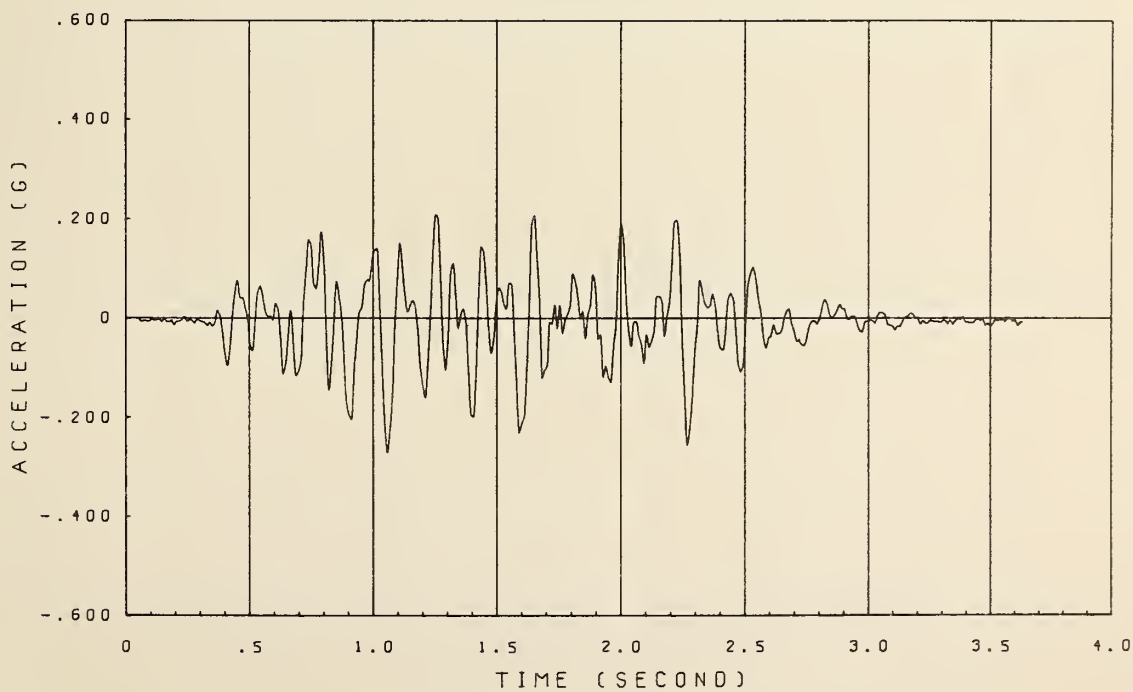


FIG. 4.15.2 VERTICAL TABLE ACCELERATION TIME HISTORY; TEST HV2

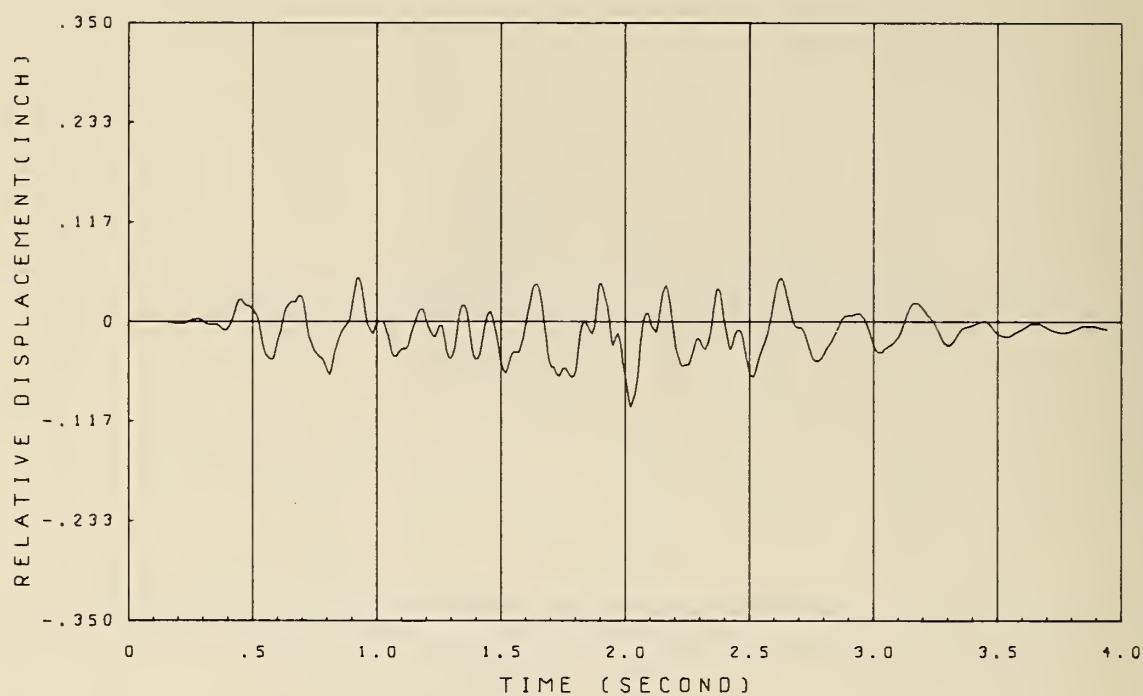


FIG. 4.16.1 MEASURED RESPONSE OF SIDE GIRDER NO. 1; LONGITUDINAL (X) DIRECTION; TEST HV2

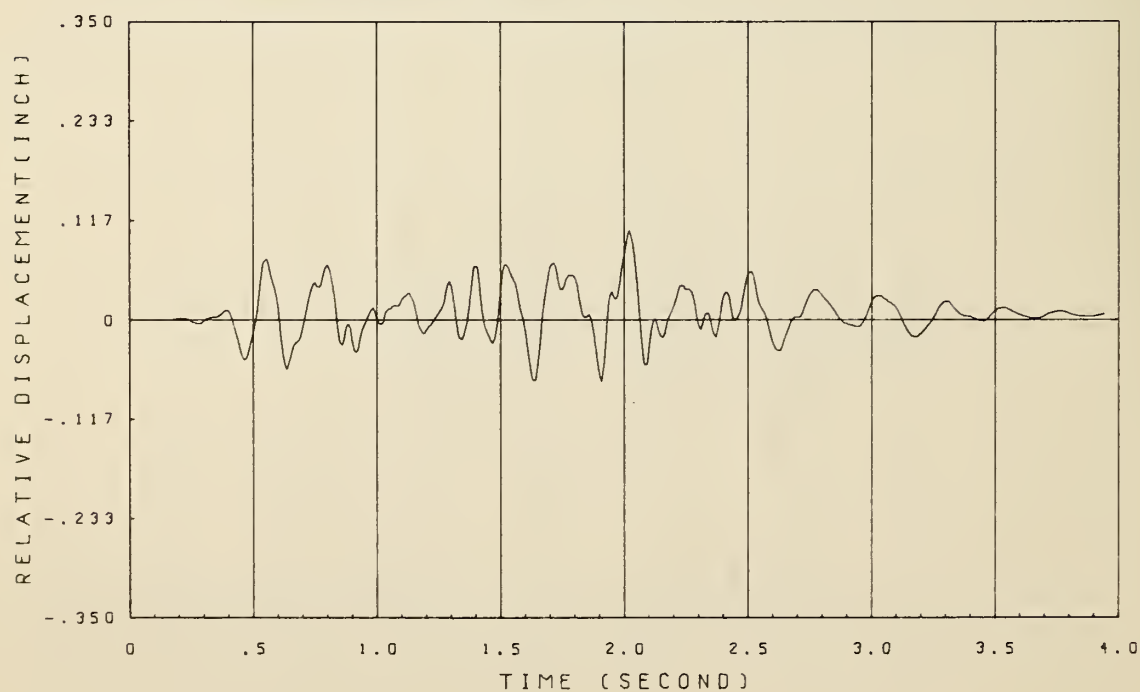


FIG. 4.16.2 MEASURED RESPONSE OF SIDE GIRDER NO. 1; TRANSVERSE (Y) DIRECTION; TEST HV2

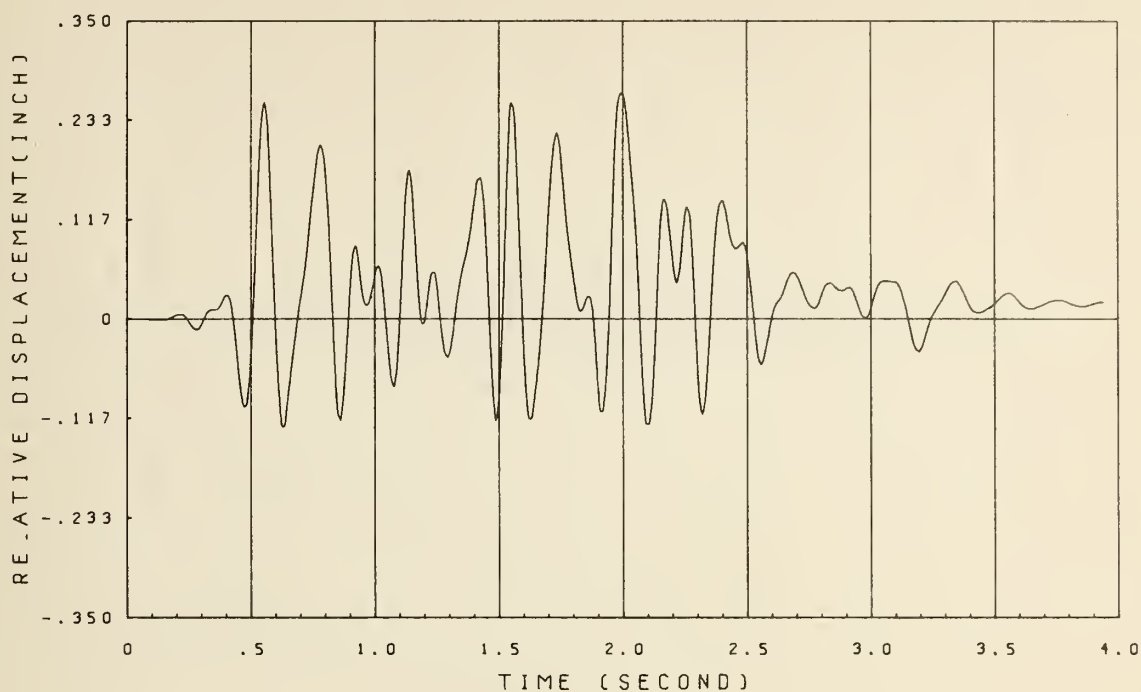


FIG. 4.16.3 MEASURED RESPONSE OF CENTER GIRDER; TRANSVERSE (Y) DIRECTION; TEST HV2

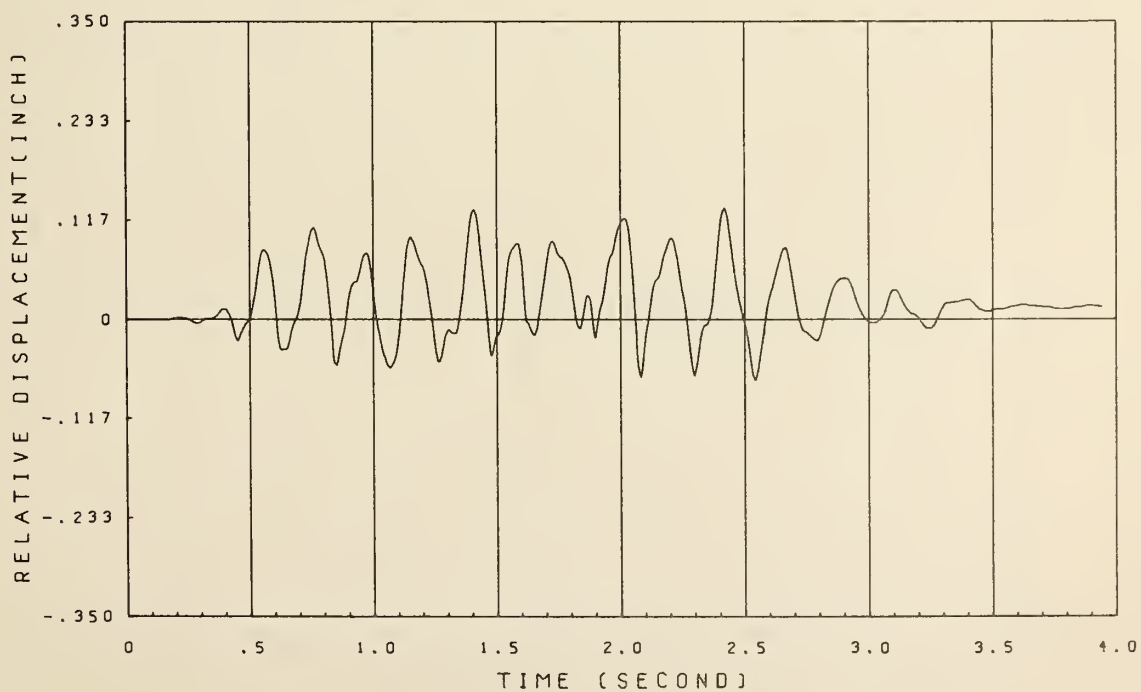


FIG. 4.16.4 MEASURED RESPONSE OF SIDE GIRDER NO. 2; LONGITUDINAL (X) DIRECTION; TEST HV2

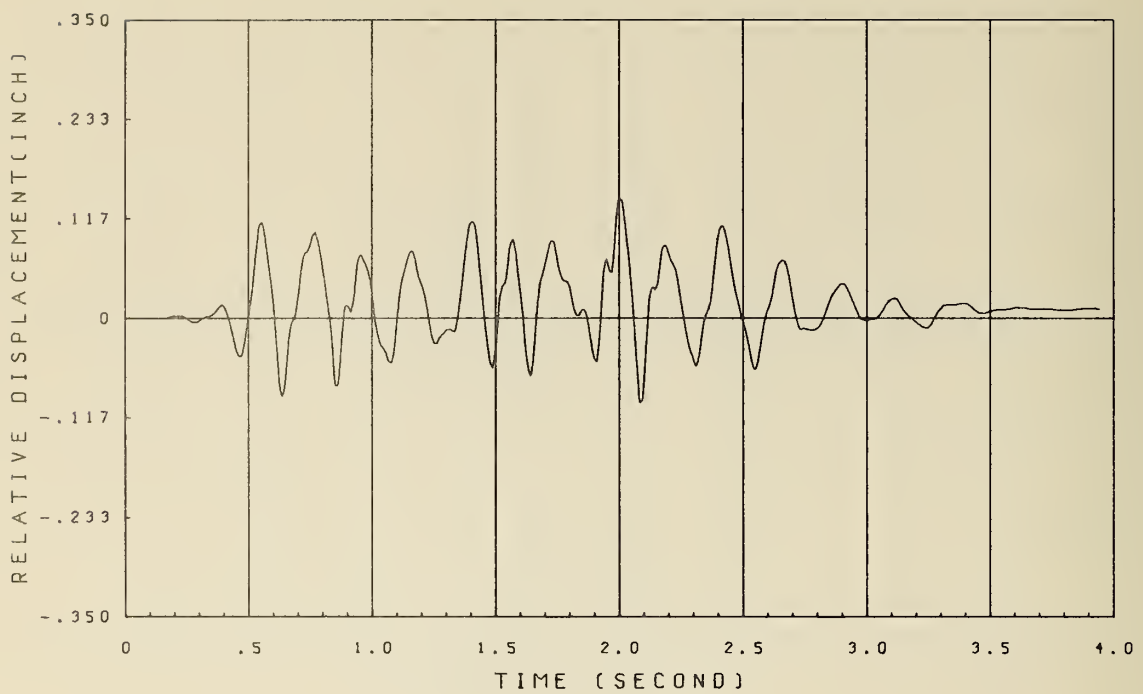


FIG. 4.16.5 MEASURED RESPONSE OF SIDE GIRDER NO. 2; TRANSVERSE (Y) DIRECTION; TEST HV2

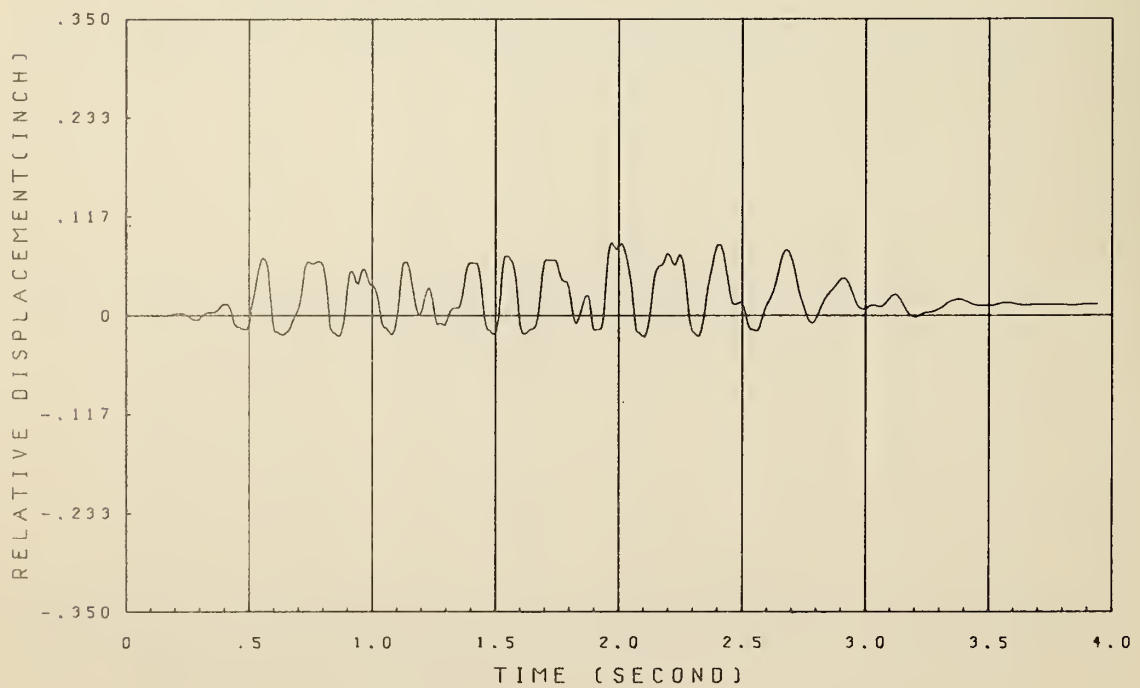


FIG. 4.16.6 MEASURED RESPONSE OF EXPANSION JOINT NO. 1; INNER SIDE; TEST HV2



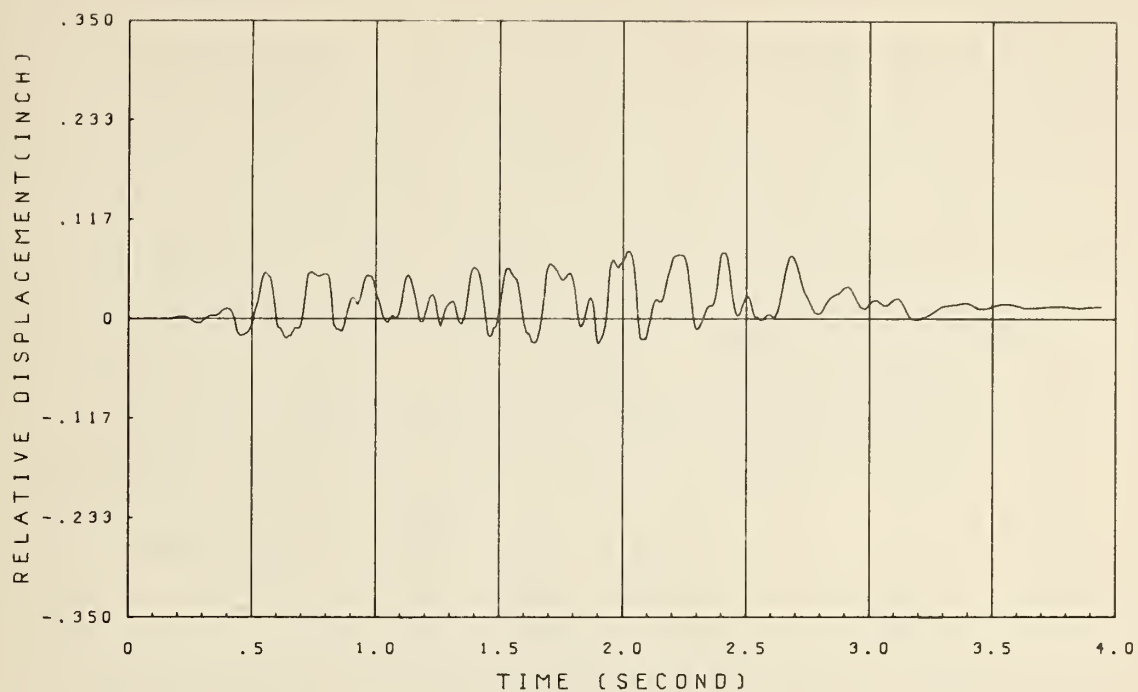


FIG. 4.16.7 MEASURED RESPONSE OF EXPANSION JOINT NO. 1; OUTER SIDE;  
TEST HV2

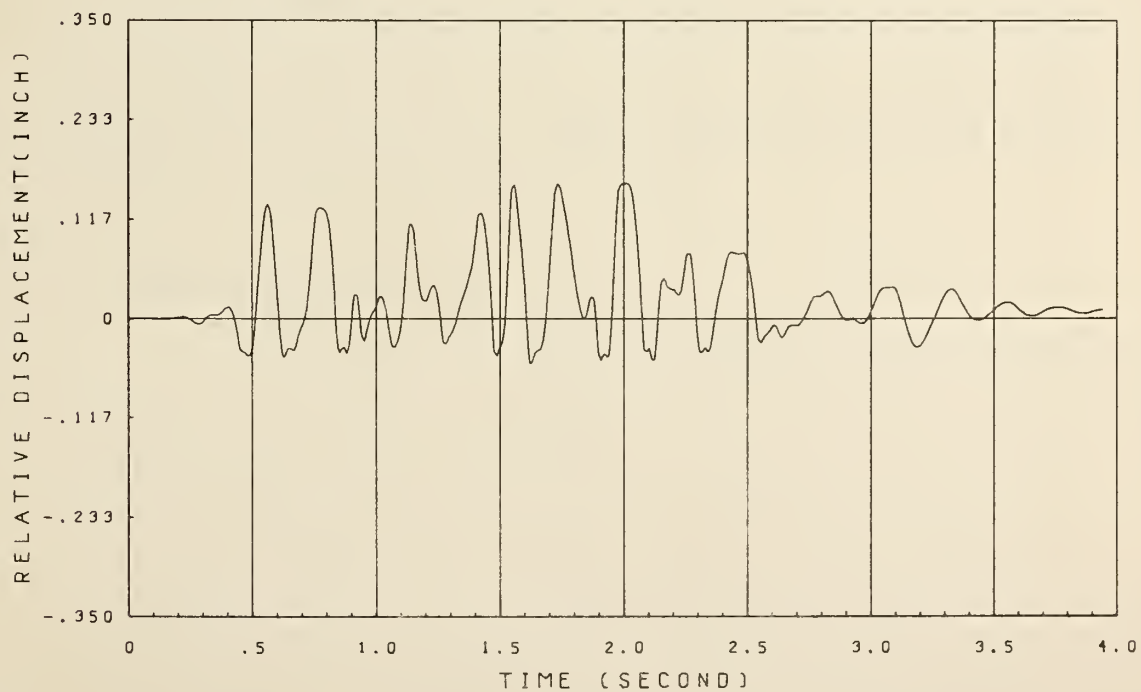


FIG. 4.16.8 MEASURED RESPONSE OF EXPANSION JOINT NO. 2; INNER SIDE;  
TEST HV2

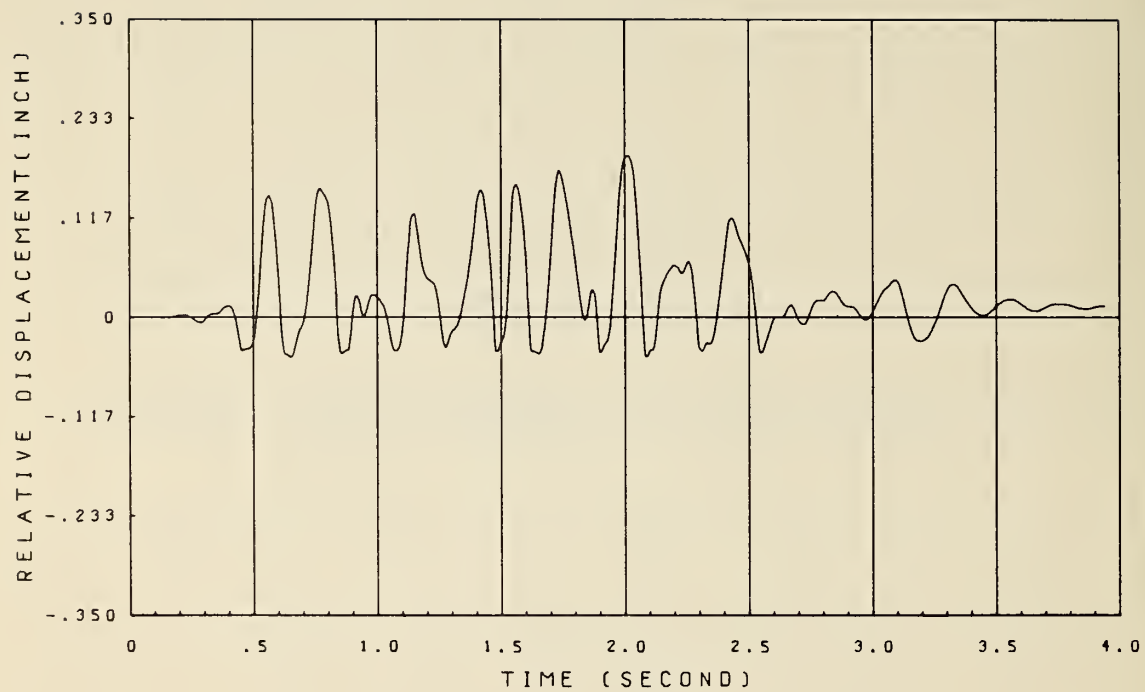


FIG. 4.16.9 MEASURED RESPONSE OF EXPANSION JOINT NO. 2; OUTER SIDE;  
TEST HV2

## V. FORMULATION OF A BASIC ANALYTICAL MODEL

The purpose of this chapter is to integrate the component stiffness properties and boundary conditions previously described into a basic analytical model that satisfies the dynamic characteristics of the experimental model observed under small amplitude free vibration and forced harmonic conditions. These small amplitude characteristics are considered a fundamental requirement of the analytical model to be used in predicting seismic responses of the experimental model.

### A. IDEALIZATION OF EXPERIMENTAL MODEL

During the free vibration and forced harmonic excitation tests, all components of the bridge model remained elastic. Therefore, the bridge model was treated as a linear three-dimensional discrete parameter system consisting of 55 nodal points. In this idealization, 24 linear curved beam elements representing the superstructure, 24 linear straight beam elements representing the columns, 2 linear elements representing the expansion joints and 2 boundary elements representing the abutments were used as shown in Fig. 5.1.

### B. BASIC ANALYTICAL MODEL

The component stiffness properties and boundary conditions previously presented are summarized again in Table 5.1. Except for the expansion joint properties, these characteristics have been fully verified for including in the basic analytical model. The various constraints provided by the expansion joint need further clarification however since they are important factors controlling the dynamic response characteristics of the analytical model. As previously shown in Fig. 4.4,

the force vs. relative displacement relation of the expansion joints is very complicated showing numerous changes in stiffness with relative displacement. When the relative displacement is very small, the effects of tie bars are negligible and slippages and collisions do not occur. In such cases, only the transverse shear key, the vertical restrainers and the rubber pad resist the relative movement between girders. Therefore in defining the analytical model, it is necessary that these constraints under small amplitude response be adequately modeled. First, a set of linear elastic springs were selected to resist the relative translational and rotational movements between the girders. The longitudinal stiffness  $k_x^{EJ}$  and the rotational stiffness  $k_{\theta z}^{EJ}$  around a vertical (z) axis were evaluated considering the shear stiffness of the rubber pad; thus,

$$\begin{aligned} k_x^{EJ} &\approx k_x^R = 2.28 \times 10^4 \text{ lbs/inch} \\ k_{\theta z}^{EJ} &\approx d^2/12 \cdot k_x^R = 1.4 \times 10^5 \text{ lb. inches/rad.} \end{aligned} \tag{71}$$

in which  $d$  represents width of the superstructure. Next, the vertical restrainers and the transverse shear key were assigned infinite stiffness to prevent vertical and transverse relative motions, respectively. With these prescribed constraints, three degrees of freedom were permitted in the joint, namely, rotations around  $x$  and  $y$  axes and uniform joint separation. These prescribed conditions (71) together with the stiffness and boundary conditions of Table 5.1 resulted in the following analytically predicted frequencies

$$\begin{aligned} f_L &= 4.1 \text{ Hz} && \text{longitudinal vibration} \\ f_T &= 7.0 \text{ Hz} && \text{transverse vibration} \\ f_V &= 9.2 \text{ Hz} && \text{vertical vibration} \end{aligned} \tag{72}$$

As described in Chapter IV, the measured natural frequencies of the experimental model were

$$\begin{aligned}
 F_L &\approx 5 \text{ Hz} && \text{longitudinal vibration} \\
 F_T &\approx 6.6 \text{ Hz} && \text{transverse vibration} \\
 F_V &\approx 9 \sim 10 \text{ Hz} && \text{vertical vibration}
 \end{aligned}
 \tag{73}$$

Comparing both sets of frequencies, it is apparent that the calculated frequencies are fairly close to their corresponding experimental values. Even so, this discrepancy was judged to be too great to satisfy modelling of the small amplitude dynamic characteristics of the experimental model. The reason for the discrepancy derived from disregarding the effects of tie bars, shear key, etc.

To remove the discrepancy, a parameter study was carried out by changing the pair of expansion joint stiffnesses. First, this study provided information on the effects of each individual stiffness on the low frequency characteristics of the model, and second it indicated the proper combination of stiffnesses to give best agreement of analytical and experimental frequencies. Table 5.2 shows the final results of this parameter study. Clearly, they show that stiffnesses  $k_x^{EJ}$ ,  $k_{\theta z}^{EJ}$  and  $k_y^{EJ}$  are more sensitive parameters than are stiffnesses  $k_{\theta x}^{EJ}$  and  $k_{\theta y}^{EJ}$ . The effects of the former three parameters on the calculated natural frequencies may be written as

$$\begin{aligned}
 f_L &\propto k_{\theta z}^{EJ} \\
 f_T &\propto k_x^{EJ} \quad \text{and} \quad k_y^{EJ}
 \end{aligned}
 \tag{74}$$



Further, it was found that the combination of stiffnesses giving best correlations of frequencies was

$$\begin{aligned}k_x^{EJ} &= 1.9 \times 10^4 \text{ lbs/inch} \\k_y^{EJ} &= 5 \times 10^4 \text{ lbs/inch} \\k_{\theta z}^{EJ} &= 10^7 \text{ lb. inches/rad.}\end{aligned}\tag{75}$$

The resulting natural frequencies were

$$\begin{aligned}f_L &= 5.0 \text{ Hz} \\f_T &= 6.7 \text{ Hz} \\f_V &= 9.3 \text{ Hz}\end{aligned}\tag{76}$$

It is interesting to note that the primary changes in stiffnesses given by Eqs. (71) and (75) are the introduction of  $k_y^{EJ}$  and a significant change in  $k_{\theta z}^{EJ}$ . Transverse stiffness  $k_y^{EJ}$  which resists relative transverse movement between the girders was incorporated into the analytical model not only to adjust the calculated natural frequencies but also because observations during experimental tests indicated that small transverse relative motions actually took place during high intensity excitations even though the transverse shear key prevented large relative motions to occur [26]. The high stiffness of  $5 \times 10^4$  lbs/inch selected for  $k_y^{EJ}$  was considered realistic in allowing small transverse relative motions to develop in the analytical model. The change in stiffness  $k_{\theta z}^{EJ}$  can be explained since  $k_{\theta z}^{EJ}$  as given by Eq. (71) was derived considering only the shear stiffness of the rubber pad. Actually, however, the transverse shear key gives some contribution

to  $k_{\theta z}^{EJ}$  since its corners and edges resist rotational movement, and the joint restrainer tie bars also make a contribution; thus, the incremental change in  $k_{\theta z}^{EJ}$  from Eq. (71) to Eq. (75) is reasonable.

Finally, the calculated lowest vibration mode shapes in the three major directions, namely, transverse, longitudinal and vertical, were checked against the observed vibration modes of the experimental model. As is shown in Fig. 5.2, it is apparent that all three of the calculated modes are very similar to the corresponding experimental modes.

Based on the discussion above, it is clear that the analytical model having stiffness properties and boundary conditions as shown in Table 5.1 and having the idealized expansion joint constraints as represented by Eq. (75) adequately satisfies the small amplitude dynamic characteristics of the experimental model. It should be noted however that since the spring stiffnesses representing the expansion joint constraints were modeled so that the low frequency characteristics of the analytical model correspond with those of the experimental model, all errors involved in determining the stiffness properties and the boundary conditions of the model are absorbed in the selected set of spring stiffnesses of expansion joints.

TABLE 5.1 STIFFNESS PROPERTIES AND BOUNDARY CONDITIONS OF EXPERIMENTAL MODEL

Component	Stiffnesses	Units	Determined Value	Procedure of Determination		
				Direct Measurement	Undirect Measurement	Calculated or Estimated
Super-Structure	Flexural Rigidity in Transverse Direction	lb. inches <sup>2</sup>	$1.8 \times 10^8$ for all girders	0		
	Flexural Rigidity in Vertical Direction	lb. inches <sup>2</sup>	$5.0 \times 10^8$ for all girders		0	0
	Axial Rigidity	lbs	$1.24 \times 10^7$ for all girders			0
	Torsional Rigidity	lb. inches <sup>2</sup>	$3.92 \times 10^7$ for all girders			0
Columns	Flexural Rigidity around Strong Axis	lb. inches <sup>2</sup>	$1.90 \times 10^7$ for COL-1A $1.90 \times 10^7$ for COL-2A $5.59 \times 10^6$ for COL-1B $5.41 \times 10^6$ for COL-2B	0		
	Flexural Rigidity around Weak Axis	lb. inches <sup>2</sup>	$3.39 \times 10^6$ for COL-1A $3.50 \times 10^6$ for COL-2A $1.39 \times 10^6$ for COL-1B $1.58 \times 10^6$ for COL-2B	0		

TABLE 5.1 - CONTINUED -

Component	Stiffnesses	Units	Determined Value	Procedure of Determination		
				Direct Measurement	Undirect Measurement	Calculated or Estimated
Columns	Axial Rigidity	lbs	$3.04 \times 10^7$ for COL-1A & 2A $1.43 \times 10^7$ for COL-1B & 2B			0
	Torsional Rigidity	lb. inches <sup>2</sup>	$6.00 \times 10^6$ for COL-1A & 2A $1.46 \times 10^6$ for COL-1B & 2B			0
Abutments	Rotational Stiffness around y axis	lb. inches/rad.	0	0		0
	Rotational Stiffness around z axis	lb. inches/rad.	$8 \times 10^6$		0	0
Expansion Joints	Shear Stiffness of Rubber Pad	lbs/inch	22800	0		
	Coefficient of Friction	—	0.4			0
	Elastic Stiffness of Tie Bar	lbs/inch	$6.47 \times 10^4$	0		
	Yield Strength of Tie Bar	lbs	650	0		

TABLE 5.2 EFFECT OF EXPANSION JOINT CONSTRAINTS ON CALCULATED LOW FREQUENCY CHARACTERISTICS OF BRIDGE MODEL

No. of Case	Purpose	Stiffnesses Representing EJ Constraints						Calculated Natural Frequencies		
		$k_x^{EJ}$	$k_y^{EJ}$	$k_{\theta x'}^{EJ}$	$k_{\theta y}^{EJ}$	$k_{\theta z}^{EJ}$		$f_L$	$f_T$	$f_V$
1	EFFECT OF $k_x^{EJ}$	$2.28 \times 10^4$	fixed	free	free	$1.4 \times 10^5$		4.07	6.95	9.23
2		$1.9 \times 10^4$	fixed	free	free	$1.4 \times 10^5$		4.06	6.66	9.20
3		$1.7 \times 10^4$	fixed	free	free	$1.4 \times 10^5$		4.05	6.47	9.18
4	EFFECT OF $k_{\theta z}^{EJ}$	$1.9 \times 10^4$	fixed	free	free	$10^6$		4.35	6.69	9.29
5		$1.9 \times 10^4$	fixed	free	free	$10^7$		4.95	6.73	9.33
6		$1.9 \times 10^4$	fixed	free	free	$10^8$		5.14	6.74	9.34
7	EFFECT OF $k_y^{EJ}$	$1.9 \times 10^4$	$10^5$	free	free	$10^7$		4.95	6.71	9.33
8		$1.9 \times 10^4$	$5 \times 10^4$	free	free	$10^7$		4.95	6.68	9.33
9		$1.9 \times 10^4$	$10^4$	free	free	$10^7$		4.93	6.49	9.30
10	EFFECT OF $k_{\theta x}^{EJ}$	$1.9 \times 10^4$	$5 \times 10^4$	fixed	free	$10^7$		5.07	6.74	9.33
11	EFFECT OF $k_{\theta y}^{EJ}$	$1.9 \times 10^4$	$5 \times 10^4$	free	fixed	$10^7$		5.00	6.71	11.39

1) Units - lbs/inch for translational stiffnesses and lb. inches/rad. for rotational stiffnesses

2)  $f_L$ : lowest natural frequency (Hz) in longitudinal (X) direction

$f_T$ : lowest natural frequency (Hz) in transverse (Y) direction

$f_V$ : lowest natural frequency (Hz) in vertical (Z) direction



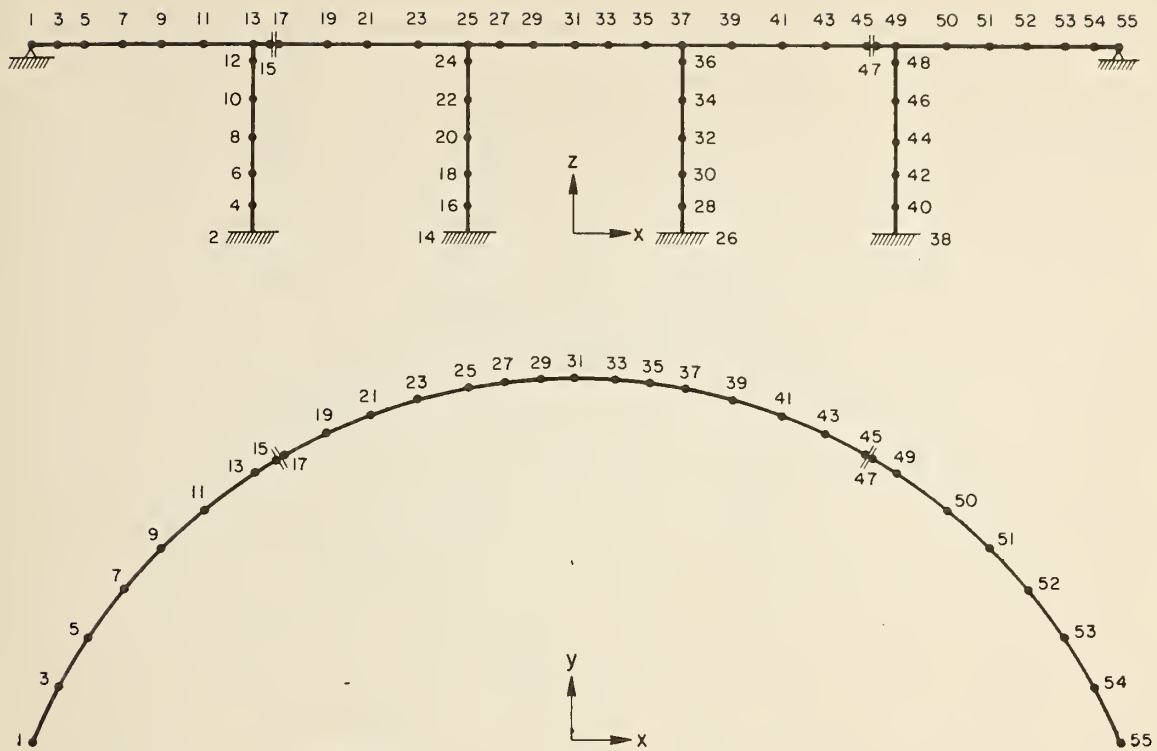


FIG. 5.1 ANALYTICAL MODEL OF BRIDGE MODEL

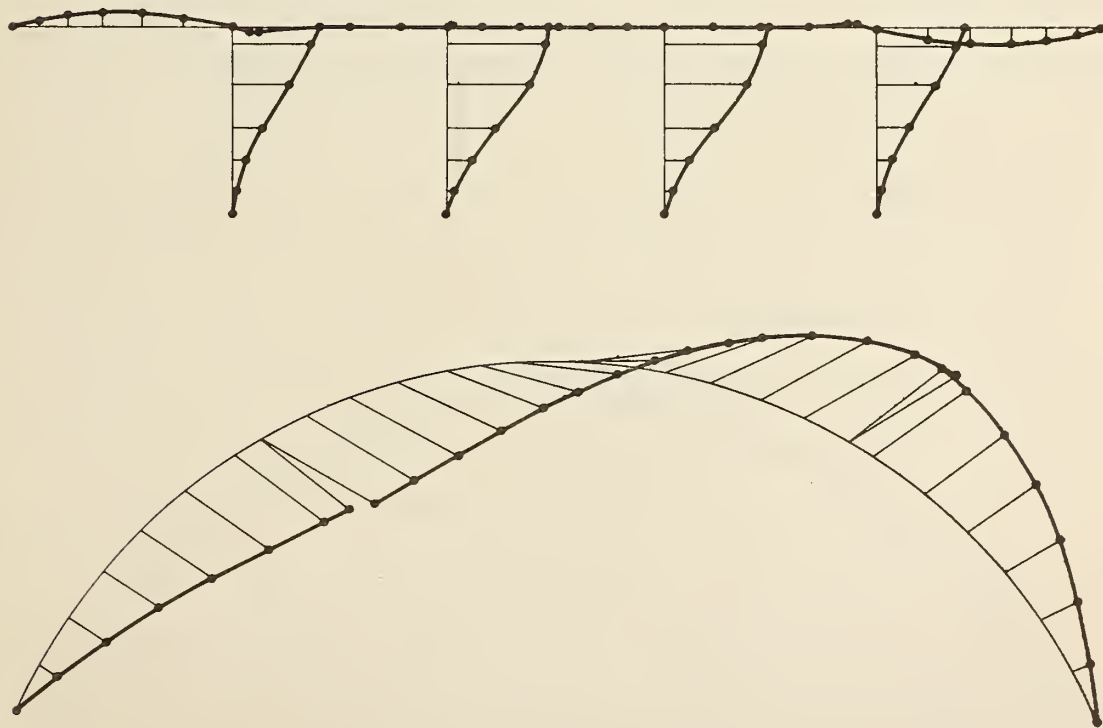


FIG. 5.2.1 CALCULATED LOWEST VIBRATION MODE; LONGITUDINAL (X) DIRECTION

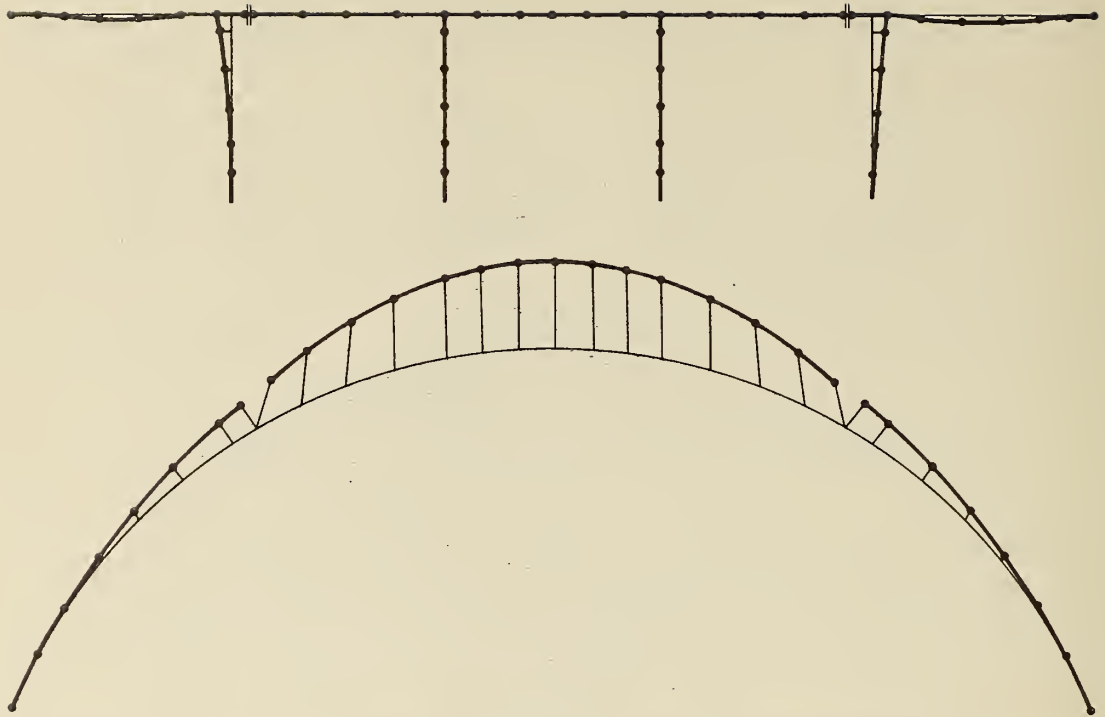


FIG. 5.2.2 CALCULATED LOWEST VIBRATION MODE; TRANSVERSE (Y) DIRECTION

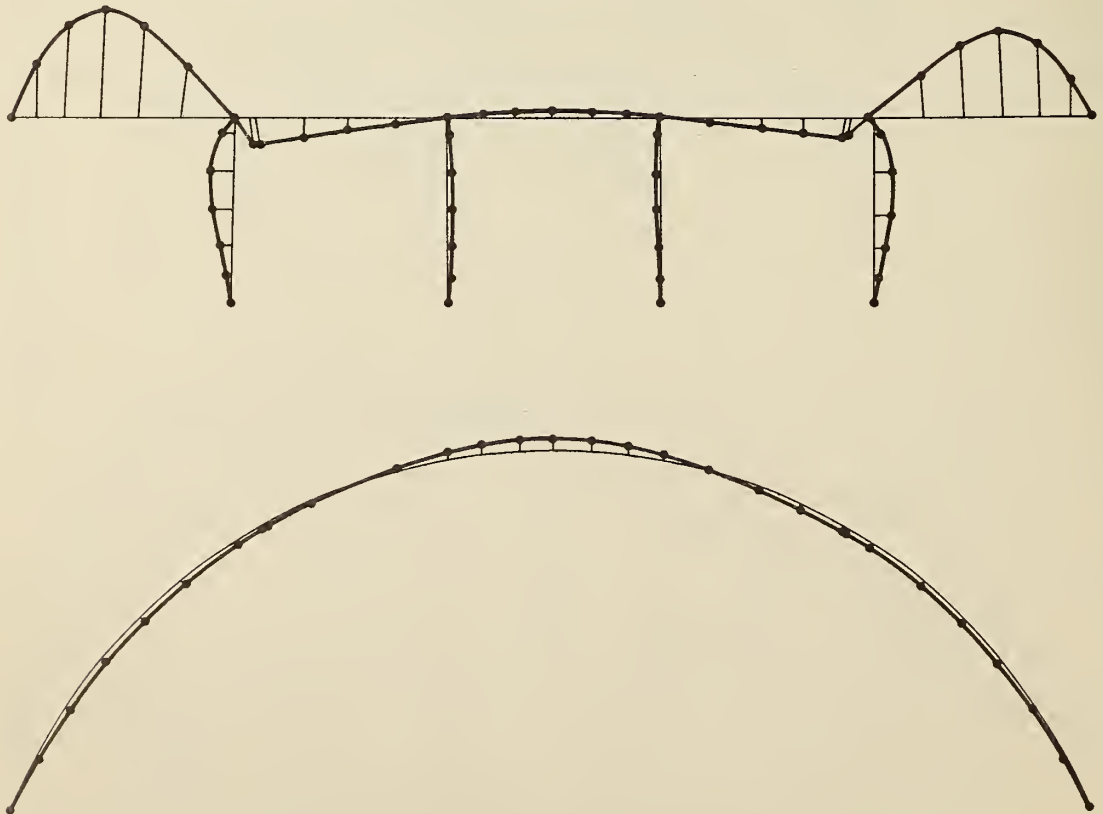


FIG. 5.2.3 CALCULATED LOWEST VIBRATION MODE; VERTICAL (Z) DIRECTION

## VI. ANALYTICAL PREDICTION OF SEISMIC RESPONSES

The purpose of this chapter is to correlate the measured responses of displacement of the experimental model with the linear and nonlinear responses determined analytically for the three seismic excitations, i.e. for Tests H1, H3 and HV2. The correlation was initiated with Test H1, since this test represented essentially linear elastic behavior. The correlation derived from this test was basic as it also represented the initial low amplitude behavior of the model during Tests H3, and HV2 which subsequently experienced high amplitude nonlinear behavior.

The correlation was made by comparing predicted and measured responses, paying particular attention to the agreement of maximum responses, phase relations, and the overall dynamic behavior.

### A. LOW INTENSITY SEISMIC EXCITATION (TEST H1)

1. Linear Analysis Correlation - The basic analytical model that satisfied the small amplitude dynamic characteristics of the experimental model was used in predicting seismic responses for Test H1. It was subjected to the table acceleration time-history shown in Fig. 4.11 in its transverse direction. A time interval of 0.01025 second was adopted for the numerical integration. A damping ratio of 6% of critical was assumed based on experimental evidence. Eq. (69) obtained from low intensity forced harmonic tests at amplitudes of vibration comparable to those developed in the Test H1.

Displacement response time-histories were calculated under these conditions and were compared with the corresponding experimental results. From these comparisons, it was found that although global behavior of the predicted response was similar to the measured response,

the correlation of individual peak amplitudes and their phase relations was relatively poor. Further, the predominant frequency of the predicted response was slightly higher than that of the measured response. This implied that the total stiffness of the basic analytical model was slightly higher than that of the experimental model under this particular seismic excitation. It was then decided to modify the stiffness of the analytical model slightly in order to make the phase lag discrepancies as small as possible. The overall stiffness of the expansion joints was chosen for this purpose since it dominated the low frequency characteristics of the model and also since it was the most uncertain property established from experimental evidence. Based on the parameter study represented by Eq. (74), it was apparent that either stiffness  $k_x^{EJ}$  or  $k_y^{EJ}$  should be changed in order to reduce the natural frequency of vibration in the transverse direction. As described in the previous chapter,  $k_y^{EJ}$  was introduced into the basic analytical model to permit some small transverse relative motions to develop at the expansion joints. It was clear therefore that stiffness of  $k_y^{EJ}$  should not be decreased from its original value since such a reduction would cause large transverse relative motions to take place. On the other hand, stiffness  $k_x^{EJ}$  was derived from the combined effects of the tie bars, slippages, etc.; thus, significant uncertainty was present in setting its numerical value. Hence,  $k_x^{EJ}$  was chosen to adjust the frequency and after some calculations, it was set at the value

$$k_x^{EJ} = 18400 \text{ lbs/inch} \quad (77)$$

giving lowest natural frequencies as follows:



$$\begin{aligned}
 f_L &= 4.9 \text{ Hz} && \text{longitudinal vibration} \\
 f_T &= 6.6 \text{ Hz} && \text{transverse vibration} \\
 f_V &= 9.3 \text{ Hz} && \text{vertical vibration}
 \end{aligned}
 \tag{78}$$

The resulting predicted response of displacement is shown in Fig. 6.1 together with the measured result. From this comparison it is seen that the predicted response agrees fairly well with that of the experimental model. The amplitudes of the predicted response are very close to those of the response which indicates that the established damping ratio of 6% was appropriate. As one would expect, the predicted response is essentially symmetric both in the outward and inward directions while the measured response is somewhat unsymmetric due to differences in the joint restrainer tie bar properties. This feature can be observed more clearly by comparing the responses of expansion joints.

The above correlation clearly indicates that the measured response during Test H1 could be predicted with fairly good accuracy using a linear analytical model provided its fundamental natural frequency in the direction of excitation agreed well with the experimental value and provided the proper damping factor was introduced into the analysis. It is quite evident however that the unsymmetric response caused by differences in the discontinuous expansion joint constraints cannot be predicted using the linear analytical model.

2. Nonlinear Analysis Correlation - For this correlation study, the linear expansion joint element previously used was replaced by the nonlinear element. It was necessary therefore to change the stiffnesses associated with the tie bars. In the linear analysis correlation, the constraints of the expansion joints were modeled by the following set of linear spring stiffnesses:



$$\begin{aligned}
 k_x^{EJ} &= 18400 \text{ lbs/inch}, \quad k_y^{EJ} = 50000 \text{ lbs/inch} \\
 k_{\theta z}^{EJ} &= 10^7 \text{ lb. inches/rad.}
 \end{aligned}
 \tag{79}$$

For the present nonlinear analysis correlation, it is not necessary to change  $k_y^{EJ}$  since the tie bars do not affect relative transverse motion at the expansion joints. On the other hand, stiffnesses  $k_x^{EJ}$  and  $k_{\theta z}^{EJ}$  are directly dependent upon the tie bars. Therefore, they must be modified. To accomplish these changes, the force vs. relative displacement relation shown in Fig. 4.4 was used. In Test H1 the maximum relative movements developed at the expansion joints were approximately + 0.01 inch (separation) and - 0.025 inch (closing). When a Coulomb friction coefficient of 0.4 is prescribed, the elastic shear deformation of the rubber pad is approximately 0.01 inch beyond which slippage takes place between the contact surface of the expansion joint. By comparing the amount of relative movement developed during excitation and the amount of shear deformation possible in the rubber pad, it is clear that maximum slippages of the order of 0.015 inch took place at the expansion joints. Since the amount of slippage in Test H1 was very small, it was decided not to introduce Coulomb type friction force in this analysis. It was then decided to take account of the small slippages approximately by linearizing the force vs. relative displacement relation. Thus, the longitudinal linearized stiffness  $k_{x,\ell}^{EJ}$  was estimated from Fig. 4.4 as

$$k_{x,\ell}^{EJ} \approx 9000 \text{ lbs/inch} \tag{80}$$

The stiffness  $k_{\theta z}^{EJ}$  was also changed for the same reason described above resulting in the value

$$k_{\theta z}^{EJ} = 6 \times 10^6 \text{ lb. inches/rad.} \quad (81)$$

Damping coefficients  $\alpha$  and  $\beta$  were assigned values so that the damping ratio of 6% of critical would be achieved for the first and second normal modes of vibration as calculated by the linear analytical model. The initial tie gaps  $\Delta_T$  were assigned zero values based on measurements taken just prior to the test which showed that they were very small.

The nonlinear analytical model defined above was subjected to the table acceleration time-history as used in the linear analysis correlation. A time interval of 0.01025 second was adopted for the numerical integration. Equilibrium iteration was used both alone and with the subdivision of time intervals into 3 equidistant sub-time intervals, when needed. The tolerances used to control the equilibrium iteration and the subdivision defined in Eqs. (51) and (62) were

$$\begin{aligned} \Delta_{ps} &= 0.01 && \text{equilibrium iteration} \\ \Delta_{ps} &= 0.08 && \text{subdivision} \\ \Delta_{us}^I &= 0.001 \end{aligned} \quad (82)$$

The predicted displacement response was compared with the experimentally measured result and it was found that the predicted response was substantially improved as compared with the linear analysis correlation although discrepancies were still observed both in the peak amplitudes and their phase relations. The largest discrepancy was seen at the expansion joints where openings of the gaps were excessively suppressed by the tie bars. Because of this discrepancy, it was decided

to change the originally assumed zero tie gaps to small realistic values. Hence, both the assumed linearized stiffness of  $k_{x,\ell}^{EJ}$  and the initial tie gaps were adjusted; finally, giving good correlation under the conditions

$$\begin{aligned} k_{x,\ell}^{EJ} &= 10000 \text{ lbs/inch} \\ \Delta_T &= 0.05 \text{ inch for both expansion joints} \end{aligned} \tag{83}$$

The comparative plots of predicted and measured responses are shown in Fig. 6.2. Excellent agreement can be seen for these responses at the center point of the model and at both expansion joints, and the unsymmetrical vibration shown by the experimental response is well followed in the analysis. The predicted responses of force induced in the tie bars are shown in Fig. 6.3. Since the maximum value of the predicted tie bar force is approximately 400 lbs, yielding of the tie bar was not indicated by analysis which is consistent with the observed results.

#### B. HIGH INTENSITY SEISMIC EXCITATION (TEST HV2)

1. Linear Analysis Correlation - To carry out the linear analysis correlation for Test HV2, the same linear model previously described for Test H1 was used. This analytical model was subjected to the measured table accelerations in both the transverse and vertical directions. A time interval of 0.01026 second was used throughout the correlation. Although it was somewhat questionable if the same viscous damping ratio as used in Test H1 should be used for this test due to the high amplitude motion, it was decided to use the same 6% of critical as a first trial.

The responses predicted on this basis were compared with the measured results as shown in Fig. 6.4. As can be seen, the predicted



response is significantly different from the measured response both in the magnitude of peak amplitudes and in the frequency characteristics. It soon became apparent from this correlation that several collisions within the joints and yielding of the tie bars do not allow the linear analysis acceptable correlations. Therefore, to obtain reasonable correlation, one must introduce these effects into the analytical model. Thus, further correlation using the linear analytical model after adjusting parameters was not attempted for Test HV2.

2. Nonlinear Analysis Correlation - In order to introduce the effects of collisions and yielding of tie bars into the analysis, the nonlinear analytical model formulated for the correlation of the Test H1 was further modified.

First, the modeling of constraints in the expansion joint was reviewed. The assumed force vs. relative displacement relation shown in Fig. 4.4 was again used for this purpose. A principal difference in the seismic responses between this test and the Test H1 is the amplitude level. For example, the maximum relative displacements at expansion joint No. 2 are approximately + 0.2 inch (opening) and - 0.05 inch (closing) in this test which are roughly 10 times those values developed during Test H1. It is apparent from these large relative movements that slippages of large amplitude took place during the excitation. Thus, instead of using the linearized stiffness  $k_{x,l}^{EJ}$  as in Test H1, one must now introduce the Coulomb friction which can be modeled by an elastoplastic hysteretic relation. The initial elastic slope of this Coulomb friction relation was taken equal to the shear stiffness of the rubber pad  $k_x^R$ . By doing so, the assumed relation of Fig. 4.4 can be exactly modeled in the analysis. Stiffnesses  $k_y^{EJ}$  and  $k_{\theta z}^{EJ}$  were

unchanged from Test H1 since they do not affect the Coulomb friction force.

Impact springs were incorporated into the analytical model to take account of joint collisions. The stiffness of the impact spring  $k_I$  was taken equal to  $10^7$  lbs/inch which is nearly the same magnitude as the longitudinal stiffnesses of the curved beam elements representing the superstructure. The initial joint gaps  $\Delta_G$  were determined from the measured experimental responses of expansion joints. Since the joint gaps were changing with each collision and also were not identical between the inner and outer edges, the following joint gaps were obtained by taking averages

$$\begin{aligned}\Delta_G &= 0.025 \text{ inch} && \text{expansion joint No. 1} \\ \Delta_G &= 0.040 \text{ inch} && \text{expansion joint No. 2}\end{aligned}\tag{84}$$

Finally, initial tie gaps  $\Delta_T$  were prescribed on the basis of measured information as

$$\begin{aligned}\Delta_T &= 0.01 \text{ inch} && \text{expansion joint No. 1} \\ \Delta_T &= 0.02 \text{ inch} && \text{expansion joint No. 2}\end{aligned}\tag{85}$$

Since no experimental data was available to estimate damping factors for the experimental model under high intensity excitations, the same damping coefficients  $\alpha$  and  $\beta$  used for the correlation of Test H1 were adopted as a first trial. As before, these values represent 6% viscous damping in the first and second normal modes of vibration.

After introducing these data into the nonlinear analytical model, it was subjected to the table accelerations in the same manner as done



previously for the linear analysis correlation. The equilibrium iteration was used both alone and with the subdivision of time intervals into 5 equidistant sub-time intervals, when needed. The tolerances used to control the equilibrium iteration and the subdivision of time interval were

$$\begin{aligned}\Delta_{ps} &= 0.01 && \text{equilibrium iteration} \\ \Delta_{ps} &= 0.07 && \text{subdivision} \\ \Delta_{us}^I &= 0.005\end{aligned}\tag{86}$$

From this first correlation, it was found that although the overall response was substantially improved as compared with the linear analysis correlation, it was not satisfactory. The discrepancies were primarily derived from excessive constraint of the tie bars at both expansion joints and from over estimation of the damping force. The former reason indicated that the assumed initial tie gaps were too small; therefore, similar to the correlation of Test H1, the assumed initial tie gaps were increased. In order to interpret the latter reason, all three sources of damping in the analytical model were examined, i.e. the 6% viscous damping which was proportional to both mass distribution and stiffness distribution, Coulomb type damping associated with slippages at the expansion joints, and hysteretic damping associated with yielding of the tie bars. The 6% viscous damping was originally derived from the results of small amplitude forced harmonic excitations. The actual damping in these tests however was probably more in the form of structural damping due to the form of energy dissipation at the expansion joints and abutments. Particularly in view of the fact that damping in the sound microconcrete of the superstructure and columns would be small.

Therefore, when collisions take place and high frequency vibration response is induced, modelling of damping using the same 6% of viscous damping most likely would overestimate this form of energy dissipation.

Thus, changing both the assumed initial tie gaps and the viscous damping ratio, a best correlation was achieved under the conditions

$$\xi = 2\% \text{ of critical for first and second modes of vibration} \quad (87)$$

and

$$\begin{aligned} \Delta_T &= 0.03 \text{ inch} && \text{expansion joint No. 1} \\ \Delta_T &= 0.045 \text{ inch} && \text{expansion joint No. 2} \end{aligned} \quad (88)$$

Comparative plots of the predicted response with the measured response are shown in Fig. 6.5. Apparently the nonlinear analysis correlation is greatly superior to the linear analysis correlation. Clearly, the effect of multiple collisions and constraints of the joint restrainer tie bars are realistically represented in the nonlinear analytical model, see Fig. 6.6. Severe yielding of the tie bars developed maximum ductility factors  $\mu_T$ , defined as the ratio of the maximum tie elongation to its yield elongation, i.e.,

$$\mu_T = \frac{u_T^E + u_T^P}{u_T^E} \quad (89)$$

where

$$\begin{aligned} u_T^E &: \text{elastic elongation of tie bar} \\ u_T^P &: \text{plastic elongation of tie bar} \end{aligned}$$

equal to approximately 4 and 12 for expansion joints No. 1 and No. 2, respectively. Figure 6.7 shows the contact force between girders caused

by collisions. The maximum contact force of approximately 4000 lbs was induced at the expansion joint No. 2. Predicted stresses of the columns did not reach to their yield strength; therefore, no plastic deformation was developed during the test.

### C. HIGH INTENSITY SEISMIC EXCITATION (TEST H3)

1. Linear Analytical Correlation - Since it was apparent from the correlation of Test HV2 that the linear analysis could not achieve good results for high intensity excitations, the linear analysis correlation was performed only to provide comparative response data with the non-linear analysis correlation.

The same linear analytical model used for Test HV2 was used for Test H3. It was subjected to the table motion as measured in the transverse direction. A time interval of 0.01025 second was adopted throughout this correlation. The comparative plots of the predicted and measured response are shown in Fig. 6.8. Like test HV2, the linearly predicted response is very much different from the measured response.

2. Nonlinear Analysis Correlation - Since the general behavior of responses in this excitation test is essentially the same as in Test HV2, the nonlinear analytical model formulated for Test HV2 was again used. The same damping factors, Coulomb friction coefficient, impact springs and tie bars were employed. The initial tie and joint gaps were chosen in the same manner described previously giving

$$\begin{aligned} \Delta_T &= 0.05 \text{ inch}, & \Delta_G &= 0.04 \text{ inch} & \text{expansion joint No. 1} \\ \Delta_T &= 0.1 \text{ inch}, & \Delta_G &= 0.05 \text{ inch} & \text{expansion joint No. 2} \end{aligned} \quad (90)$$

Comparative plots of the predicted and the measured responses are shown in Fig. 6.9. Like Test HV2, the nonlinear analysis correlation is

greatly superior to the linear analysis correlation. Although permanent drifts take place in the measured response from approximately 2.1 seconds, it is beyond the scope of this analytical correlation to predict them as explained in Chapter IV. By comparing the predicted and measured responses at expansion joint No. 2, it is assessed that the critical failure of the shear key most likely was caused by a collision which took place at approximately 2 seconds. Figure 6.10 shows the predicted tie bar forces and tie yieldings of both expansion joints. The tie bar ductility factor  $\mu_T$  defined in Eq. (89) reached approximately 10 and 13 at expansion joints No. 1 and No. 2, respectively. Figure 6.11 shows the contact force between girders caused by collisions. A maximum contact force of approximately 8000 lbs was induced at expansion joint No. 2. Like Test HV2, yielding of columns did not develop during the test.

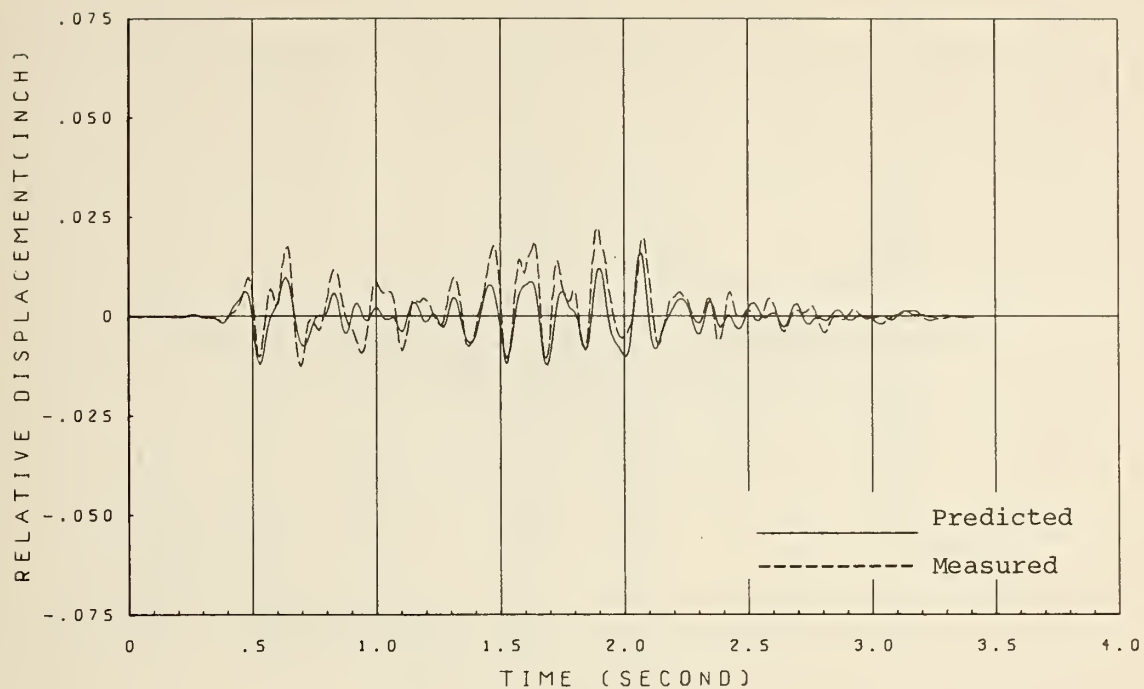


FIG. 6.1.1 LINEAR CORRELATION FOR TEST H1; SIDE GIRDER NO. 1;  
LONGITUDINAL (X) DIRECTION

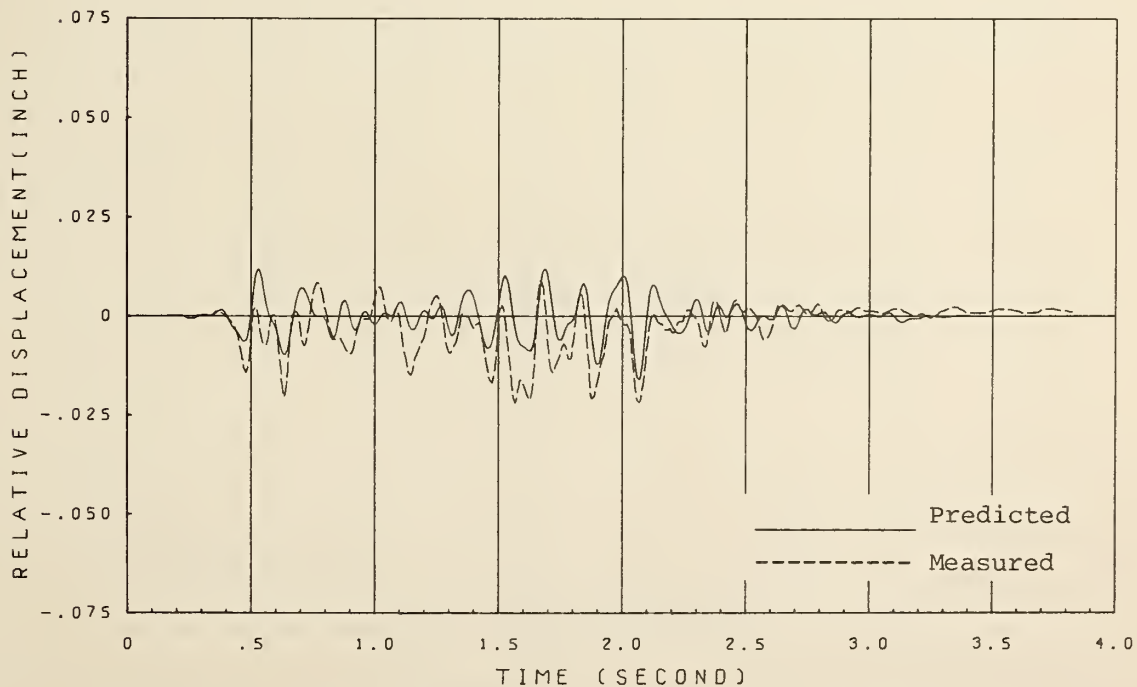


FIG. 6.1.2 LINEAR CORRELATION FOR TEST H1; SIDE GIRDER NO. 1;  
TRANSVERSE (Y) DIRECTION



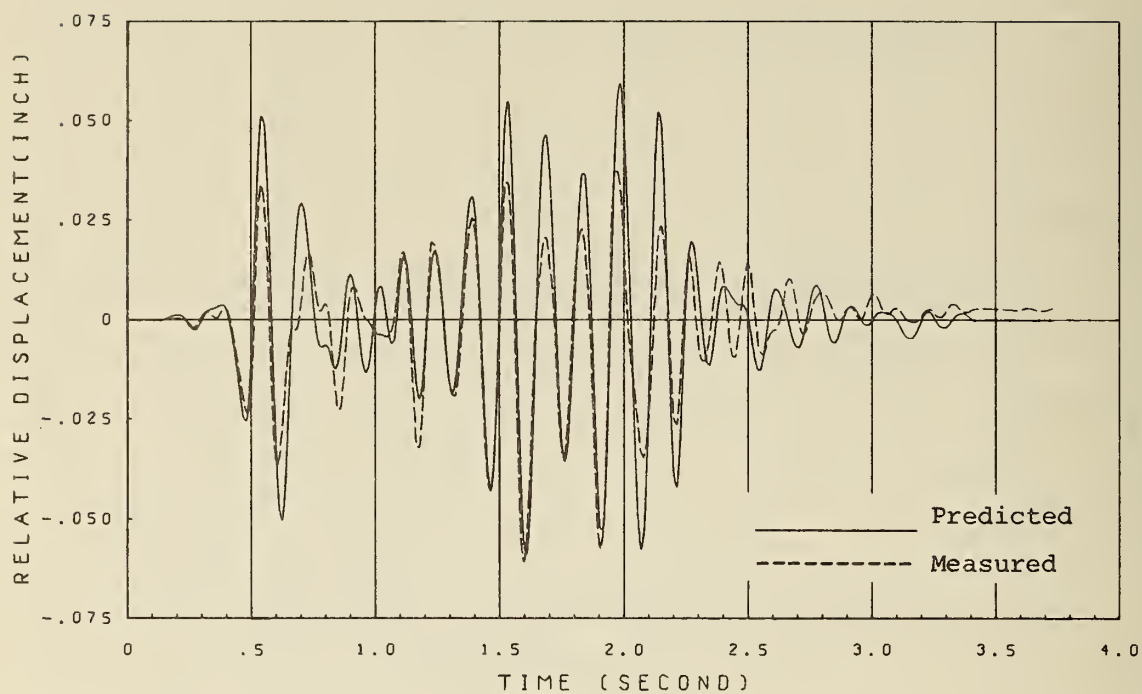


FIG. 6.1.3 LINEAR CORRELATION FOR TEST H1; CENTER GIRDER;  
TRANSVERSE (Y) DIRECTION

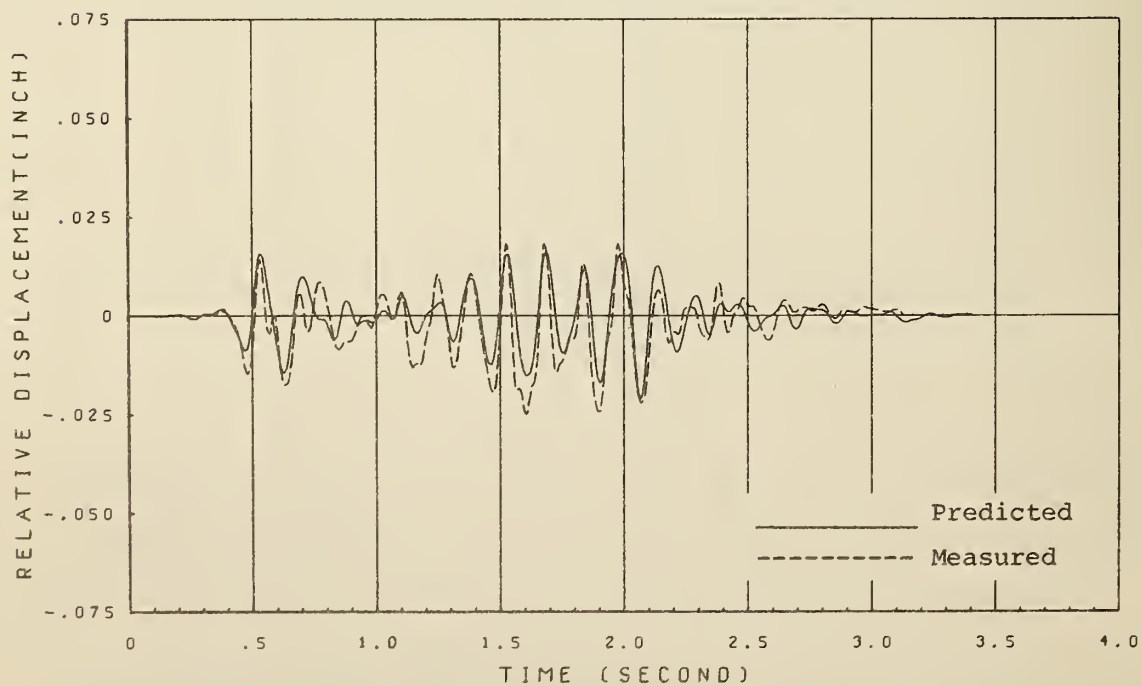


FIG. 6.1.4 LINEAR CORRELATION FOR TEST H1; SIDE GIRDER NO. 2;  
LONGITUDINAL (X) DIRECTION

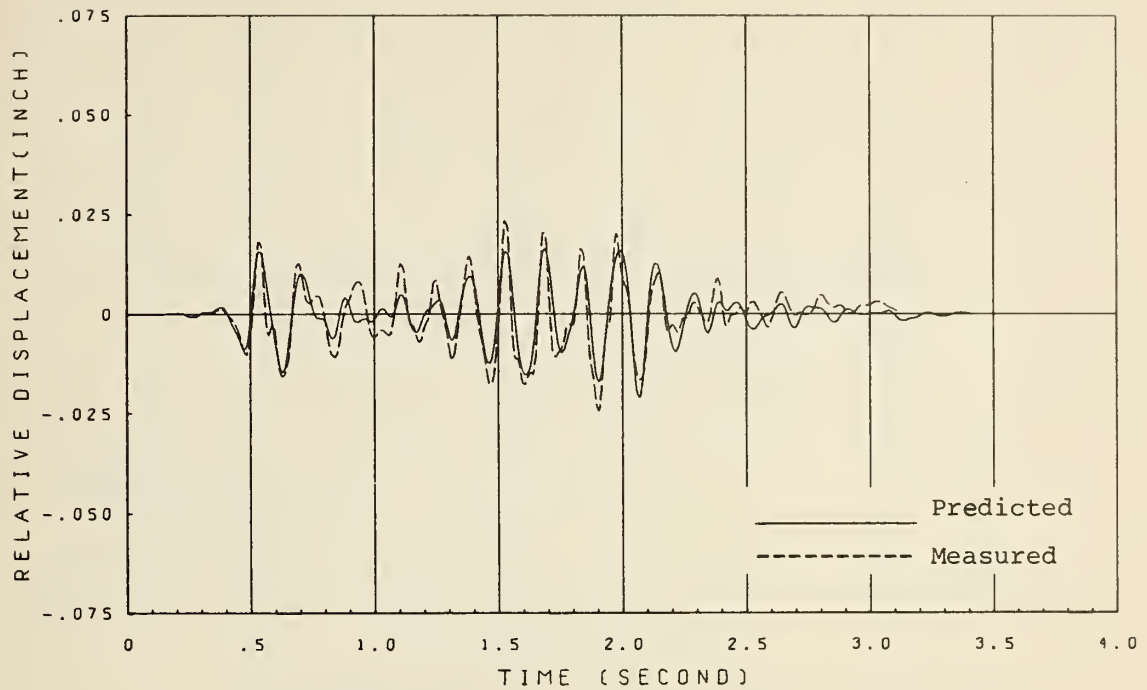


FIG. 6.1.5 LINEAR CORRELATION FOR TEST H1; SIDE GIRDER NO. 2;  
TRANSVERSE (Y) DIRECTION

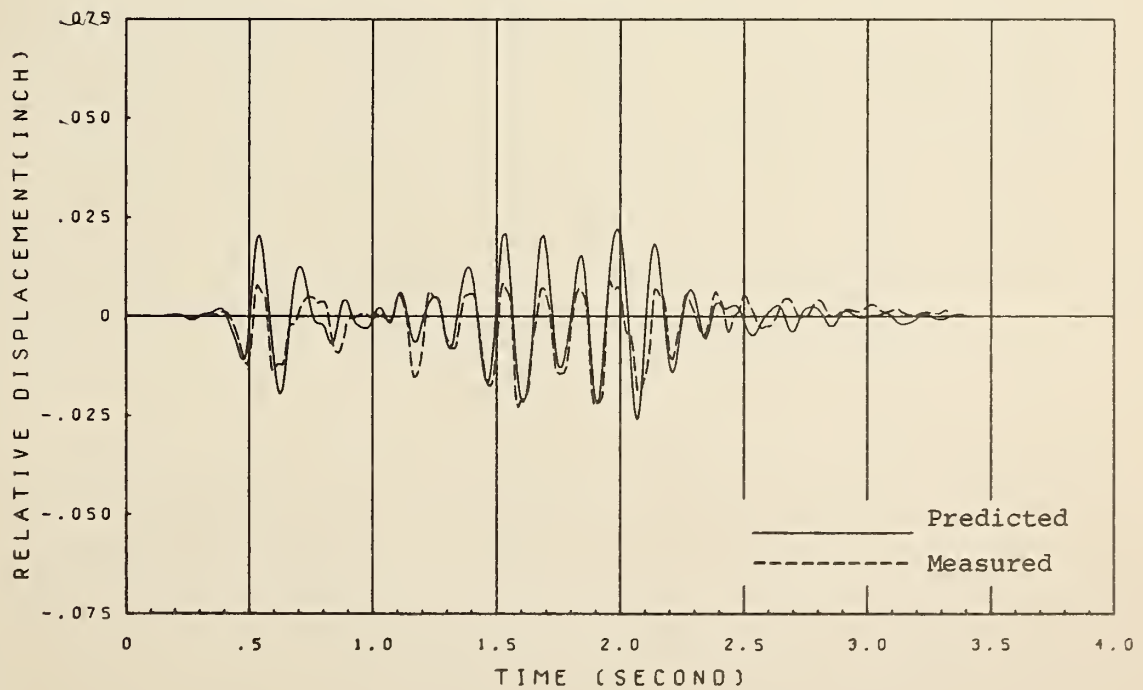


FIG. 6.1.6 LINEAR CORRELATION FOR TEST H1; EXPANSION JOINT NO. 1;  
INNER SIDE

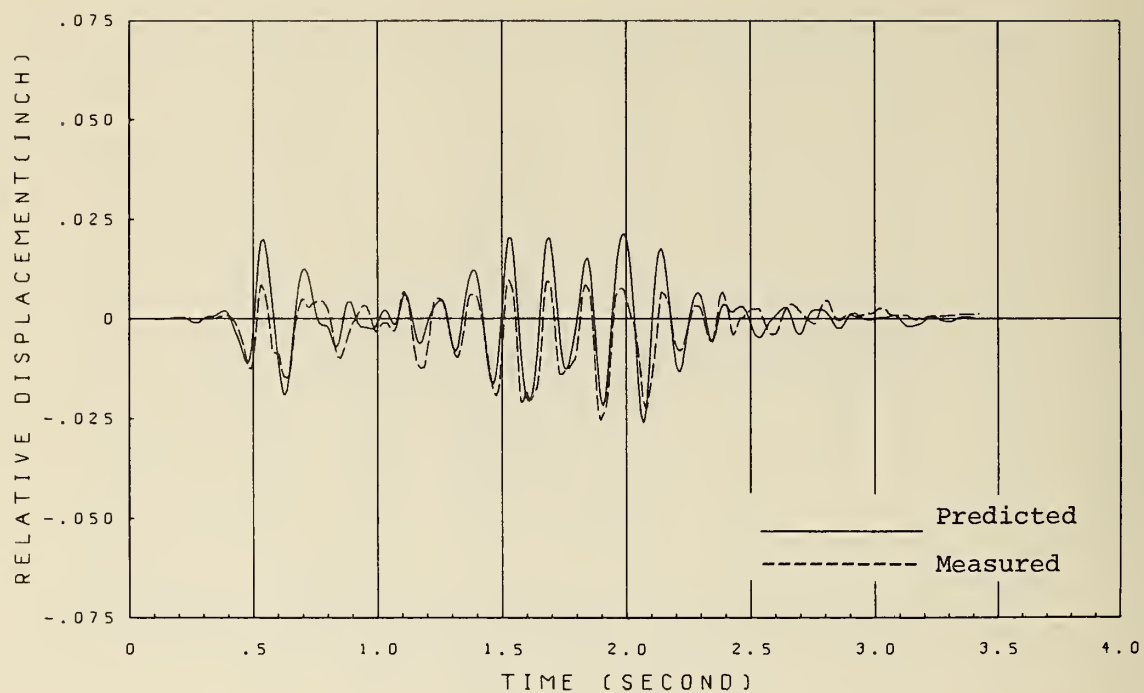


FIG. 6.1.7 LINEAR CORRELATION FOR TEST H1; EXPANSION JOINT NO. 1;  
OUTER SIDE

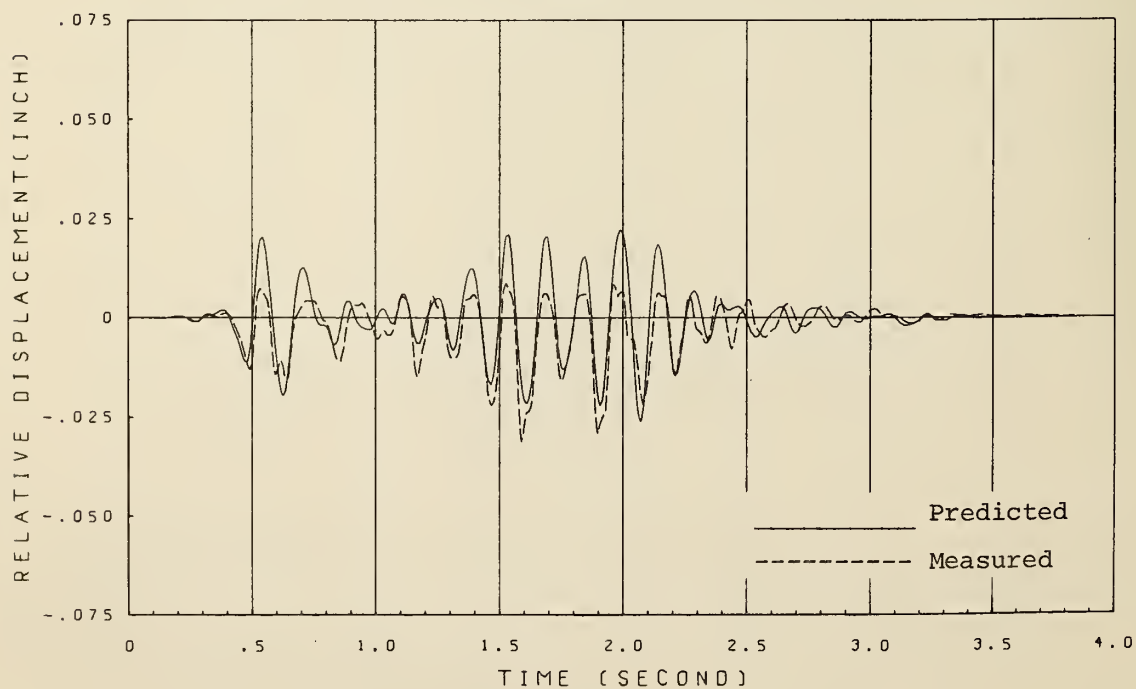


FIG. 6.1.8 LINEAR CORRELATION FOR TEST H1; EXPANSION JOINT NO. 2;  
INNER SIDE

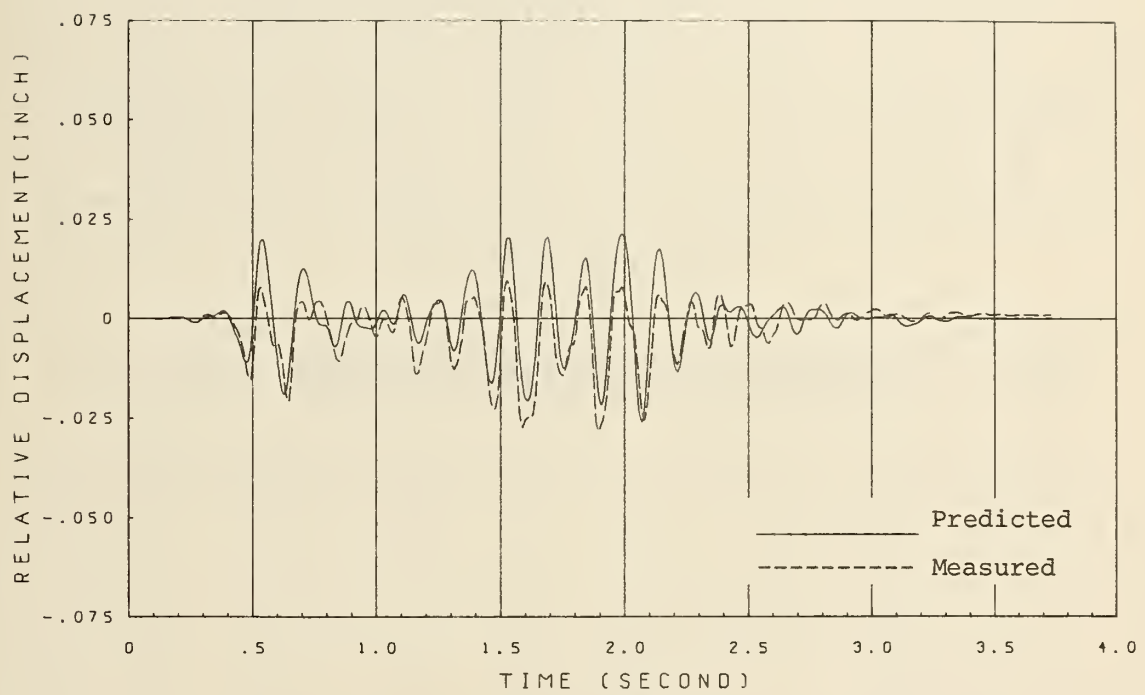


FIG. 6.1.9 LINEAR CORRELATION FOR TEST H1; EXPANSION JOINT NO. 2;  
OUTER SIDE

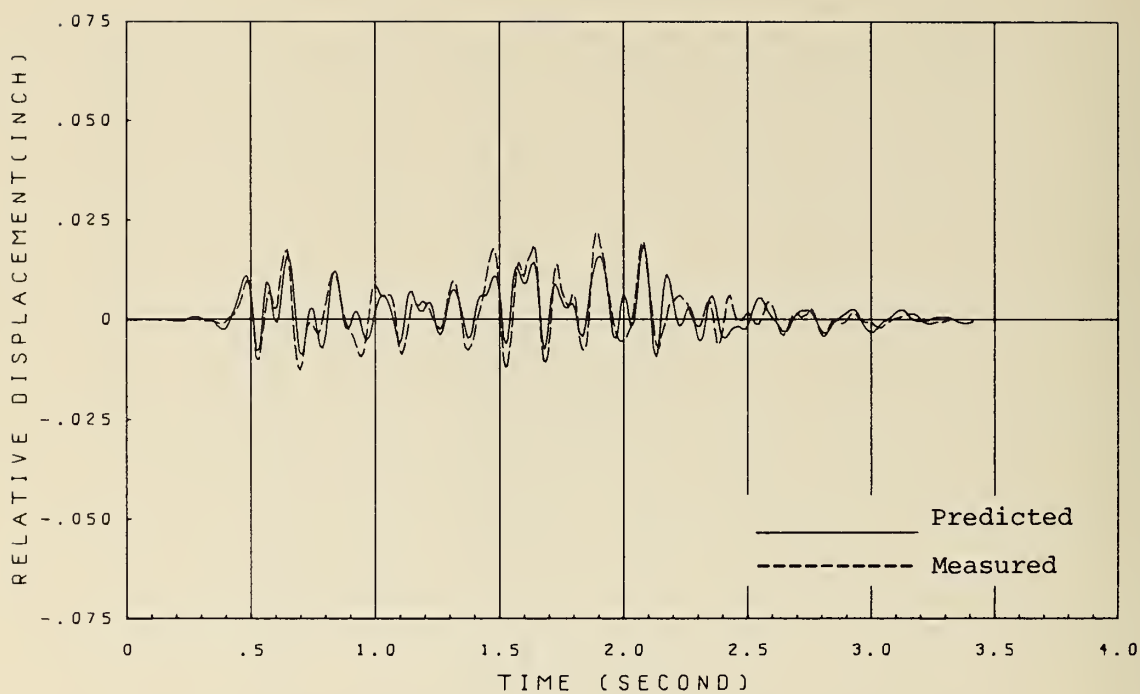


FIG. 6.2.1 NONLINEAR CORRELATION FOR TEST H1; SIDE GIRDER NO. 1;  
LONGITUDINAL (X) DIRECTION

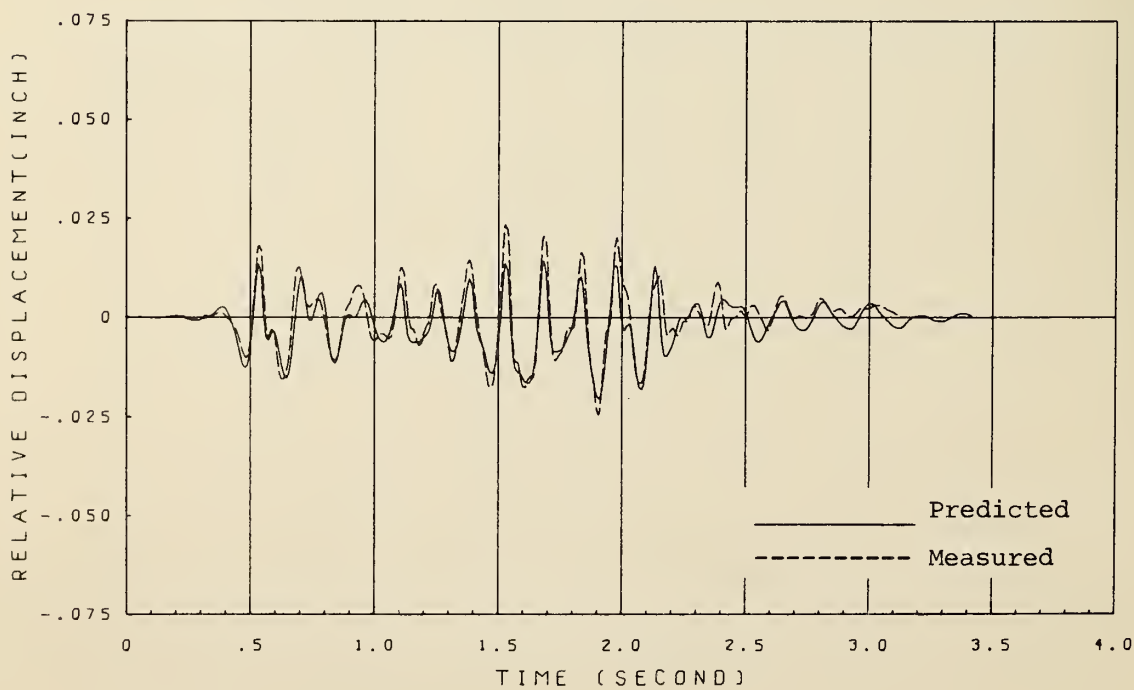


FIG. 6.2.2 NONLINEAR CORRELATION FOR TEST H1; SIDE GIRDER NO. 1;  
TRANSVERSE (Y) DIRECTION



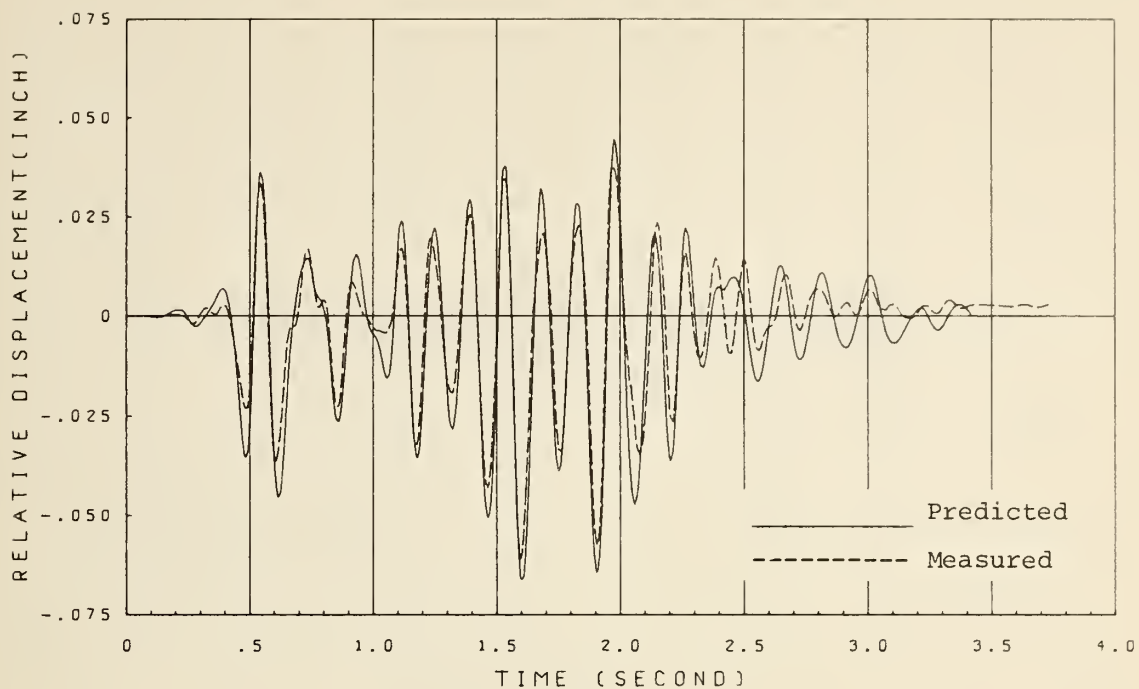


FIG. 6.2.3 NONLINEAR CORRELATION FOR TEST H1; CENTER GIRDER;  
TRANSVERSE (Y) DIRECTION

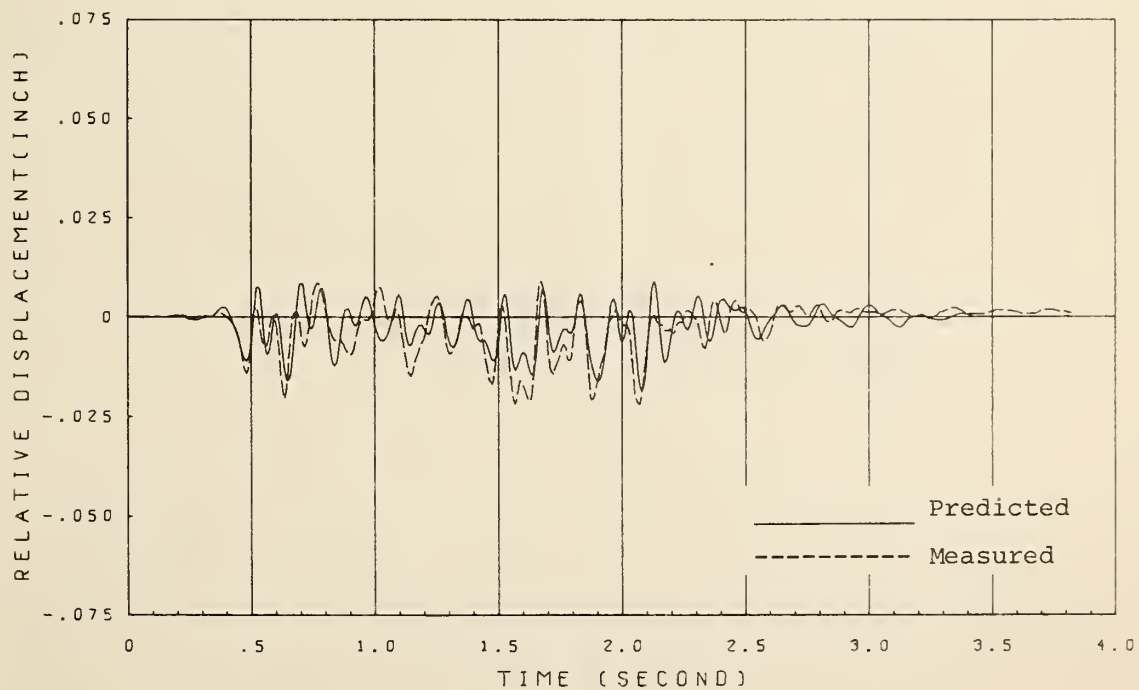


FIG. 6.2.4 NONLINEAR CORRELATION FOR TEST H1; SIDE GIRDER NO. 2;  
LONGITUDINAL (X) DIRECTION

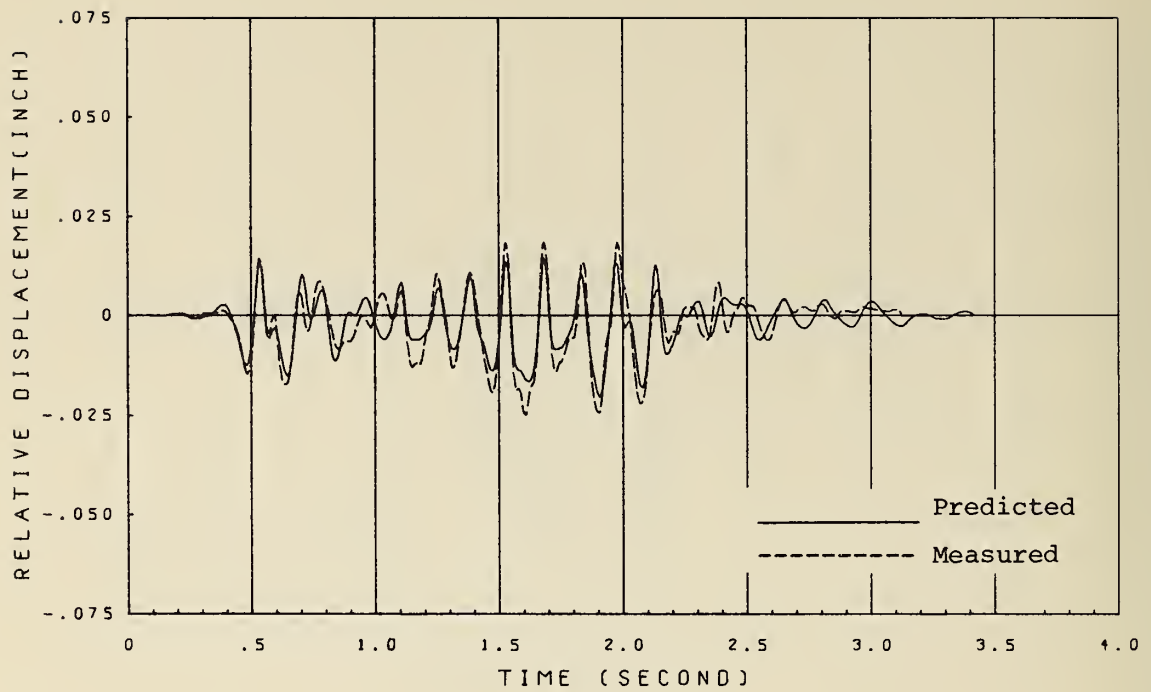


FIG. 6.2.5 NONLINEAR CORRELATION FOR TEST H1; SIDE GIRDER NO. 2;  
TRANSVERSE (Y) DIRECTION

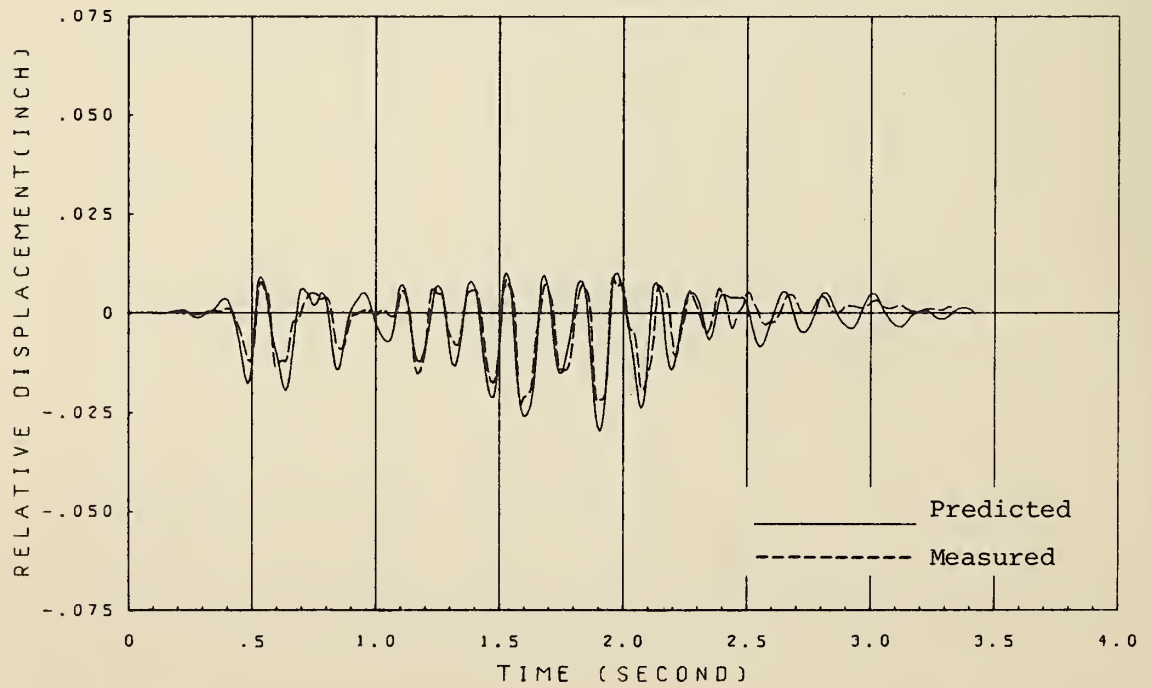


FIG. 6.2.6 NONLINEAR CORRELATION FOR TEST H1; EXPANSION JOINT NO. 1;  
INNER SIDE

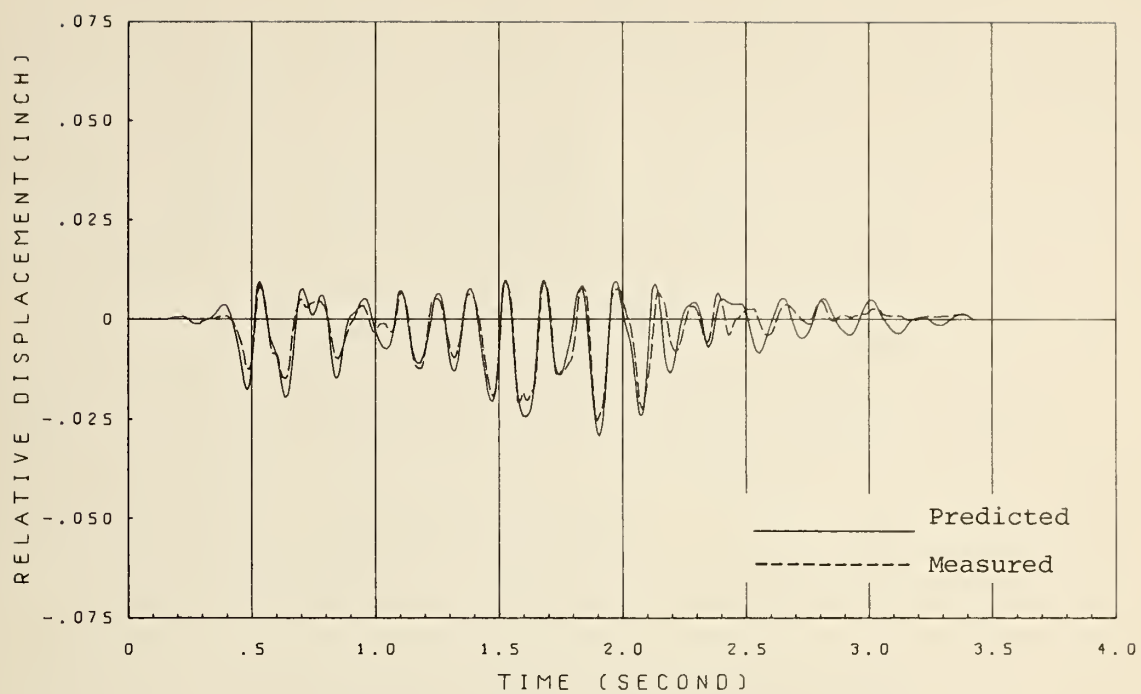


FIG. 6.2.7 NONLINEAR CORRELATION FOR TEST H1; EXPANSION JOINT NO. 1;  
OUTER SIDE

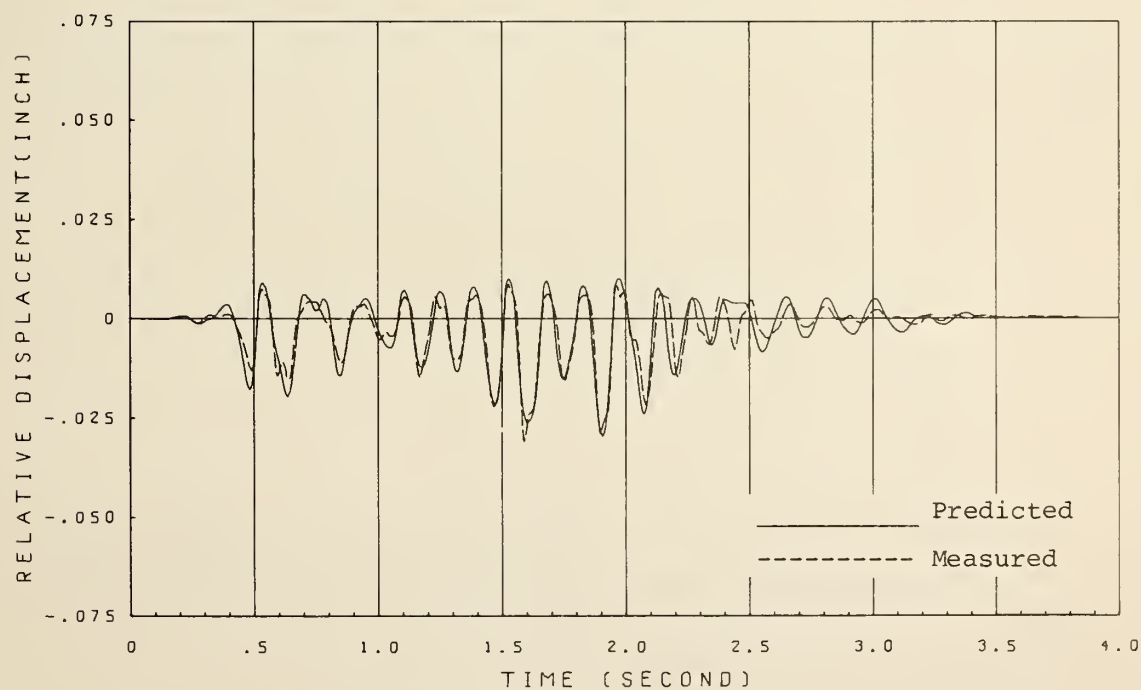


FIG. 6.2.8 NONLINEAR CORRELATION FOR TEST H1; EXPANSION JOINT NO. 2;  
INNER SIDE

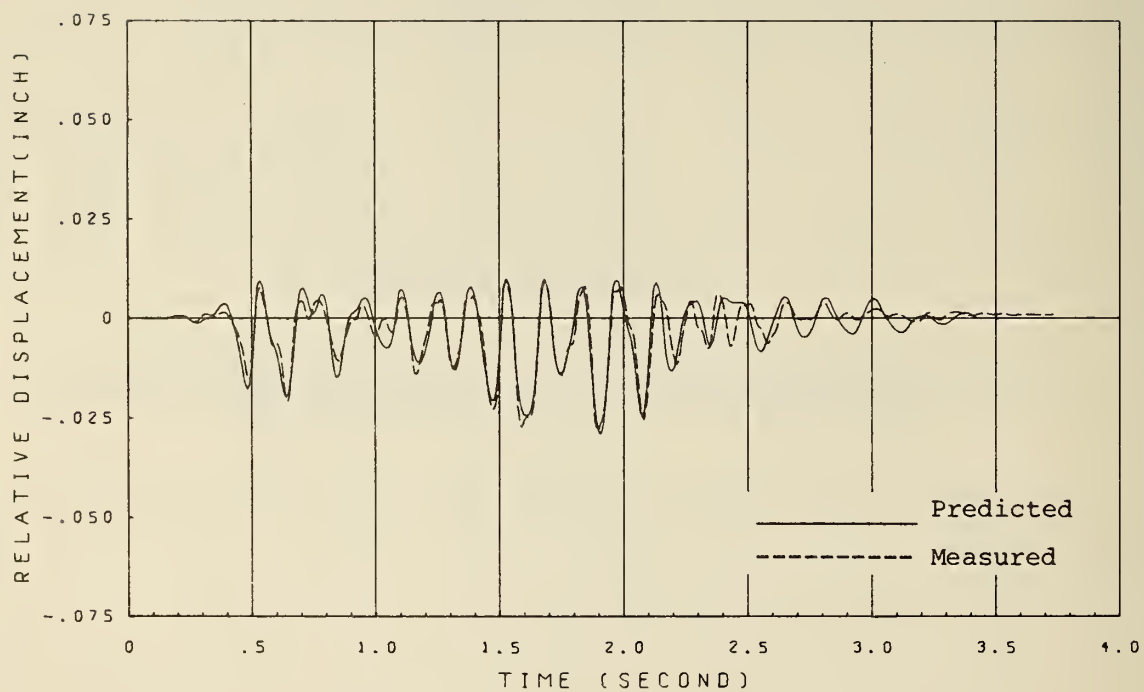


FIG. 6.2.9 NONLINEAR CORRELATION FOR TEST H1; EXPANSION JOINT NO. 2;  
OUTER SIDE

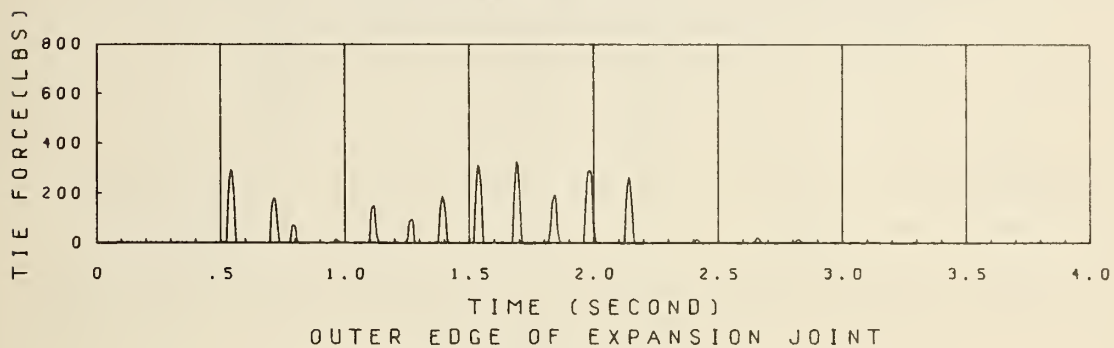
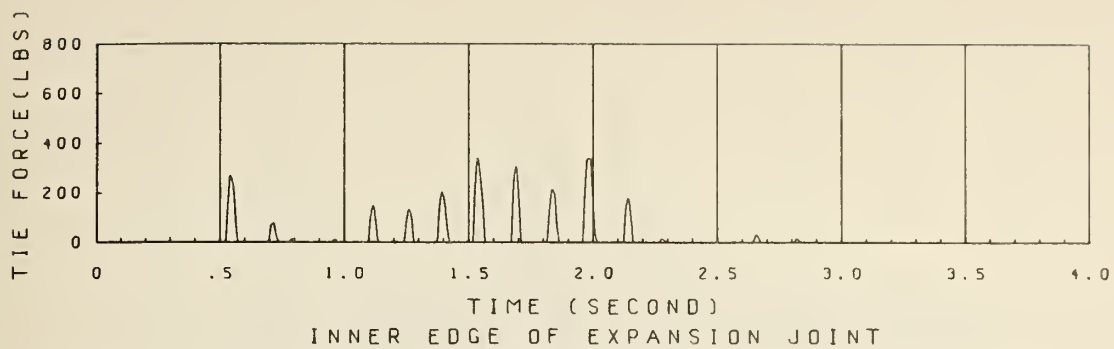


FIG. 6.3.1 PREDICTED TIE BAR FORCE FOR TEST H1; EXPANSION JOINT NO. 1

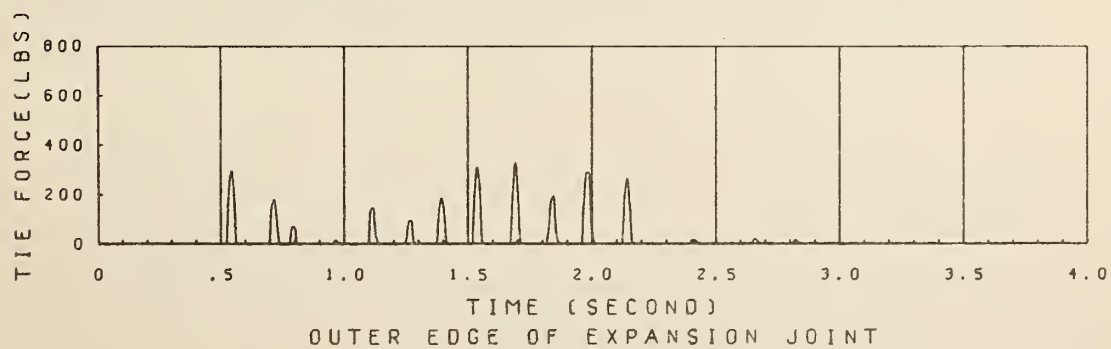
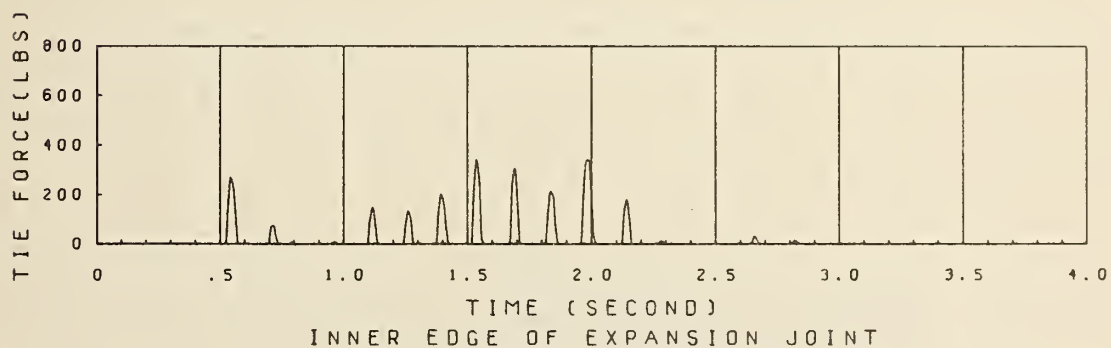


FIG. 6.3.2 PREDICTED TIE BAR FORCE FOR TEST H1; EXPANSION JOINT NO. 2



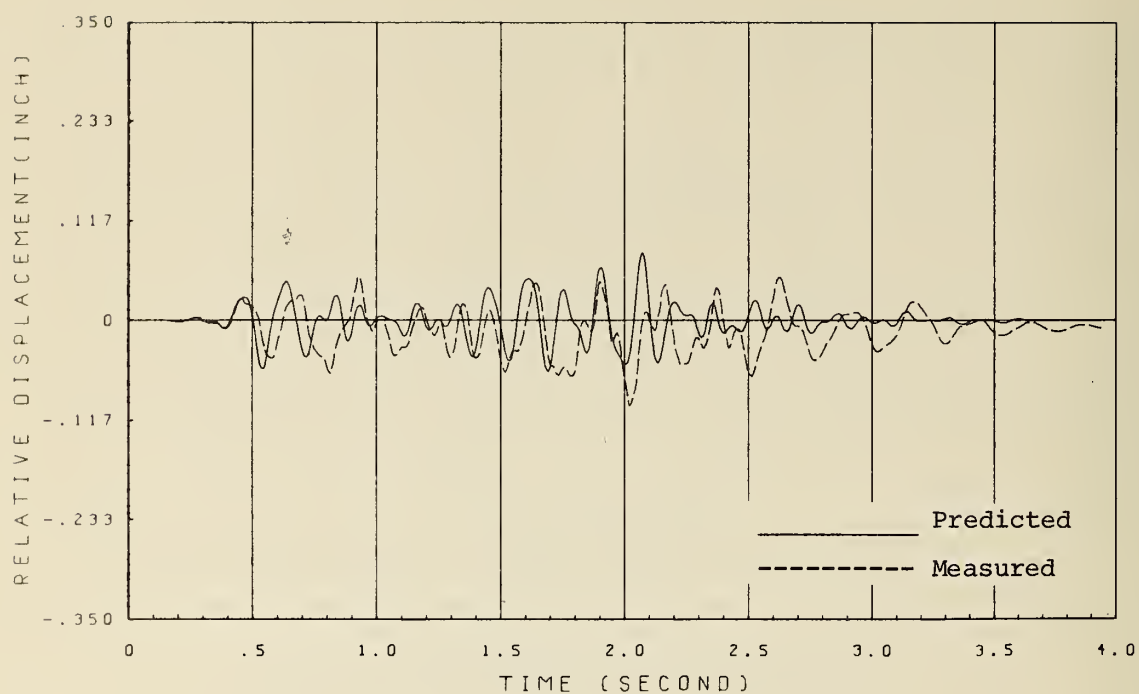


FIG. 6.4.1 LINEAR CORRELATION FOR TEST HV2; SIDE GIRDER NO. 1;  
LONGITUDINAL (X) DIRECTION

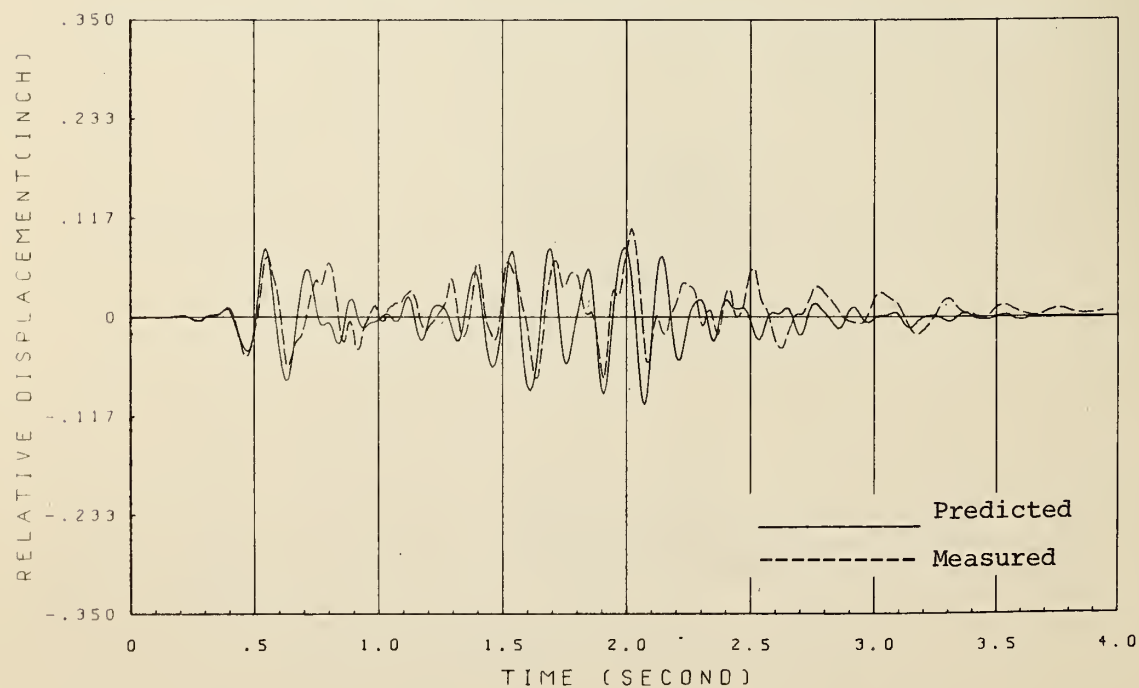


FIG. 6.4.2 LINEAR CORRELATION FOR TEST HV2; SIDE GIRDER NO. 1;  
TRANSVERSE (Y) DIRECTION

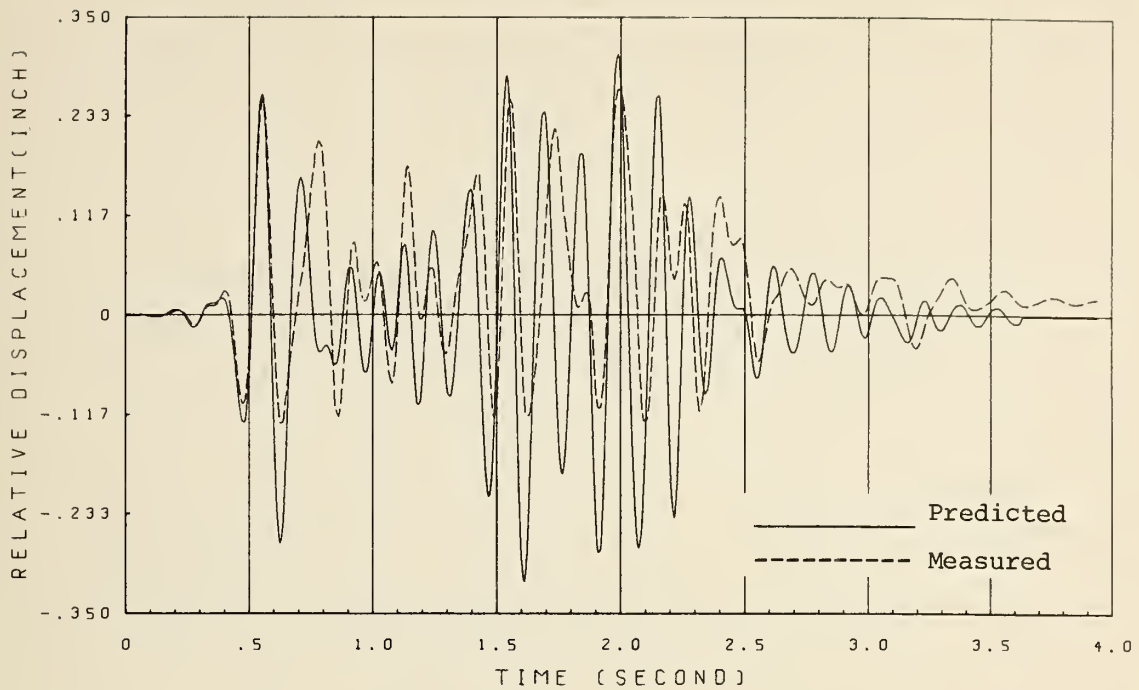


FIG. 6.4.3 LINEAR CORRELATION FOR TEST HV2; CENTER GIRDER;  
TRANSVERSE (Y) DIRECTION

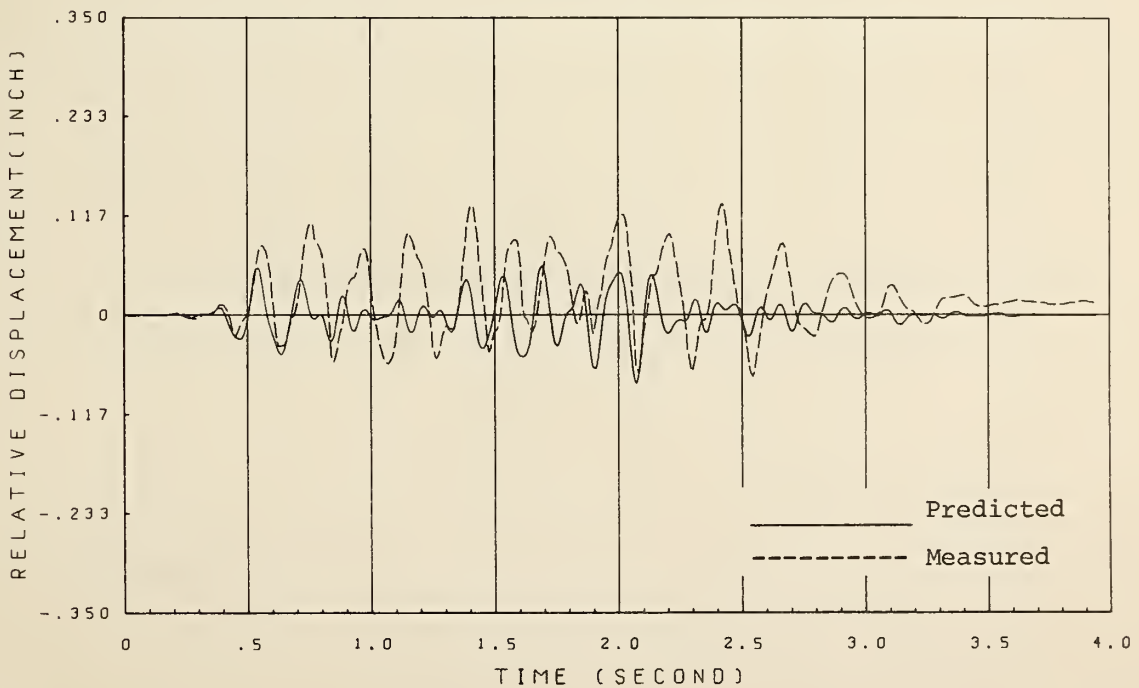


FIG. 6.4.4 LINEAR CORRELATION FOR TEST HV2; SIDE GIRDER NO. 2;  
LONGITUDINAL (X) DIRECTION

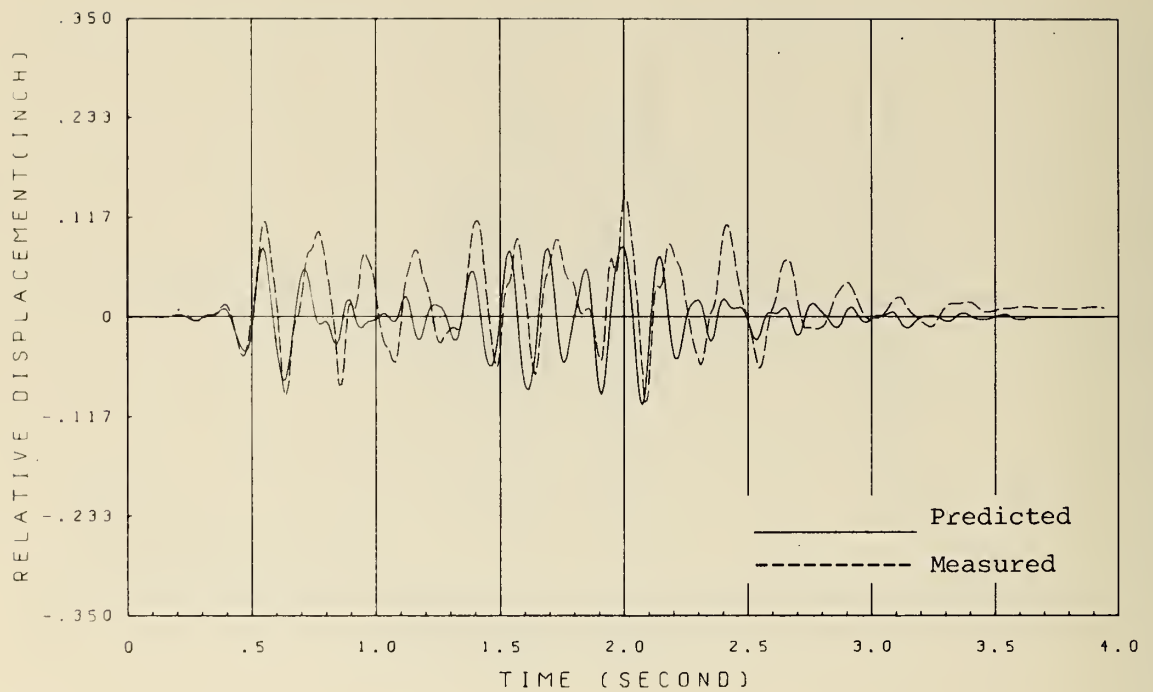


FIG. 6.4.5 LINEAR CORRELATION FOR TEST HV2; SIDE GIRDER NO. 2;  
TRANSVERSE (Y) DIRECTION

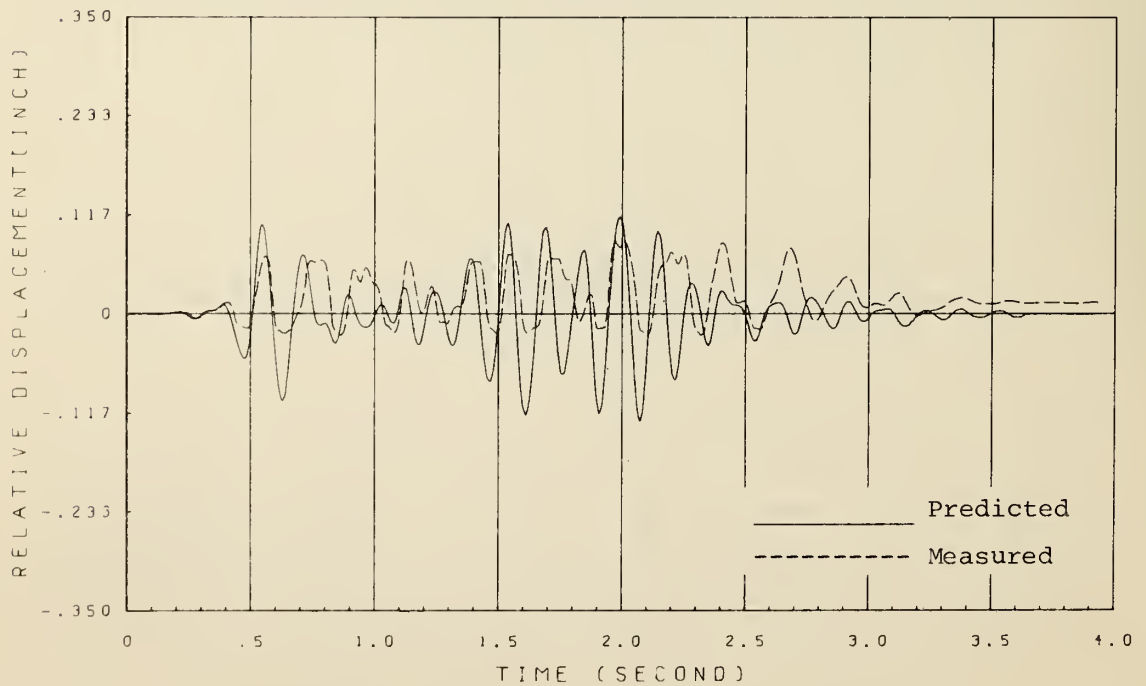


FIG. 6.4.6 LINEAR CORRELATION FOR TEST HV2; EXPANSION JOINT NO. 1;  
INNER SIDE

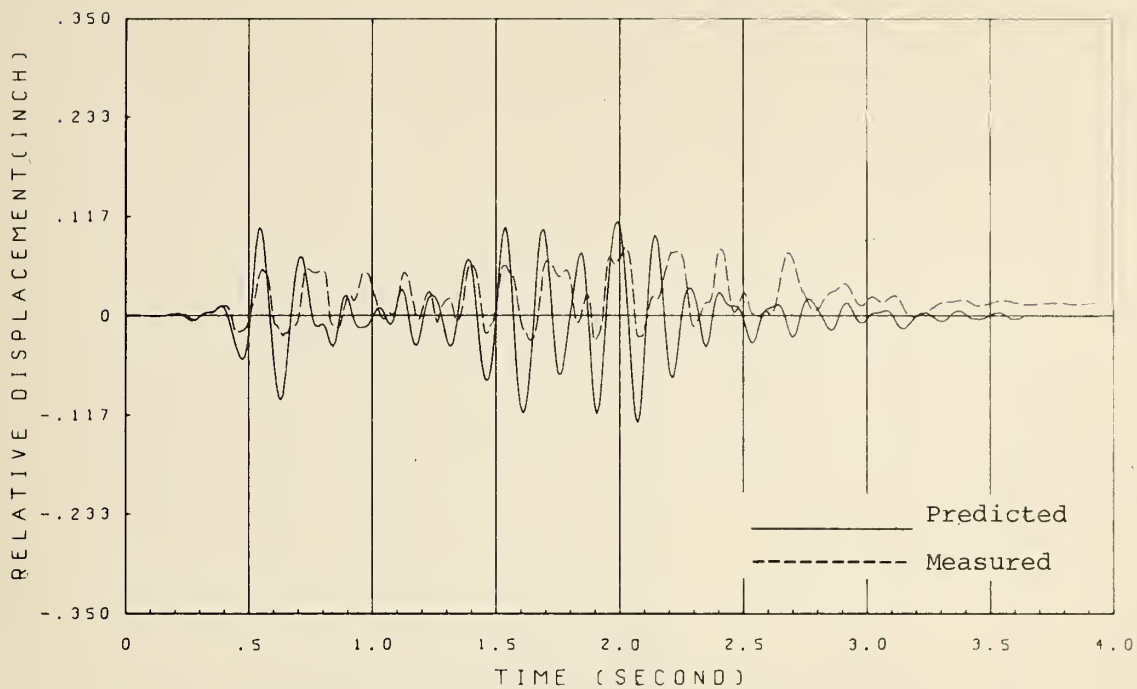


FIG. 6.4.7 LINEAR CORRELATION FOR TEST HV2; EXPANSION JOINT NO. 1;  
OUTER SIDE

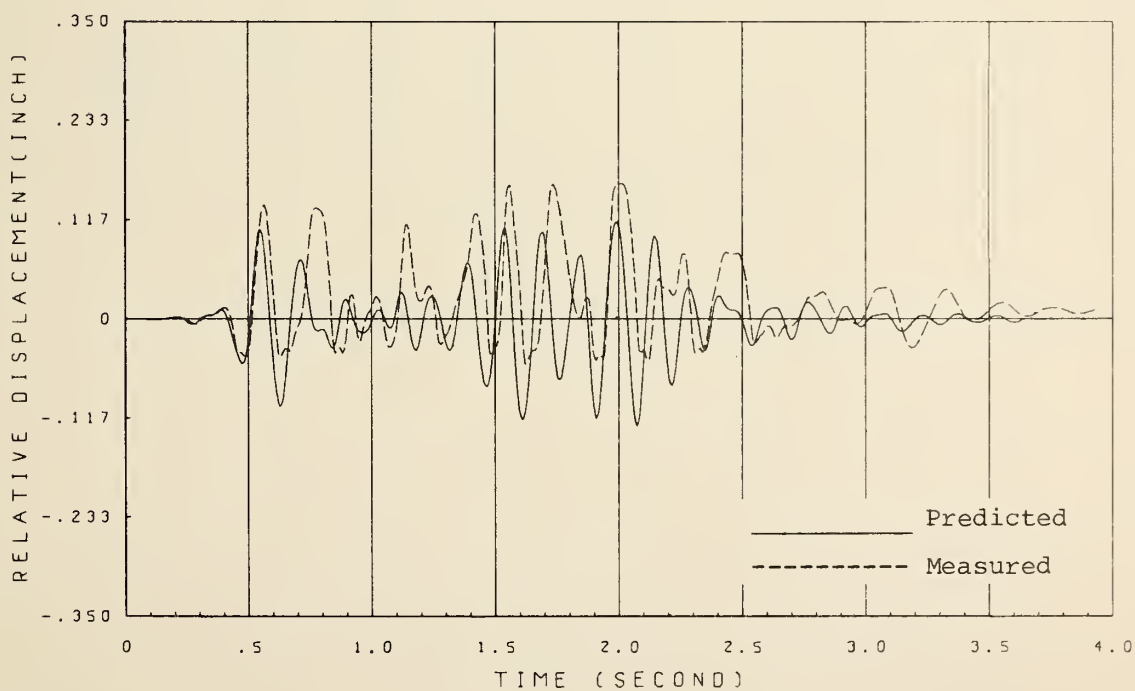


FIG. 6.4.8 LINEAR CORRELATION FOR TEST HV2; EXPANSION JOINT NO. 2;  
INNER SIDE

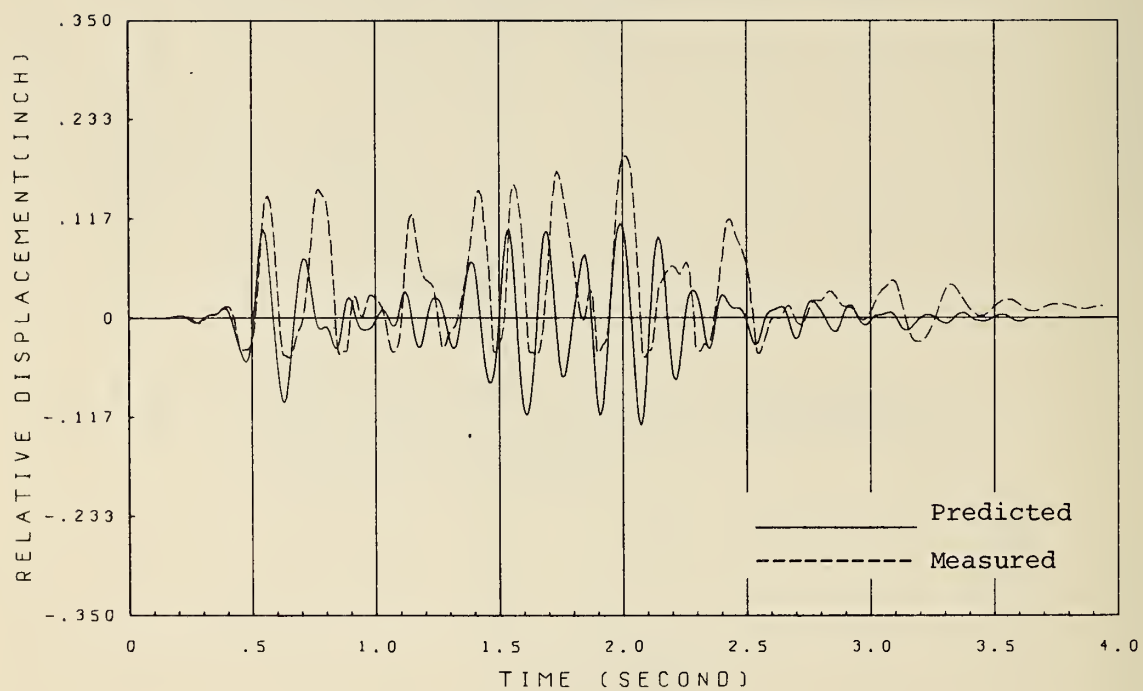


FIG. 6.4.9 LINEAR CORRELATION FOR TEST HV2; EXPANSION JOINT NO. 2;  
OUTER SIDE



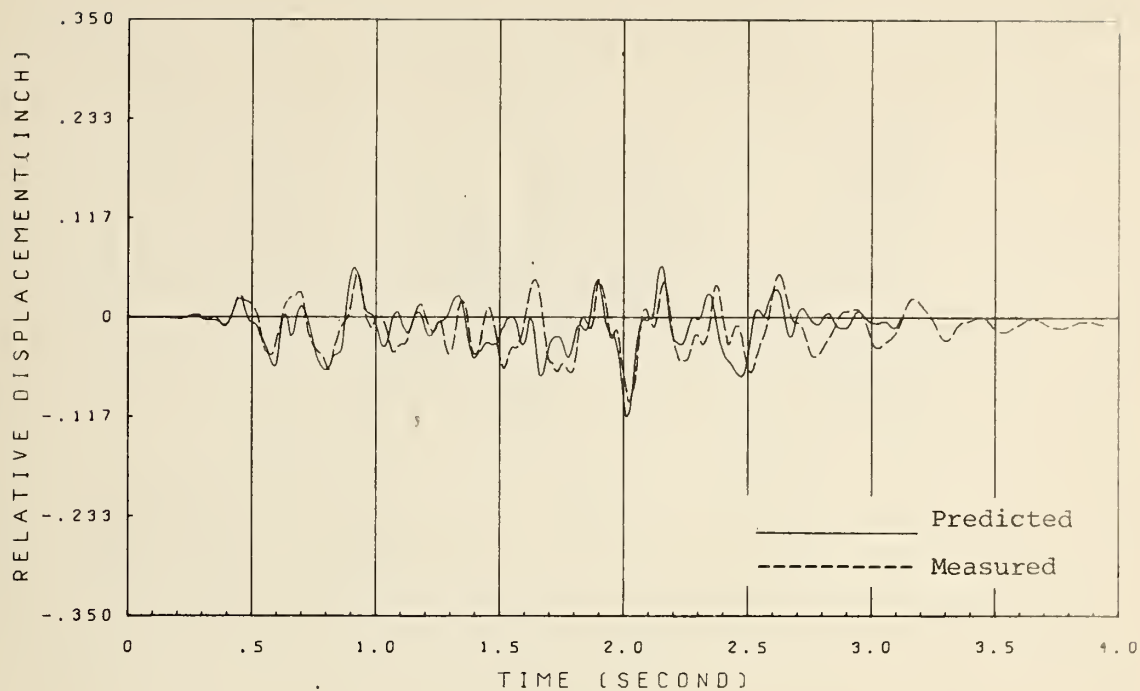


FIG. 6.5.1 NONLINEAR CORRELATION FOR TEST HV2; SIDE GIRDER NO. 1;  
LONGITUDINAL (X) DIRECTION

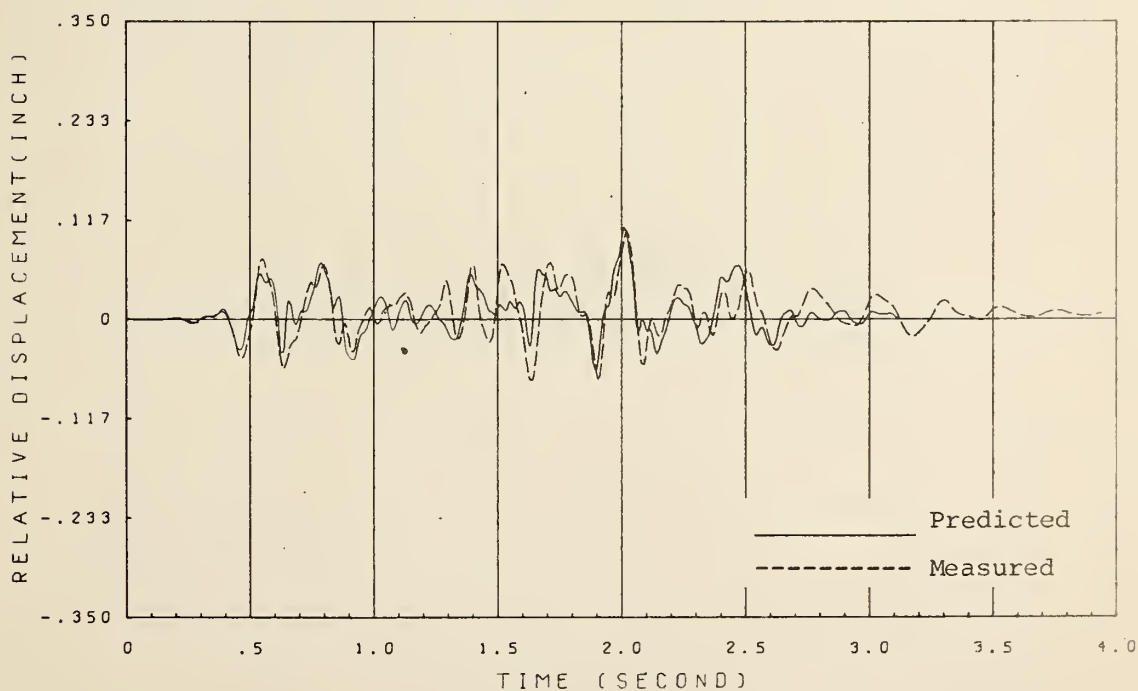


FIG. 6.5.2 NONLINEAR CORRELATION FOR TEST HV2; SIDE GIRDER NO. 1;  
TRANSVERSE (Y) DIRECTION

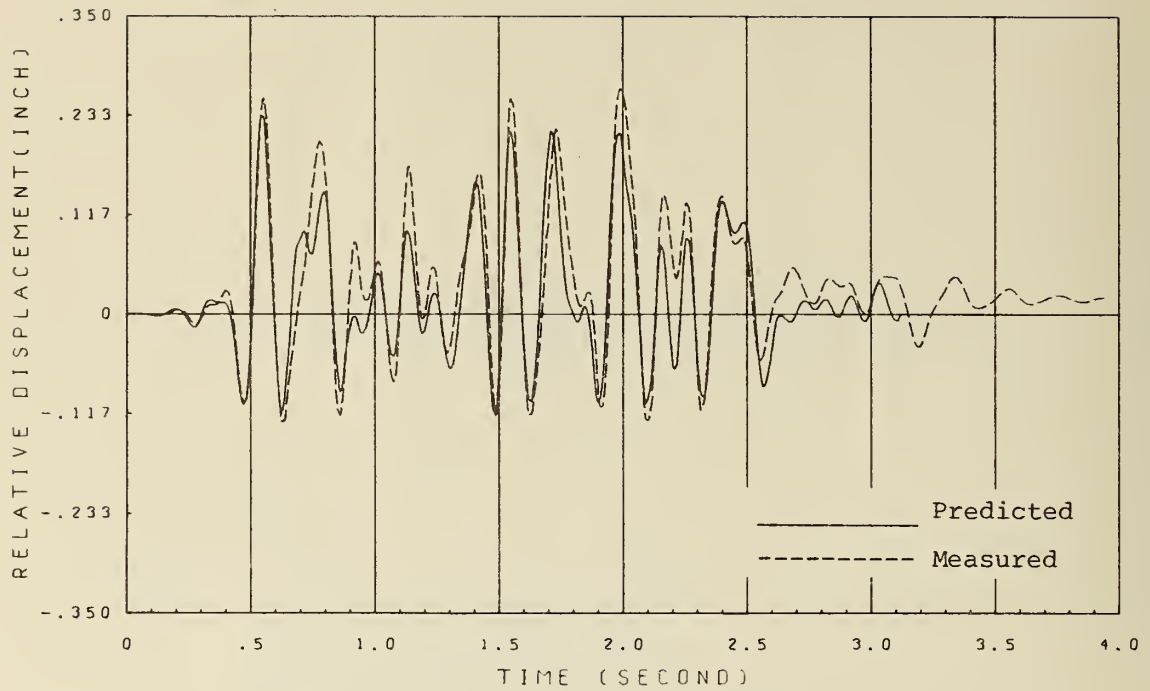


FIG. 6.5.3 NONLINEAR CORRELATION FOR TEST HV2; CENTER GIRDER;  
TRANSVERSE (Y) DIRECTION

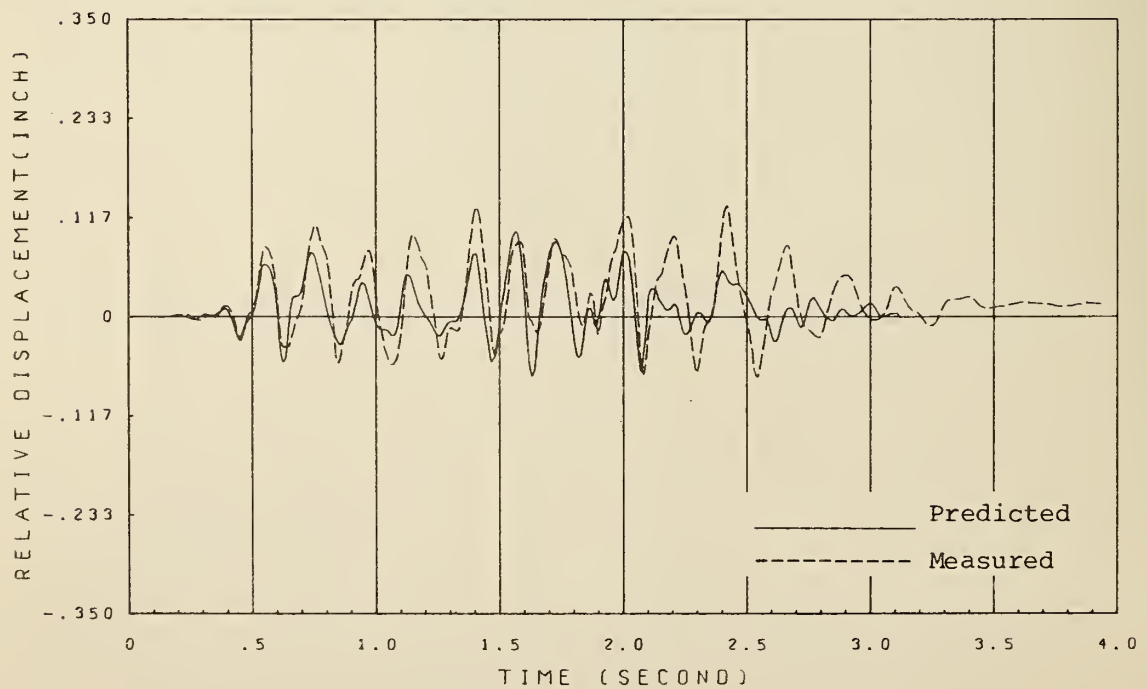


FIG. 6.5.4 NONLINEAR COORELATION FOR TEST HV2; SIDE GIRDER NO. 2;  
LONGITUDINAL (X) DIRECTION

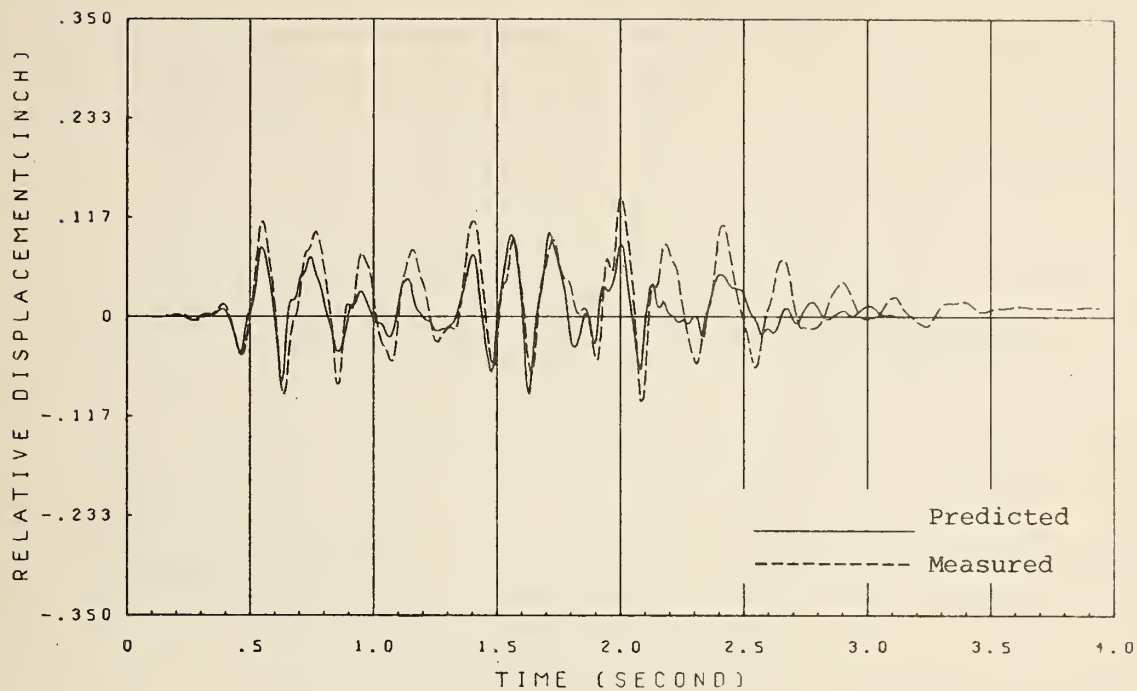


FIG. 6.5.5 NONLINEAR CORRELATION FOR TEST HV2; SIDE GIRDER NO. 2;  
TRANSVERSE (Y) DIRECTION

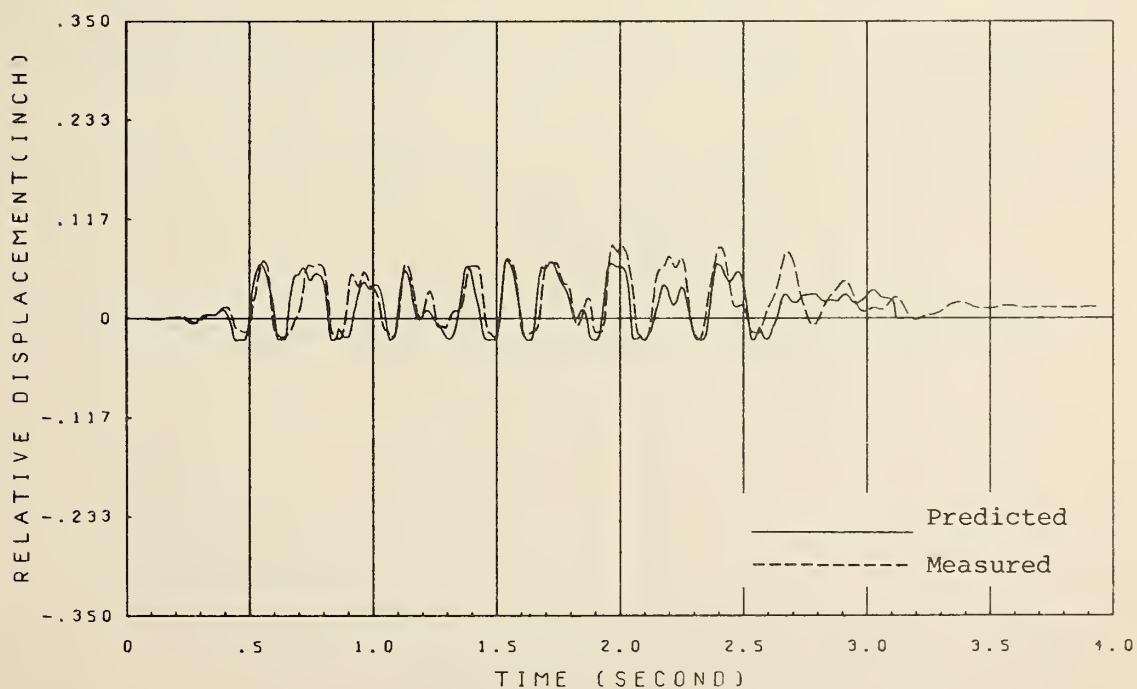


FIG. 6.5.6 NONLINEAR CORRELATION FOR TEST HV2; EXPANSION JOINT NO. 1;  
INNER SIDE

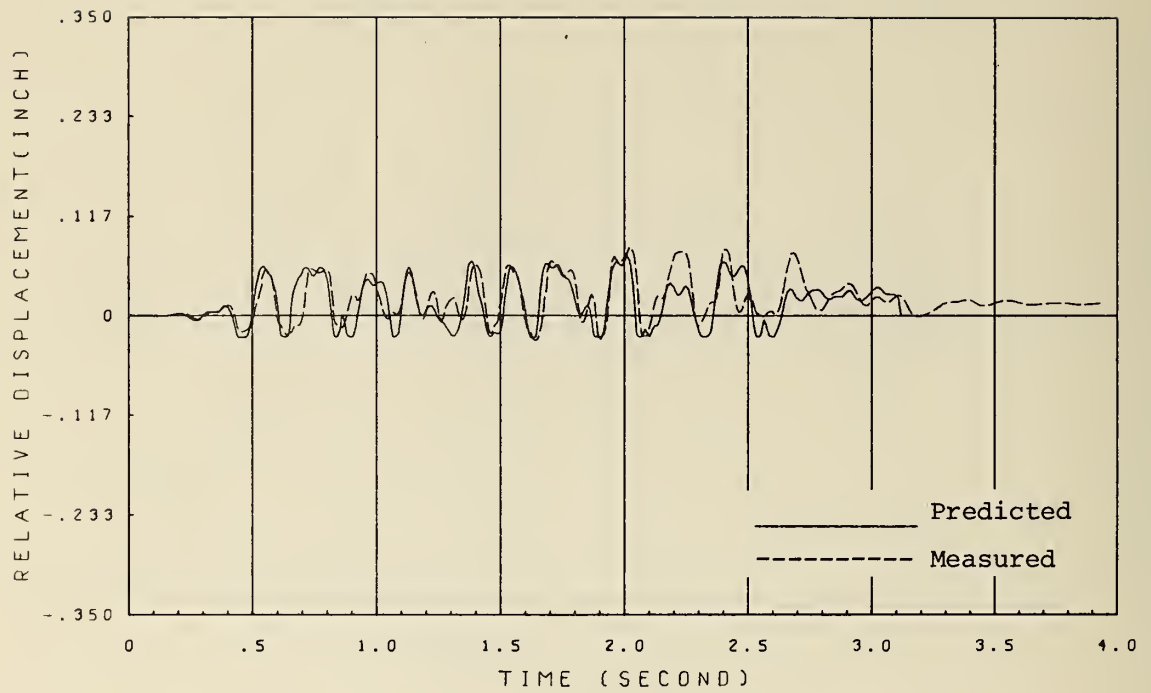


FIG. 6.5.7 NONLINEAR CORRELATION FOR TEST HV2; EXPANSION JOINT NO. 1;  
OUTER SIDE

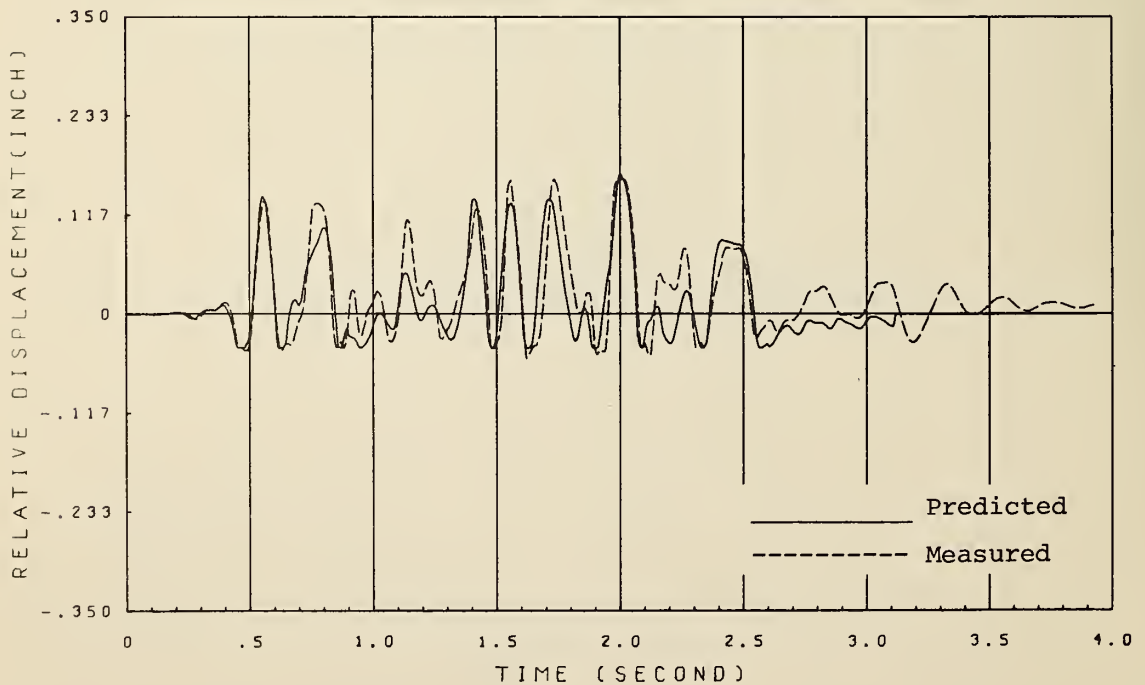


FIG. 6.5.8 NONLINEAR CORRELATION FOR TEST HV2; EXPANSION JOINT NO. 2;  
INNER SIDE

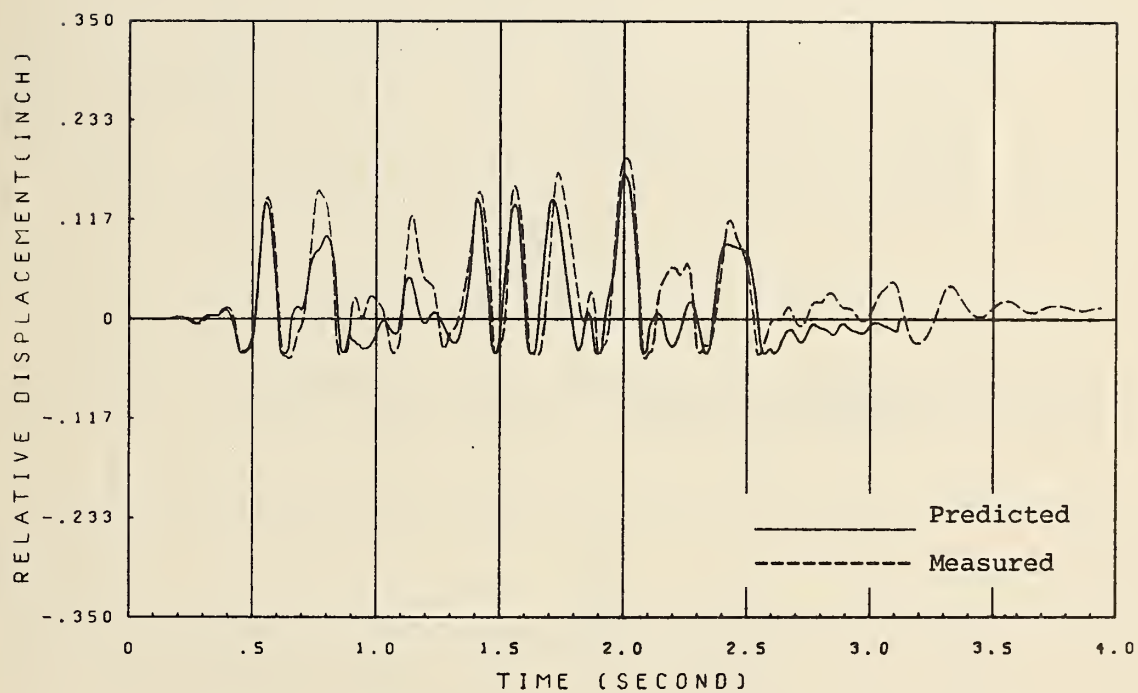


FIG. 6.5.9 NONLINEAR CORRELATION FOR TEST HV2; EXPANSION JOINT NO. 2;  
OUTER SIDE



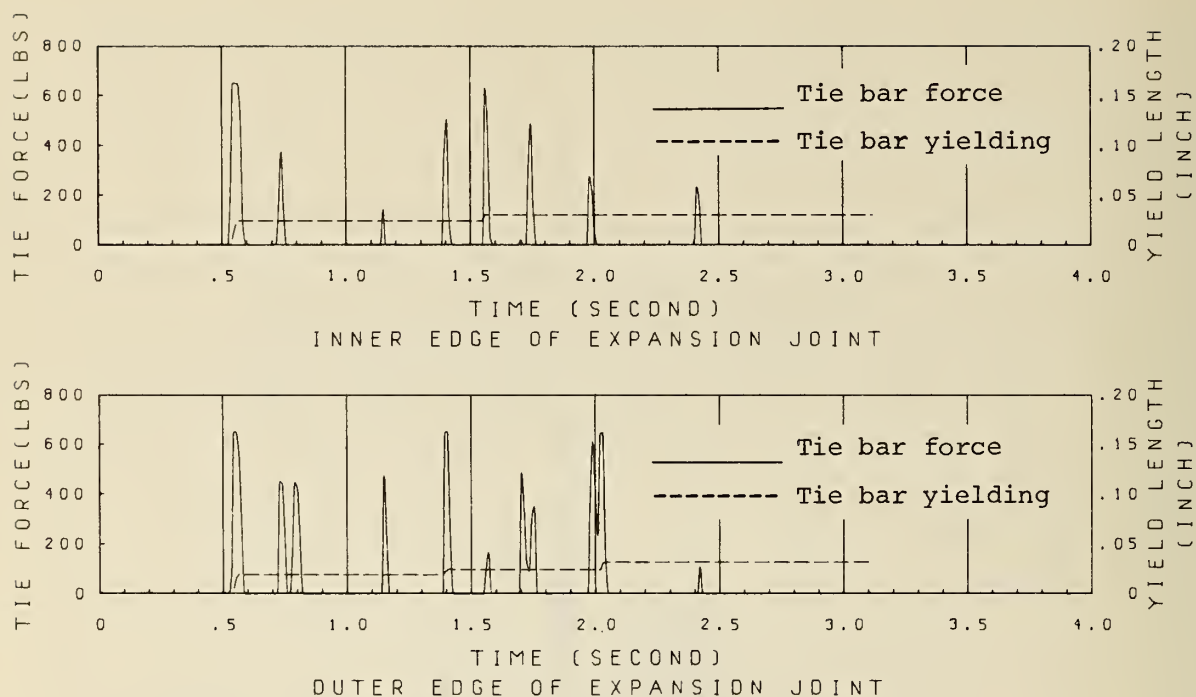


FIG. 6.6.1 PREDICTED TIE BAR FORCE AND YIELD LENGTH FOR TEST HV2;  
EXPANSION JOINT NO. 1

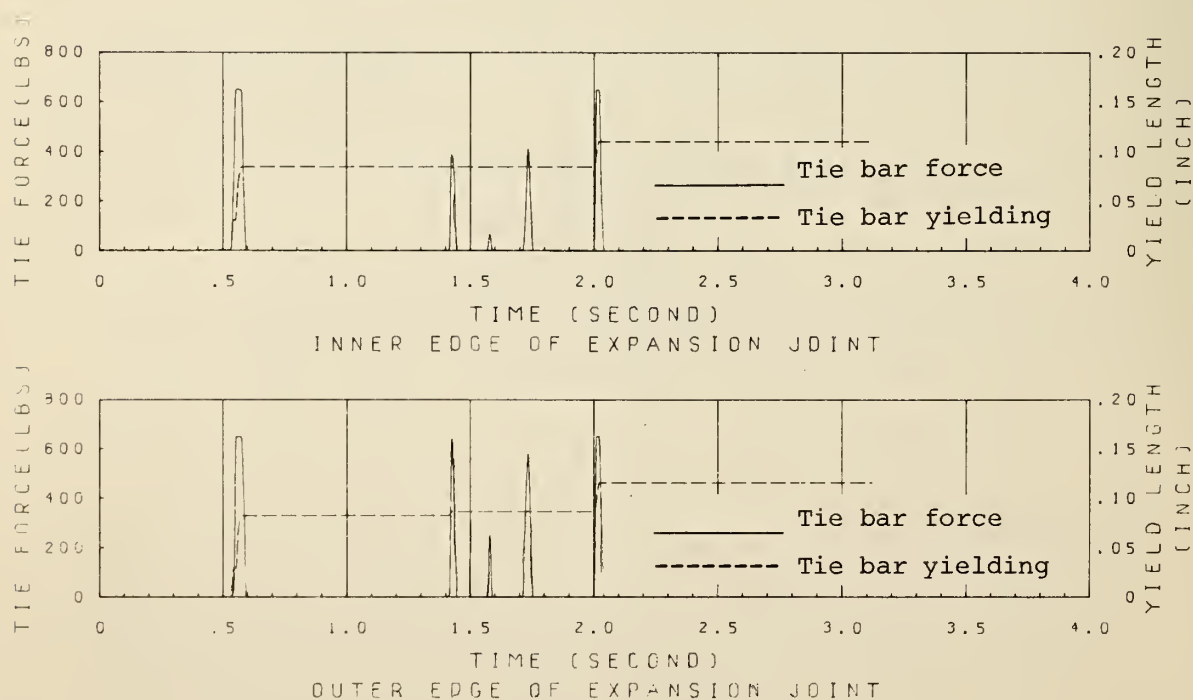


FIG. 6.6.2 PREDICTED TIE BAR FORCE AND YIELD LENGTH FOR TEST HV2;  
EXPANSION JOINT NO. 2

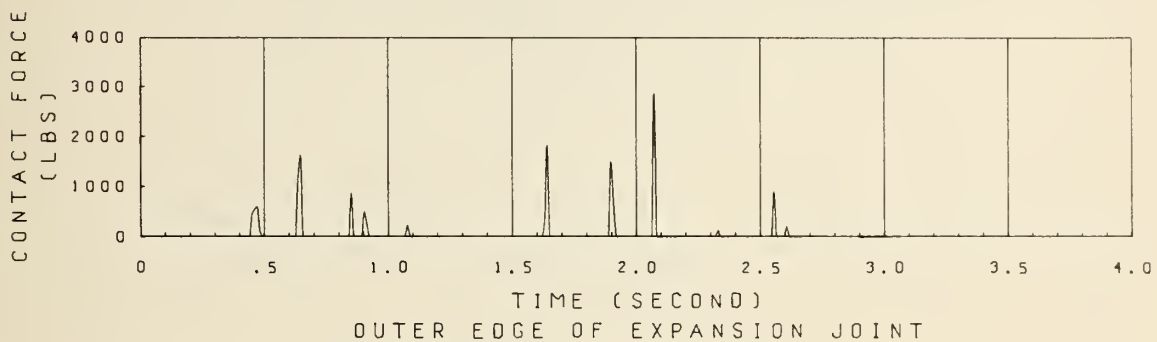
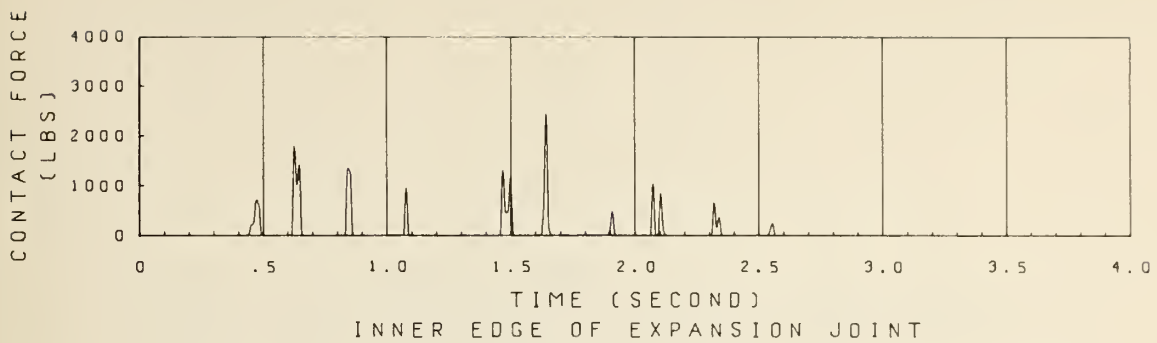


FIG. 6.7.1 PREDICTED CONTACT FORCE FOR TEST HV2; EXPANSION JOINT NO. 1

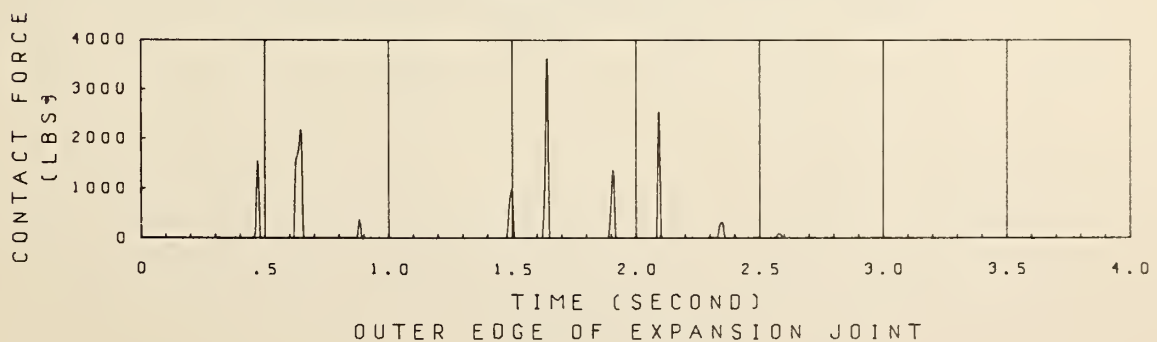
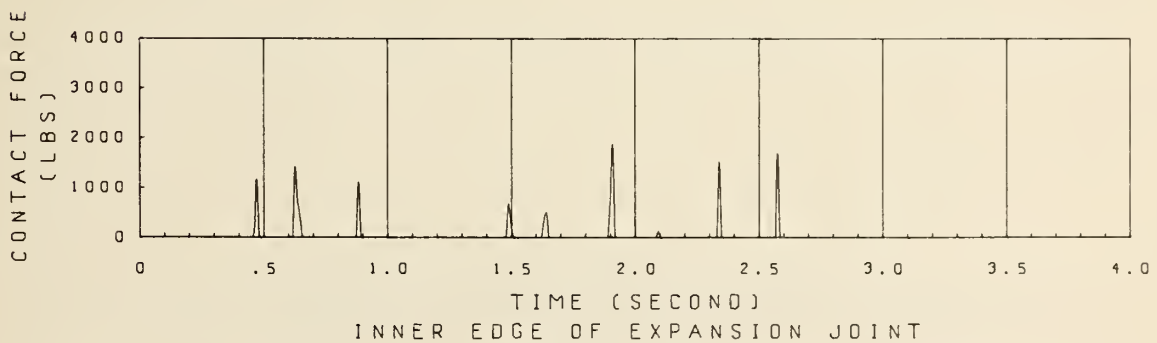


FIG. 6.7.2 PREDICTED CONTACT FORCE FOR TEST HV2; EXPANSION JOINT NO. 2

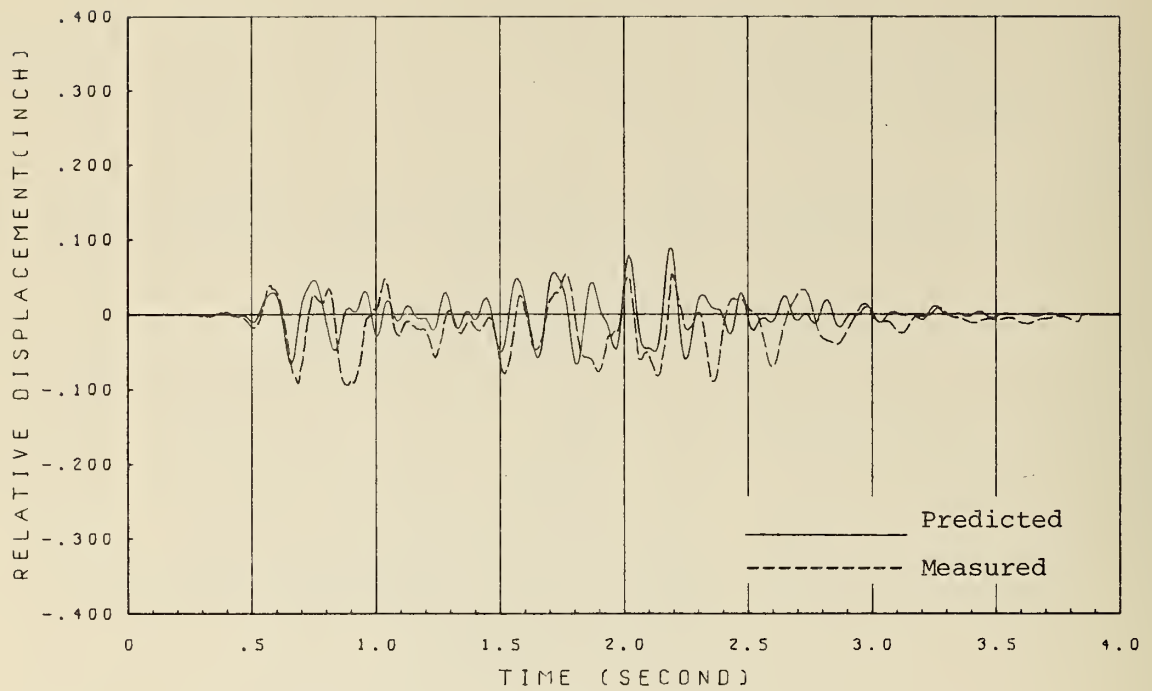


FIG. 6.8.1 LINEAR CORRELATION FOR TEST H3; SIDE GIRDER NO. 1;  
LONGITUDINAL (X) DIRECTION

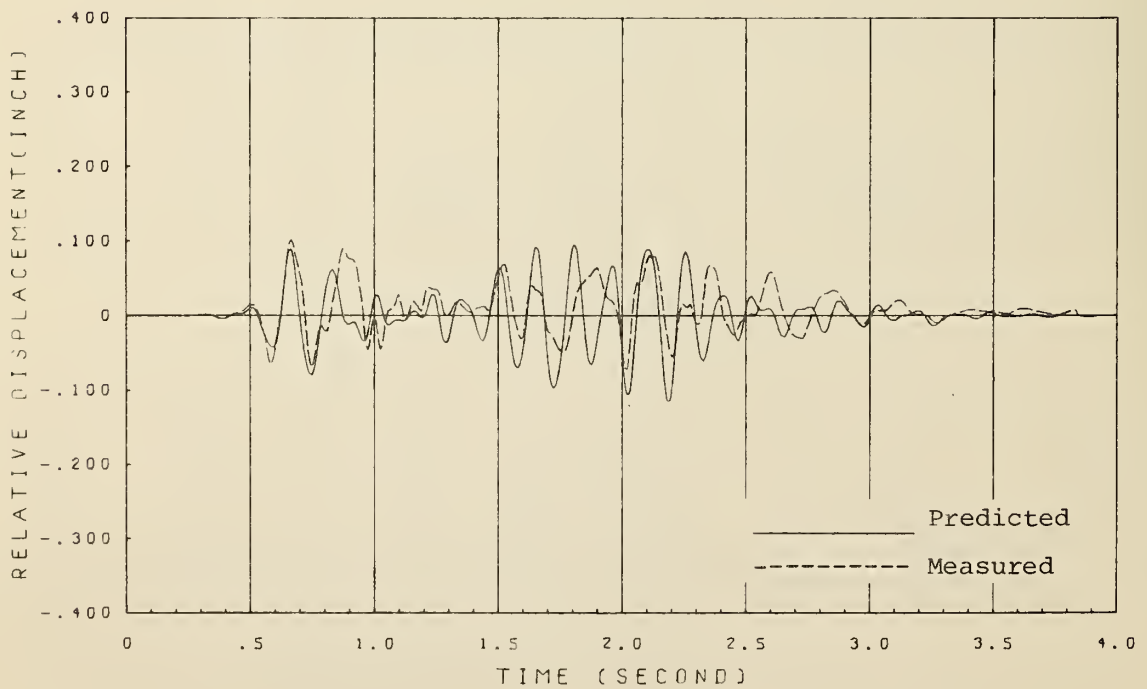


FIG. 6.8.2 LINEAR CORRELATION FOR TEST H3; SIDE GIRDER NO. 1;  
TRANSVERSE (Y) DIRECTION

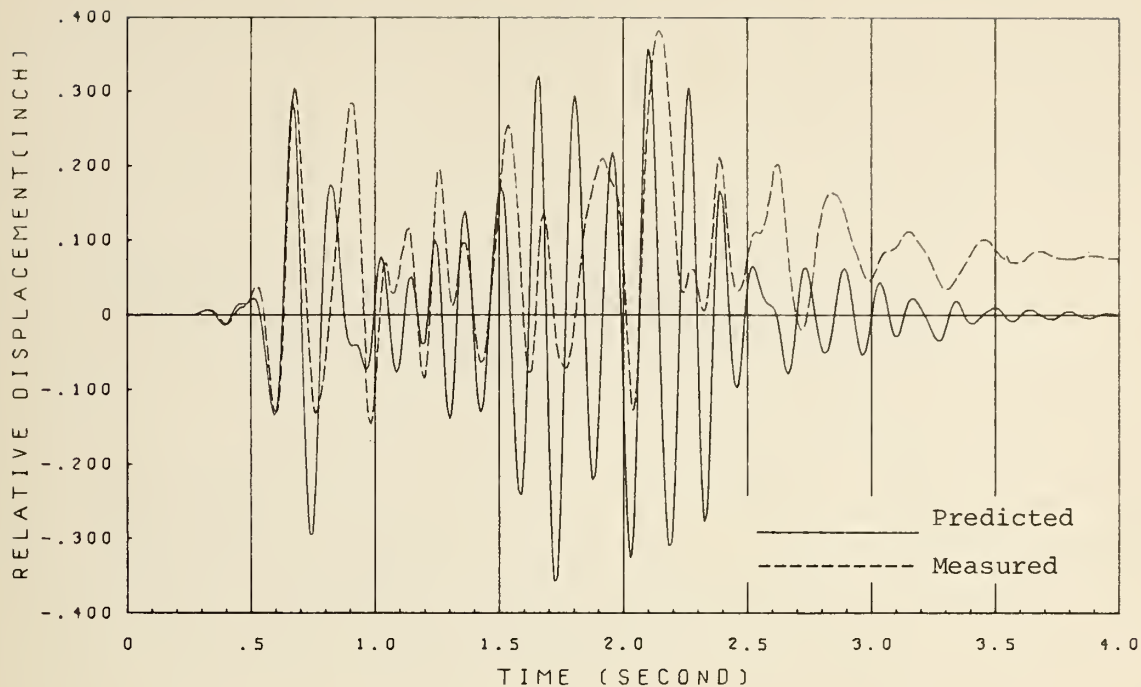


FIG. 6.8.3 LINEAR CORRELATION FOR TEST H3; CENTER GIRDER;  
TRANSVERSE (Y) DIRECTION

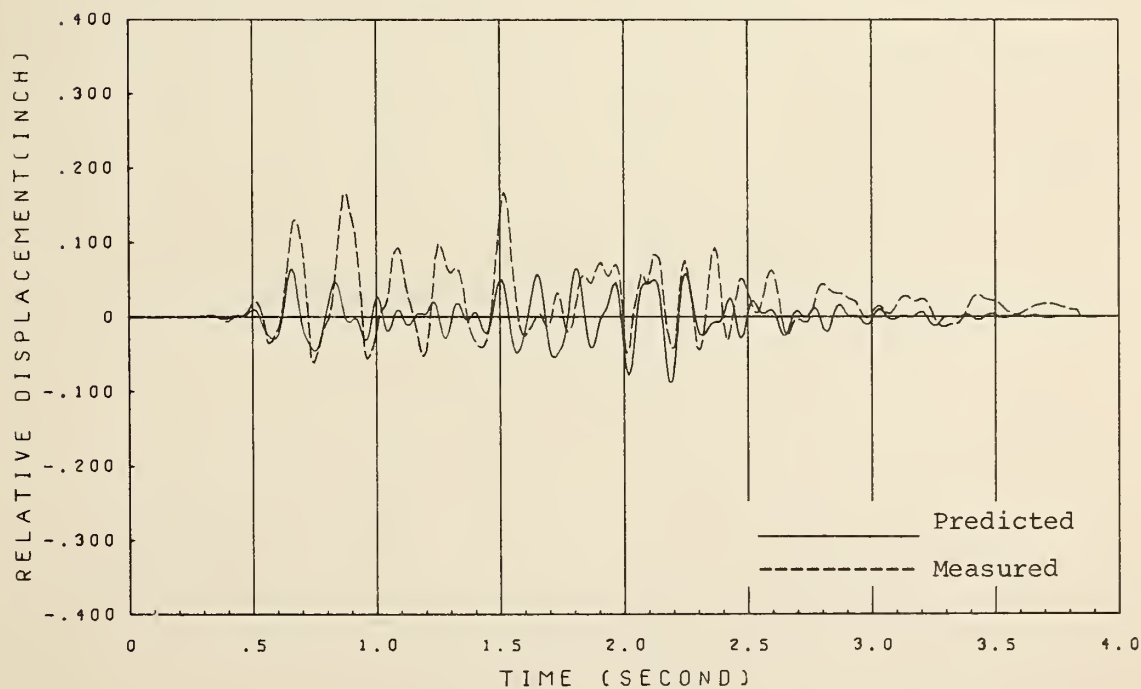


FIG. 6.8.4 LINEAR CORRELATION FOR TEST H3; SIDE GIRDER NO. 2;  
LONGITUDINAL (X) DIRECTION

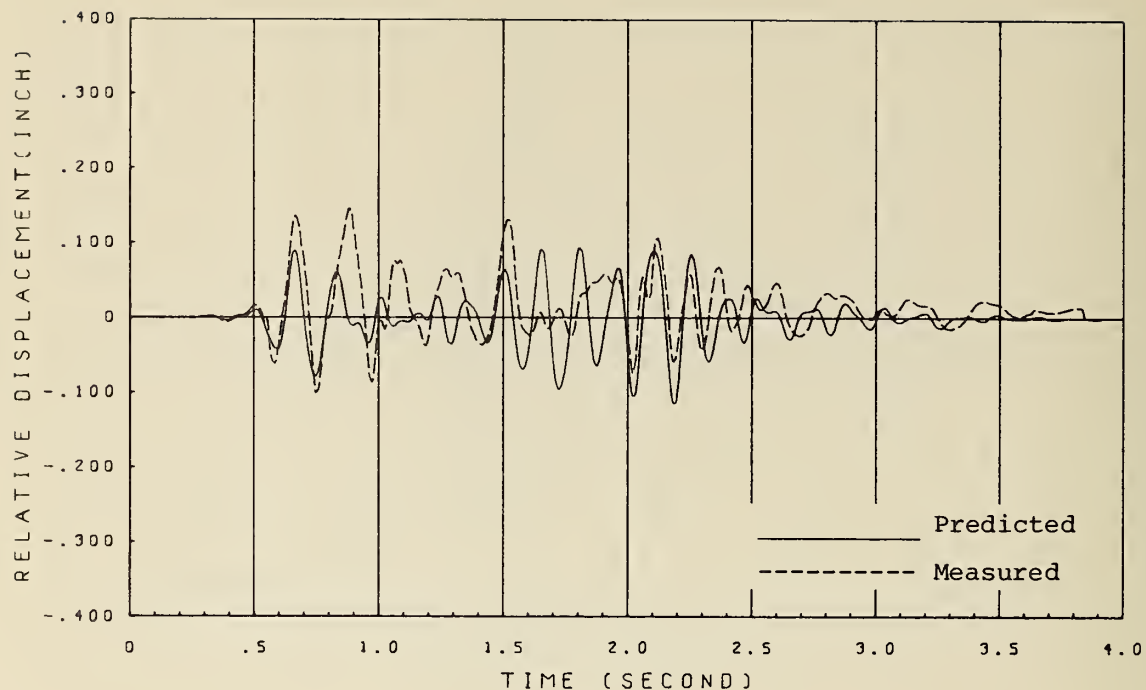


FIG. 6.8.5 LINEAR CORRELATION FOR TEST H3; SIDE GIRDER NO. 2;  
TRANSVERSE (Y) DIRECTION

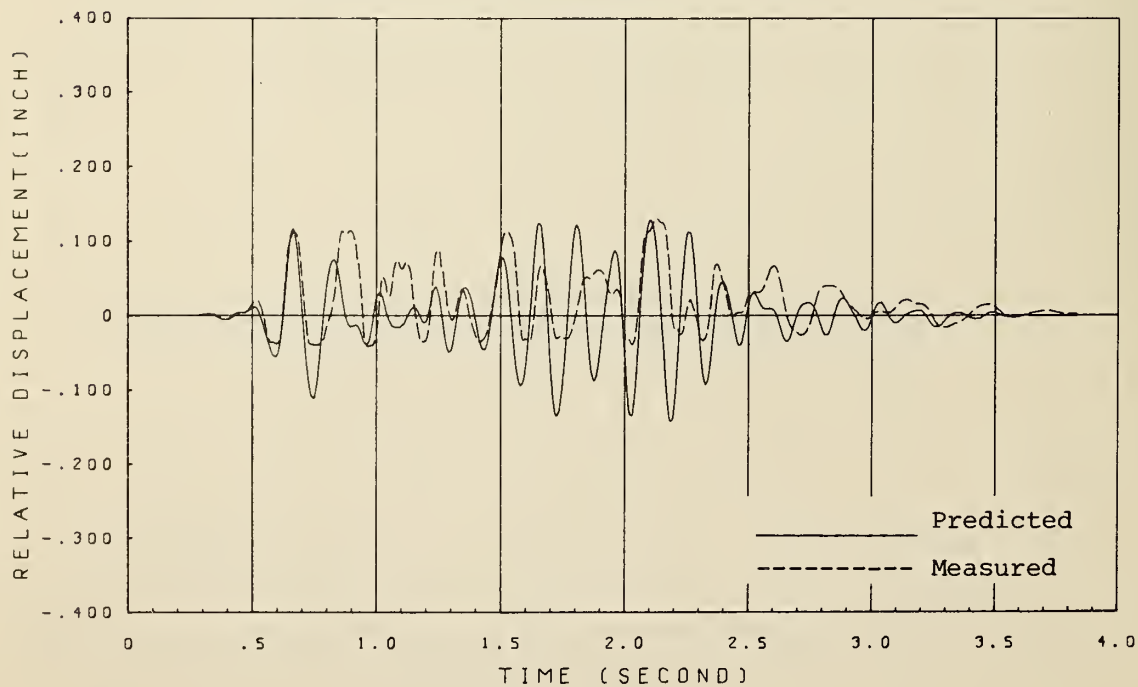


FIG. 6.8.6 LINEAR CORRELATION FOR TEST H3; EXPANSION JOINT NO. 1;  
INNER SIDE



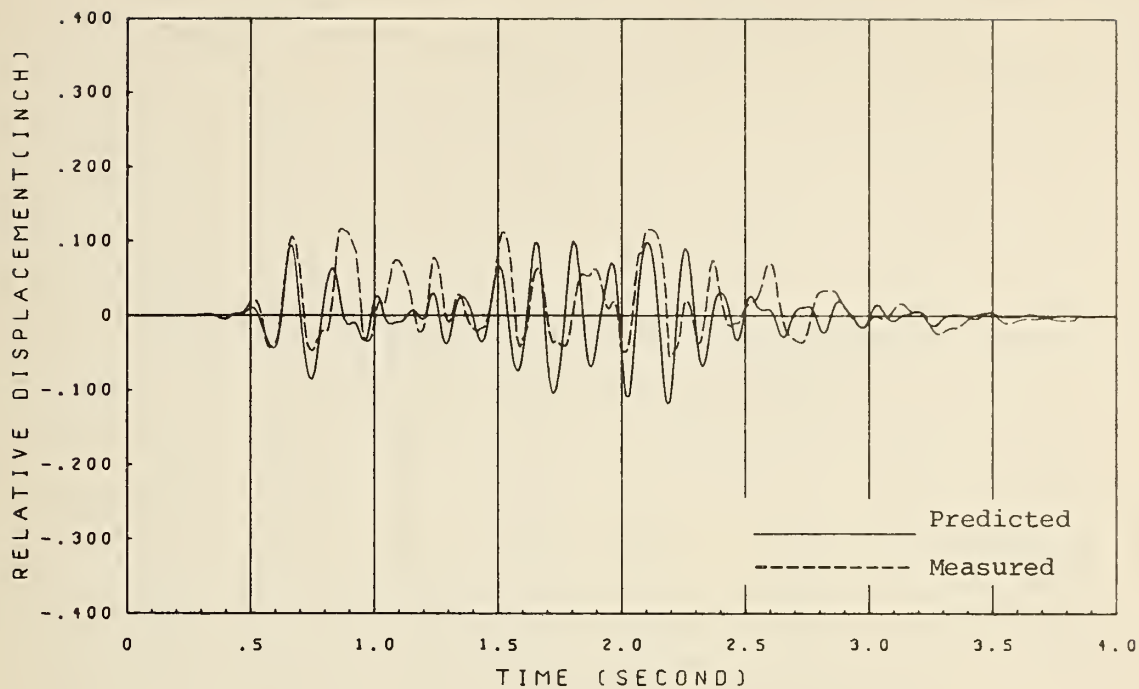


FIG. 6.8.7 LINEAR CORRELATION FOR TEST H3; EXPANSION JOINT NO. 1;  
OUTER SIDE

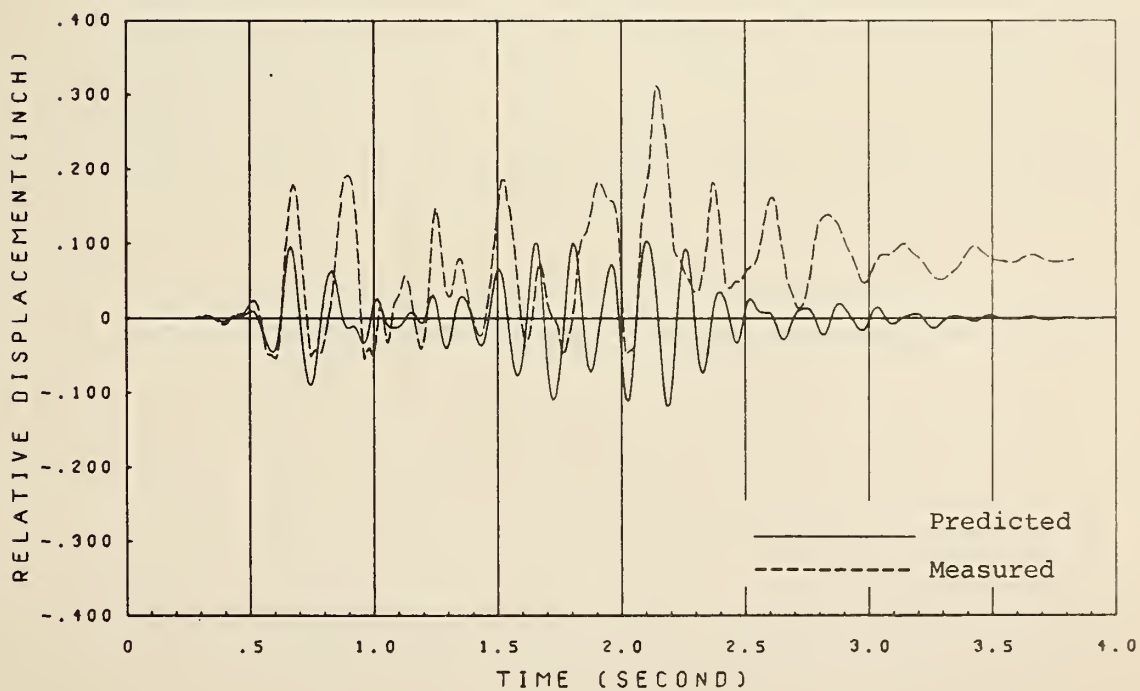


FIG. 6.8.8 LINEAR CORRELATION FOR TEST H3; EXPANSION JOINT NO. 2;  
INNER SIDE

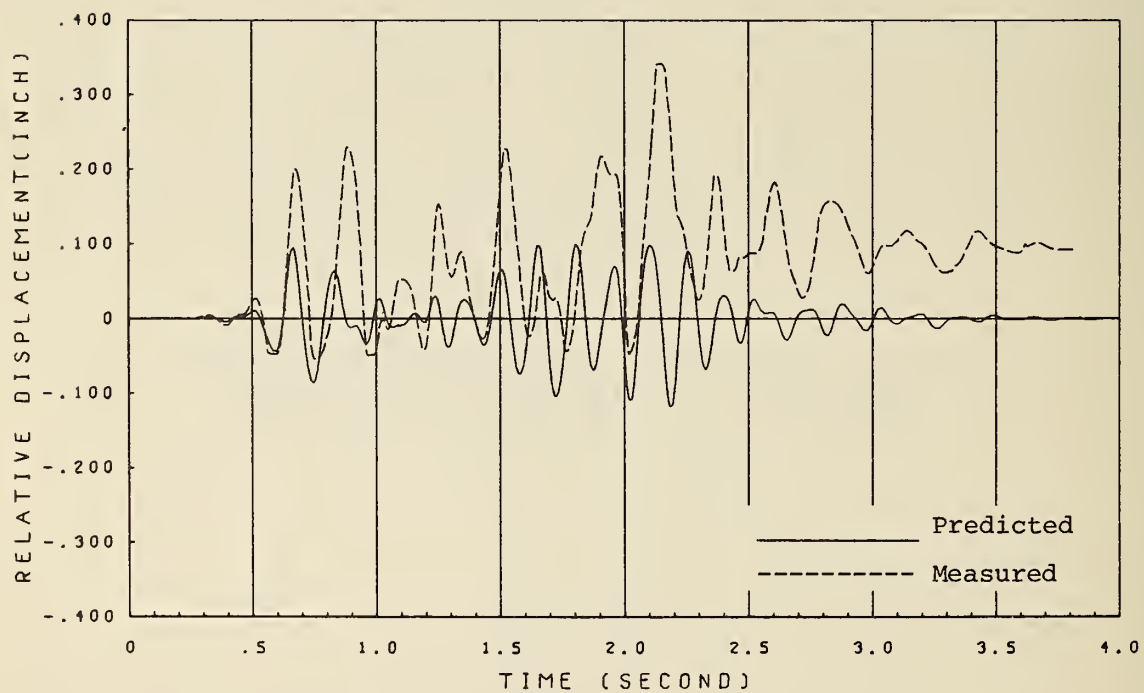


FIG. 6.8.9 LINEAR CORRELATION FOR TEST H3; EXPANSION JOINT NO. 2;  
OUTER SIDE

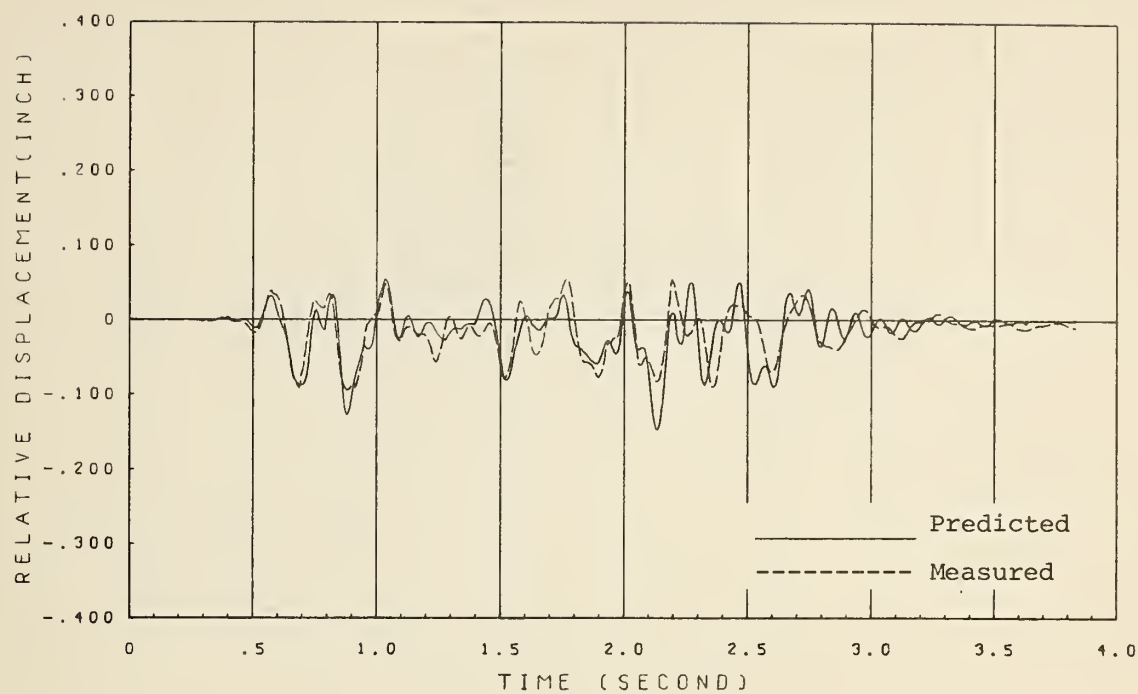


FIG. 6.9.1 NONLINEAR CORRELATION FOR TEST H3; SIDE GIRDER NO. 1;  
LONGITUDINAL (X) DIRECTION

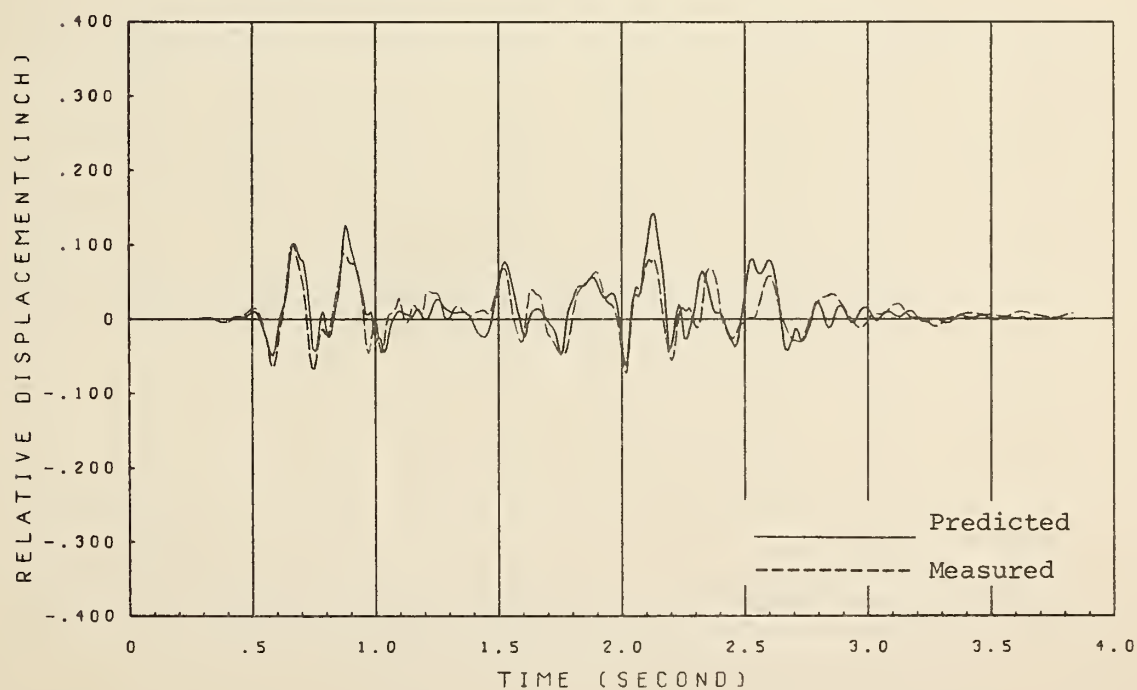


FIG. 6.9.2 NONLINEAR CORRELATION FOR TEST H3; SIDE GIRDER NO. 1;  
TRANSVERSE (Y) DIRECTION

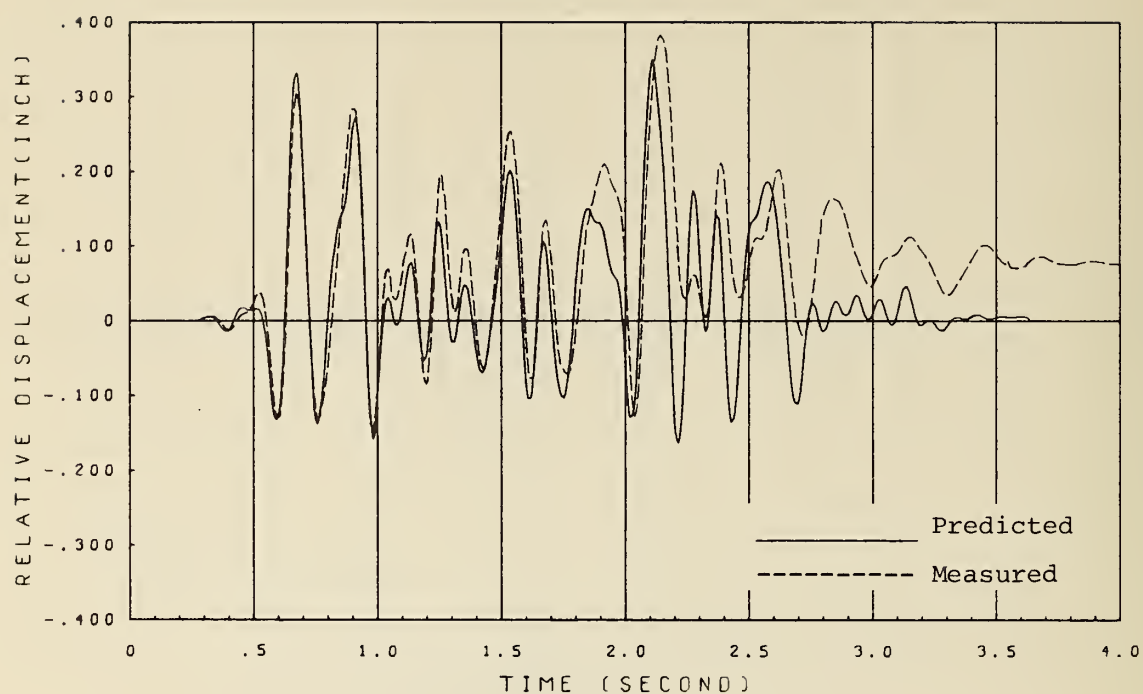


FIG. 6.9.3 NONLINEAR CORRELATION FOR TEST H3; CENTER GIRDER;  
TRANSVERSE (Y) DIRECTION

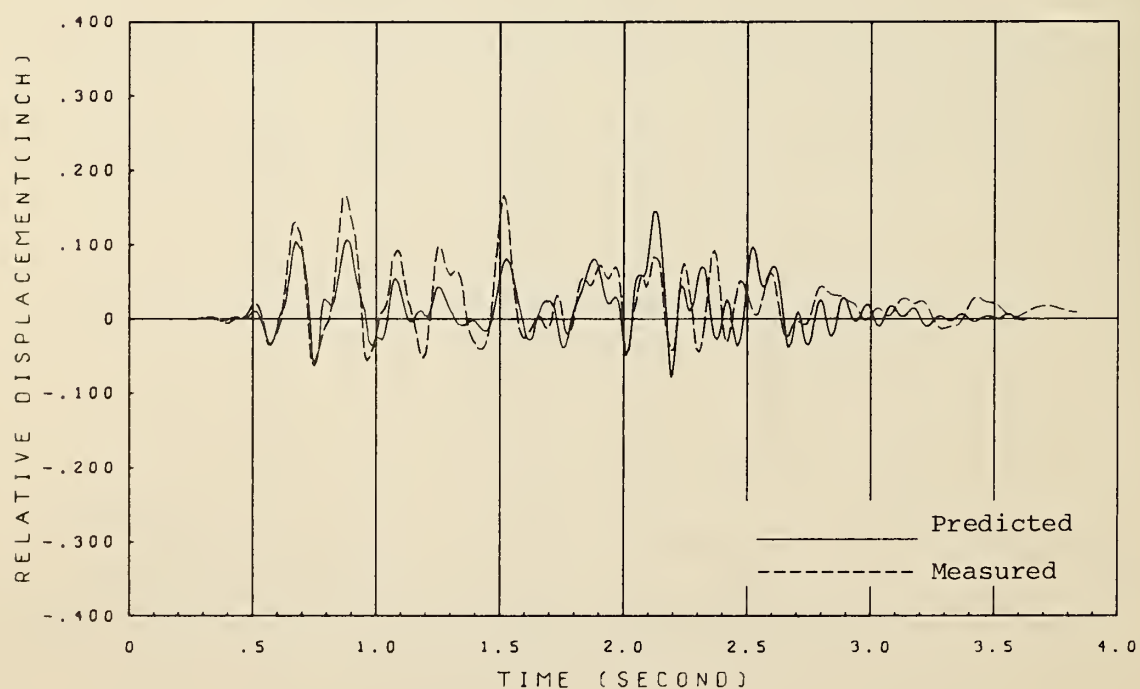


FIG. 6.9.4 NONLINEAR CORRELATION FOR TEST H3; SIDE GIRDER NO. 2;  
LONGITUDINAL (X) DIRECTION

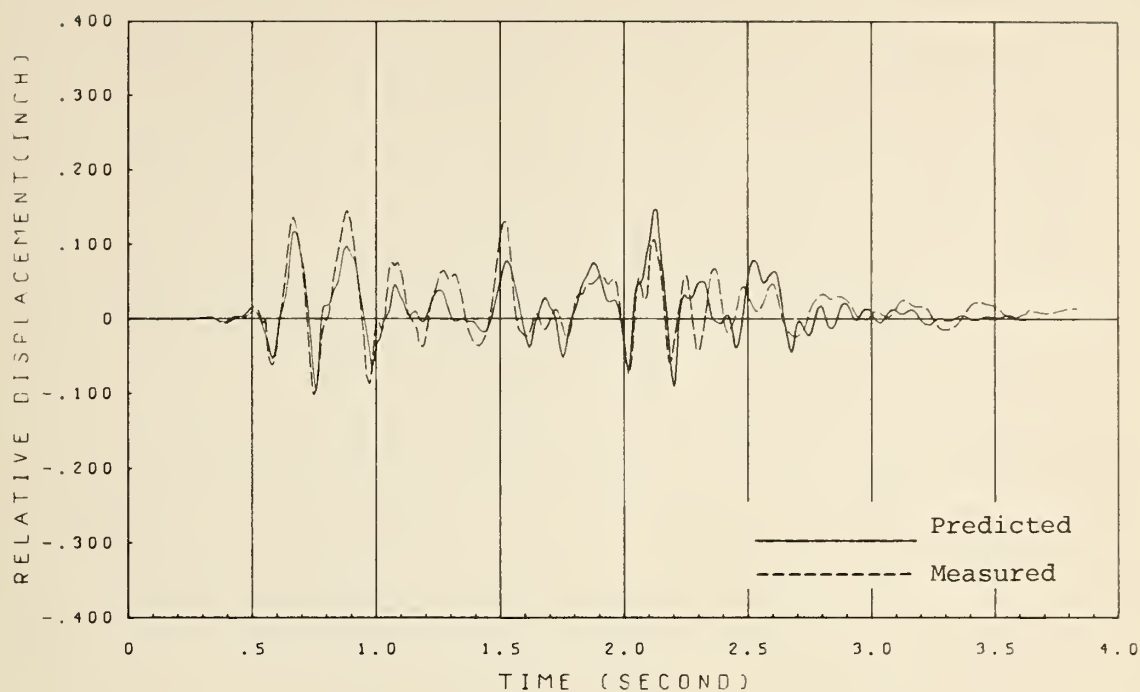


FIG. 6.9.5 NONLINEAR CORRELATION FOR TEST H3; SIDE GIRDER NO. 2;  
TRANSVERSE (Y) DIRECTION

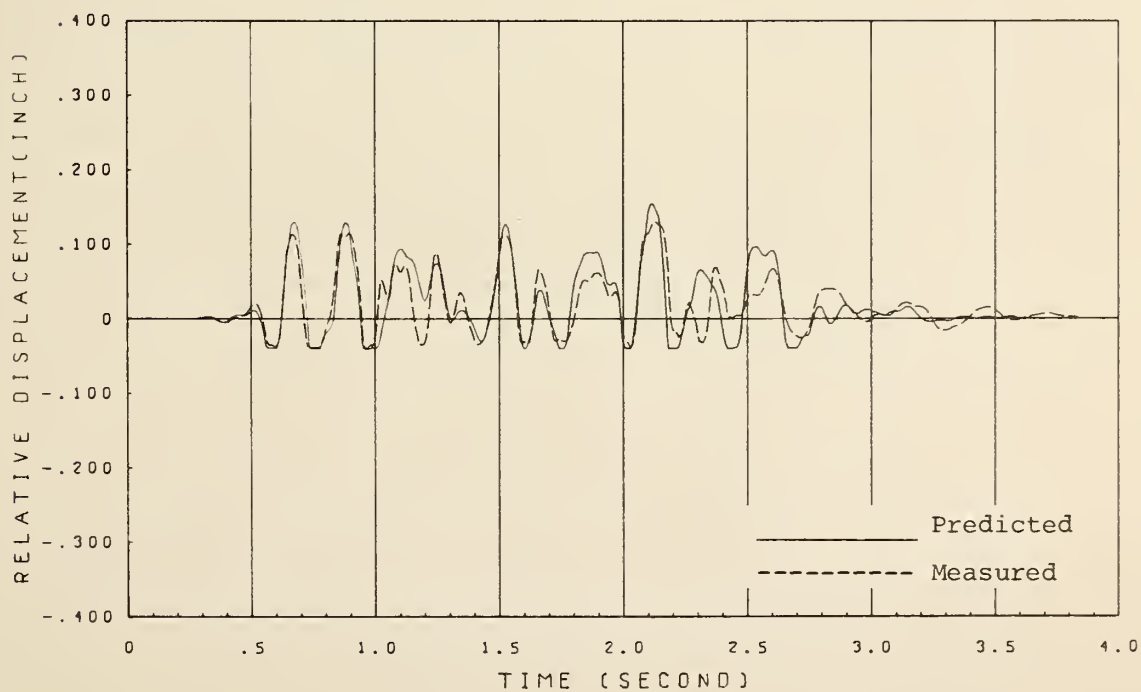


FIG. 6.9.6 NONLINEAR CORRELATION FOR TEST H3; EXPANSION JOINT NO. 1;  
INNER SIDE



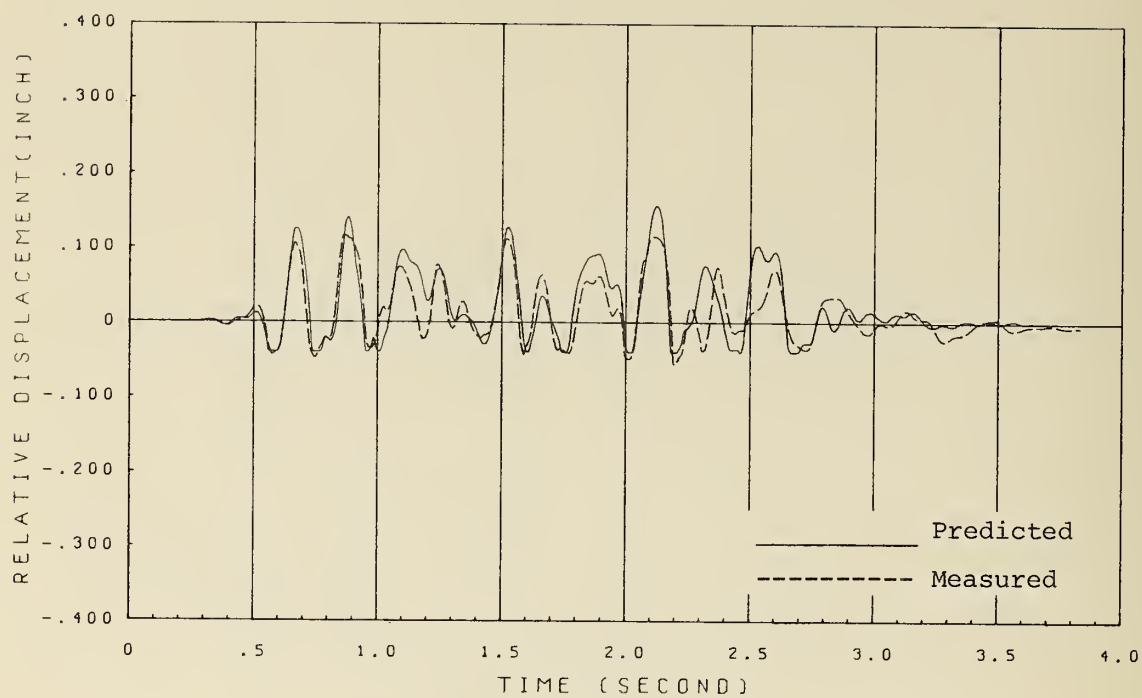


FIG. 6.9.7 NONLINEAR CORRELATION FOR TEST H3; EXPANSION JOINT NO. 1;  
OUTER SIDE

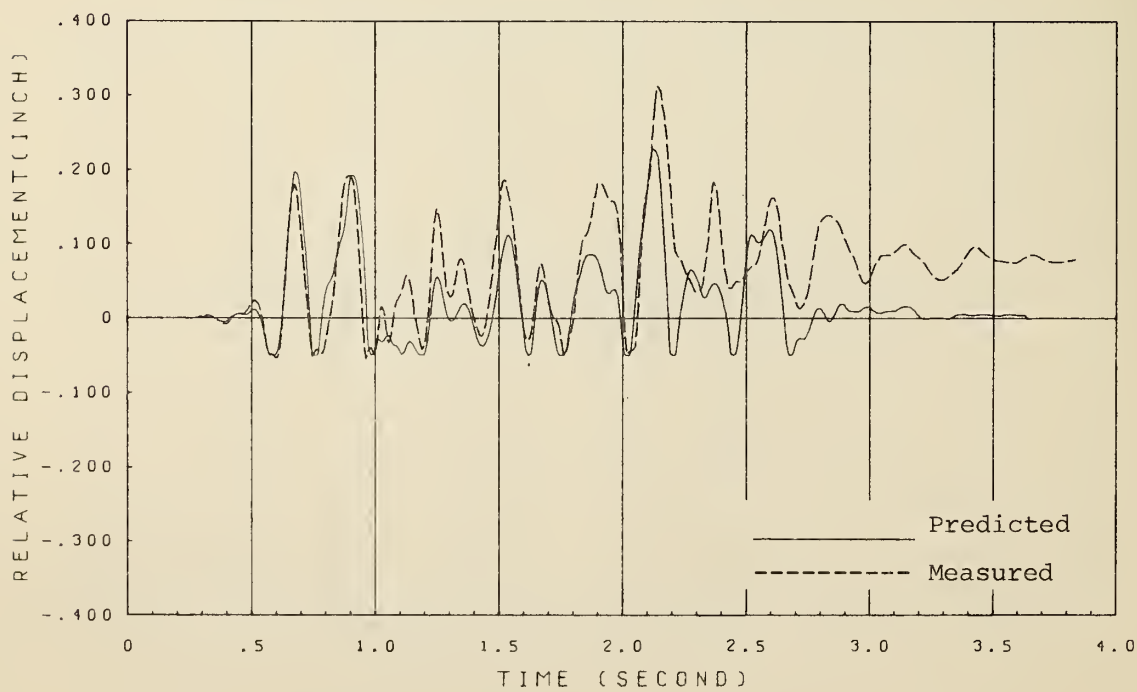


FIG. 6.9.8 NONLINEAR CORRELATION FOR TEST H3; EXPANSION JOINT NO. 2;  
INNER SIDE

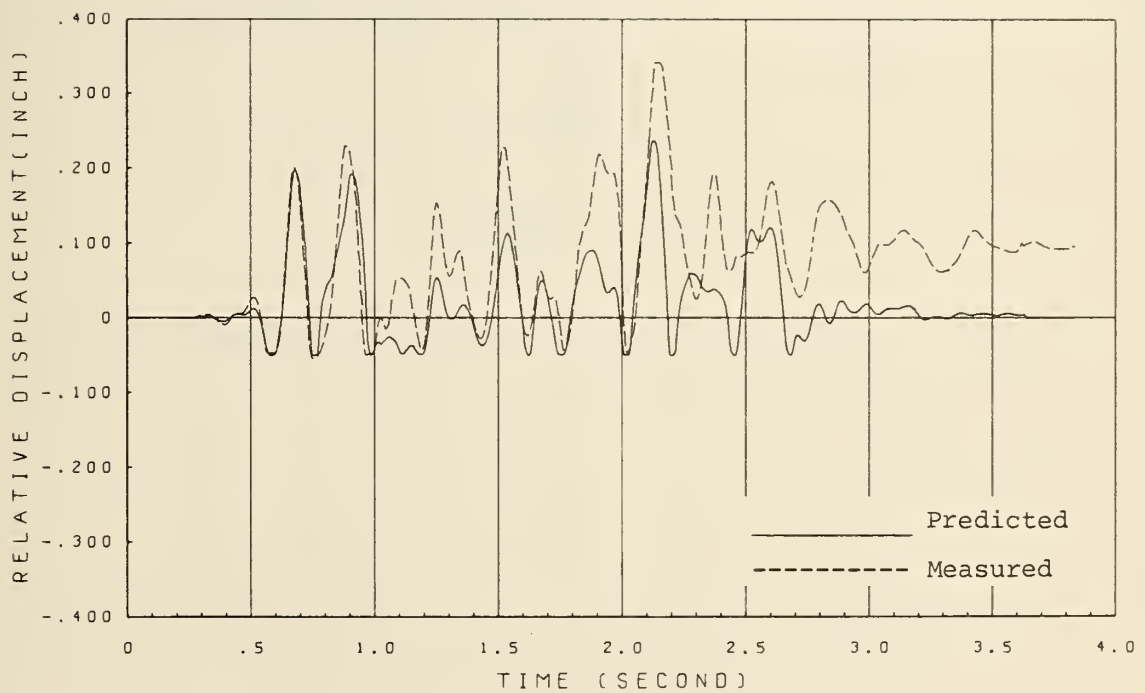


FIG. 6.9.9 NONLINEAR CORRELATION FOR TEST H3; EXPANSION JOINT NO. 2;  
OUTER SIDE

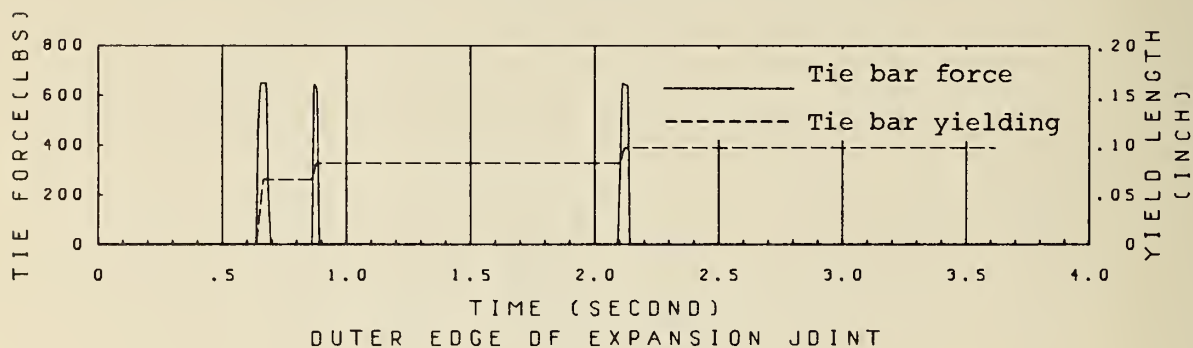
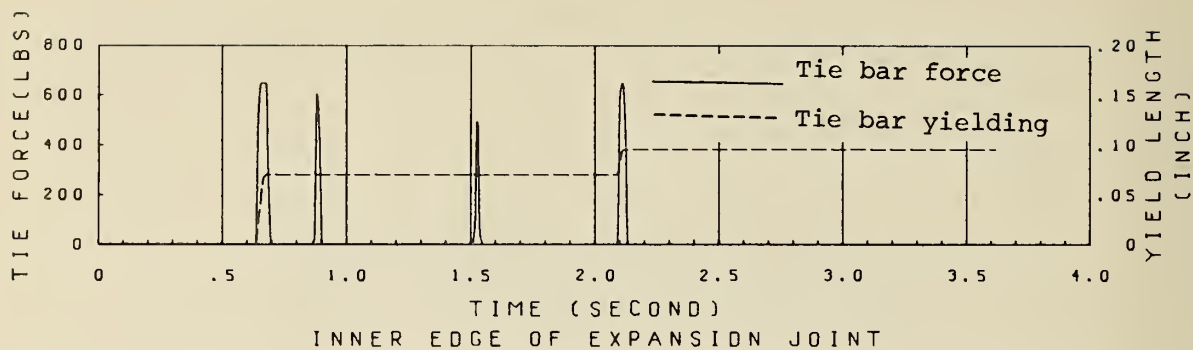


FIG. 6.10.1 PREDICTED TIE BAR FORCE AND YIELD LENGTH FOR TEST H3;  
EXPANSION JOINT NO. 1

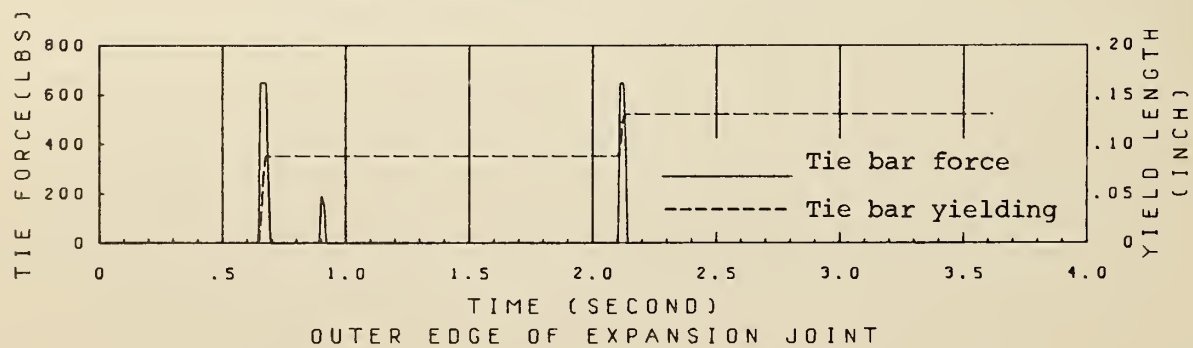
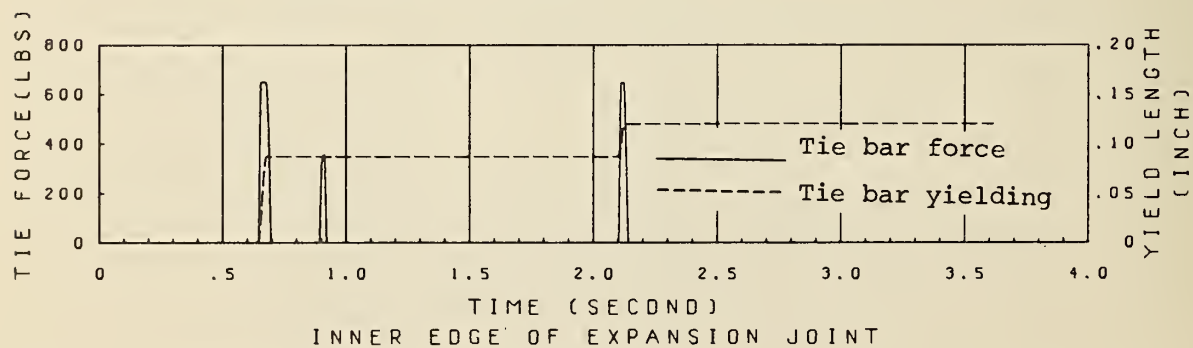


FIG. 6.10.2 PREDICTED TIE BAR FORCE AND YIELD LENGTH FOR TEST H3;  
EXPANSION JOINT NO. 2

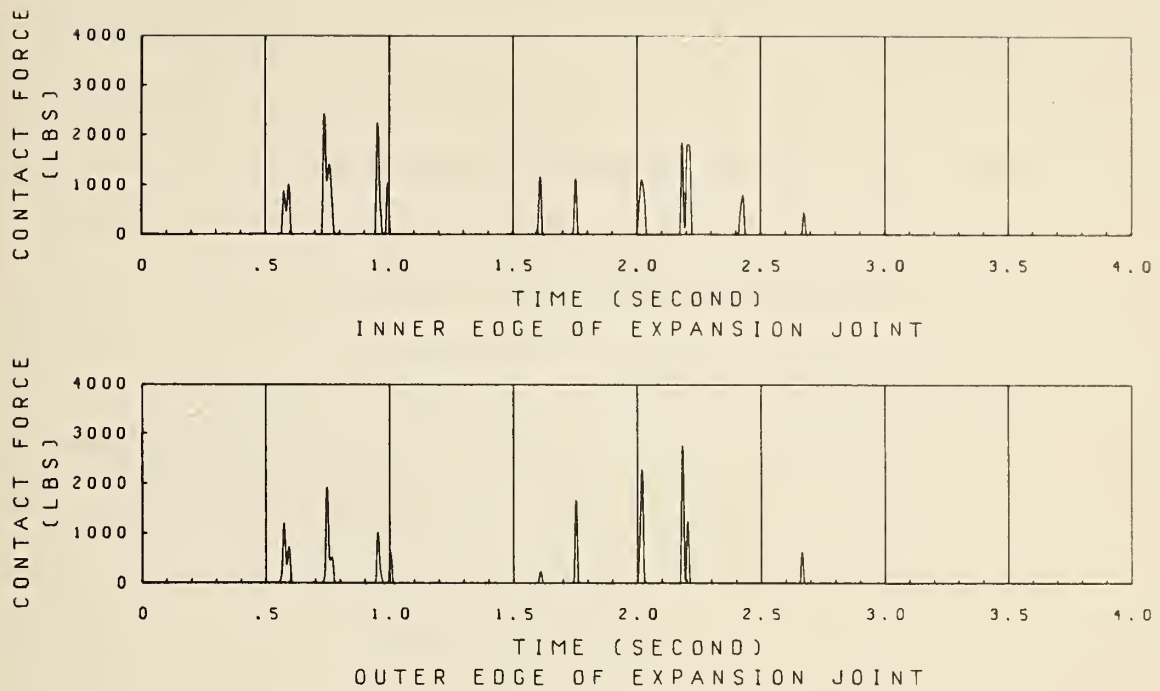


FIG. 6.11.1 PREDICTED CONTACT FORCE FOR TEST H3; EXPANSION JOINT NO. 1

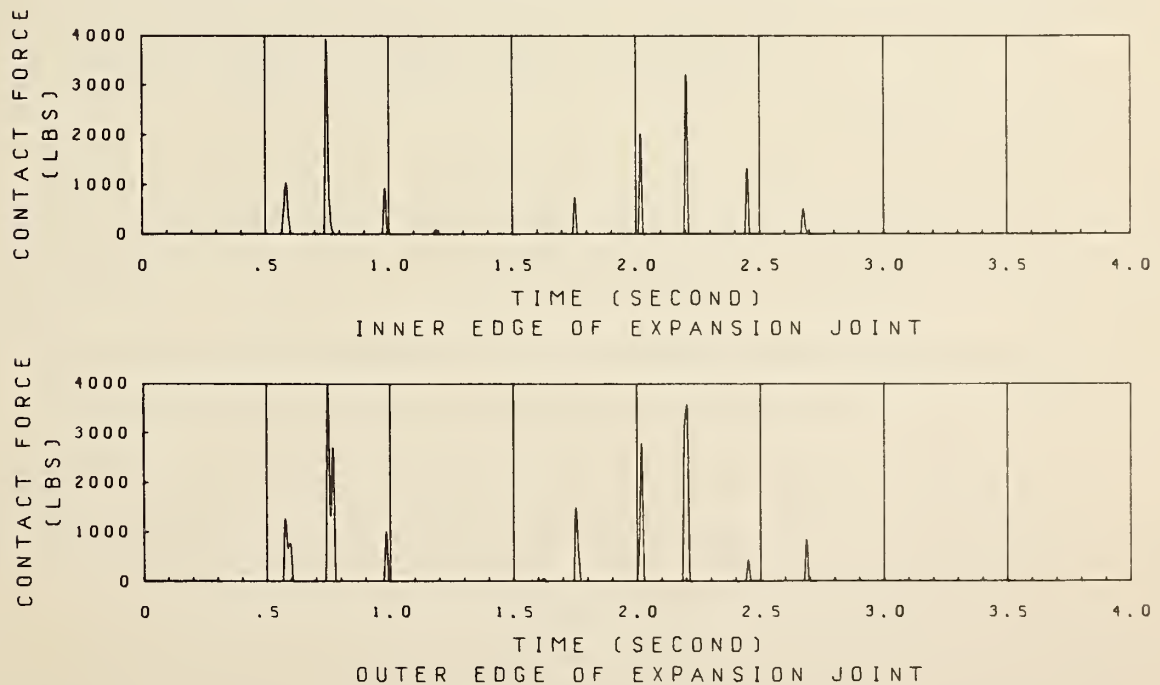


FIG. 6.11.2 PREDICTED CONTACT FORCE FOR TEST H3; EXPANSION JOINT NO. 2

## VII. DISCUSSION OF CORRELATION RESULTS

The purpose of this chapter is to comment on the correlation results presented in the previous chapter. Since Test HV2 shows the most typical response of the bridge model under high intensity excitation including the tie bar yieldings, collisions, slippages and vertical excitation, these comments will concentrate on this test.

### A. JOINT RESTRAINER TIE BARS

The experimental model consisted of three independent subassemblages having essentially different dynamic characteristics which were joined together by restrainer tie bars. The characteristics of these bars are extremely important in controlling the dynamic behavior of the bridge model both in the amplitude and in frequency content. Figure 7.1 shows an example of two different calculated responses which are compared with the corresponding predicted response adopted for the correlation of Test HV2. These three responses were calculated using the same nonlinear analytical model and damping factors but with different tie bar characteristics. In one case, the magnitude of the initial tie gap at expansion joint No. 2 was arbitrarily taken twice that value adopted for the correlation. In another case, it was assumed that no tie bars were provided at the expansion joints. It is apparent from this comparison that the joint restrainer tie bars can be extremely effective in reducing the seismic response of the bridge model, if properly designed. Further, it is apparent that small initial tie gaps are desirable for this purpose.



## B. COLLISIONS

Although the general effects of collisions on the dynamic behavior of the bridge model is apparent from a comparison of responses between the linear analysis correlation and the nonlinear analysis correlation for the Test HV2 or Test H3, the differences observed in this comparison include the effects of other factors, e.g. tie bars, slippages, etc. Therefore in an attempt to isolate the effects of collisions, one response was calculated using the same nonlinear analytical model adopted finally for the correlation of the Test HV2 but eliminating the impact springs at both expansion joints. The comparative plot between this response and the response calculated for the correlation of Test HV2 is shown in Fig. 7.2. It is seen from this comparison that collisions are a major factor affecting the general behavior of the bridge model subjected to high intensity seismic excitations. It should be noted that even if the response amplitude in the negative direction is suppressed by a collision, the rebound from that collision can appreciably increase the positive response amplitude which follows immediately.

## C. COULOMB FRICTION FORCE

Although a Coulomb friction coefficient of 0.4 was assumed throughout this study based on considerations of the surface condition of the contact plane, its actual value could be expected to vary from 0.3 to 0.6. Therefore, it is of interest to examine the sensitivity of this parameter on the dynamic behavior of the bridge model. Therefore, two responses were calculated using the nonlinear analytical model formulated for Test HV2 but with different Coulomb friction coefficients, i.e. 0.3 and 0.6. The comparative plot of these two responses is shown in Fig. 7.3 which could be compared with the response finally adopted in

the correlation of Test HV2 using a friction coefficient of 0.4. It is apparent from this comparison that the Coulomb friction coefficient has low sensitivity in controlling seismic response. For example, if a Coulomb friction coefficient of 0.6 is used which could be considered a maximum, the maximum friction force acting on one expansion joint would be only 220 lbs corresponding to a vertical contact force of 380 lbs. In comparison, the maximum tie bar force acting on one expansion joint is approximately 1300 lbs which is roughly 6 times as large. Furthermore, the predicted maximum contact force caused by collisions reached approximately 4000 lbs which is roughly 18 times as large. It is clear from this comparison that the overall response was critically controlled by the tie bars for outward motion and by collisions for inward motion with the effects of friction being relatively small.

#### D. VERTICAL EXCITATION

Vertical excitation has an important effect on the vertical response of the bridge model. It also has some effect on horizontal response due to coupling between the horizontal and vertical vibration modes which is associated with deck curvature. Further, the vertical excitation causes vertical oscillatory motion in the superstructure resulting in changes of the vertical contact force at the expansion joints. This, in turn, affects the friction forces acting at expansion joints which affect horizontal response.

To check the influence of vertical excitation, one response was calculated using the nonlinear analytical model adopted for the correlation of Test HV2 but with the vertical excitation removed from the input. The comparative plot of responses with and without vertical excitation is shown in Fig. 7.4. It is apparent from this comparison

that vertical excitation is less significant than horizontal excitation in the transverse direction. This observation is consistent with the relatively low sensitivity of Coulomb friction and relatively small effect caused by coupling of vertical and horizontal modes.

#### E. IMPACT SPRING STIFFNESS

In the analytical correlations presented in Chapter VI, the impact spring stiffness  $k_I$  of  $10^7$  lbs/inch was adopted. This value was selected so that  $k_I$  would be similar in magnitude to the longitudinal stiffness of neighboring curved beam elements representing the superstructure; see Appendix A. Since impact is important to response, the sensitivity of stiffness  $k_I$  was examined using the nonlinear analytical model adopted for the correlation of Test HV2 but using two different impact spring stiffnesses  $k_I$ , namely  $10^6$  and  $10^9$  lbs/inch which are, respectively, one tenth and a hundred times that of the impact spring stiffness adopted for the correlation study. It is apparent from the resulting responses shown in Fig. 7.5 that  $k_I$  is an insensitive parameter provided it is set sufficiently large. Therefore, the stiffness of  $10^7$  lbs/inch set in the correlation study is shown to be a proper value for the analysis purpose.

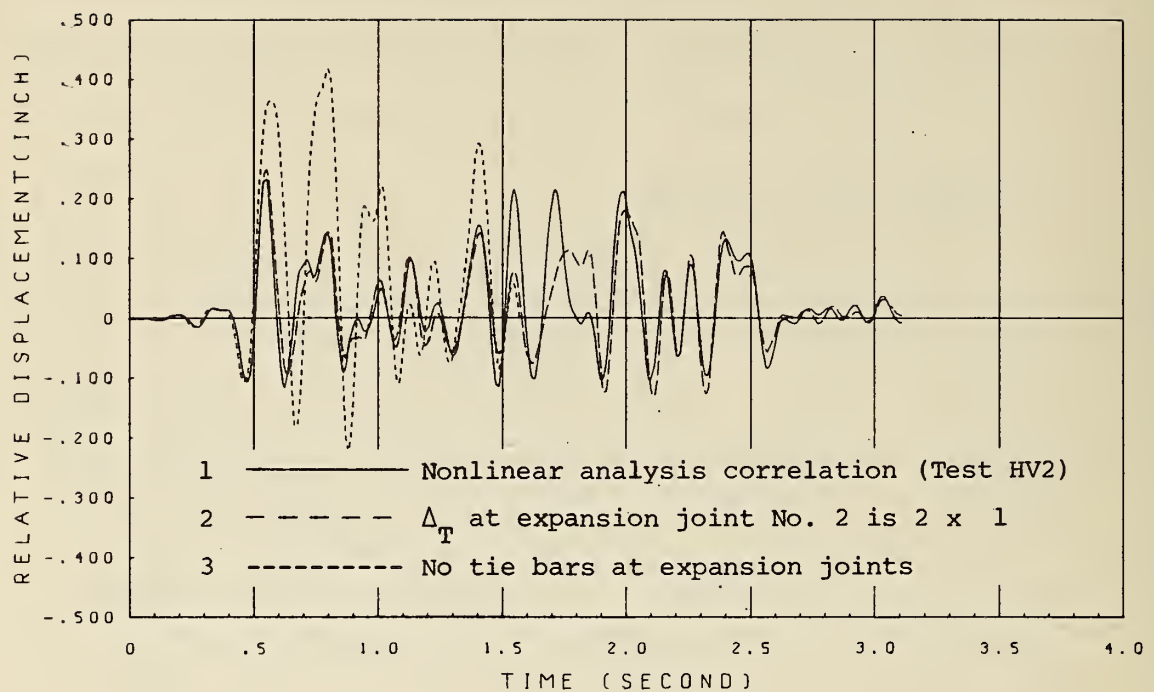


FIG. 7.1.1 EFFECT OF LONGITUDINAL RESTRAINER TIE BARS ON RESPONSE OF CENTER GIRDER; TEST HV2

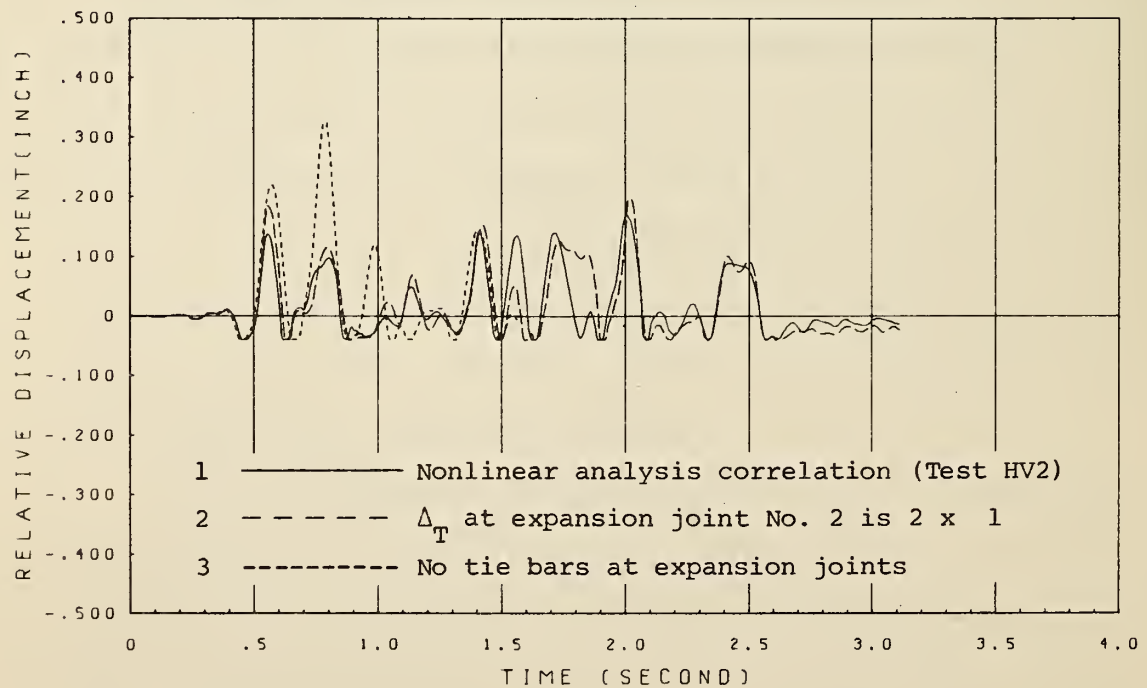


FIG. 7.1.2 EFFECT OF LONGITUDINAL RESTRAINER TIE BARS ON RELATIVE RESPONSE OF EXPANSION JOINT NO. 2 (OUTER SIDE); TEST HV2



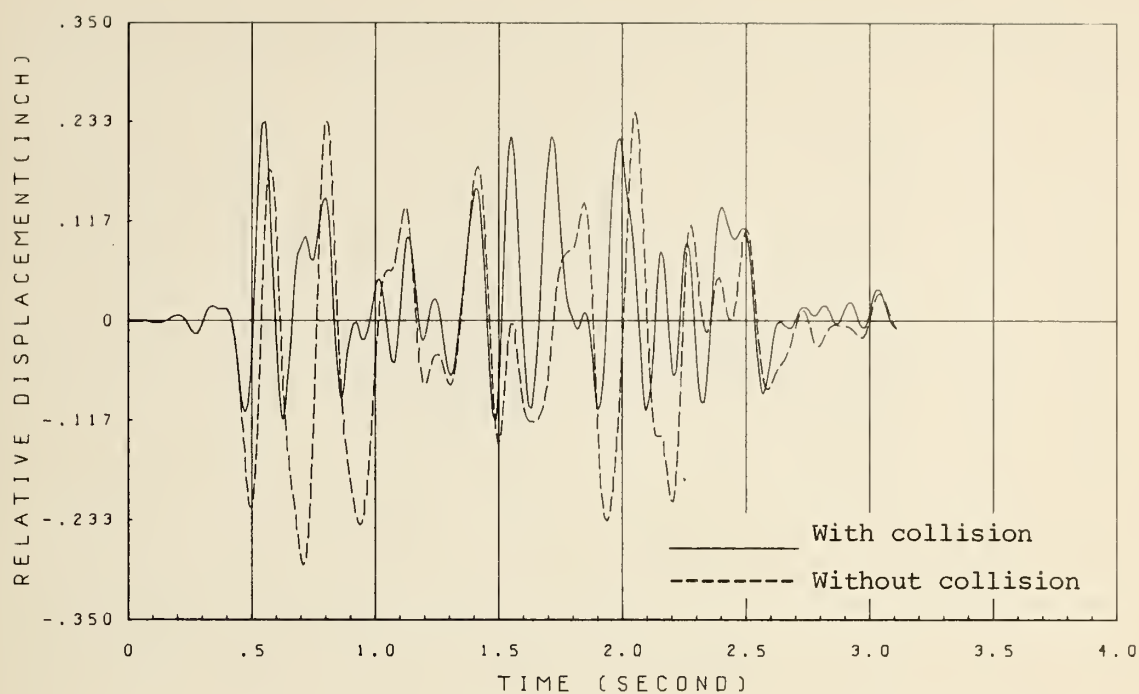


FIG. 7.2.1 EFFECT OF COLLISIONS ON RESPONSE OF CENTER GIRDER; TEST HV2

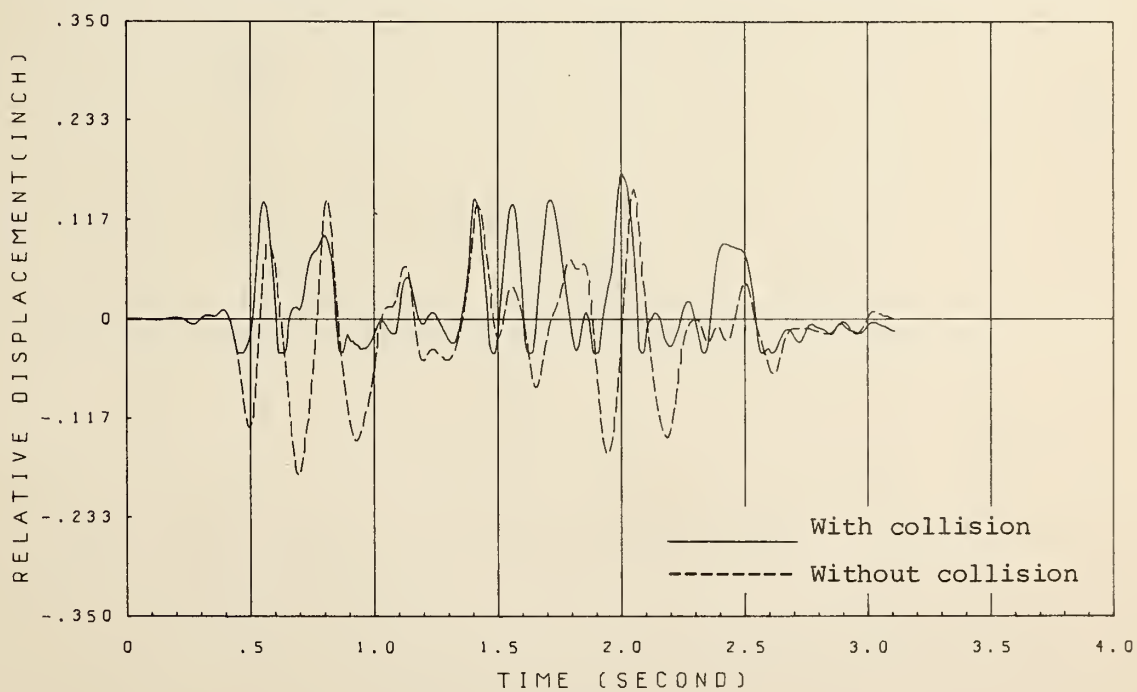


FIG. 7.2.2 EFFECT OF COLLISIONS ON RELATIVE RESPONSE OF EXPANSION JOINT NO. 2 (OUTER SIDE); TEST HV2



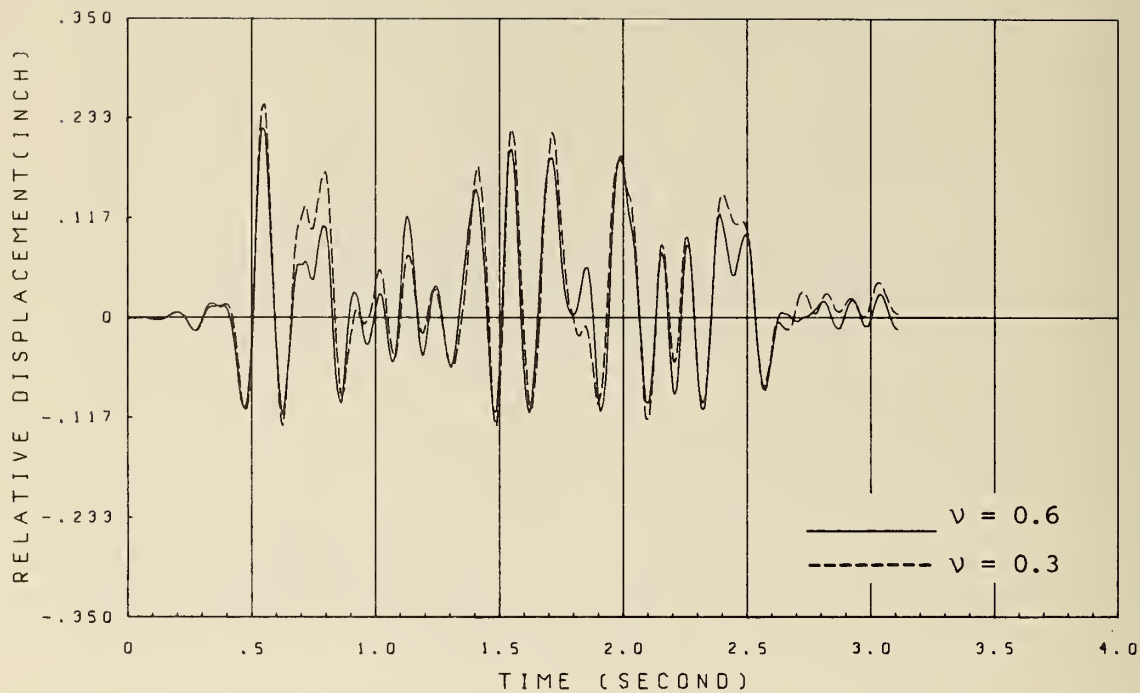


FIG. 7.3.1 EFFECT OF COULOMB FRICTION ON RESPONSE OF CENTER GIRDER;  
TEST HV2

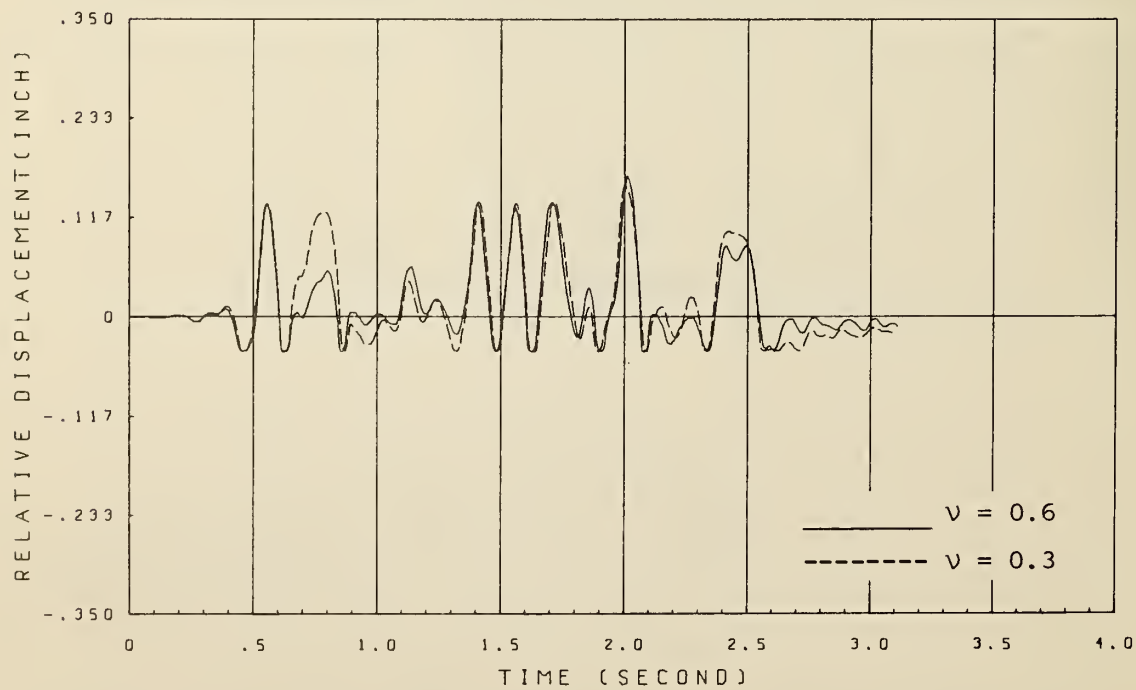


FIG. 7.3.2 EFFECT OF COULOMB FRICTION ON RELATIVE RESPONSE OF EXPANSION  
JOINT NO. 2 (OUTER SIDE); TEST HV2

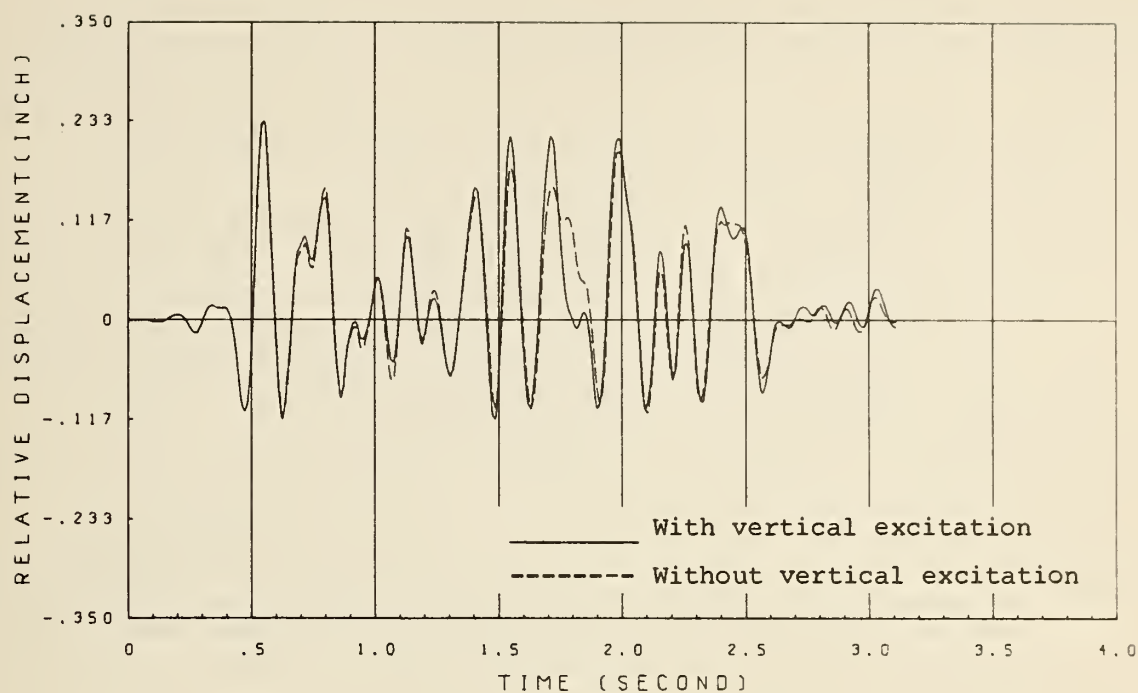


FIG. 7.4.1 EFFECT OF VERTICAL EXCITATION ON RESPONSE OF CENTER GIRDER;  
TEST HV2

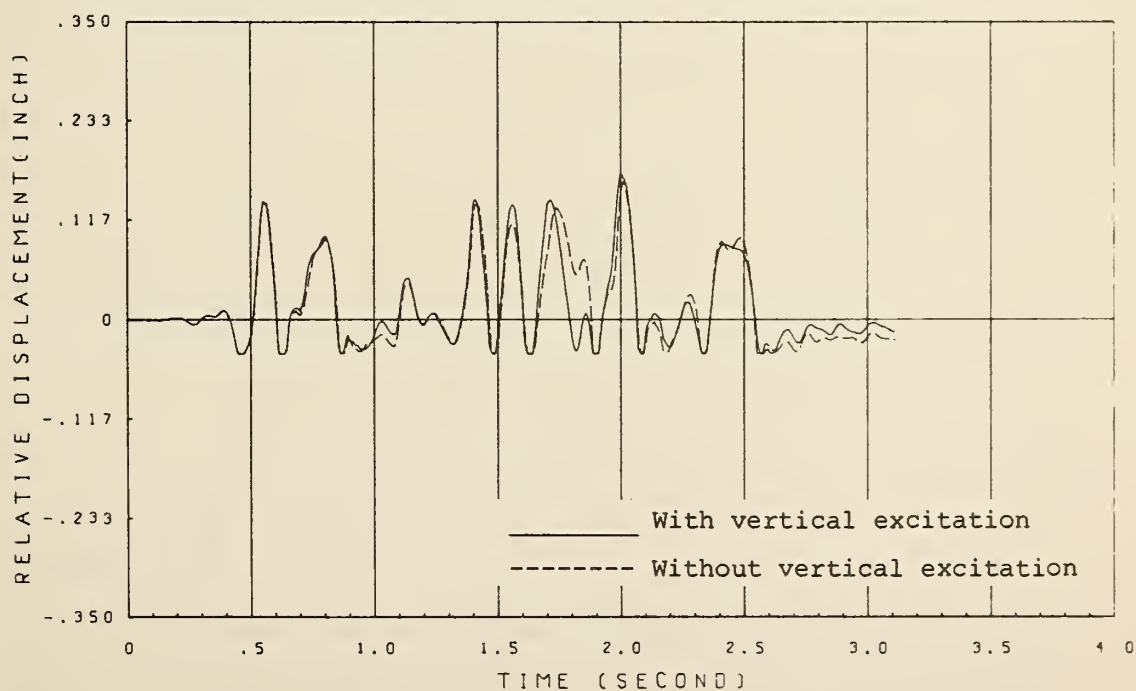


FIG. 7.4.2 EFFECT OF VERTICAL EXCITATION ON RELATIVE RESPONSE OF  
EXPANSION JOINT NO. 2 (OUTER SIDE); TEST HV2

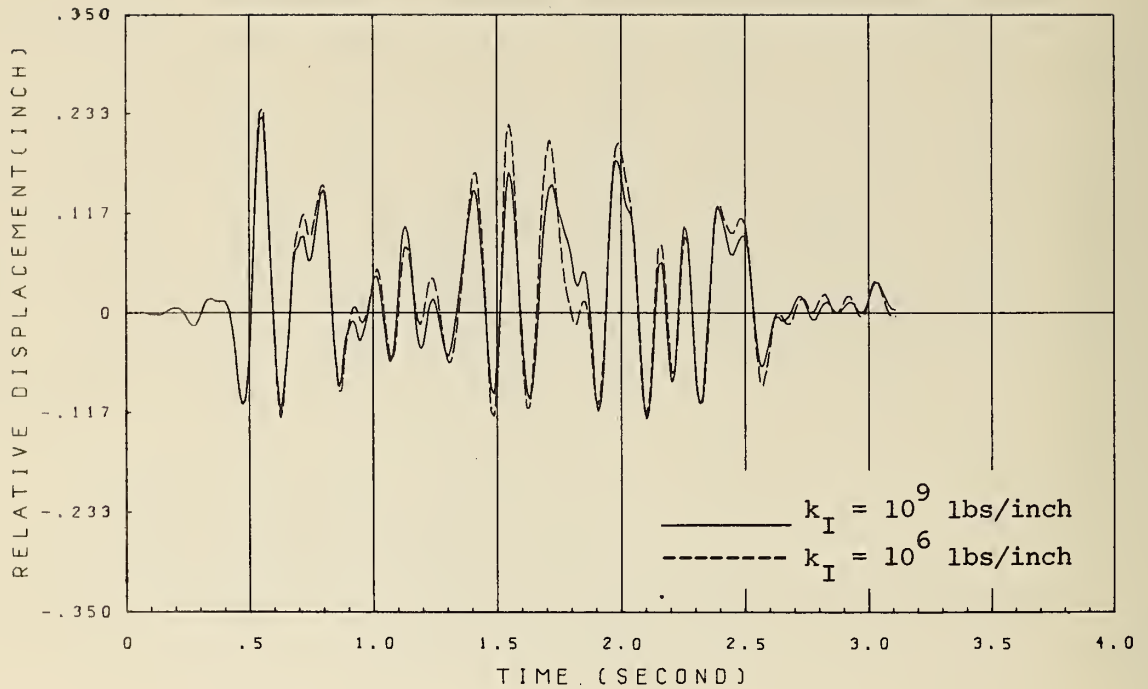


FIG. 7.5.1 EFFECT OF IMPACT SPRING STIFFNESS ON RESPONSE OF CENTER GIRDER; TEST HV2

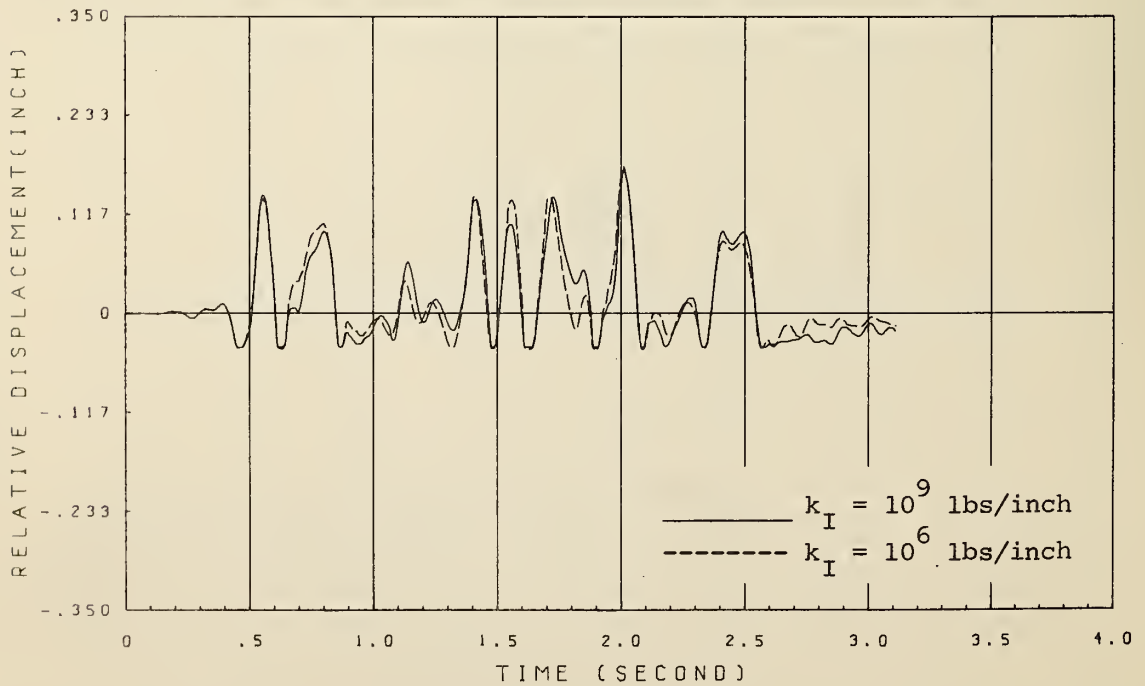


FIG. 7.5.2 EFFECT OF IMPACT SPRING STIFFNESS ON RELATIVE RESPONSE OF EXPANSION JOINT NO. 2 (OUTER SIDE); TEST HV2

## VIII CONCLUSIONS

Based on the correlation results presented, the following conclusions may be deduced:

(1) The mathematical model and analytical procedure developed in Phase 2, which were modified and improved in Phase 5, predicts realistically the nonlinear response of the bridge model under low and high intensity seismic excitations as conducted in Phase 4.

(2) The displacement seismic response of the bridge model under low intensity excitation which does not result in significant yielding of the longitudinal joint restrainer tie bars and does not produce collision of the girders can be predicted with fairly good accuracy using the linear analytical model provided the low frequency characteristics of analytical model agree well with those of the physical model and provided a proper damping factor is used in the analysis.

(3) The linear analytical model cannot satisfactorily predict the seismic response of the bridge model under high intensity seismic excitations causing appreciable yielding of tie bars and multiple collisions of the girders, even if the low frequency characteristics and the damping factor of the analytical model are adjusted.

(4) The displacement seismic response of the bridge model produced by high intensity excitations resulting in severe yielding of tie bar and collisions of the girders can be predicted realistically using the nonlinear analytical model which accounts for the effects of collisions, slippages and tie bars.

(5) The expansion joints have a controlling effect on the dynamic behavior of the bridge model; thus, their characteristics must be properly represented in a realistic mathematic model of the bridge structure.

(6) Under high intensity seismic excitations, the dynamic response of the bridge model is primarily controlled by joint restrainer tie bars for motions in the outward direction and by multiple collisions for motions in the inward direction with the effects of Coulomb friction being relatively small.

(7) Vertical excitation has an important effect on the vertical response of the bridge model. However, the effect of vertical excitation on horizontal transverse response is relatively small due to the insensitivity of coupling of vertical and horizontal modes and of Coulomb friction on horizontal response.

(8) The longitudinal restrainer tie bars are very effective in reducing transverse response of the bridge model provided they are properly designed. Smaller tie gaps are also effective in reducing transverse response.

(9) The multiple collisions which take place between girders have a major influence on both the amplitude and the frequency characteristics of response and they cause large contact forces to be developed at expansion joints. Even though a negative response amplitude is suppressed by collision, the rebound from that collision can result in an increased positive response amplitude immediately following the collision.

(10) The mathematical model, analytical procedures, and computer program NEABS can be used to predict realistic dynamic response of prototype bridge structures subjected to high intensity rigid base seismic excitation.



## BIBLIOGRAPHY

1. Iwasaki, T., Penzien, J. and Clough, R., "Literature Survey -- Seismic Effects on Highway Bridges," Report No. EERC 71-11, Earthquake Engineering Research Center, University of California, Berkeley, November 1972.
2. Tseng, W. S., and Penzien, J., "Analytical Investigations of the Seismic Response of Long Multiple Span Highway Bridges," Report No. EERC 73-12, Earthquake Engineering Research Center, University of California, Berkeley, June 1973.
3. Tseng, W. S., and Penzien, J., "Seismic Response of Highway Overcrossings," Proc. 5th World Conference on Earthquake Engineering, Rome, Italy, 1973.
4. Tseng, W. S., and Penzien, J., "Seismic Analysis of Long Multiple-Span Highway Bridges," International Journal of Earthquake Engineering and Structural Dynamics, Vol. 4, pp. 3-24, 1975.
5. Tseng, W. S., and Penzien, J., "Seismic Response of Long Multiple-Span Highway Bridges," International Journal of Earthquake Engineering and Structural Dynamics, Vol. 4, pp. 25-48, 1975.
6. Chen, M. C., and Penzien, J., "Analytical Investigations of Seismic Response of Short, Single, or Multiple-Span Highway Bridges," Report No. EERC 75-4, Earthquake Engineering Research Center, University of California, Berkeley, January 1975.
7. Goldsmith, W., "Impacts," Edward Arnold, London, 1960.
8. Clough, R. W., and Penzien, J., "Dynamics of Structure, McGraw Hill, 1975.
9. Ban, S., "Collisions of Building Structure during Earthquakes," Trans. of the Architectural Institute of Japan, Vol. 221, pp. 1-7, July, 1974, (In Japanese).
10. Takeyama, K., "Earthquake Response of A Building Collided with A Neighboring Building," Proc. of 5th World Conference on Earthquake Engineering, Rome, Italy, 1973.
11. Bathe, K. J., Wilson, E. L., and Peterson, F. E., "SAP IV -- A Structural Analysis Program for Static and Dynamic Response of Linear Systems, Report No. EERC 73-11, Earthquake Engineering Research Center, University of California, Berkeley, June 1973.
12. Newmark, N. M., "A Method of Computation for Structural Dynamics," Proc. ASCE, Vol. 85, No. EM3, pp. 67-94, July 1959.
13. Wilson, E. L., and Clough, R. W., "Dynamic Response by Step-by-Step Matrix Analysis," Proc. Symposium on the use of Computers in Civil Engineering, Lisbon, Portugal, 1962.

14. Clough, R. W., and Bathe, K. J., "Finite Element Analysis of Dynamic Response," 2nd U.S.-Japan Seminar on Matrix Methods of Structural Analysis and Design, pp. 153-179, August 1972.
15. Bathe, K. J., and Wilson, E. L., "Stability and Accuracy Analysis of Direct Integration Methods," International Journal of Earthquake Engineering and Structural Dynamics, Vol. 1, pp. 282-291, 1973.
16. Wilson, E. L., Farhoomand, I., and Bathe, K. J., "Nonlinear Dynamic Analysis of Complex Structures," International Journal of Earthquake Engineering and Structural Dynamics, Vol. 1, pp. 241-252, 1973.
17. Nickell, R. E., "Direct Integration Methods in Structural Dynamics," Proc. ASCE, Vol. 99, No. EM2, pp. 303-317, April 1973.
18. Kanaan, A. E., and Powell, G. H., "General Purpose Computer Program for Dynamics Analysis of Inelastic Plane Structures," Report No. EERC 73-6, Earthquake Engineering Research Center, University of California, Berkeley, 1973.
19. Hughes, T. J., Taylor, R. L., and Sackman, J. L., "Finite Element Formulation and Solution of Contact - Impact Problems in Continuous Mechanics," Report No. UC SESM 74-8, Structural Engineering Laboratory, University of California, Berkeley, 1974.
20. Mondkar, D. P., and Powell, G. H., "Static and Dynamic Analysis of Nonlinear Structures," Report No. EERC 75-10, University of California, Berkeley, March 1975.
21. Bathe, K. J., Wilson, E. L., and Iding, R. H., "NONSAP -- A Structural Analysis Program for Static and Dynamic Response of Nonlinear System," Report No. UC SESM 74-3, Structural Engineering Laboratory, University of California, Berkeley, 1974.
22. Bathe, K. J., Ozdemir, H., and Wilson, E. L., "Static and Dynamic Geometric and Material Nonlinear Analysis," Report No. UC SESM 74-4, Structural Engineering Laboratory, University of California, Berkeley, 1974.
23. Williams, D., and Godden, W. G., "Seismic Response of A Curved Highway Bridge Model," 54th Annual Meeting, Transportation Research Board, National Research Council, Washington, D. C., January, 1975.
24. Williams, D., and Godden, W. G., "Seismic Behavior of High Curved Overcrossings," Proc. of U. S. National Conference on Earthquake Engineering, Ann Arbor, 1975.
25. Howe, S., and Williams, D., "Private Memorandum on Test Procedures and Test Results of Model Bridge Structure," 1975.
26. Williams, D., and Godden, W. G., "16 m/m Film for Experimental Test of Model Bridge Structure, 1975.

27. Rea, D., and Penzien, J., "Dynamic Response of A 20 ft x 20 ft Shaking Table," Proc. of 5th World Conference on Earthquake Engineering, Rome, Italy, 1973.
28. Chopra, A. K., Bertero, V. V., and Mahin, S., "Response of the Olive View Medical Center Main Building during the San Fernando Earthquake," Proc. 5th World Conference on Earthquake Engineering, Rome, Italy, 1973.
29. Tang, D., and Clough, R. W., "Shaking Table Tests of A Steel Frame - A Progress Report," Report No. EERC 74-8, Earthquake Engineering Research Center, University of California, Berkeley, July 1975.
30. Tang, D., "Earthquake Simulatory Study of A Steel Frame Structure, Volume II - Analytical Results," Report No. EERC 75-36, Earthquake Engineering Research Center, University of California, Berkeley, October 1975.
31. Hidalgo, P., and Clough, R. W., "Earthquake Simulatory Study of A Reinforced Concrete Frame," Report No. EERC 74-13, Earthquake Engineering Research Center, University of California, Berkeley, December 1974.
32. Iemura, H., and Jennings, P. C., "Hysteretic Response of a Nine-Story Reinforced Concrete Building During the San Fernando Earthquake," Report No. EERL 73-7, Earthquake Engineering Research Laboratory, California Institute of Technology, Pasadena, October 1973.
33. Bouwkamp, J. G., and Rea, D., "Dynamic Testing and the Formulations of Mathematical Models," Earthquake Engineering, Wiegel, R. L., Coordinating Editor, Prentice Hall, 1970.





## LONGITUDINAL COLLINEAR COLLISION OF TWO RODS

To check the mathematical model and analytical procedures used in representing joint impact as presented in Chapters II and III, respectively, consider the collinear collision of two uniform bars initially travelling in opposite directions with the same initial velocity  $V_0$  as shown in Fig. A.1. The approximate solution of the post-impact behavior obtained by these procedures can be compared with the exact solution obtained by classical wave propagation theory [7].

Assume both bars have the same properties as given by

$$\begin{aligned} E \text{ (modulus of elasticity)} &= 100 \\ A \text{ (cross-sectional area)} &= 1 \\ \rho \text{ (mass density)} &= 0.1 \\ L \text{ (rod length)} &= 10 \\ V_0 \text{ (initial rod velocity)} &= \pm 0.1 \end{aligned} \tag{A-1}$$

in which any convenient units may be used. For this example problem, the impact contact duration  $T_I$  is 0.2 units of time as given by the exact solution. This duration corresponds to the time required for a wave to propagate twice the length of the rod, i.e.

$$T_I = \frac{2L}{c_0} \tag{A-2}$$

where  $c_0$  is the longitudinal wave velocity given by

$$c_0 = \sqrt{E/\rho} \tag{A-3}$$

In both the exact and approximate solutions, it is convenient to monitor the separation and rate of change of separation between the two bars as given by



$$\begin{aligned} u &= u^R - u^L \\ \dot{u} &= \dot{u}^R - \dot{u}^L \end{aligned} \tag{A-4}$$

where  $u^R$  and  $\dot{u}^R$  represent the displacement and velocity, respectively, of the contact surface of the right bar and  $u^L$  and  $\dot{u}^L$  represent the displacement and velocity, respectively, of the contact surface of the left bar. A positive value of  $u$  represents a separation of the contact surfaces while a negative value of  $u$  represents an overlap of the contact surfaces. A negative value of  $u$  is, of course, not possible in reality as given by the exact solution.

Using the modelling procedures of Chapter II, the two bars can be represented by an impact spring and finite elements as shown in Fig. A-2. In this case, a zero value of  $u$  represents that position of the bars when initial contact is made on both sides with the impact spring; thus, a negative value of  $u$  is possible which corresponds to the shortening of the impact spring.

In modelling the two bar system in Fig. A-2, the impact spring stiffness  $K^I$ , the numerical time interval of integration  $\Delta t$ , and the number of finite elements  $n$  representing each rod are all factors influencing the predicted dynamic response following impact. The constant acceleration integration procedure with equilibrium iteration has been used in this example parameter study. The tolerances controlling the equilibrium iteration, as defined in Eqs. (51) and (63), were specified as

$$\begin{aligned} \Delta_{ps} &= 0.001 \\ \Delta_{ps}^I &= 0.001 \end{aligned} \tag{A-5}$$

Responses  $u$  and  $\dot{u}$  as predicted by exact wave propagation theory are shown in Fig. A.3. Before collision, the relative separation velocity  $\dot{u}$  equals  $-0.2$  which instantaneously changes to zero upon collision. This velocity stays at a value of zero during the contact duration equal to  $0.2$  and then instantaneously changes to a value of  $+0.2$ . It should be noted that the instantaneous change in velocity represents a Dirac delta change in the acceleration, i.e. a pure acceleration pulse of duration and amplitude which tend to zero and infinity, respectively.

Turning now to the approximate solution, consider first the effect of the magnitude of the impact spring stiffness  $K^I$  upon response. Using a time interval of integration  $\Delta t$  equal to  $0.01 T_I$ , a value of  $10$  for  $n$ , and five different values for  $K^I$  ( $10, 10^2, 10^3, 10^4$  and  $10^5$ ), responses  $u$  and  $\dot{u}$  as shown in Fig. A.4 were obtained. Comparing the relative displacement results in this figure with the corresponding results for the exact solution given in Fig. A.3 shows that the exact and approximate values of  $u$  are in good agreement for  $K^I$  equal to  $10^2$  and  $10^3$  but they are significantly in error for the larger values of  $K^I$ . Comparing the relative velocity results in these same figures shows considerable differences for all 5 values of  $K^I$  and it shows considerable vibrations taking place following unit time zero. These vibrations in velocity  $\dot{u}$  increase in amplitude with increasing values of  $K^I$ . It is interesting to note that when the larger values of  $K^I$  are used, contact and separation of the bar ends are repeated many times during period  $T_I$ . To judge the best value of  $K^I$  it is convenient to introduce the dimensionless parameter

$$\gamma = \frac{K^I L}{n EA} \quad (A-6)$$

which represents the ratio of the impact spring stiffness to an individual rod element stiffness. Comparing responses  $u$  and  $\dot{u}$  in Figs. A.3 and A.4, it appears that a value of unity for  $\gamma$  yields the best overall correlation of the approximate results with exact results. This suggests that the numerical value of  $K^I$  should be approximately equal to the stiffness of its neighboring elements.

Let us now consider the effect of the magnitude of  $\Delta t$  upon response. Using  $K^I$  equal to 100 ( $\gamma = 1$ ),  $n$  equal to 10, and  $\Delta t$  equal to  $0.5 T_I$ ,  $0.05 T_I$ , and  $0.01 T_I$ , responses  $u$  and  $\dot{u}$  were obtained as shown in Fig. A.5. The displacement response  $u$  agrees well with the exact response shown in Fig. A.3 for  $\Delta t$  equal to  $0.05 T_I$  and  $0.01 T_I$  but shows considerable error for  $\Delta t$  equal to  $0.5 T_I$ . These and similar results for other values of  $\Delta t$  indicate that the approximate response  $u$  will agree reasonable well with the exact response provided  $\Delta t$  is assigned a value less than  $0.2 T_I$ . The velocity response  $\dot{u}$  in Fig. A.5 shows an erroneous oscillation for  $\Delta t$  equal to  $0.05 T_I$  and  $0.01 T_I$ . However, if a smooth curve is drawn through these oscillations, it would agree reasonable well with the exact relation shown in Fig. A.3. The velocity response in Fig. A.5 for  $\Delta t$  equal to  $0.5 T_I$  is greatly in error which again shows that  $\Delta t$  must be taken much smaller than  $0.5 T_I$ .

Further, let us consider the effect of the value of  $n$  on dynamic response. Using  $K^I$  equal to 100,  $\Delta t$  equal to  $0.01 T_I$ , and  $n$  equal to 2, 10, and 40, responses  $u$  and  $\dot{u}$  were obtained as shown in Fig. A.6. The approximate displacement response for all three values of  $n$  agrees very closely with the exact response; however, the approximate velocity response agrees closely with the exact response

only for the case of  $n$  equal to 40. Considerable disagreement in the velocity response is noted for  $n$  equal to 10 and an even larger disagreement is noted for  $n$  equal to 2.

Finally, let us consider the variations of particle velocity and longitudinal stress with position along both bars for the case of  $n$  equal to 10,  $K^I$  equal to 100 ( $\gamma = 1$ ), and  $\Delta t$  equal to  $0.05 T_I$ . The resulting variations along both bars for instantaneous times  $t$  equal to 0,  $0.25 T_I$ ,  $0.50 T_I$ ,  $0.75 T_I$ ,  $1.00 T_I$ , and  $1.25 T_I$  are shown in Fig. A.7. The ordinates representing particle velocity and stress have been normalized by dividing by the initial bar velocity (0.1) and the exact intensity of the stress wave ( $\bar{V}_O \rho E = 0.2 \rho E$ ), respectively. Comparing these variations with the exact solution shows that reasonably accurate results can be obtained by the approximate method employing an impact spring.

Based on the above discussion, the effects of parameters  $K^I$ ,  $\Delta t$ , and  $n$  on the dynamic response of two colliding rods can be summarized as shown in Table A.1.



TABLE A-1 EFFECTS OF VARIOUS PARAMETERS ON PREDICTED RESPONSE OF COLLIDING RODS

EFFECTS PARAMETERS	Overlap Between Contact Planes	Velocity Change After Collision	Numerical Oscillation of $\dot{u}$ and $\ddot{u}$	Numerical Duration of Collision $T_I'$	Stress During Collision
Increase of $K^I$	decreased	less significant	increased but approaches to a certain level	$T_I' \approx T_I$ for $\gamma \geq 1$ $T_I' > T_I$ for $\gamma \ll 1$	less significant for $\gamma \geq 1$ becomes small for $\gamma \ll 1$
Increase of $n$	less significant	less significant	decreased	less significant	less significant
Decrease of $\Delta t$	less significant	less significant	less significant	$T_I' \approx T_I$ for $\Delta t < \left(\frac{1}{4} \sim \frac{1}{6}\right) T_I$ $T_I' > T_I$ for $\Delta t > \left(\frac{1}{4} \sim \frac{1}{6}\right) T_I$	less significant as long as $\Delta t$ is small enough to provide realis- tic solution



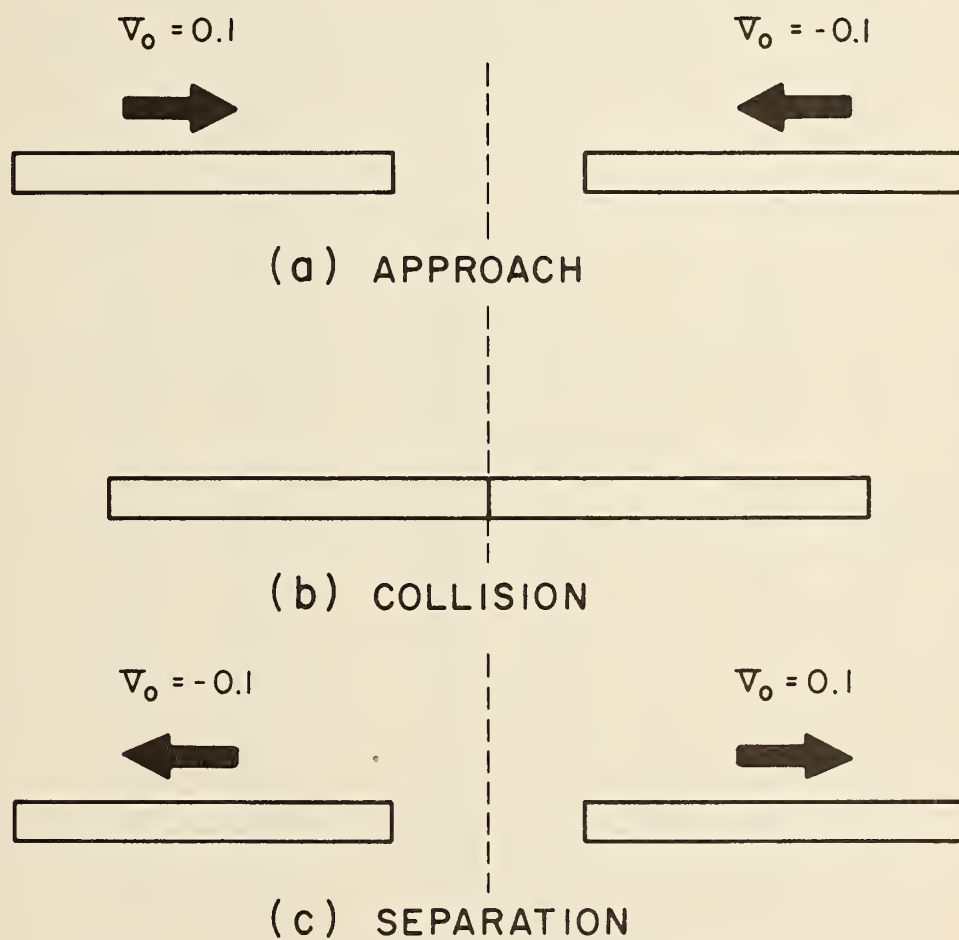
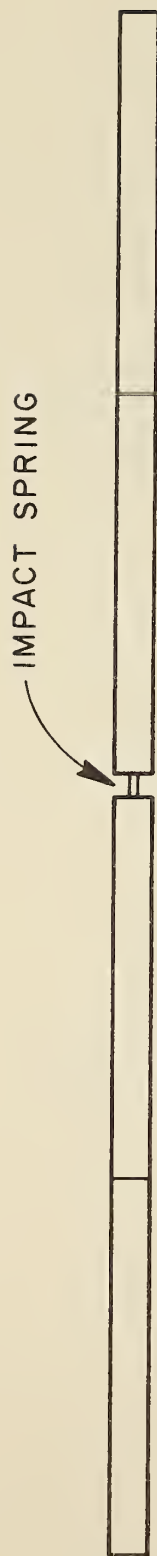


FIG. A.1 LONGITUDINAL COLLINEAR COLLISION OF TWO RODS



(a) NUMBER OF ELEMENTS PER ROD = 2



(b) NUMBER OF ELEMENTS PER ROD = 10



(c) NUMBER OF ELEMENTS PER ROD = 40

FIG. A.2 ANALYTICAL MODEL FOR COLLISION OF RODS

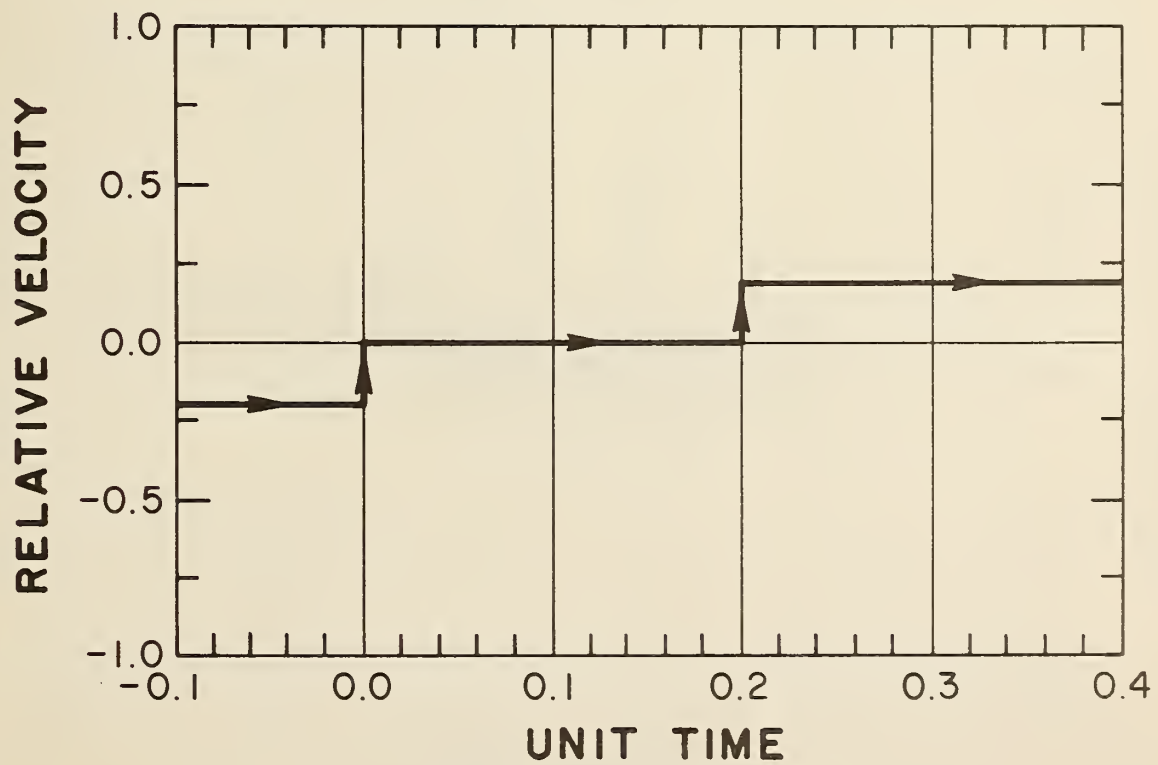
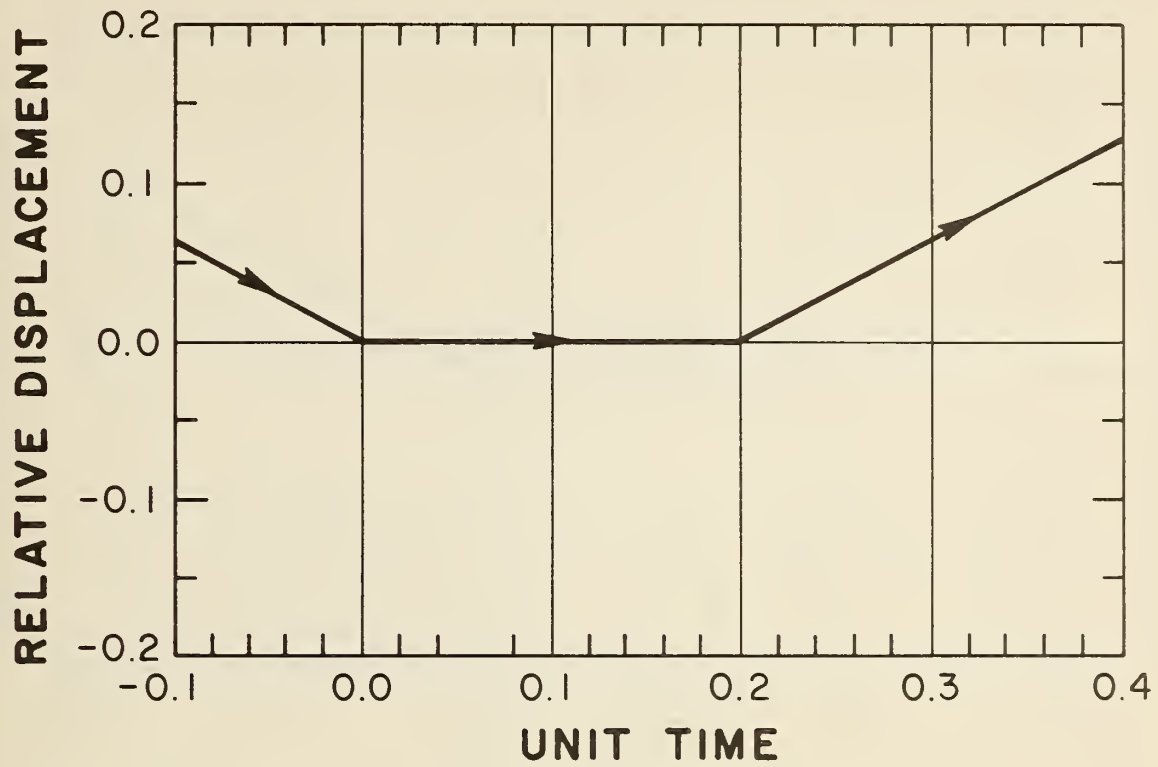


FIG. A.3 EXACT SOLUTION OF RELATIVE DISPLACEMENT AND RELATIVE VELOCITY

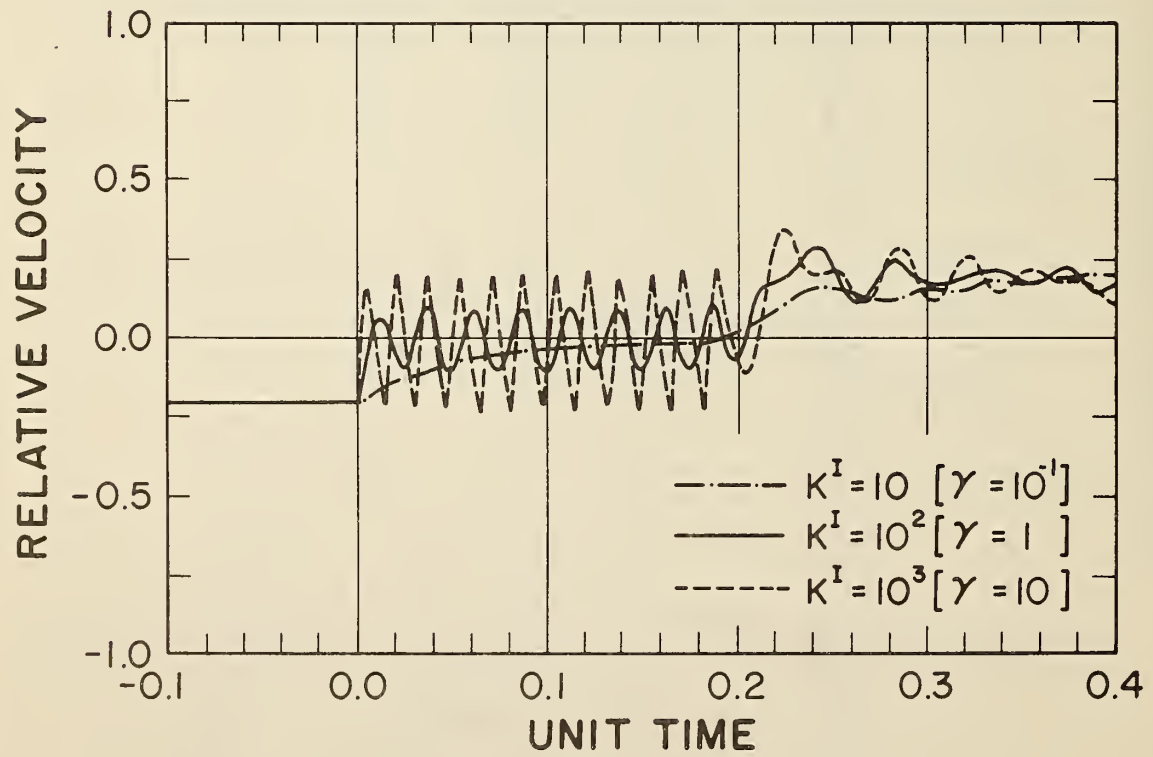
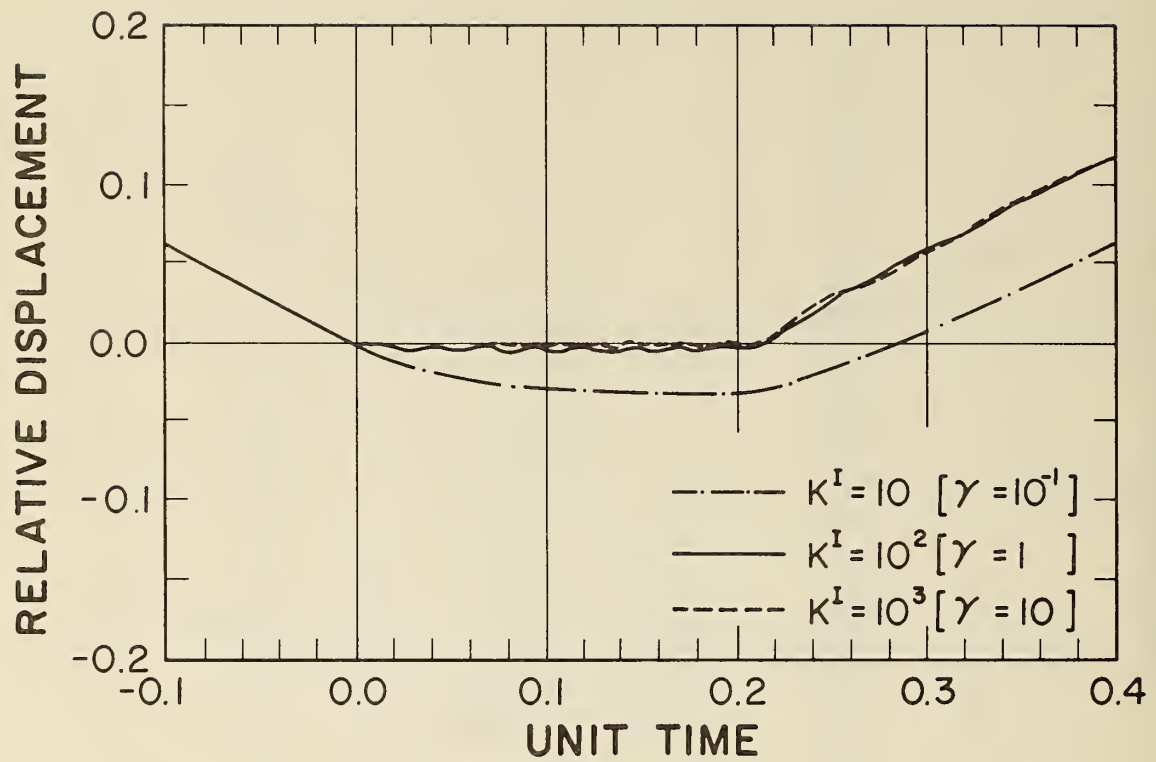


FIG. A.4.1 EFFECT OF IMPACT SPRING STIFFNESS ON RELATIVE RESPONSE OF RODS ( $K^I = 10, 10^2$  and  $10^3$ )

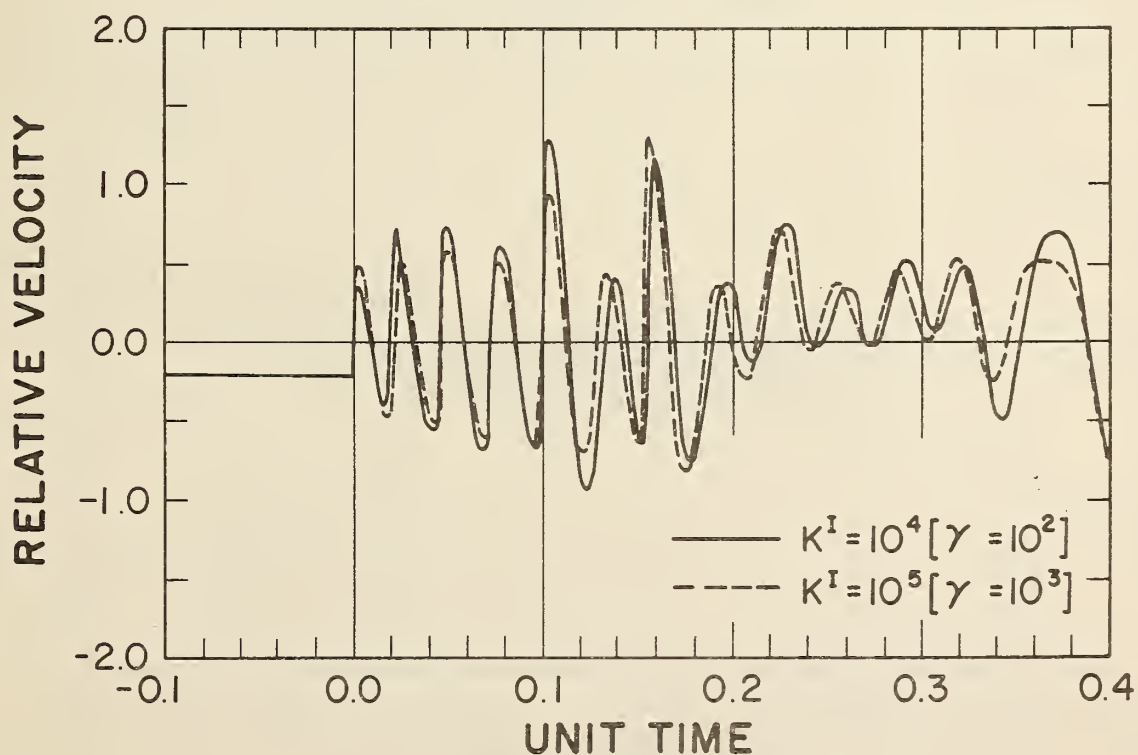
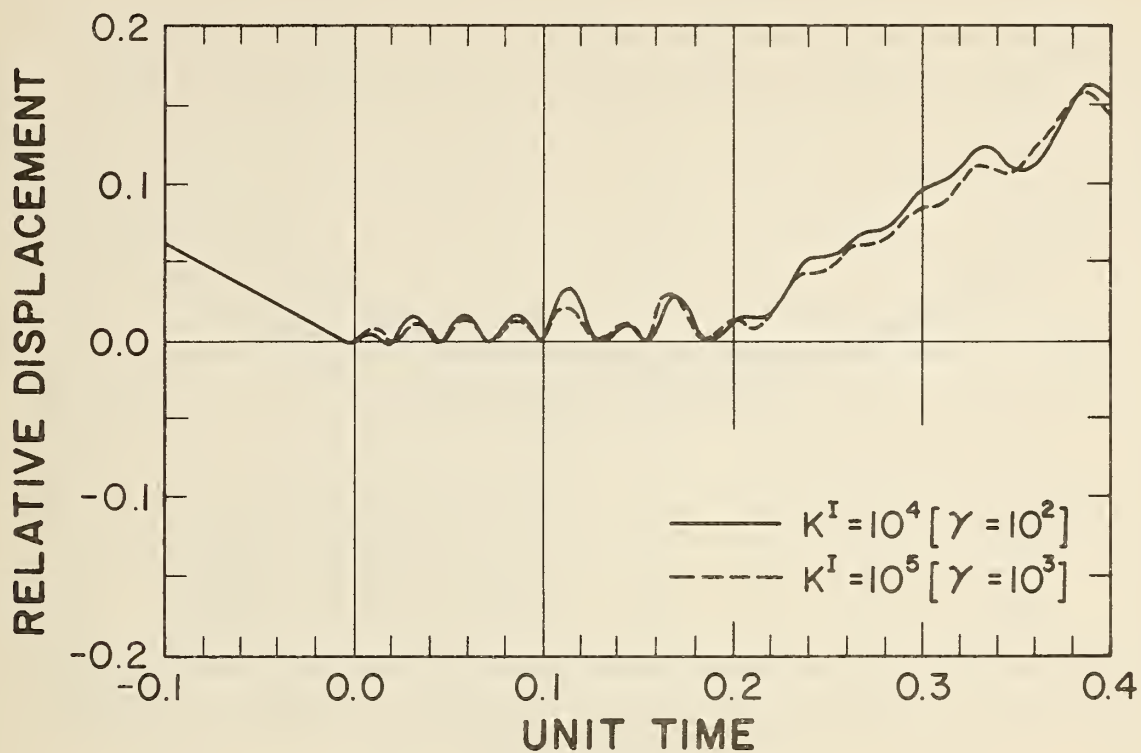


FIG. A.4.2 EFFECT OF IMPACT SPRING STIFFNESS ON RELATIVE RESPONSE OF RODS ( $K^I = 10^4$  and  $10^5$ )



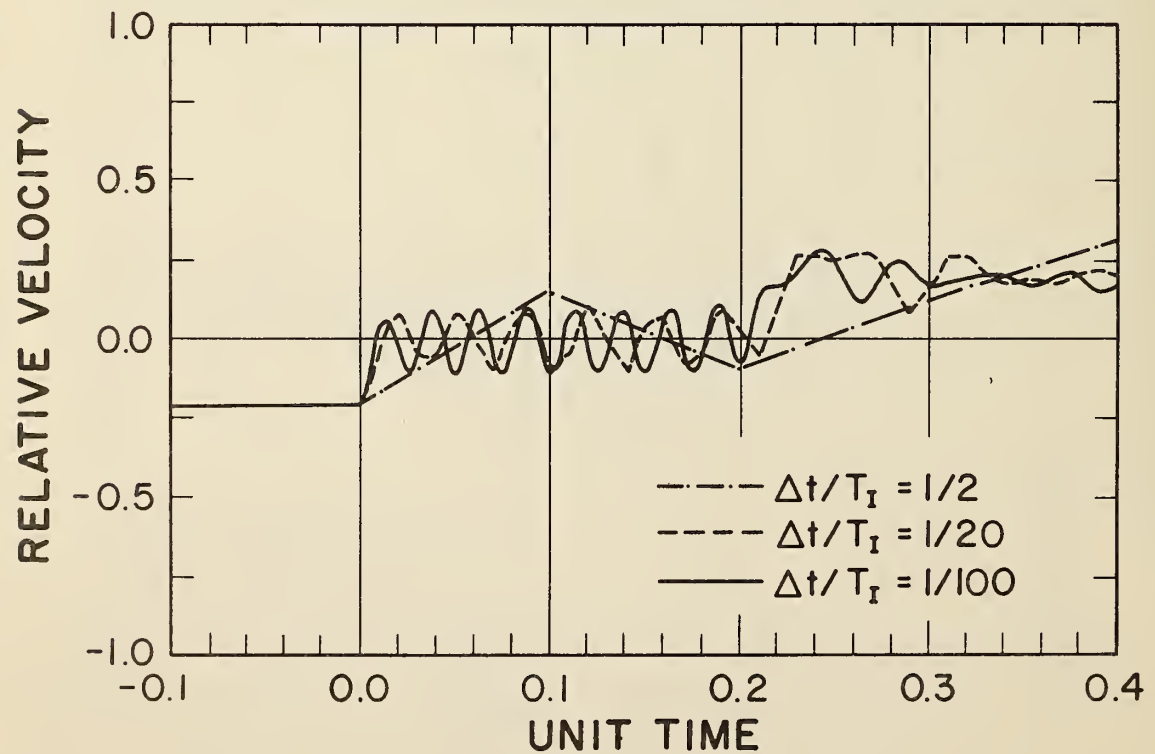
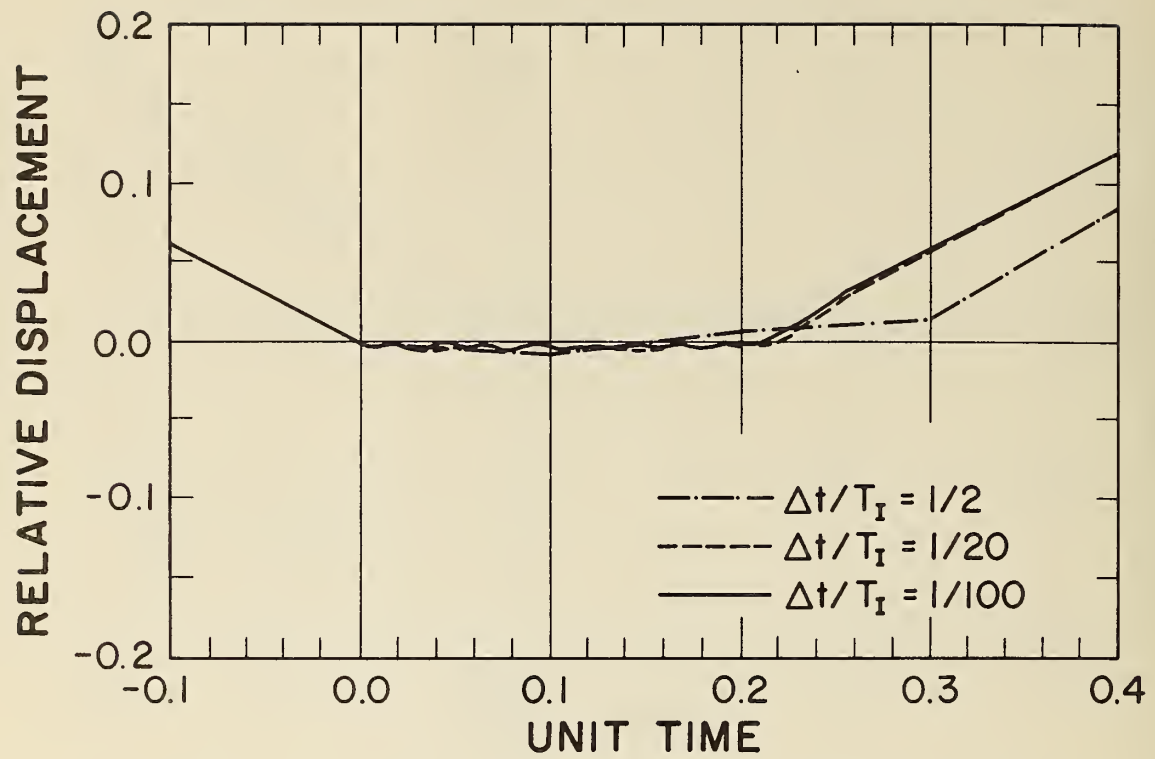


FIG. A.5 EFFECT OF TIME INTERVAL ON RELATIVE RESPONSE OF RODS

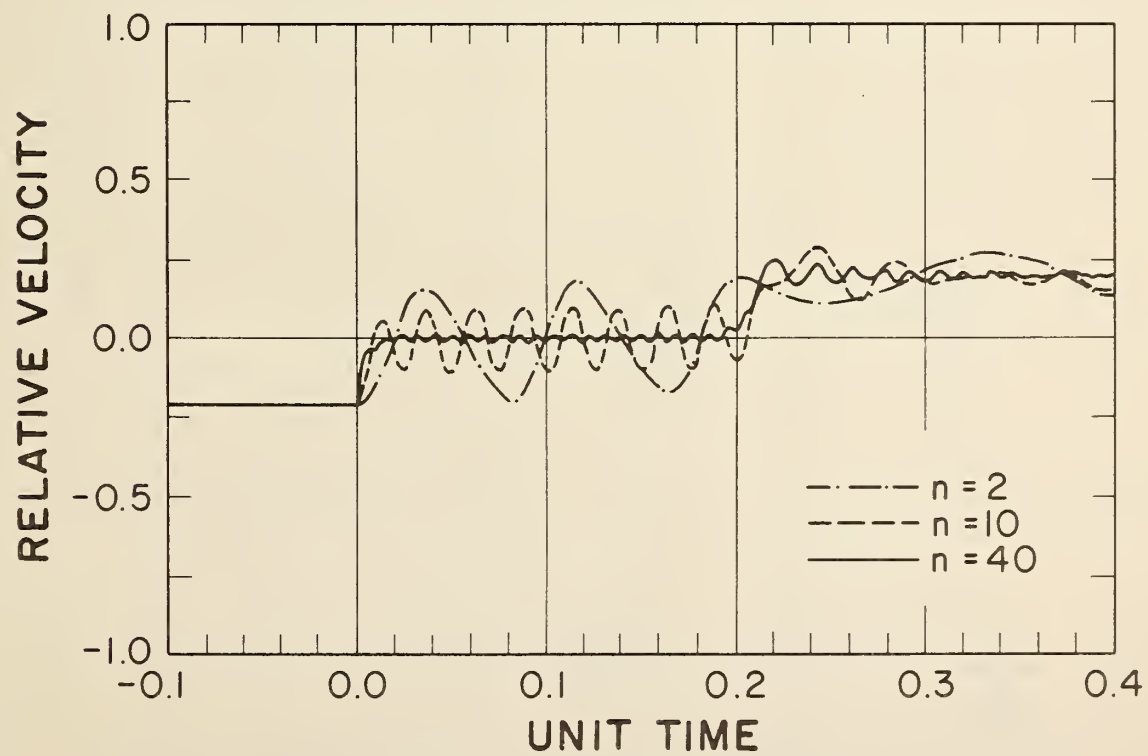
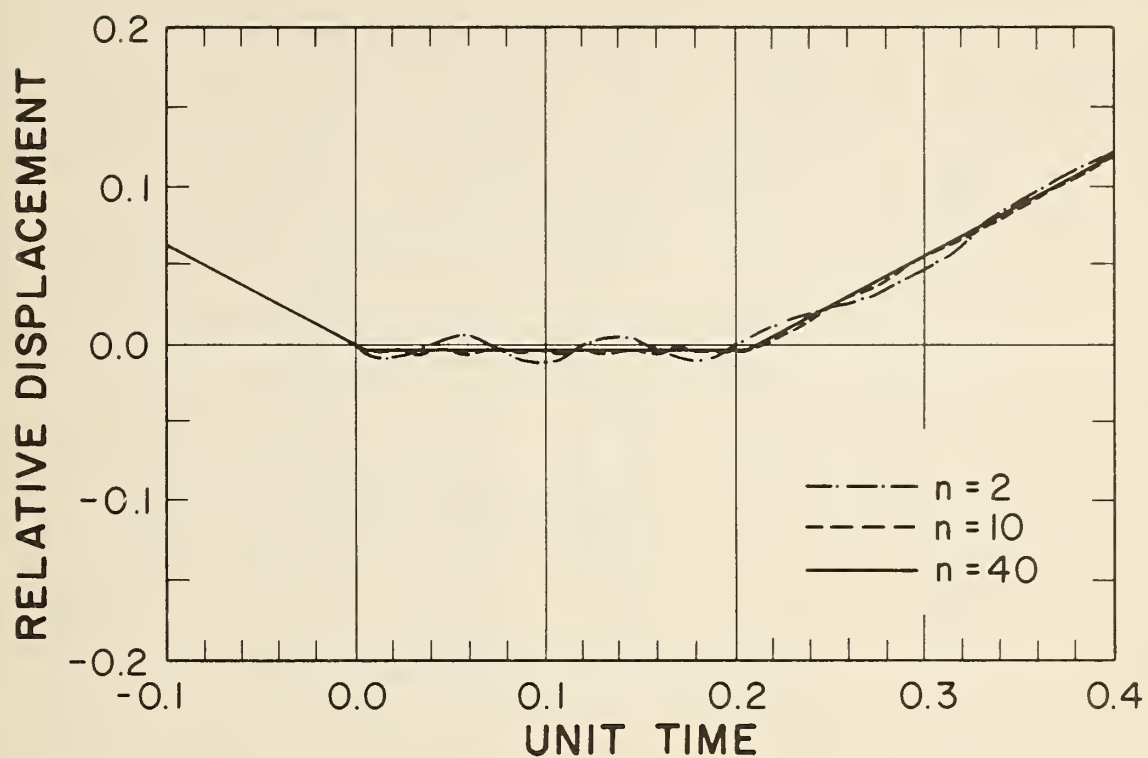


FIG. A.6 EFFECT OF ELEMENT NUMBER ON RELATIVE RESPONSE OF RODS

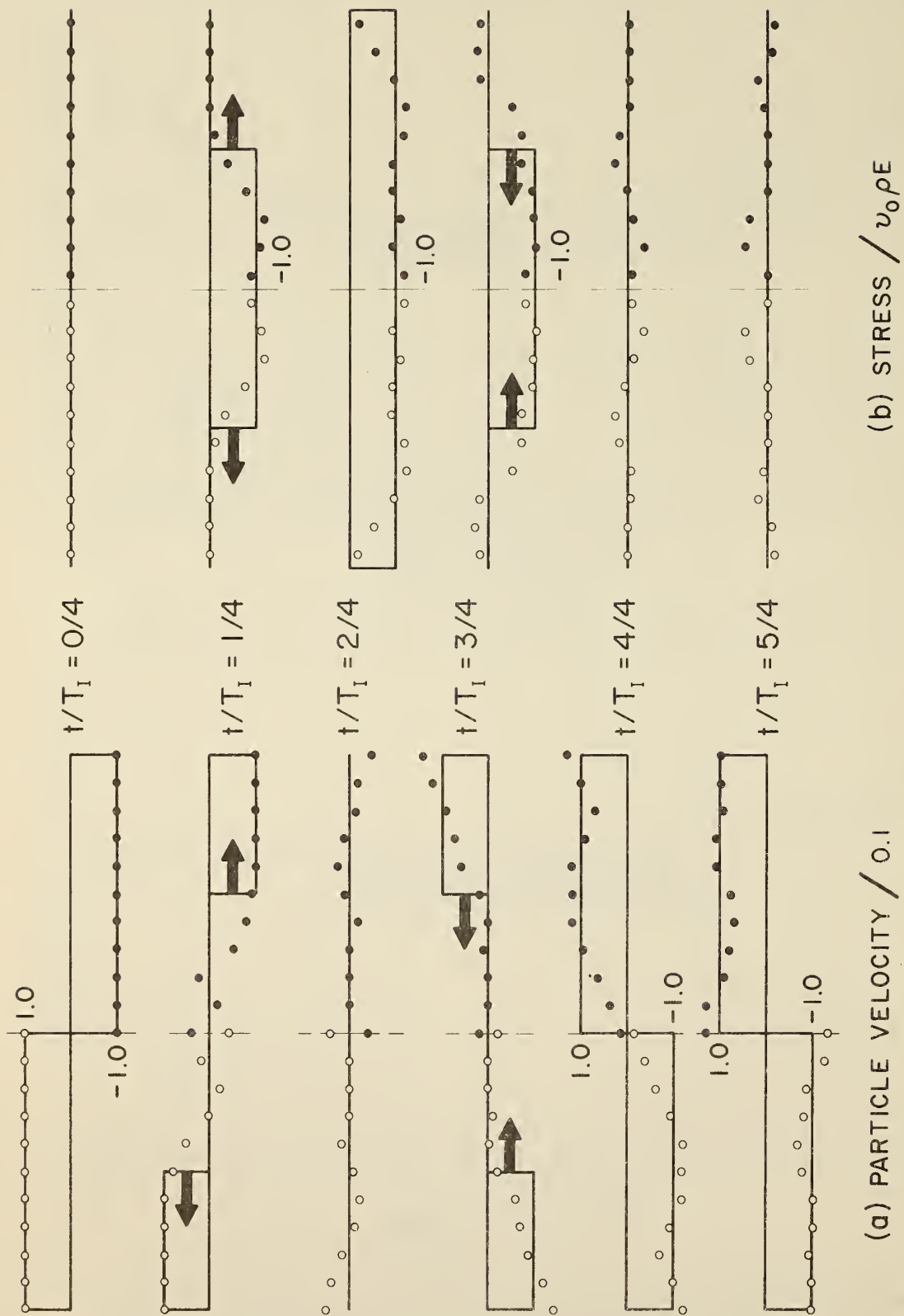


FIG. A.7 PREDICTED PARTICLE VELOCITY AND STRESS OF RODS

## APPENDIX B

### FREE VIBRATION OF A SINGLE SPRING-MASS SYSTEM WITH COULOMB FRICTION

Consider the rigid mass  $m$  shown in Fig. B.1 which is attached to a linear elastic spring of stiffness  $k$  and is supported on a surface which can develop Coulomb friction having a maximum absolute value of  $\nu mg$  ( $\nu$  = Coulomb friction coefficient). If the mass is displaced to the right, elongating the spring by an amount  $x_0$ , where  $x_0 \gg \Delta$  and where

$$\Delta = \frac{F}{k} = \frac{\nu mg}{k} \quad (B-1)$$

, and it is then released from rest, the free vibration equation of motion becomes

$$m \ddot{x} + k x = - F \operatorname{sign}(\dot{x}) \quad (B-2)$$

Introducing two new variables, namely

$$\begin{aligned} x_1 &\equiv x + \Delta \\ x_2 &\equiv x - \Delta \end{aligned} \quad (B-3)$$

, Eq. (B-2) can be written in the double form

$$\begin{aligned} m \ddot{x}_1 + k x_1 &= 0 & \dot{x} &> 0 \\ m \ddot{x}_2 + k x_2 &= 0 & \dot{x} &< 0 \end{aligned} \quad (B-4)$$

, having solutions

$$\begin{aligned} x_1 &= A \cos(\omega_n t - \gamma) & \dot{x} &> 0 \\ x_2 &= A' \cos(\omega_n t - \gamma') & \dot{x} &< 0 \end{aligned} \quad (B-5)$$

where  $\omega_n = \sqrt{k/m}$  and  $A$ ,  $A'$ ,  $\gamma$ , and  $\gamma'$  are arbitrary constants. The solution of Eq. (B-2) can now be written as

$$\begin{aligned}
 x &= -\Delta + A \cos(\omega_n t - \gamma) & \dot{x} &> 0 \\
 x &= \Delta + A' \cos(\omega_n t - \gamma') & \dot{x} &< 0
 \end{aligned}
 \tag{B-6}$$

As an example, let  $x_0$  equal  $12\Delta$ . The resulting motion of the mass as represented by Eq. (B.6) is that motion shown in Fig. B.2. It is well known that the frequency of free vibration of the system with Coulomb friction is the same as the free vibration frequency with no damping. Further, it is well known that the amplitude of oscillation diminishes by an amount  $4\Delta$  with each full cycle. The block finally comes to rest in the first extreme position which is less than  $\Delta$ . For this example, the final rest is reached at time  $t = 6\pi/\omega_n$ .

The above example problem has also been solved using the mathematical model and analytical procedures defined in Chapter II and III, respectively. The numerical data used in this approximate solution were the following:

$$\begin{aligned}
 m &= 80/386.4 \text{ lbs sec}^2/\text{inch} \\
 k &= 400 \text{ lbs/inch} \\
 v &= 0.5 \\
 f_n &= \frac{1}{2\pi} \sqrt{\frac{(400)(386)}{80}} = 6.98 \text{ c/s} \\
 \omega_n &= 2\pi (6.98) = 43.8 \text{ c/s} \\
 \Delta &= \frac{F}{k} = \frac{(0.5)(80)}{400} = 0.1 \text{ inch} \\
 x_0 &= 12 \Delta = 1.2 \text{ inch}
 \end{aligned}
 \tag{B-7}$$

In the numerical calculation, it is convenient to introduce the elastic deformation



$$u^e \equiv \frac{F}{k^e} \quad (B-8)$$

where  $F = \gamma mg$  and  $k^e$  is the elastic stiffness of the Coulomb friction elastoplastic model defined in Fig. 2.4. The constant acceleration integration procedure with equilibrium iteration is used for the analysis. The tolerances controlling the equilibrium iteration were specified as

$$\delta R_t \leq 0.1 \quad ; \quad \delta R_t^{(i)} \leq 0.01 \quad (B-9)$$

where  $\delta R_t$  and  $\delta R_t^{(i)}$  represent the residual forces at time  $t$  and during the  $i$ th iteration, respectively.

First, let us examine the effect of the value of  $u^e$  on response. Using a time interval  $\Delta t$  equal to  $0.05(2\pi/\omega_n)$  throughout the calculations, the displacement response shown in Fig. B.3 is obtained. Clearly, the approximate solution approaches the exact solution with decreasing values of the ratio  $u^e/\Delta$ . Quite good agreement is shown when this ratio is assigned the value 0.1, particularly for the higher amplitude oscillations.

Now let us examine the effect of the value of  $\Delta t$  on response. For this examination, let  $u^e$  equal  $0.1 \Delta$  and compare the resulting responses for  $\Delta t$  equal to  $0.05(2\pi/\omega_n)$ ,  $0.10(2\pi/\omega_n)$ , and  $0.166(2\pi/\omega_n)$  as shown in Fig. B.4. It is quite apparent from these results that the approximate solution is improved by decreasing the time interval  $\Delta t$ .

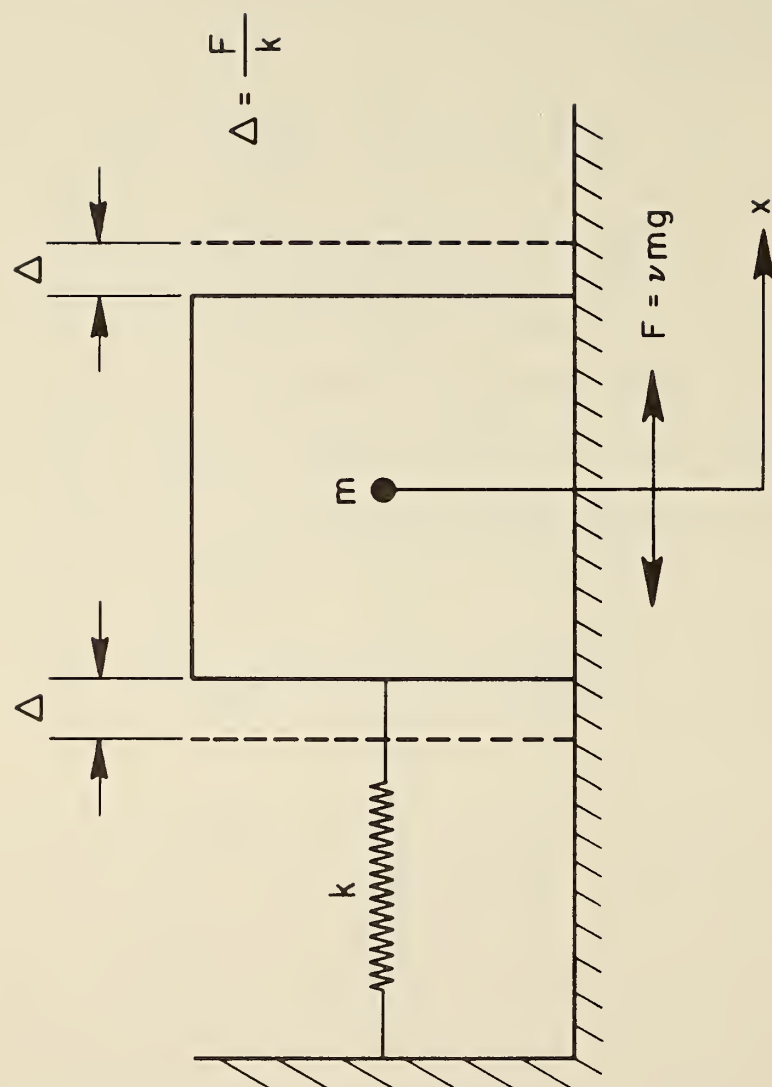


FIG. B.1 FREE VIBRATION OF A BLOCK WITH COULOMB FRICTION

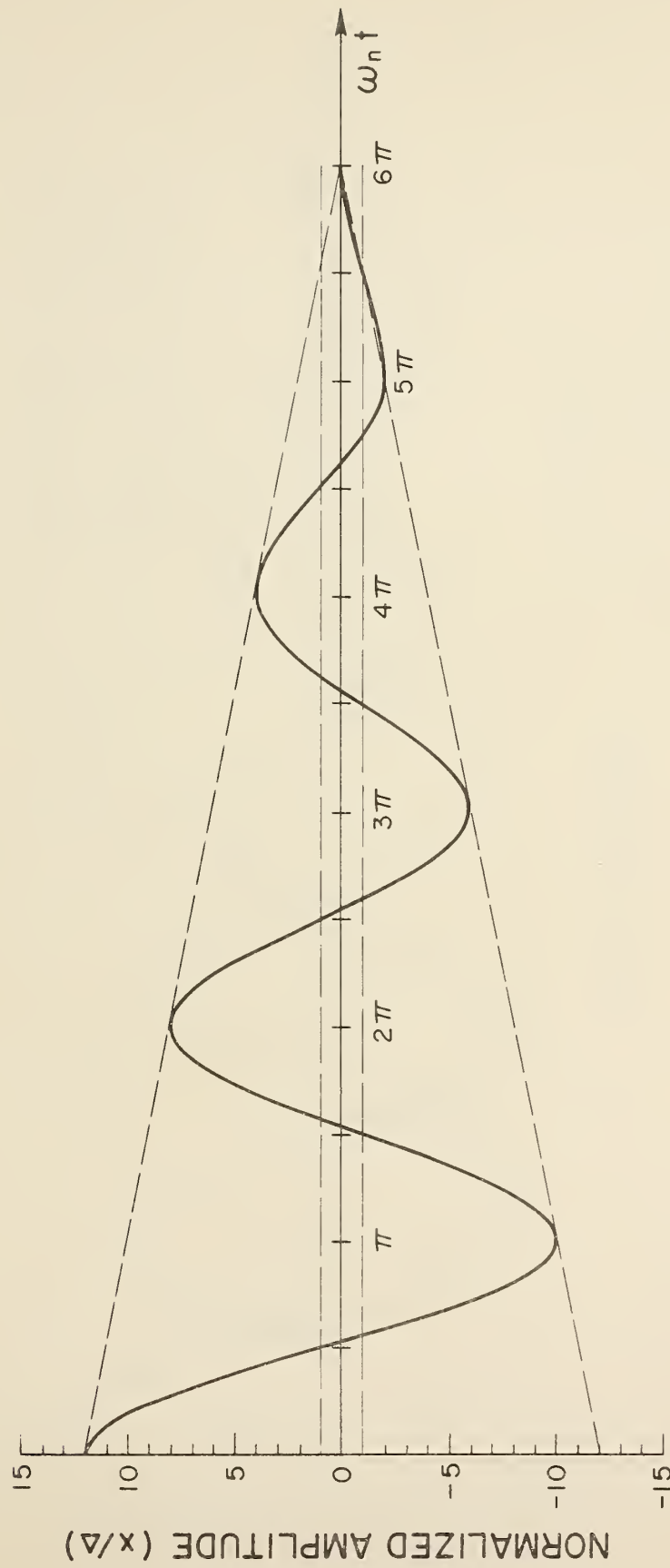


FIG. B.2 FREE VIBRATION RESPONSE OF A BLOCK WITH COULOMB FRICTION

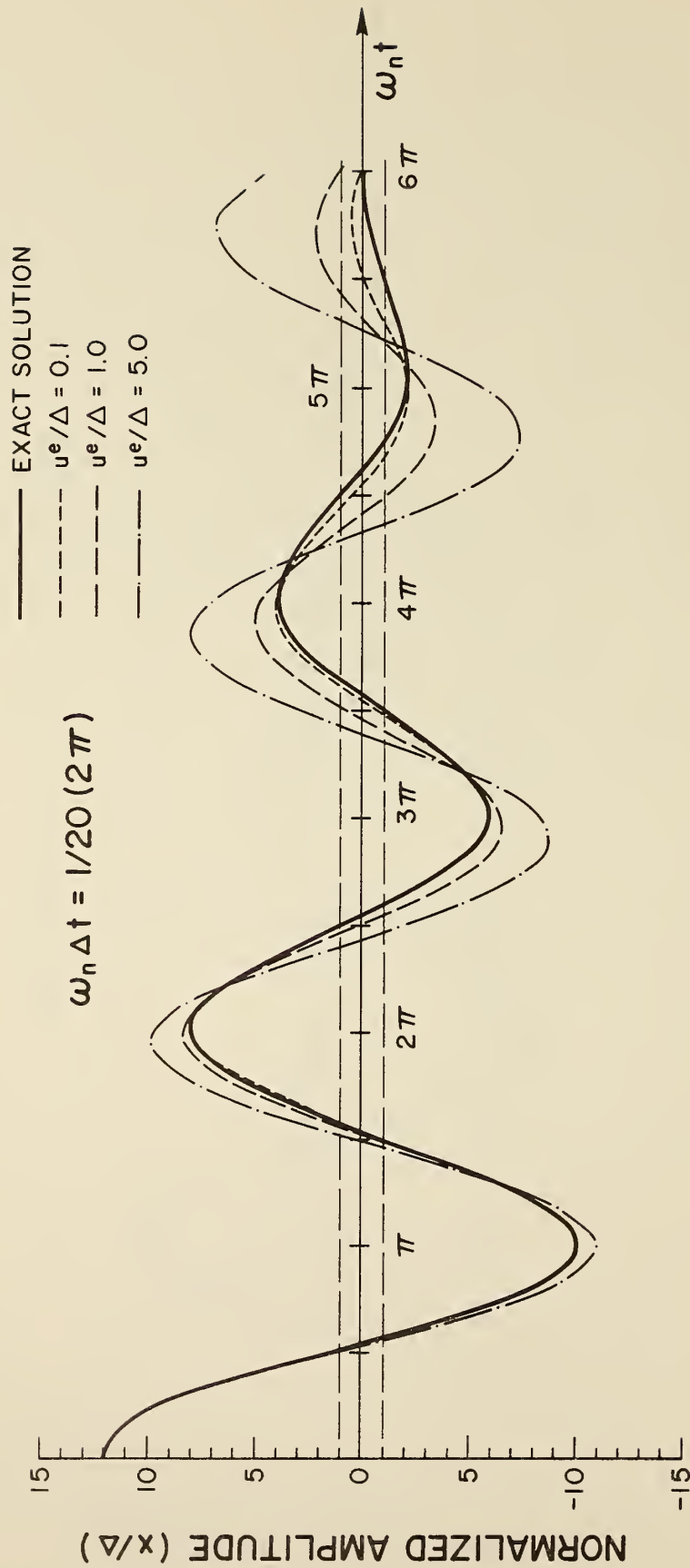


FIG. B.3 EFFECT OF MAGNITUDE OF  $u^e$  ON FREE VIBRATION RESPONSE OF A BLOCK

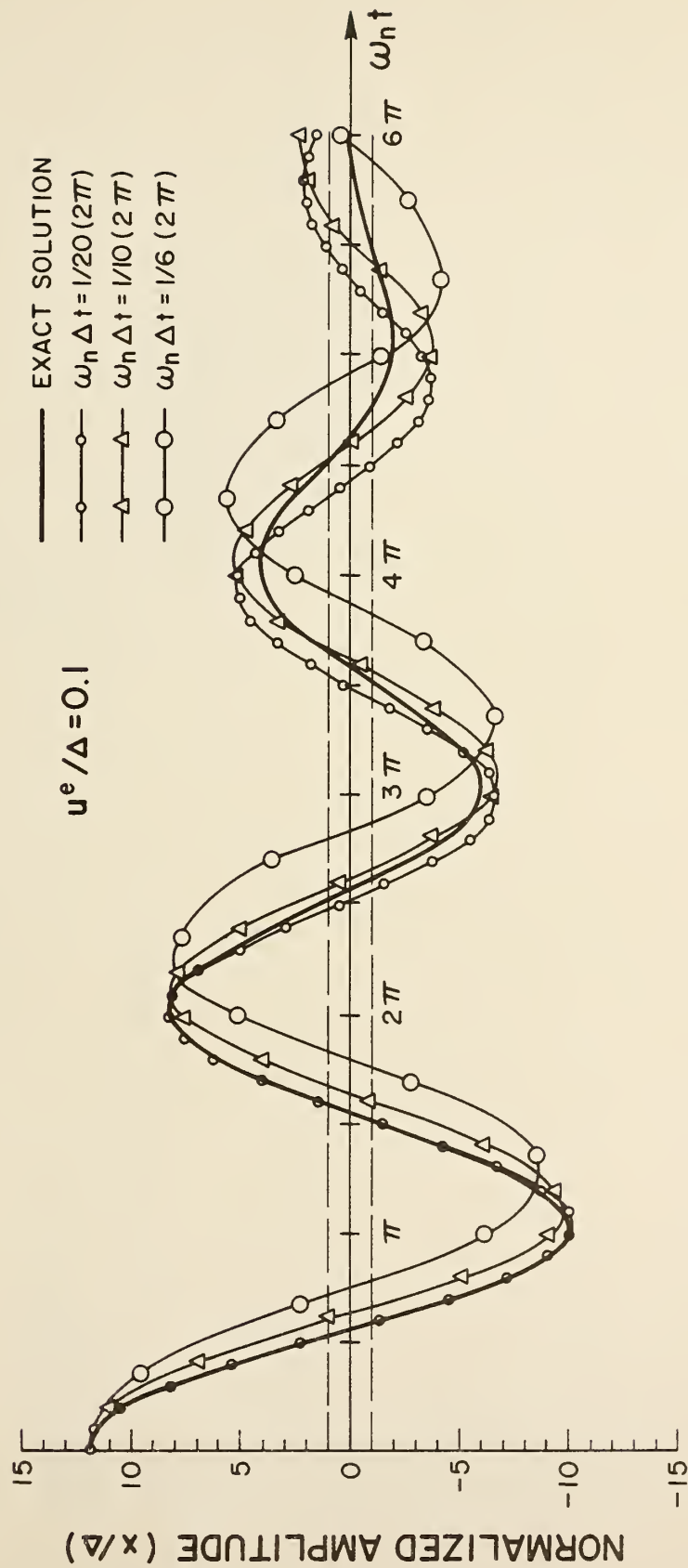


FIG. B.4 EFFECT OF TIME INTERVAL ON FREE VIBRATION RESPONSE OF A BLOCK





## COMPUTER LISTING OF NEABS

C-1

```

*DIAGN ERROR
C SURRELTIME (ERROR (MODE,N,PH)
C
C PRINT APPROPRIATE ERROR MESSAGE...
C
C GC TC (1,2,3,4,5,6,7,8,9) MODE
C
C ERROR MODE 1
C
C ) WRITE(6,2001) N,PH
C GC TC 100
C
C ERROR MODE 2
C
C ) WRITE(6,2002) N,PH
C GC TC 100
C
C ERROR MODE 3
C
C ) WRITE(6,2003) N,PH
C GC TC 100
C
C ERROR MODE 4
C
C ) WRITE(6,2004) N,PH
C GC TC 100
C
C ERROR MODE 5
C
C ) WRITE(6,2005) N,PH
C GC TC 100
C
C ERROR MODE 6
C
C ) WRITE(6,2006) N,PH
C GC TC 100
C
C ERROR MODE 7
C
C ) WRITE(6,2007) N,PH
C GC TC 100
C
C ERROR MODE 8
C
C ) WRITE(6,2008) N,PH
C GC TC 100
C
C ERROR MODE 9
C
C ) WRITE(6,2009) N,PH
C 100 STOP
C
2001 FORMAT (1F1,4H*****DIMENSION IN BLANK COMMON A EXCEEDED BY,16,
. 20F
AT SUBROUTINE ,A7/27H *****EXECUTION TERMINATED.)
2002 FORMAT (1F1,42H*****WRONG INPLT FOR TCAL NO. OF ELEMENTS ,16,
. 20F AT SUBROUTINE ,A7/27H *****EXECUTION TERMINATED.)

```

```

2003 FORMAT (1F1,4H*****ELEMENT NCNLINER PARAMETER NC. INPUT WRONG,
. 10F FOR NU. ,16,17H ELEMENT OF ,A7/
. 27F *****EXECUTION TERMINATED.)
2004 FORMAT (1F1,50H*****ELEMENT DATA INPUT IN WRONG ORDER DETECTED AT,
. 3FAC.,16,17H ELEMENT OF ,A7/27H *****EXECUTION TERMINATED.)
2005 FORMAT (1F1,16H*****ELEMENT NC. ,16,9H OF ,A7,12HHAS C LENGTH
. 27F *****EXECUTION TERMINATED.)
2006 FORMAT (1F1,16H*****ELEMENT NC. ,16,9H CF ,A7,17HHAS WRONG K
.NODE. /27H *****EXECUTION TERMINATED.)
2007 FORMAT (1F1,37H*****DATA INPUT NOT IN ORDER FOR NCDE,16,
. 15F DETECTED AT ,A7/27H *****EXECUTION TERMINATED.)
2008 FORMAT (1H1,41H*****MULTIPLE GROUND MCTION INPUT AT NODE,16/
. 50F NOT COMPATIBLE WITH THAT OF JCINT INPUT CODE ,
. 13F DETECTED AT ,A7/27H *****EXECUTION TERMINATED.)
2009 FORMAT (1F1,25H*****NCNLINER ELEMENT NO ,16,16H IS SINGULAR,
. 15F DETECTED AT ,A7/27H *****EXECUTION TERMINATED.)
END

```

```

*CHECK SETUP
C SUBROUTINE SETUP
  CCMPCN/EPAR/ NPAR(14),NUMNP,NELTYP,NUMFL,NUMNEL,NEQ,MEAND,MTOT,
    N1,N2,N3,N4,N5,N6,N7
  CCMPCN/ENTX/ GQQ(2043)
  CCMPCN/PLSC/ NFN,NOP,NT,NCT,JJULID)
  CCMPCN/JUNK/ JUK(205)
  CCMPCN AI(1)

  C INPUT JCINT UATA-----JCINT ID CODE ARRAY STORED CN TAPE 8
  C
  C
  C N1=1
  C N2=N1+NUMNP*6
  C N3=N2+NUMNP
  C N4=N3+NUMNP
  C N5=N4+NUMNP
  C IF (N5.GT.MTOT) CALL ERROR (1,N5-MTOT,7HINPUTM )
  C CALL INPUTM (AIN1),AIN2),AIN3),AIN4),ALMAP,NEQ)

  C INPUT ELEMENT DATA AND FORM ELEMENT STIFFNESSES---
  C STIFFNESS CN TAPE 2, STRESS CN TAPE 1, NONLINEAR DATA ON TAPE 3.
  C
  C N6=N5+NUMEL
  C IF (N6.GT.MTOT) CALL ERROR (1,N6-MTOT,7HELSTF )
  C CALL ELSTF (AIN5),NUMEL)
  C WRITE(6,2000) NEQ,MEAND

  C INPUT HOVAL LOADS AND MASSES-----ON TAPE 5
  C
  C N3=N2+NUMNP
  C N4=N3+NUMNP*6
  C N5=N4+NEQ
  C IF (N5.GT.MTOT) CALL ERROR (1,N5-MTOT,7HIALM )
  C CALL INLM (AIN1),AIN2),AIN3),AIN4),NUMNP,NEQ)

  C ASSEMBLE TOTAL STIFFNESS,LOAD-----ON TAPE 4, MASSES-----ON TAPE 9
  C
  C N2=N1+NEQ
  C N3=N2+NEQ*MBAND
  C N4=N3+NEQ
  C IF (N4.GT.MTOT) CALL ERROR (1,N4-MTOT,7HACDSTF )
  C CALL ACDSF (AIN1),AIN2),AIN3),NEQ,MBAND,ALMEL)
  C RETURN

  C 2000 FORMAT (//////2RH SYSTEM SETUP INFORMATION... ///
    * 30H TOTAL NUMBER OF ECLATIONS = 15//
    * 30H BAND WIDTH = 15)
    * END
  C

```

```

*DECK INPUT
C SUBROUTINE INPUTM (ID,X,Y,Z,NUMNP,NEQ)
C
C DIMENSION ID(NUMNP*6),X(1),Y(1),Z(1),NID(6)
C
C ACCAL POINT INPUT AND GENERATION
C
C REMIND 8
C ND=6
C WRITE(6,200)
C WRITE(6,204)
C KO=1
C DO 10 ID, I=1,6
C ID NID(I)=0
C 11 READ (5,100) N,(ICIN,I),I=1,6),X(IN),Y(IN),Z(IN),KN
C WRITE(6,203) N,(ICIN,I),I=1,6),X(IN),Y(IN),Z(IN),KN
C DO 30 I=1,6
C IF (ICIN,I) 21,22,23
C 21 NID(I)=-1
C IDIN,I)=1
C GO TC 30
C 22 IF (NID(I).EQ.-1) ICIN,I)=1
C GO TC 30
C 23 NID(I)=0
C 30 CONTINUE
C
C CHECK IF GENERATION NEEDED THEN GENERATE NEW NODES
C
C IF (KU.CQ.1) GO TO 32
C IF (KN) 33,33,34
C 32 KO=0
C 33 CONTINUE
C NUMINT=1
C GO TC 45
C 34 NUMINT=(N-NID)/KN
C OX=(X(IN)-X(NID))/NUMINT
C OY=(Y(IN)-Y(NID))/NUMINT
C OZ=(Z(IN)-Z(NID))/NUMINT
C CC 41 J=1,NUMINT
C NN=NI+J*KN
C X(NN)=X(INN-KN)+OX
C Y(NN)=Y(INN-KN)+OY
C Z(NN)=Z(INN-KN)+OZ
C
C SET LUF CODES SAME AS FIRST JOINT IN THE SERIES
C
C GO 40 JJ=1,6
C IF (ICIN,JJ)=1) 37,36,35
C 35 IDIN,JJ)=ICIN,JJ)+J*KN
C GO TC 40
C 36 IDIN,JJ)=IDIN,JJ)
C GO TC 40
C 37 ICIN,JJ)=0
C 40 CONTINUE
C 41 CONTINUE
C 45 NI=NI

```





```

WRITE(6,2002) (I,INC(I),I=1,NUMEL)
WRITE (H) INC
RETURN

C
1001 FORMAT (14I5)
2000 FCMPAT (1H1,3H#TOTAL NUMBER OF NONLINEAR ELEMENTS = ,15 //)
2001 FCMPAT (1H ,3H#ELEMENT TYPE OF L/NL INDICATOR,.... //
* FCMPAT 1P ,5(14H ELEMENT INC //1P ,5(14P NUMBER TYPE))
2002 FCMPAT (1P ,5(17,16,1X))
END

C
*DTCK WRITET
SUBROUTINE WRITET (PARAM,NOIF)
C
COMMON/EPAR/ NPAR(14),NUMNP,NCLTYP,NUMEL,NUMNEL,NEC,NBAND,PTOT,
* CCMPCN/EMTX/ LPI(24),NF,NS,S(24,4),PI(24,4),XMI(24),ST(12,24),
* TT(12,4)
C
CALCULATE RANG WIDTH AND WRITE ELEMENT INFORMATION CN TAPES
C
MIN=100000
MAX=0
DO 450 L=1,ND
IF (LM(L).EQ. 0) GO TO 450
IF (LM(L).GT.NEC) GO TO 450
IF (LM(L).GT.MAX) MAX=LM(L)
IF (LM(L).LT.MIN) MIN=LM(L)
450 CONTINUE
NDIF=MAX-MIN+1
IF (NDIF.GT.NBAND) NBAND=NDIF
C
WRITE (1) NS,ND,LM,ST,TT
WRITE (2) LM,ND,NS,S,P,XM
C
RETURN
END

```

```

60 CONTINUE
DO 70 I1=1,NS
  SALL1,NO+1)=SALL1,I)*01
70 SALL1,NO+2)=SALL1,I)*02
C
  S(ND+1,NO+1)=S(I1,I)*01**2
  S(ND+2,NO+2)=S(I1,I)*02**2
  S(ND+1,NO+2)=S(I1,I)*01*02
  S(ND+2,NO+1)=S(ND+1,NO+2)
  NO=ND+2
80 CONTINUE
C
  SET ROTATIONS
C
  DO 90 J=1,3
    K=NF+J+2
    IF (LM(K).GT.0) GO TO 90
    M=-LM(K)
    LM(K)=IDIM+J+3)
  90 CONTINUE
C
  100 CONTINUE
C
  RETURN
END

```

```

*DECK INLM
12
SUBROUTINE INLM (ID,IN,TL,XL,NLMNP,NEQ)
C
  DIMENSION ID(NLMNP,1),IN(1),TL(NLMNP,1),XL(NEQ)
  CCMPCN/JUNK/ NT,KSHF,NE,NR(6),NN,11,JJ,JLK(192)
C
  KSHF=0
  RE=INL ?
  1 DO 5 I=1,NLMNP
    IN(I)=0
    DO 5 J=1,6
      5 TL(I,J)=0.0
      DO 10 I=1,NEQ
        10 XL(I)=0.
C
  INPUT NCDAL MASSES AND/OR LOADS
C
  NE=0
  100 READ(5,1001) N,R
  NE=NE+1
  IF (N.EQ.0) GO TO 300
  IF (N.EQ.1) GO TO 120
  IF (KSHF.EQ.0) WRITE (6,2003)
  IF (KSHF.EQ.1) WRITE (6,2002)
  120 WRITE (6,2001) N,R
  DO 150 J=1,6
    150 TL(N,J)=R(J)
    IN(N)=1
    GO TO 100
C
  ASSEMBLE LOADS AND MASSES IN CCRE
C
  300 DO 500 NN=1,NLMNP
    IF (IN(NN)) 500,500,310
  310 DO 400 J=1,6
    11=IC(NN,J)
    IF (11) 400,400,350
  350 XL(11)=TL(NN,J)
  400 CONTINUE
  500 CONTINUE
C
  WRITE (9) XL
  IF (KSHF) 600,600,700
  600 KSHF=1
  GO TO 1
  700 RETURN
C
  1001 FORMAT (15,5X,6F10.0)
  2001 FORMAT (15,5X,6F12.3)
  2002 FORMAT (23HINCDAL POINT LOADS..... / 1CH NODE
    . 14APPLIED LOADS / 1CH NO.
    . 2HRY 1CX 2HRZ 1CX 2HMZ 1CX 2HMY 1CX 2HPZ )
  2003 FORMAT (23HINCDAL PCINT MASSES.... // 1CH NODE
    . 19PCONCENTRATED MASSES / 1CH NO.
    . 2HRY 1CX 2HMZ 1CX 3H1/Y 9X 3H1/Z )
  END

```

```

27X
6X 2HRX 10X
27X
8X 2HPX 10X

```

```

*DFCN ADDSTF
SUBROUTINE ADDSTF (E,A,TM,NEQ,MBAND,NUMEL)
C
DIMENSION B(NEQ),A(NFC,MBAND),TM(NEQ),STIF(722)
CCMPCN/EMTK/ LM(24),UL,NS,S(24,24),P(24,4),XM(24),ST(12,24),
* CCMPCN/JUNK/ ST(12,4),LPM,II,JJ,N,I,J,JUK(195)
EQUIVALENCE (STIF,LPM)
C
FORM GLOBAL EQUILIBRIUM EQUATION IN CORE
C
L=1
NMA=NEQ*MBAND
REWIND 2
REWIND 4
REWIND 9
DO 40 I=1,4
40 STR(I)=0.
WRITE (6,20001)
READ (5,1001) STR
WRITE (6,2001) L,(STR(1),I=1,4)
C
DO 100 I=1,NMA
100 A(I)=0.
C
READ (9) TM
READ (9) B
REWIND 9
DO 500 N=1,NUMEL
READ (2) STIF
DO 400 I=1,N0
II=LPM(I)
IF (II.LE.0.OR.II.GT.NEQ) GO TO 400
LMN=1-II
TM(II)=TM(II)+XM(I)
DO 240 J=1,4
240 B(II)=B(II)+P(I,J)*STR(J)
DO 300 J=1,N0
JJ=LPM(J)
IF (JJ.LE.0.OR.JJ.GT.NEQ) GO TO 300
JJ=JJ+LMN
IF (JJ) 300,300,250
250 A(II,JJ)=A(II,JJ)+S(1,J)
300 CONTINUE
400 CONTINUE
500 CONTINUE
C
WRITE (4) (A(I),I=1,NMA)
WRITE (9) (TM(I),I=1,NEQ)
RETURN.
C
1001 FORMAT (4F10.0)
ZCCC FORMAT (777749H ELEMENT LCAC MULTIPLIER FOR STATIC ANALYSIS.....//
* 10P STRUCTURE 6X 24P ELEMENT LOAD MULTIPLIER /
* 10P LOAD CASE 7X 14H 9X 14B 5X 14C 9X 14D 77)
2001 FORMAT (16,5X,4F10.3)
END

```

```

15
*DFCN STATIC
SUBROUTINE STATIC
CCMPCN/EPAR/ NPAR(14),NUMNP,NELTYP,NUMEL,NUMNEL,NEQ,MBAND,MTOT,
* 11,N2,N3,N4,N5,N6,N7
CCMPCN/EMTK/ QCCQ(2043)
CCMPCN/MISC/ REN,NGM,NT,NOT,JJJ(10)
CCMPCN/JUNK/ JUK(205)
CCMPCN ALL)
C
C COMPUTE STATIC RESPONSE--- SOLVE FOR DISPLACEMENT UNKNOWNNS
C
N2=N1+NEQ
N3=N2+NEQ*MBAND
N4=N3+NEQ
IF (N4.GT.MTOT) CALL ERROR (1,N4-MTOT,7HCCQSOL )
CALL CCQSOL (1(N1),A(N2),A(N3),NEQ,MBAND)
C
C OUTPUT DISPLACEMENTS
C
N3=N2+NUMNP*6
N4=N3+NUMNP*6
N5=N4+NUMNP
IF (N5.GT.MTOT) CALL ERROR (1,N5-MTOT,7HPRINTO )
CALL PRINTO (A(N1),A(N2),A(N3),A(N4),NEQ,NUMNP)
C
C OUTPUT STATIC STRESSES OF EACH ELEMENT
C
N3=N2+NUMEL
IF (N3.GT.MTOT) CALL ERROR (1,N3-MTOT,7HSTRESS )
CALL STRESS (A(N1),A(N2),NEQ,NUMEL)
C
RETURN
END

```

```

*DECK COSCL
SUBROUTINE COSCL (B,A,NBMAX,NEQ,MBAND)
C
C   DIMENSION B(1),A(1),NBMAX(1)
C
C   TRIANGULARIZE BANDED MATRIX BY GAUSSIAN ELEMENTATION
C
  IF (NEQ.EQ.1) RETURN
  NMA=NEQ*MBAND
  NE=NEQ-1
  DO 300 N=1,NE
    NBMAX(N)=0
    DO 100 I=N,NMA,NEQ
      IF (A(I).NE.0.) NBMAX(N)=I
    100 CONTINUE
  C
  IF (A(N).EQ.0.) GO TO 300
  IL=N*NEQ
  IH=NBMAX(N)
  L=N
  DO 200 I=IL,IH,NEQ
    L=L+1
    IF (A(I).EQ.0.) GO TO 200
    C=A(I)/A(N)
    J=L-1
    DO 150 K=I,IH,NEQ
      IF (A(K).EQ.0.) GO TO 150
      A(K+J)=A(K+J)-C*A(K)
    150 CONTINUE
    A(I)=C
  200 CONTINUE
  300 CONTINUE
C
C   REDUCTION OF LUAD VECTOR
C
  IL=NEQ
  DO 400 N=1,NEQ
    C=B(N)
    IF (A(N).NE.0.) B(N)=B(N)/A(N)
    IF (N.EQ.NEQ) GO TO 450
    IL=IL+1
    IH=NBMAX(N)
    K=N+1
    DO 350 I=IL,IH,NEQ
      IF (A(I).EQ.0.) GO TO 350
      B(K)=B(K)-A(I)*C
    350 K=K+1
  400 CONTINUE
C
C   BACK-SUBSTITUTION
C
  450 IL=NEQ*2
  500 IL=IL-1
  N=N-1
  IF (N.EQ.0) RETURN
  IH=NBMAX(N)

```

```

K=N+1
DO 600 I=IL,IH,NEQ
  IF (A(I).EQ.0.) GO TO 600
  B(K)=B(K)-A(I)*B(K)
600 K=K+1
GO TO 500
END

```





```

304 IF (INTAG.EQ.0) WRITE(6,20C4)
   WRITE(6,30C4) MM,L,(SIG(I),I=1,6)
   GO TO 500
C
105 IF (INTAG.EQ.0) WRITE(6,20C5)
   WRITE(6,30C5) MM,L,(SIG(I),I=1,12)
C
50C MM=MM+1
   INTAG=1
   WRITE (8) NS,SIG
1000 CONTINUE
   RETURN
C
200C FORMAT (27H1,STATIC STRESS OUTPUT.....) //
2001 FORMAT (/26H0,....TRUSS MEMBER FORCES //
   46H0 MEMBER LOAD STRESS FORCE )
2002 FORMAT (/36H0,....STRAIGHT BEAM FORCES AND MOMENTS//
   10F0BEAM LOAD 5X 5FAXIAL 217X,5HSHEAR),5X 7HTORSION
   215X,7HBENDING// 10F NC. NC. 8X 2HR1 10X 2HR2 10X
   2HR3 10X 2HR1 10X 2HR2 10X 2HR3)
2003 FORMAT (/36H0,....CLAVED BEAM FORCES AND MOMENTS//
   10F0BEAM LOAD 5X 5FAXIAL 217X,5HSHEAR),5X 7HTORSION
   215X,7HBENDING// 10F NC. NC. 8X 2HR1 10X 2HR2 10X
   2HR3 10X 2HR1 10X 2HR2 10X 2HR3)
2004 FORMAT (/40H0,....BUCROARY SPRING FORCES AND MOMENTS //
   10F0 ED. LOAD 5X 5FAXIAL 217X 5HSHEAR) 5X 7HTORSION
   215X 7HBENDING) /1CH NO NC 8X 2HR1 10X 2HR2 10X 2HR3 10X
   2HR1 10X 2HR2 10X 2HR3 )
20C5 FORMAT (/40H0,....EXPANSION JCINT FORCES AND MOMENTS //
   10F0 JT. LOAD,5X,5HAXIAL,217X,5HSHEAR),7X,5HAXIAL,5X,7HBENDING,
   5X,7H SHEAR/10H NC. NC. ,8X,2HR1,10X,2HR2,10X,2HR3,
   10X,2HR4,10X,2HR5,10X,2HR6)
3001 FORMAT (218,F15.5,F15.3)
3002 FORMAT (15,14,1PE11.3,5E12.3/8X,6E12.3/)
3003 FORMAT (15,14,1PE11.3,5E12.3/8X,6E12.3/)
3004 FORMAT (15,14,1PE11.3,5E12.3)
3005 FORMAT (15,14,1PE11.3,5E12.3/8X,6E12.3/)
END
C
*CFCK LOADS 21.
SUPERCLUTINE LOADS
C
CCMPCN/EPAR/ NPAR(14),NUMNP,NELTYP,NUMEL,NUMMEL,NEQ,MBAND,*TOT,
   N1,N2,N3,N4,N5,N6,N7
   CCMPCN/EMIX/ CQCQ(2C43)
   CCMPCN/MISC/ VFN,NGM,NT,NCT,OT,ALFA,BETA,INTG,IGM(3),FGM(3)
   CCMPCN/JUNK/ JUK(205)
   CCMPCN/ITSO/ NSDIV,ITITYP,MAXIT,RTCLU,RTCLS,RTOLI,CCAN(34)
   CCMPCN A(1)
C
READ ANL PRINT LCAC INPUT CONTROL DATA
C
READ (5,1000) OT,ALFA,BETA,INTG
   WRITE(6,2000) DT,NT,NCT,NFN
   WRITE(6,2001) INTG,ALFA,BETA
C
READ ANL PRINT SUBDIVISION CONTROL DATA
C
READ (5,1100) NSDIV,RTOLS
   WRITE(6,2100) NSDIV,RTCLS
C
READ ANL PRINT EQUILIBRIUM ITERATION CONTROL DATA
C
READ (5,1200) MAXIT,ITITYP,RTOLI,RTOLU
   WRITE(6,2200) MAXIT,ITITYP,RTOLI,RTCLU
C
INPUT GROUND MOTION
C
READ (5,1002) IGM,FGM
   WRITE(6,2002) IGM,FGM
   NG=0
   DC 5 I=1,3
   IF (IGM(I).LE.0) GO TO 5
   IF (FGM(I).EQ.0.) FGM(I)=1.C
   IF (IGM(I).LE.NG) GC TO 5
   NG=NG+1
   IF (NG.LE.NFN) GO TO 5
   WRITE(6,3000) I
   STOP
5 CONTINUE
   GO TO I=1,3
   IF (IGM(I).LE.NFN) GO TO 10
   WRITE(6,3000) I
   STOP
1C CCATINUE
C
SETUP NODAL DYNAMIC LOAD COEFFICIENT MATRIX
C
N1=1
N2=N1+NEQ*NFH
N3=N2+NUMNP*6
N4=N3+NEQ
N5=N4+NEQ
CALL LCAOR (A(N1),A(N2),A(N3),A(N4),NEC,NFN,NUMNP)
C

```

```

C
C
C INPUT HISTORIES OF LOAD FUNCTIONS
C
N3=N2*NT*NFN
MAX=IMCT-N3)/2
IF IMAX-GE-NT) GO TO 20
N4=2*INT-MAX)
CALL ERROR I1,N4,7H-INTHIS )
20 N4=N3*MAX
CALL INTHIS IAIN2),A(N3),AIN4),NFN,NT,OT,MAX)
C
C FCRP DYNAMIC NOLAL LOAD VECTOR
C
N4=N3*HEQ
CALL LOADV IAIN1),AIN2),AIN3),NEQ,NFN,NT)
C
C
C RETURN
1000 FORMAT (3F10.0,15)
1002 FCRPAT (315,3F10.0)
1100 FORMAT (15,F10.0)
1200 FORMAT (215,2F10.0)
2000 FCRPAT (37H-DYNAMIC LCAC INPUT CONTROL DATA..... ///
. 32H TIME INCREMENT DT ISEC) = F8.3//
. 32H TOTAL NUMBER OF TIME STEPS = 15 //
. 32H OUTPUT INTERVAL = 15 //
. 32H NUMBER OF TIME FUNCTIONS = 15 //
2001 FCRPAT (177749H STEP-BY-STEP DYNAMIC ANALYSIS CONTROL DATA.....///
. 32H INTEGRATION INDICATOR = 15 //
. 32H DAMPING FACTOR ALPHA = 1PE12.3//
. 32H DAMPING FACTOR BETA = 1PE12.3 )
2002 FCRPAT (30H-GROUND MOTION INPUT KEY..... ///
. 30X, 9H-DIRECTION/24X,1HX,7X,1HY,7X,1HZ //
. 20H FUNCTION NUMBER... ,15,21H //
. 20H SCALE FACTOR.....,3F8.3)
2100 FCRPAT (49H-SUBDIVISION OF TIME INCREMENT CONTROL DATA ..... ///
. 43H NUMBER OF SUBDIVISION = 15//
. 43H RELATIVE TOLERANCE OF SUBDIVISION = F15.7 )
2200 FCRPAT (41H-EQUILIBRIUM ITERATION CONTROL DATA ..... ///
. 43H MAXIMUM NUMBER OF ITERATION = 15//
. 43H TYPE OF ITERATION = 15//
. 43H RELATIVE TOLERANCE TO USE ITERATION = F15.7//
. 43H RELATIVE TOLERANCE FOR CONVERGENCE = E15.7 )
3000 FCRPAT (65H-ERROR.....INPUT DATA FOR GROUND MOTION FUNCTION NLP8E
. R INCORRECT/11X,20H-EXECUTION TERMINATED )
C
END

```



```

200 K=1
L=1
TIME=F(1)
<10 L=L+1
IF (INT-L) 300,220,220
220 OUT=T(L)-T(L-1)
COF=FILE-FIL-1)
IF (OUT) 225,210,230
225 WRITE (6,2003) T(L),FIL)
GO TO 210
<30 SLCPE=DDF/DDT
235 IF (T(L)-T(MC) 210,240,240
240 Z(K,J)=FIL-1)+(TIME-T(L-1))*SLCPE
TIME=TIME+DT
K=K+1
IF (INT-K) 300,235,235
300 WRITE (6,2004) NT,OT
310 K=0
OC 350 I=1,NT,8
K=K+1
IF (K=7
IF (IH.GT.NT) IH=NT
350 WRITE (6,2005) K,Z(L,J),L=1,IH)
400 CONTINUE
DC 450 I=1,NT
450 WRITE (10) (Z(I,J),J=1,NFN)
RETURN
C
1000 FORMAT (12A6/15,3F10.0)
1001 FORMAT (10F8.5)
1002 FORMAT (12F8.0,8X)
2000 FORMAT (17HITIME HISTORY NO. ,13,5H,.....,12A6 ///
. 5X,30H NUMBER OF DATA POINT = ,15 //
. 5X,30H SCALING FACTOR = ,F10.4//
. 5X,30H TIME INCREMENT OF DATA (SEC) = ,F10.6//
. 5X,30H ZERO CORRECTION = ,F10.4//
. 5X,30H TIME INPUT )///)
2001 FORMAT (5X,(F8.3,F10.6,2X))
2002 FORMAT (5X,20HDATA POINT ,F8.3,F10.6)
2003 FORMAT (53HGENERATED TIME HISTORY FOR RESPONSE CALCULATION,.....//
. /5X,30H NUMBER OF DATA GENERATED = ,15 //
. 5X,30H TIME INCREMENT OF DATA (SEC) = ,F10.4//)
2005 FORMAT (18,24,8F13.3)
3000 FORMAT (38H1,.....,ERRCK,....,INPL TIME HISTORY NO. ,13,5H ,FAS,16,
. 13P DATA POINTS /15X,30H WHICH IS GREATER THAN THE MAX. ,16,
. 24P ALLOWED IN THIS PROGRAM /15X,2CHEXECUTION TERMINATED )
END

```







```

34.
195 CONTINUE
200 XX=PEXT(I)-PU(I)-PN(I)-PM(I)*(CONT(9)*X1(I)+CONT(10)*X2(I))
    K=I
    IF (MB.LT.1) GO TO 210
    DO 205 J=1,MB,NEQ
    IF (B(J).EQ.0.) GO TO 205
    XX=XX+B(J)*PMIK)
205 K=K+1
210 IF (1.EQ.1) GO TO 215
    N2=N1-1
    IF (PH.LT.N2) GO TO 215
    K=1-1
    DO 212 J=N2,MH,NEQ1
    IF (B(J).EQ.0.) GO TO 212
    XX=XX+B(J)*PMIK)
212 K=K-1
215 FIT(I)=XX
C
C SOLVE FOR DYNAMIC INCREMENT
C
CALL TRIA (A,NBMAX,NEQ,MBAND)
CALL BACK (A,NBMAX,FIT,NEQ)
C
C COMPUTE NEW DISPLACEMENT, VELOCITY AND ACCELERATION
C
DO 218 I=1,NEQ
    OD=FIT(I)
    XX1=X1(I)
    XX2=X2(I)
    X2(I)=X2(I)+CONT(1)*OC-CONT(2)*XX1-CONT(3)*XX2
    X1(I)=X1(I)+CONT(4)*CC-CONT(5)*XX1-CONT(6)*XX2
    DX(I)=OC
218 DX(I)=OC
C
C FORM NONLINEAR ELEMENT FORCE AND STIFFNESS MATRIX
C
CALL NELSTF (A,B,X,X1,X2,UX,XM,MBMAX,MHMAX,PEXT,FIT,PU,PN,PP,REF,
    * STR,STRF,UPL,LPLF,NINC,NSS,NEG,MBAND,NLMNEL,1,ISDIV,
    * ICR,RTOL)
C
C CHECK CURRENTNESS OF SOLUTION
C
IF (NSDIV.EQ.0) GO TO 220
IF (RTOL.GT.RTOLS) GO TO 23C
22C IF (MAXIT.EQ.0) GO TO 500
IF (RTOL.GT.RTOL1) GO TO 400
GC TC 500
C
C INITIALIZATION FOR SUBDIVISION OF TIME STEP
C
230 IF (ISDIV) 290,250,200
250 ISDIV=1
    MSCIV=MSDIV+1
    ICR=1
    DO 260 I=1,NEQ

```

```

35.
    OO=DX(I)
    XX1=X1(I)
    XX2=X2(I)
    X2(I)=CC-CCNB(1)*CC-CCNB(2)*XX1-CCNB(3)*XX2
    X1(I)=CCNB(4)*CC-CCNB(5)*XX1-CCNB(6)*XX2
    X(I)=X(I)-DO
260 OX(I)=O.
    DO 270 I=1,I2
270 CCNT(I)=CONS(I)
    DO 275 I=1,NUMNEL
    DO 275 J=1,I2
    STR(I,J)=STRF(I,J)
275 UPL(I,J)=UPLF(I,J)
    DO 276 I=1,I2
276 USP(I)=USPF(I)
    DO 280 I=1,NEQ
    XX=PP(I)
    PP(I)=(PEXT(I)-XX)/ASDIV
280 PEXT(I)=XX
C
CALL NELSTF (A,B,X,X1,X2,UX,XM,MBMAX,MHMAX,PEXT,FIT,PU,PN,PP,REF,
    * STR,STRF,UPL,LPLF,NINC,NSS,NEG,MBAND,NLMNEL,2,ISDIV,
    * ICR,RTOL)
C
    GO TC 110
29C CCNTINUE
C
EQUILIBRIUM ITERATION
C
IF (MAXIT.EQ.0.CC.RTOL.LE.RTOL1) GO TO 500
40C ICR=1
    MTRN=MTRN+1
    CALL ITERN (A,B,X,X1,X2,OX,FIT,REF,PL,PN,PM,PEXT,NBMAX,PPMAX,
    * MHMAX,NINC,NSS,STR,STRF,UPL,LPLF,NEG,MBAND,NUMNEL,
    * ISDIV,ICR,NOT,NITRN)
C
C CHECK FOR LAST SUBDIVISION
C
50C IF (NSDIV.EQ.0.CC.RTOL.EQ.0) GO TC 600
IF (ISDIV.EQ.NSCIV) 3C TO 510
    ISDIV=ISDIV+1
    GC TC 110
51C DC 520 I=1,I2
52C CCNT(I)=CONI(I)
C
C COMPUTE GROUPD ACCELERATION
C
60C READ(10) (PK(I),I=1,NFN)
    DC 610 I=1,NEQ
    XG(I)=O.
    J=MASS(I)
    IF (J.LE.0) GO TO 610
    JJ=ICM(J)
    IF (JJ.LE.C) GO TO 610
    XG(I)=FCM(J)*PR(JJ)
610 CONTINUE
C

```

50.

```

C      STORE DISPLACEMENT AND ABSOLUTE ACCELERATION ON TAPE 8
C      DC 650 I=1,NEQ
C      650 XG(I)=XG(I)+X2(I)
C      IF (NDT.EQ.NOUT) WRITE(8) (X(I),I=1,NEQ),(XG(I),I=1,NEQ)
C
C      STORE NONLINEAR STRESS AND DEFORMATION ON TAPE 9
C      IF (NDT.EQ.NOUT) WRITE(9) NSS,STR,UPL
C
C      STORE FORMER EXTERNAL FORCE
C      IF (NSDIV) 705,715,705
C      705 DC 710 I=1,NEQ
C      710 PP(I)=PEXT(I)
C      715 CONTINUE
C
C      CHECK FOR LAST TIME STEP
C      IF (NDT.EQ.NOUT) NOUT=NOUT+NDT
C      NDT=NCT+1
C      IF (NDT-NT) 100,100,800
C
C      800 IF (NSDIV.NE.0) WRITE(6,2300) MSDIV
C      IF (MAXIT.NE.0) WRITE(6,2400) MITRN,NITRN
C
C      RETURN
C
C      2000 FORMAT(1H,5HNDT=,15)
C      2100 FORMAT(1H,10X,7HISCV=,15)
C      2200 FORMAT(1H,25X,38P-RELATIVE NORM OF UNBALANCED FORCE.....,F15.7)
C      2300 FORMAT(1H,15X,38P-NUMBER OF TIME STEP FOR WHICH SUBDIVISION WAS USED..
C      ..,15//)
C      2400 FORMAT(1H,15X,38P-NUMBER OF TIME STEP FOR WHICH ITERATION WAS USED.....
C      ..,15//)
C      2500 FORMAT(1H,15X,38P-TOTAL NUMBER OF ITERATION.....,15//)
C
C      END

```

1

51.

```

*CHECK TRIA
SUBROUTINE TRIA (A,NBMAX,NEQ,MBAND)
C
C      DIMENSION A(1),NBMAX(1)
C
C      TRIANGULARIZE BANCEC MATRIX BY GAUSS ELIMINATION
C
C      IF (NEQ.EQ.1) RETURN
C      MM=NEQ*MBAND
C      NE=NEQ-1
C      DD 300 N=1,NE
C
C      DETERMINE VARIABLE BAND WIDTH
C
C      NBMAX(N)=0
C      DD 100 I=N,MM,NEQ
C      IF (A(I).NE.0.0) NBMAX(N)=I
C      100 CONTINUE
C
C      REDUCTION OF EQUATIONS WITHIN BAND
C
C      IF (A(N).EQ.0.0) GO TO 300
C      IL=N+NEQ
C      IH=NBMAX(N)
C      L=N
C      CC 200 I=IL,IH,NEQ
C      L=L+1
C      IF (A(I).EQ.0.0) GO TO 200
C      C=A(I)/A(N)
C      J=L-1
C      CD 150 K=I,IH,NEQ
C      IF (A(K).EQ.0.0) GO TO 150
C      A(K+J)=A(K+J)-C*A(K)
C      150 CONTINUE
C      A(I)=C
C      200 CONTINUE
C      300 CONTINUE
C      RETURN
C      END

```

```

*OECK BACK SUBROUTINE BACK (A,NBMAX,B,NEQ)
C
C DIMENSION A(1),NBMAX(1),B(1)
C
C REDUCTION OF LOAO VECTOR AND BACKSUBSTITUTION
C
IL=NEQ
DO 400 N=1,NEQ
C=B(N)
IF (A(N).NE.0.0) B(N)=B(N)/A(N)
IF (N.EQ.NEQ) GO TO 450
IL=IL+1
IH=NBMAX(N)
K=N
DO 350 I=IL,IH,NEQ
K=K+1
IF (A(I).EQ.0.) GO TO 350
B(K)=B(K)-A(I)*C
350 CONTINUE
400 CONTINUE
C
450 IL=2*NEQ
500 IL=IL-1
N=N-1
IF (N.EQ.0) RETURN
IH=NBMAX(N)
K=N
DO 600 I=IL,IH,NEQ
K=K+1
IF (A(I).EQ.0.) GO TO 600
B(N)=B(N)-A(I)*B(K)
600 CONTINUE
GO TO 500
END

29.
*OECK NELSTF (A,B,X,X1,X2,OX,YM,MBMAX,MHMAX,PEXT,FIT,PU,PN,PM
REF,STR,STRF,UPL,UPLF,MNO,NSS,NEQ,MBANC,NUMNEL
ICONO,ISOIV,ICOR,RTOL)
C
C DIMENSION A(NEQ,MBANC),B(NEQ,MBANC),X(1),X1(1),X2(1),OX(1),YM(1),
MBMAX(1),MHMAX(1),PEXT(1),FIT(1),PU(1),PN(1),PM(1),
REF(1),STR(NUMNEL,12),STRF(NUMNEL,12),UPL(NUMNEL,12),
UPLF(NUMNEL,12),NINC(1),NSS(1),STIF(1),131)
CCMPCN/ENTX/ MTYPE,LM(24),NCON,ASAI(24),SAI(12,24),S(12,12),
FNP(24),TTT(72),ASSAI(24,24),SSA(12,24),OF(24),
F(12),UPI(12)
CCMPCN/NEW / EX(24),EXI(24),OEX(24),OFF(12),OP(12),FF(12),P(12),
SS(12,12),U(12),EFI(12)
CCMPCN/ITSD/ NSCIV,ITYP,MAXIT,RTOL,RTOLS,RTOLL,COAN(34)
CCMPCN/MISC/ MP(4),OT,ALFA,BETA,INTG,LL(16)
CCMPCN/JUNK/ I,II,J,JJ,LMN,JUK(200)
CCMPCN/COLB/ USP(10,2),USPF(1C,2),KF(6),LP(12),LPSLIP(2)
EQUIVALENCE (STIF,MTYPE)
C
C INITIALIZATION
C
REWIND 3
DO 10 I=1,NEQ
PU(I)=0.
10 PN(I)=0.
IF (ICONO.EQ.2) GO TO 13
DO 12 I=1,20
12 USPF(I)=USP(I)
13 CONTINUE
C
IF (ITYP.EQ.0.ANC.ICONC.EQ.3.ANO.ICOR.NE.0) GO TO 20
DO 15 I=1,NEQ
DO 15 J=1,MBANC
15 A(I,J)=B(I,J)
20 CONTINUE
IF (NUMNEL.EQ.0) RETURN
C
C COMPUTE NONLINEAR ELEMENT STIFFNESS MATRIX AND FORCE
C
M=0
DO 700 N=1,NUMNEL
C
DO 50 I=1,24
EX(I)=0.
EXI(I)=0.
50 OEX(I)=0.
C
REAC(3) STIF
C
DO 100 I=1,NU
II=LM(I)
IF (II.LE.0.OR.II.GT.NEQ) GO TO 100
EX(II)=X(II)
EXI(II)=X(II)
OEX(II)=OX(II)

```

40.

```

100 CONTINUE
C
  DO 200 I=1,12
    F(I)=STR(N,I)
  200 UP(I)=UPL(N,I)
  IF (INSCIV.EQ.0.OR.ICONC.NE.1.OR.ISOIV.NE.0) GO TO 220
  DO 210 I=1,12
    STRF(N,I)=F(I)
  210 UPLF(N,I)=UP(I)
  220 CONTINUE
C
  INC=NINC(N)
  GC TC (310,320,330,340,350) MTYPE
C
  C NONLINEAR TRUSS ELEMENT.....SKIP
C
  310 GO TC 400
C
  C ELASTIC-PLASTIC BEAM ELEMENT.....SKIP
C
  320 GO TC 400
C
  C NONLINEAR CURVED BEAM ELEMENT.....SKIP
C
  330 GO TO 400
C
  C BILINEAR BOUNDARY ELEMENT.....SKIP
C
  340 GO TO 400
C
  C NONLINEAR EXPANSION JOINT ELEMENT
C
  350 M=M+1
    CALL NEXPJT (M,INO)
C
  400 NINC(N)=INC
C
  C COMPUTE NONLINEAR RESTORING FORCE
C
  IF (INO) 410,440,410
  410 DC 435 I=1,NO
    II=LM(I)
    IF (II.LE.0.OR.II.GT.NEQ) GO TO 435
    PN(II)=PN(II)+EF(I)
  435 CONTINUE
  440 CONTINUE
C
  C COMPUTE COULOMB FRICTIONAL FORCE
C
  IF (MTYPE.NE.5) GO TO 525
  DO 520 I=1,NO
    II=LM(I)
    IF (II.LE.0.OR.II.GT.NEQ) GO TO 520
    PU(II)=PU(II)+OF(I)
  520 CONTINUE
  525 CONTINUE

```

C-19

41.

```

ASSEMBLE NEW TOTAL STIFFNESS MATRIX
C
C
  IF (ITYP.EQ.0.ANC.ICCND.EQ.3.AND.ICOR.NE.0) GO TO 555
  IF (INC.EQ.0.AND.MTYPE.NE.5) GC TO 555
  DO 550 I=1,NO
    II=LM(I)
    IF (II.LE.0.OR.II.GT.NEQ) GO TO 550
    LMN=I-II
    DO 540 J=1,NO
      JJ=LM(J)
      IF (JJ.LE.0.OR.JJ.GT.NEQ) GO TO 540
      JJ=JJ+LMN
      IF (JJ) 540,540,535
      535 A(II,JJ)=A(II,JJ)+ASSA(II,JJ)-ASSA(II,J)
      540 CONTINUE
      550 CONTINUE
      555 CONTINUE
C
  C UPDATE NONLINEAR ELEMENT STRESS AND DEFORMATION
C
  IF (ICONC.EQ.2) GO TO 580
  IF (ITYP.EQ.0.ANC.ICONC.EQ.3.AND.ICOR.NE.0) GO TO 580
  ASS(N)=NS
  DO 570 I=1,12
    STR(N,I)=P(I)
  570 UPL(N,I)=UP(I)
  580 CONTINUE
C
  700 CONTINUE
C
  C COMPUTE RESIDUAL FORCE
C
  GO TO (710,720,710) ICONC
  710 CALL RESIDF(B,XM,X,X1,X2,PEXT,PBMAX,MMAX,PM,REF,PA,NEC,
    MBAND,RTOL,PU)
C
  720 RETURN
  END

```



42.

```

*OECK RESIDF
SUBROUTINE RESIDF (B,XM,X,X1,X2,PEXT,MBSMAX,MHMAX,PM,REF,PN,NEC,
    MBAND,RTOL,PU)
C
C DIMENSION B(1),XM(1),X(1),X1(1),X2(1),PEXT(1),MBMAX(1),MHMAX(1),
    PM(1),PN(1),REF(1),PL(1)
C COMMON/MISC/ MM(4),DT,ALFA,BETA,INTG,LL(6)
C COMMON/JUNK/ FNM1,FNM2,DFNM,NEC1,I,XX,MB,PH,K,J,N2,JUK(194)
C COMMON/COLR/ USP(10,2),LSPF(10,2),KF(6),LPSLIP(2)
C
C COMPUTE RESIDUAL FORCE
C
FNM1=0.
FNM2=0.
OFNM=0.
RTOL=0.0
NEC1=NEC-1
DO 10 I=1,NEQ
10 PM(I)=X(I)+BETA*X1(I)
XX=-PM(I)-XM(I)*(X2(I)+ALFA*X1(I))-PU(I)
MB=MHMAX(I)
MH=MHMAX(I)
K=1
IF (MB.LT.1) GO TO 30
DO 20 J=1,MB,NEQ
IF (B(J).EQ.0.) GO TO 20
XX=XX-B(J)*PM(K)
20 K=K+1
30 IF (I.EQ.1) GO TO 100
N2=I+NEQ1
IF (MH.LT.N2) GO TO 100
K=I-1
DO 50 J=N2,MH,NEQ1
IF (B(J).EQ.0.) GO TO 50
XX=XX-B(J)*PM(K)
50 K=K-1
100 REF(I)=PEXT(I)+XX
FNM1=FNM1+PEXT(I)**2
FNM2=FNM2+XX*XX
OFNM=OFNM+REF(I)**2
150 CONTINUE
C
XX=SQRT(FNM1)+SQRT(FNM2)
IF (XX.EQ.0.) GO TO 200
RTOL=SQRT(OFNM)/XX
C
200 RETURN
END

```

43.

```

*OECK ITERN
SUBROUTINE ITERN (A,B,XM,X,X1,X2,OX,FIT,REF,PU,PN,PM,PEXT,NBMAX,
    MBMAX,MHMAX,NINC,NSS,STR,STRF,UPL,UPLF,REC,MBAND,
    NUMNEL,(SOIV,ICOR,NOT,NITRN))
C
C DIMENSION A(1),B(1),XP(1),X(1),X1(1),X2(1),OX(1),FIT(1),REF(1),
    PU(1),PN(1),PM(1),PEXT(1),NBMAX(1),MBMAX(1),MHMAX(1),
    NINC(1),NSS(1),STRINUMNEL(12),STRFNUMNEL(12),
    UPL(NUMNEL,12),UPLF(NUMNEL,12)
C COMMON/EPAR/ CONT(14),NNNN(14)
C COMMON/TSO/ NSD(4),ITYP,MAXIT,RTOL,RTCLS,RTOLI,CCAN(134)
C COMMON/MISC/ MM(14)
C COMMON/JUNK/ I,J,MB,MP,N1,DO,JLK(199)
C COMMON/COLR/ USP(10,2),USPF(10,2),KF(6),LPSLIP(2)
C
C ITERATION OF EQUATION OF MOTION
C
XNM1=0.
DO 5 I=1,NEQ
5 XNM1=XNM1+X(I)**2
IF (XNM1.EQ.0.) GO TO 200
C
ITRN=0
6 ITRN=ITRN+1
WRITE(6,1000) ITRN
C
FORM EFFECTIVE DYNAMIC STIFFNESS MATRIX AND LOAD VECTOR
C
IF (ITYP) B,20,B
8 DO 10 I=1,NEQ
10 PM(I)=CONT(11)*X1(I)+CONT(12)*X2(I)-X(I)
DO 15 I=1,NEQ
A(I)=A(I)+CONT(7)*XM(I)+CONT(8)*B(I)
MB=MBMAX(I)
MH=MHMAX(I)
N1=I+NEQ
IF (MH.LT.N1) GO TO 15
DO 12 J=N1,MH,NEQ
IF (B(J).EQ.0.) GO TO 12
A(J)=A(J)+CONT(8)*B(I)
12 CONTINUE
15 CONTINUE
C
C TRIANGULARIZE EFFECTIVE DYNAMIC STIFFNESS MATRIX
C
CALL TRIA (A,NBMAX,NEG,MBAND)
20 CONTINUE
C
SOLVE FOR CORRECTIVE DISPLACEMENT INCREMENT
C
CALL BACK (A,NBMAX,REF,NEG)
C
C COMPUTE DISPLACEMENT, VELOCITY AND ACCELERATION
C
OXNM=0.
XNM2=0.

```

44.

```

OC 50 I=1,NEQ
OD=REF(1)
X(1)=X(1)+DC
X1(1)=X1(1)+CONT(4)*OD
X2(1)=X2(1)+CONT(1)*OD
DX(1)=OD
XNM2=XNM2+X(1)*2
50 CXNP=DXNM+CD*OD
C
C CHECK CORRECTNESS OF NEW SOLUTION
C
C RTOL=SQRT(10*XNM)/(1+SQRT(XNM1))+SQRT(XNM2))
C IF (RTOL*LT,RTOL) ICOR=0
C WRITE(6,1200) RTOL
C
C COMPLETE NEW STIFFNESS MATRIX AND RESIDUAL FORCE
C
C CALL NELSTF (A,B,X,X1,X2,DX,XP,MBMAX,PHMAX,PEXT,FIT,PU,PN,PM,REF,
C STR,STRF,UPL,UPLF,NINC,NSS,REQ,MBANO,NUMNEL,3,ISDIV,
C ICOR,RTOL)
C
C CHECK FOR NUMBER OF ITERATION
C
C IF (ICOR.EQ.0) GO TO 20C
C IF (ITRN*LT,MAXIT) GO TO 6
C WRITE(6,1100) NOT,ITRN
C STOP
C
C 200 NITRN=NITRN+1ITRN
C RETURN
C
C 1000 FORMAT(1H,20X,21NUMBER OF ITERATION =,I5)
C 1100 FCPRAT(1H,51H*****EQUILIBRIUM ITERAT(CN FAILED TO CONVERGE*****
C /SHNCT =,I5/3X+6HITRN =,I5/26H*****EXECUTION TERMINATED. )
C 1200 FCPRAT(1H,25X,45HRELATIVE NORM OF CORRECTIVE DISPLACEMENT.....,
C F15.7)
C
C END

```

45

```

*CHECK OUTPUT SUBROUTINE OUTPUT
C
C COMPCN/EPAR/ PAR(14),NUMNP,NELTYP,NUMEL,NUMNEL,NEQ,MBANO,MTCT,
C NL,N2,N3,N4,N5,N6,N7
C COMPCN/EMIX/ QQQ(2043)
C COMPCN/MISC/ NFN,NGM,NT,NOT,OOT,LL(9)
C COMPCN/JUNK/ NCS,GT,KK1,KK2,ISP1,ISP2,NSC,NSS,NNS,MCIS,MSTR,
C NOISE,MSTRB,MBC,NBS,JUK(190)
C COMPCN A(1)
C
C INPUT SPECIFICATIONS FOR OUTPUT OF RESPONSE TIME HISTORIES
C
C DT=DDT
C N1=1
C N2=N1+NUMNEL*12
C N3=N2+NEQ
C N4=N3+NUMEL
C CALL INCUT (AIN1),AIN2),A(N3),A(N4),NUMNP,NEQ,NUMEL,NUMNEL)
C
C PACK RESPONSE TIME HISTORIES IN BLOCKS
C
C DT=NCT*OT
C NOS=NT/NOT
C NCISB=(MTCT-N3-NEQ*2)/(MOTS*2)
C MCISB=(MTCT-N3-9*NCS)/(MOTS*2)
C IF (NOISB-GT,MCISB) NOISB=MCISB
C IF (NCISB-GT,NCS) NCISB=NCS
C NBC=(NOS-1)/NOISB+1
C
C MSTRB=(MTCT-N3-4*NUMEL*25)/(MSTR*2)
C MSTRB=(MTCT-N3-9*NCS)/(MSTR*2)
C IF (MSTRB-GT,MSTRB) MSTRB=MSTRB
C IF (MSTRB-GT,NOS) MSTRB=NOS
C NBS=(NOS-1)/MSTRB+1
C
C N4=N3+NEQ
C N5=N4+NEQ
C N6=N5+MCIS*NDISB
C
C N7=N3+NUMNEL
C N8=N7+NUMNEL*12
C N9=N8+NUMNEL*12
C N10=N9+MSTR*MSTRB
C N11=N10+MSTR*MSTRB
C CALL REPACK (AIN1),AIN2),A(N3),A(N4),A(N5),A(N6),
C A(N3),A(N7),A(N8),A(N9),A(N10),NOS,NEQ,
C MCIS,NCISB,NUMNEL,MSTR,MSTRB,MBC,NBS )
C
C MT=0
C NFLE=0
C IF (KK1.EQ.4) NFLE=NFLE+NNO*2
C IF (KK2.EQ.4) NFLE=NFLE+NSS+NNS
C IF (NFLE.EQ.0) GO TO 100
C MT=30
C REWIND MT

```



```

      K=K+1
      L=0
      150 CONTINUE
      GO TO 100
C
C
C
      READ AND PRINT STRESS OUTPUT SPECIFICATIONS
C
      200 NSC=K
      WRITE(6,4000) KK1,ISP1
C
      READ (8) INC
      L=0
      LL=0
      K=0
      KK=0
      READ (5,1000) KK2,ISP2
      NREAD=1
      NTYPE=0
      NUMNE=0
C
      00 600 N=1,NUMEL
      MTYPE=INO(N)
      IF (MTYPE.GT.0) GO TO 205
      MTYPE=-MTYPE
      GO TO 210
      205 NUMNE=NUMNE+1
      210 IF (NTYPE.FQ.MTYPE) GO TO 220
      NTYPE=MTYPE
      NUME=0
      220 NUME=NUME+1
      READ (1) NS,NO,LM,SA
      READ (8) NOOF,SIG
      IF (NREAD.EQ.0) GO TO 300
      225 READ (5,1000) NELTY,NEL,IS
      IF (NEL.GT.0) GO TO 250
      IF ( L .EQ.0) GO TO 230
      WRITE (4) KO,SO,L
      WRITE (7) KLM,SSA,NC
      K=K+1
      230 IF (LL .EQ.0) GO TO 700
      WRITE (2) NKS,SNO,LL
      KK=KK+1
      GO TO 700
C
      250 IF (N.EQ.1) WRITE(6,3000)
      WRITE(6,3002) NELTY,NEL,IS
C
      300 IF (NELTY.EQ. NTYPE.AND.NEL.EQ.NUME) GO TO 350
      NREAD=0
      GO TO 600
      350 NREAD=1
      IF (INO(N)) 400,400,500
C
C
C
      STRESSES FOR LINEAR ELEMENTS
C
      400 00 450 I=1,NS

```

```

C
DO 720 I=N,NUMEL
  READ (8)
720 CONTINUE
C
750 MOIS=0
  MSTR=0
  DO 800 I=1,NEQ
    IF (IDIS(I).EQ.0) GO TO 800
    MOIS=MOIS+1
    IOISI=MOIS
800 CONTINUE
C
DO 900 I=1,NUMNEL
  DO 900 J=1,12
    IF (ISTR(I,J).EQ.0) GO TO 900
    MSTR=MSTR+1
    ISTR(I,J)=MSTR
900 CONTINUE
C
  RETURN
C
1000 FORMAT (14I5)
2000 FORMAT (36H1015PLACEMENT COMPONENTS FOR WHICH /
  36H OUTPUT TIME HISTORY IS REQUIRED,... //
  5H NODE 4X 23H15PLACEMENT COMPONENTS /)
2001 FORMAT (15,4X,6I4)
3000 FORMAT (36HELEMENT STRESS COMPONENTS FOR WHICH /
  36H OUTPUT TIME HISTORY IS REQUIRED,... //
  40H ELEMENT DESIRED STRESS COMPONENTS /
  10H TYPE NO. /)
3002 FORMAT (2I4,5X,12I3)
4000 FORMAT (/16H OUTPUT TYPE.....,I2 /
  16H PLOT SPACING.....,I2 )
4001 FORMAT (15,4X,14,4X,21HFIXED DCF...NO OUTPUT )
END

C
*DECK REPACK
SUBROUTINE REPACK (ISTR,IOIS,X,X2,XH,X2H,NSS,STR,UPL,STH,UPH,
  NOS,NEQ,MOIS,NOISB,NUMNEL,MSTR,NSTRB,NBO,NBS)
C
  DIMENSION ISTR(NUMNEL,1),IOISI(1),XINEQ,XHIMOIS,NCTISB,
  NSS(NUMNEL),STR(NUMNEL,12),UPL(NUMNEL,12),
  STH(MSTR,NSTRB),UPH(MSTR,NSTRB),X2(NEQ),X2HIMOIS,NOISB)
C
  PACK RESPONSE TIME HISTORY IN OPTIMAL AVAILABLE STORAGE BLOCKS
C

```



```

*CHECK OUTHIS
SUBROUTINE OUTHIS (ISTR,IOIS,I,X,XH,UH,NEL,NOS,NOI,KOJ,
  NOB,NH8,KKK,KKI,ISPI,IT,ITKT,MT,IF)
C
C OI'PENSION ISTR(NEL,I),IOIS(I),T(I),X(8,NCS),XH(NOI,KOJ),
  UH(NOI,KOJ)
C CMPCN/EMTX/ KLM(8,24),SA(8,24),NO,SM(8)
C CMPCN/JUNK/ NPT,CT,NDATA(13),L,K,KOI(4,8),XO(8),TM(8),XP(8)
C DATA SM /1H1,1HA,1H2,1H8,1H3,1FC,1H4,1HC/
C
C OUTPUT RESPONSE TIME HISTORIES ON SPECIFIED DISPLAY MEDIUM
C
C TAPE IT INPUT TAPE STORE KOI(4,8),XC(8),L
C TAPE JT INPUT TAPE STORE XH(ICI,NCJ),UH(NOI,NCJ),K
C TAPE KT INPUT TAPE STORE KLM(8,24),SA(8,24),NO
C TAPE MT OUTPUT TAPE STORE IF,KKK,L,KC,XM,X(8,NCS)
C
C IF (NOB.EQ.0) RETURN
C
C O0 900 M=1,NOH
  IF=IF+1
  RE=ND- JT
  READ (IT) KO,XO,L
  IF (KKK.EQ.3) READ (KT) KLM,SA,NO
  O0 100 I=1,8
  TM(I)=0.
  XM(I)=0.
10C CONTINUE
C
C PRINT APPROPRIATE TITLE
C
C GO TC (110,200,130,110) KKI
C
110 GC TC (111,112,113,114) KKK
111 WRITE(6,1001) M,IF
  WRITE(6,1002) (KO(I,1),KO(3,1),I=1,L)
  GO TC 200
112 WRITE(6,2001) M,IF
  WRITE(6,1002) (KC(I,1),KO(3,1),I=1,L)
  GO TC 200
113 WRITE(6,3001) M,IF
  WRITE(6,3002) (KC(1,1),KO(2,1),KO(3,1),I=1,L)
  GO TC 200
114 WRITE(6,4001) M,IF
  WRITE(6,4002) (KO(1,1),KO(2,1),KO(3,1),I=1,L)
  GO TC 200
C
13C IF (M.GI.1) GO TO 200
  GO TC (131,132,133,131) KKK
131 WRITE(6,1003)
  WRITE(6,1010)
  GO TC 200
132 WRITE(6,2003)
  WRITE(6,2010)
  GO TC 200
133 WRITE(6,3003)

```

```

C
C10 DO 611 N=1,NOS
C11 WRITE(6,1004) T(N),(X(I,N),I=1,L)
    WRITE(6,1005) (XM(I),I=1,L)
    WRITE(6,1006) (TM(I),I=1,L)
    GC TC 900
C
C    PLOT RESPONSE TIME HISTORIES
C
C 620 GO TO (621,623,625,627) KKK
C
C 621 ISO=1
    WRITE(6,1008) M
    WRITE(6,1010)
    GC TC 624
C 623 ISO=1
    WRITE(6,2008) M
    WRITE(6,2010)
    GO TC 629
C 624 WRITE(6,2011) (KO(1,I),KO(2,I),KO(3,I),XM(I),TM(I),I=1,L)
    GO TC 629
C 625 ISO=1
    WRITE(6,3008) M
    WRITE(6,3010)
    WRITE(6,3011) (KO(1,I),KO(2,I),KO(3,I),XM(I),TM(I),I=1,L)
    GO TC 629
C 627 ISO=2
    WRITE(6,4009) M
    WRITE(6,4010)
    DO 628 I=1,L,2
        II=I+1
        WRITE(6,4011) KO(1,I),KO(2,I),KO(3,I),XM(I),TM(I),SM(I)
        WRITE(6,4012) XM(II),TM(II),SM(II)
C 628
C 629 CALL PLCT (X,XM,L,DT,NOS,ISPI,ISO)
    GO TC 900
C
C    PRINT MAXIMUM RESPONSE ONLY
C
C 630 GO TC (631,635,637) KKK
C 631 WRITE(6,1007) (KO(1,I),KO(2,I),XM(I),TM(I),I=1,L)
    GC TC 900
C 635 WRITE(6,3007) (KO(1,I),KO(2,I),KO(3,I),XM(I),TM(I),I=1,L)
    GO TC 900
C 637 DO 638 I=1,L,2
    II=I+1
    WRITE(6,4007) KC(1,I),KO(2,I),KO(3,I),XM(I),TM(I)
C 638 WRITE(6,4008) XM(II),TM(II)
    GO TO 900
C
C    STORE RESPONSE TIME HISTORIES ON OUTPUT TAPE MT
C
C 640 IF (KK1.EC.4) WRITE (MT) IF,KKK,L,KO,XM,X
    GO TC 610
C
C 900 CONTINUE
    RETURN
END

```

```

*DECK PLCT
SUBROUTINE PLOT (X,M,L,OT,NDS,ISP,ISO)
C
C DIMENSION X(8,1),M(8),PM(8),Q(8),SM(8),IP(8)
CCPMCN/EMTX/ PP(101)
DATA PM /1H1,1H2,1H3,1H4,1H5,1H6,1H7,1H8/
DATA CM /1H1,1H2,1H3,1H4,1H5,1H6,1H7,1H8/
DATA EL,V,P /1H ,1H.,1H+/
C
C ACRPALIZED PLOT OF TIME HISTORIES OF TIME FUNCTIONS
C
C DO 30 I=1,L
GO TC (10,20) ISO
10 SM(I)=PM(I)
GO TC 30
20 SM(I)=QM(I)
30 CONTINUE
C
C DO 100 I=1,L
IF (X(I)) 50,100,50
50 XM(I)=50./XM(I)
100 CONTINUE
TT=0.
WRITE(6,2000)
WRITE(6,2001)
WRITE(6,2002) TT,P,(V,I=1,24),P,(V,I=1,24),P,(V,I=1,24),P,
(V,I=1,24),P,TT
C
C K=1
DC 200 I=2,100
PP(I)=BL
NDS1=NDS-I
DO 500 N=1,NDS1
PP( 1)=V
PP( 51)=V
PP(101)=V
II=(SP
210 IF (II.LE.0) GO TO 250
WRITE(6,2003) PP
II=II-1
GO TC 210
250 TT=TT+DT
DO 300 I=1,L
XX=XM(I)*X(I,N)
M=XX
M=M+51
IP(1)=M
300 PP(M)=SM(I)
IF (K.LT.10) GO TO 320
PP( 1)=P
PP( 51)=P
PP(101)=P
K=1
WRITE(6,2002) TT,PP,TT
GO TC 340
320 WRITE(6,2003) PP

```

58.

```

K=K+1
C
C RESET PP(101)
C
C 340 DO 360 I=1,L
M=IP(I)
360 PP(M)=BL
500 CONTINUE
C
C TT=TT+DT
WRITE(6,2002) TT,P,(V,I=1,24),P,(V,I=1,24),P,(V,I=1,24),P,
(V,I=1,24),P,TT
C
C WRITE(6,2001)
RETURN
C
C *CARRIAGE CCTRL CHARACTER Z SURPRESS SKIP OVER PAGE FOLDS
C
C 2000 FORMAT (1/56X,8HORDINATE )
2001 FORMAT (1/12H2 TIME -1.0,21X,4F-C.5,22X,3H0.0,22X,3H0.5,22X,3H1.0,
X,4HTIME )
2002 FORMAT (1H2,F7.2X,101A1,F7.2)
2003 FORMAT (1H2,9X,101A1)
END

```

59.

```

*DECK SBEAM
SUBROUTINE SBEAM
C
C GPMCN A(1)
CCPMCN/EPAR/ NPAR(14),NUMNP,NELTYP,NUMEL,NUMMEL,MEQ,MBANO,MTOT,
C
C CCPMKN/JUNK/ STR(4),PP,L,K,NTAG,NDYN,SIG(12),EXRA(184)
C
C N7=N6+NPAR(5)
N8=N7+NPAR(5)
N9=N8+NPAR(5)
N10=N9+NPAR(4)*12
N11=N10+NPAR(3)*6
N12=N11+NPAR(6)*12
IF (N12.GT.MTOT) CALL ERROR (1,N12-MTOT,7HBEAM )
CALL TEAM (NPAR(2),NPAR(3),NPAR(4),NPAR(5),NPAR(6),
A(N1),A(N2),A(N3),A(N4),A(N5),A(N6),A(N7),A(N8),
A(N9),A(N10),A(N11),NUMNP,MBANC,NUMEL)
C
C RETURN
END

```

```

*OECA TEAM
SURFCUTINE TEAM (NBEAM,NUMETP,NUMFIX,NUMPAT,NUMPAR,1D,X,Y,Z,1NO,
E,G,RC,SFT,CCPROP,ENPRCP,NUMNP,MEANO,NUMEL)
C
C DIMENSION IC(NUMNP,1),X(1),Y(1),Z(1),INC(1),EL(1),G(1),RO(1),
SFT(NUMFIX,1),CCPROP(NUMETP,1),ENPROP(NUMPAR,1),
SFT(72),LPS(12),EC(12),T(3,3)
CCPCPN/EMTX/ LM(24),NC,NS,ASA(24),RF(24,4),XM(24),SA(12,24),
SF(12,4),ENPAR(24),S(12,12),F(48),TTT(72)
CCPCPN/JUNK/ LC(4),JK(6),MELTYP,OL,MATTYP,ILC(4),TS(2,2),LS(4),
EMUL(3,4)
ECLIVALENCE (STIF,LP),(LMS,TTT(1)),(EC,TTT(13)),(T,TTT(25))
C
C FCRPS 3-0 BEAM STIFFNESS AND STRESS ARRAYS
C
C WRITE (6,2005) NBEAM,NUMETP,NUMFIX,NUMPAT,NUMPAR
DD 5 I=1,1346
5 STIF(1)=0.
C
C READ AND PRINT MATERIAL PROPERTY DATA
C
C WRITE (6,2001)
DO 10 I=1,NUMMAT
READ (5,1001) N,E(IN),G(N),RO(N)
WRITE (6,2002) N,E(IN),G(N),RO(N)
10 G(N)=0.5*E(N)/(1.+G(N))
C
C READ AND PRINT GEOMETRIC PROPERTIES OF COMMON ELEMENTS.
C
C WRITE (6,2003)
DO 30 I=1,NUMETP
READ (5,1002) N,(CCPROP(N,J),J=1,6)
IF (ICPROP(N,1).NE.C.0).AND.(CCPROP(N,4).NE.0.0).AND.
1 (CCPROP(N,5).NE.C.0).AND.(CCPROP(N,6).NE.0.0) GO TO 20
WRITE (6,2013)
CALL EXIT
20 WRITE (6,2004) N,(CCPROP(N,J),J=1,6)
30 CONTINUE
C
C ELEMENT LOAD MULTIPLIERS
C
C READ (5,1006) ((EMUL(I,J),J=1,4),I=1,3)
WRITE (6,2006) ((EMUL(I,J),J=1,4),I=1,3)
C
C READ AND PRINT FIXED END FORCES IN LOCAL COORDINATES
C
C IF (NUMFIX .EQ. 0) GO TO 56
WRITE (6,2010)
DO 55 I=1,NUMFIX
READ (5,1005) N,(SFT(N,J),J=1,12)
55 WRITE (6,2011) N,(SFT(N,J),J=1,12)
56 CONTINUE
C
C READ AND PRINT ELEMENT NONLINEAR PARAMETERS
C
C IF (NUMNP.EQ.0) GO TO 59
WRITE (6,2020)
CC 58 I=1,NUMNP
READ (5,1007) N,(ENPROP(N,J),J=1,12)
WRITE (6,20,1) (N,(ENPROP(N,J),J=1,12),N=1,NUMNP)
59 CCATINUE
C
C READ AND PRINT ELEMENT DATA. GENERATE MISSING INPLT.
C
C WRITE (6,4000)
L=0
60 KKK=0
READ (5,3000) INEL,INI,INJ,INK,IPAT,IMEL,ILC,INELKJ,INC,100
IF (ICD.GT.NUMNP) CALL ERROR (3,INEL,7HBEAM )
IF (INEL.NE.1) GO TO 15
NI=INI
NK=INK
NJ=INJ
15 IF (INC.EC.0) INC=1
65 L=L+1
KKK=KKK+1
ML=(INEL-L
IF (ML) 66,67,68
66 CALL FRKR (4,INEL,7HBEAM )
67 NEL=INEL
NI=INI
NJ=INJ
NK=INK
MATTYP=IMAT
MELTYP=IMEL
DO 90 I=1,4
90 LC(I)=ILC(I)
NEKCD=INELKI
NEKCLJ=INELKJ
NINO=100
GO TO 69
68 NEL=INEL-ML
NI=IN+KKK*INCR
NJ=JN+KKK*INCR
69 CONTINUE
WRITE (6,4001) NEL,NI,NJ,NK,MATTYP,MELTYP,LC,NEK001,NEK00J,NINO
C
C 74 OX=X(INJ)-X(INI)
OY=Y(INJ)-Y(INI)
DZ=Z(INJ)-Z(INI)
DL=SCRT(DX*OX+OY*OY+OZ*OZ)
IF(OL) 75,75,76
75 CALL ERROR (5,NEL,7HBEAM )
C
C FORM GLOBAL TO LOCAL COORDINATE TRANSFORMATION.
C
C 76 T(1,1)=OX/OL
T(1,2)=OY/OL
T(1,3)=OZ/OL
A1=X(INJ)-X(INI)
A2=Y(INJ)-Y(INI)

```



```

A3=Z(NJ)-Z(NI)
B1=X(NK)-X(NI)
B2=Y(NK)-Y(NI)
B3=Z(NK)-Z(NI)
AA=A1*A1+A2*A2+A3*A3
AB=A1*B1+A2*B2+A3*B3
U1=AA*B1-AB*A1
U2=AA*B2-AB*A2
U3=AA*B3-AB*A3
UU=U1*U1+U2*U2+U3*U3
UU=SQRT(UU)
IF (UU.GT.O.) GO TO 77
CALL ERROR (6,INEL,7H BEAM )
77 T(2,1)=U1/UU
T(2,2)=U2/UU
T(2,3)=U3/UU
T(3,1)=T(1,2)*T(2,3)-T(1,3)*T(2,2)
T(3,2)=T(1,3)*T(2,1)-T(1,1)*T(2,3)
T(3,3)=T(1,1)*T(2,2)-T(1,2)*T(2,1)
CHECK IF NEW STIFFNESS NEEDED
C
C
IF (NFL-EQ.1) GO TO 80
IF (ABS(CS-OL).GT.EL/100.) GO TO 80
IF (INT(NE-MATYP).CR.(ME-NE.RELTYP)) GO TO 80
IF ((JK(1).NE.NEKOCJ).OR.(JK(2).NE.NEKOCJ)) GO TO 80
OO 78 I=1,4
IF (LS(1).NE.LC(1)) GO TO 80
78 CONTINUE
OO 79 I=1,2
OO 79 J=1,2
IF (ABS(TS(1,J)-T(1,J)).GT.ABS(T(1,J)/100.)) GO TO 80
79 CONTINUE
GO TO 150
C
B0 OS=OL
MT=MATYP
ME=RELTYP
OO 81 I=1,2
OO 81 J=1,2
B1 TS(1,J)=T(1,J)
OO 82 I=1,4
B2 LS(1)=LC(1)
JK(1)=NEKOCJ
JK(2)=NEKOCJ
C
C
FORM NEW STIFFNESS
C
CALL NEW8M (E,C,RD,COPROP,SFT,NUMFIX,NUMETP)
C
FORM ELEMENT LOCATION MATRIX
C
150 DO 170 M=1,6
LM(M)=IQ(NI,M)
LM(M+12)=0
LM(M+18)=0

```

```

170 LM(M+6)=IQ(NJ,M)
NS=12
NO=12
C
C TRANSFORM TO MASTER DEGREES OF FREEDOM
C
CALL SLAVE (X,Y,Z,IC,NUMNP,NI,NJ)
C
WRITE ELEMENT INFORMATION ON TAPE
C
CALL WRITET (MEANG,NDIF)
C
C SET NONLINEAR ELEMENT INDICATOR AND STORE NONLINEAR INFORMATION
C
NN=NUMEL+NEL
IF (INCL.LE.0) GO TO 200
INC(NN)=2
OO 190 I=1,12
190 EMPAR(I)=ENPROP(INC,I)
MTYPE=2
WRITE (3) MTYPE,LM,NO,NS,ASA,SA,S,ENPAR,TTT
GO TO 250
200 INC(NN)=2
C
C CHECK FOR LAST ELEMENT
C
250 IF (NBLAM-NEL) 66,500,260
260 IF (PL.GT.0) GO TO 65
IN=INI
JN=INJ
INCR=INC
GO TO 60
500 RETURN
C
1001 FORMAT (15,F10.0)
1002 FORMAT (15,F10.0)
1005 FORMAT (15,6F10.0/F15.0,5F10.0)
1006 FORMAT (4F10.0)
1007 FORMAT (15,4F10.0/8F10.0)
2001 FCMPAT (24H MATERIAL PROPERTIES.... ///
. 54H NUMBER MODULUS POISSON S RATIO
. 54H MATERIAL YOUNG S
2002 FORMAT (1H,15,3X,F12.0,F14.5,F14.5)
2003 FCMPAT (17730H BEAM GEOMETRIC PROPERTIES.....//
1 48H ELEMENT AREA AREA AREA AREA
2 60H INERTIA INERTIA INERTIA INERTIA
3 / 48H TYPE X Y Z
4 30H X Y Z
2004 FORMAT (1H,15,2X,6F12.3)
2005 FCMPAT (39H1.....THREE DIMENSIONAL BEAM ELEMENTS///
. 36H NUMBER OF BEAMS =,15//
. 36H NUMBER OF GEOMETRIC PROPERTY SETS =,15//
. 36H NUMBER OF FIXED END FORCE SETS =,15//
. 36H NUMBER OF MATERIALS =,15//
. 36H NUMBER OF BEAM N/L PROPERTY SETS =,15)
2006 FORMAT (17730H ELEMENT LOAD MULTIPLIERS...../12X,1HA,14X,1HB,14X,

```







```

*DECK TRANSFM
C
      SUBROUTINE TRANSFM (RD,COPROP,NUMETP)
C
      DIMENSION RC(1),COPROP(NUMETP,1)
      CCMPCN/EMTX/ LM(24),NC,NS,ASA(24),RF(24,4),XM(24),SA(12,24),
      * SF(12,4),ENPAR(24),S(12,12),F(48),LMS(12),EC(12),TI(3,3),TJ(3,3)
      * CCMPCN/JUNK/ LC(4),JK(6),MELTYP,DL,MATTYP,BETA,B,DP,O,RA,AX,
      * EMUL(3,4),ILC(4),LS(4),R(12),C(12),EL(3,4)
C
      PERFORM LOCAL TO GLOBAL TRANSFORMATION
C
      DC 31 I=1,288
      31 SA(1)=0.
      DO 150 LA=1,10,3
      LB=LA+2
      DO 150 MA=1,10,3
      MB=MA-1
      DO 150 I=LA,LF
      DO 150 JM=1,3
      J=JM+MB
      XX=0.
      IF (J.GT.6) GO TO 152
      DO 151 K=1,3
      151 XX=XX+SI(I,K+MB)*TI(K,JM)
      DO 152 K=1,3
      152 DO 153 N=1,3
      153 XX=XX+SI(I,K+MB)*TJ(K,JM)
      150 SA(I,J)=XX
C
      DO 32 I=1,576
      32 ASA(I)=0.
C
      DO 160 LA=1,10,3
      LB=LA-1
      DO 160 MA=1,10,3
      MB=MA+2
      DO 160 IL=1,3
      I=IL+LB
      DO 160 J=MA,MB
      XX=0.
      IF (I.GT.6) GO TO 162
      DO 161 K=1,3
      161 XX=XX+TI(K,IL)*SAIK+LB,J)
      DO 162 K=1,3
      162 DO 163 N=1,3
      163 XX=XX+TJ(K,IL)*SAIK+LB,J)
      160 ASA(I,J)=XX
C
      DO 170 LA=1,10,3
      LB=LA-1
      DO 170 IL=1,3
      I=IL+LB
      DO 170 N=1,4
      XX=0.
      IF (I.GT.6) GO TO 172
      DO 171 K=1,3

```

```

      171 XX=XX-TI(K,IL)*SF(K+LB,N) 40.
      GO TO 170
      DO 173 K=1,3
      173 XX=XX-TJ(K,IL)*SF(K+LB,N)
      170 RF(I,N)=XX
C
      FORM MASS MATRIX
C
      XL =RABETA
      XLP =RUMATTYP)*AX*XL/2.0
      XXPX=XXMP*(COPROP(MATTYP,4)/AX)
      XXPY=XXMP*(XL**2/210.*COPROP(MATTYP,5)/(5.*CAX))
      XXPZ=XXMP*(XL**2/210.*COPROP(MATTYP,6)/(5.*CAX))
      DO 180 M=1,3
      XM(M)=XXM
      XM(M+6)=XXM
      XM(M+5)=XXPX*TI(1,M)**2+XXPY*TI(2,M)**2+XXMZ*TI(3,M)**2
      XPI*P*9)=XXMX*TI(1,P)**2+XXMY*TI(2,P)**2+XXMZ*TI(3,P)**2
      RETURN
      END

```

```

*DECK CBEAM
C
      SUBROUTINE CBEAM
C
      CCMPCN A(1)
      CCMPCN/EPAR/ NPAR(14),NUMNP,NELTYP,NUMEL,NUMNEL,NEG,MEANO,PTOT,
      * CCMPCN/JUNK/ STR(4),PP,L,K,NTAG,NDYN,SIG(12),EXRA(164)
C
      NT=N6+NPAR(5)
      N8=N7+NPAR(5)
      N9=N8+NPAR(5)
      A10=N9+NPAR(4)*12
      N11=N10+NPAR(3)*6
      N12=N11+NPAR(6)
      N13=N12+NPAR(7)*12
      IF (N13.GT.PTOT) CALL ERROR (1,N13-PTOT,THCBEAM )
      CALL CTEAM (NPAR(2),NPAR(3),NPAR(4),NPAR(5),NPAR(6),NPAR(7),
      * A(N1),A(N2),A(N3),A(N4),A(N5),A(N6),A(N7),A(N8),
      * A(N9),A(N10),A(N11),A(N12),ALP,NP,MBAND,NUMEL)
      RETURN
      END

```

```

*DECK CTEAP
SUBROUTINE CTEAP (NCREAM,NUMETP,NUMFIX,NUMMAT,NUMRAD,NUMPAR,
  IC,X,Y,Z,INC,E,G,RO,SFT,CCPROP,RAC,ENPRCP,
  NUMNP,MBAND,NUMEL)
  C
  C FCRM 3-C CURVED BEAM STIFFNESS AND STRESS-DISP. ARRAYS
  C
  C DIMENSION IC(NUMNP,1),X(1),Y(1),Z(1),INC(1),E(1),G(1),RO(1),
  C SFT(NUMFIX,1),CCPROP(NUMETP,1),RAD(1),ENPROP(NUMPAR,1),
  C STIFF(7221),LMS(112),EC(112),TT(13,3),TJ(13,3)
  C CCMPCN/ENTX/ LMS(24),NC,NS,ASA(24,24),RF(24,4),XP(24),SA(12,24),
  C SFI(12,4),ENPAR(24),S(12,12),F(48),TTT(72)
  C CCMPCN/JUNK/ LC(4),JK(16),MELTYP,OL,MATYP,BETA,B,OP,O,RA,AREA,
  C ECUVALENCE (STIFF,LP),(LMS,TTT11),(EC,TTT(13)),(TT,TTT(25)),
  C (TJ,TTT(34))
  C
  C WRITE (6,2005) NCREAM,NUMETP,NUMFIX,NUMMAT,NUMRAD,NUMPAR
  C DO 5 I=1,1346
  C 5 STIFF(I)=0.
  C
  C READ AND PRINT RADII OF CURVATURE DATA
  C
  C WRITE (6,2000)
  C DO 8 I=1,NUMRAD
  C READ (5,1000) N,RAD(N)
  C IF (RADIN).NE.0.0) GO TO 7
  C WRITE (6,2014)
  C CALL EXIT
  C 7 WRITE (6,2015) N,RAC(N)
  C 8 CONTINUE
  C
  C READ AND PRINT MATERIAL PROPERTY DATA
  C
  C WRITE (6,2001)
  C DO 10 I=1,NUMMAT
  C READ (5,1001) N,E(N),G(N),RO(N)
  C WRITE (6,2002) N,E(N),G(N),RO(N)
  C 10 G(N)=0.5*E(N)/(1.+G(N))
  C
  C READ AND PRINT CROSS SECTIONAL PROPERTIES
  C
  C WRITE (6,2003)
  C DO 30 I=1,NUMETP
  C READ (5,1002) N,ICCPROP(N,J),J=1,6)
  C IF (ICCPROP(N,1).NE.0.0).AND.(ICCPROP(N,4).NE.0.0).AND.
  C (CCPROP(N,5).NE.0.0).AND.(CCPROP(N,6).NE.0.0)) GO TO 20
  C WRITE (6,2013)
  C CALL EXIT
  C 20 WRITE (6,2004) N,(CCPROP(N,J),J=1,6)
  C 30 CONTINUE
  C
  C ELEMENT LOAD MULTIPLIERS
  C
  C READ (5,1006) ((FMULT(I,J),J=1,4),I=1,3)
  C WRITE (6,2006) ((FMULT(I,J),J=1,4),I=1,3)

```

```

  C
  C READ AND PRINT FIXED END FORCES IN LOCAL COORDINATES
  C
  C IF(NUMFIX.EQ.0) GO TO 56
  C WRITE (6,2010)
  C DO 55 I=1,NUMFIX
  C READ (5,1005) N,(SFT(N,J),J=1,12)
  C 55 WRITE (6,2011) N,(SFT(N,J),J=1,12)
  C 56 CONTINUE
  C
  C READ AND PRINT ELEMENT NONLINEAR PARAMETERS
  C
  C IF (NUMPAR.EQ.0) GO TO 59
  C WRITE (6,2020)
  C DO 58 I=1,NUMNPAR
  C READ (5,1007) N,(ENPRCP(N,J),J=1,12)
  C WRITE (6,2021) N,(ENPROP(N,J),J=1,12),N=1,NUMNPAR)
  C 58 CONTINUE
  C
  C READ AND PRINT ELEMENT DATA FOR EACH ELEMENT
  C
  C WRITE (6,4000)
  C L=0
  C 60 READ (5,3000) INEL,INI,INJ,INK,IPAT,IPEL,ILC,INELKI,INELKJ,IRAO,IQ
  C IF (IC.GT.NUMNPAR) CALL ERROR (3,INEL,7+ICBEAM )
  C L=L+1
  C M=INEL-L
  C IF (M.LT.66) GO TO 67,66
  C 66 CALL ERROR (4,INEL,7+ICBEAM )
  C 67 NEL=INEL
  C NI=INI
  C NJ=INJ
  C NK=INK
  C MATYP=IPAT
  C MELTYP=IPEL
  C DO 68 I=1,4
  C LC(I)=ILC(I)
  C 68 NEKCDI=INELKI
  C NEKCCJ=INELKJ
  C NR=IRAC
  C NI=0
  C WRITE (6,4001) NEL,NI,NJ,NK,MATYP,MELTYP,ILC,NEKCDI,NEKCCJ,NR,NINC
  C
  C FCRM GLOBAL TO LOCAL COORDINATE TRANSFORMATION.
  C
  C 74 CX=X(NJ)-X(NI)
  C DY=Y(NJ)-Y(NI)
  C CZ=Z(NJ)-Z(NI)
  C CL=SQRT(CX*CX+DY*DY+CZ*CZ)
  C IF (CL) 75,75,76
  C 75 CALL ERROR (5,NEL,7+ICBEAM )
  C 76 RA=RAD(NR)
  C ARGU=DL/(12.0*RA)
  C BETA=2.0*ASIN(ARGU)
  C B= SIN(BETA)
  C CP=CCS(BETA)

```

```

14.
O = 1.0-OP
BX=X(N1)-X(NK)
BY=Y(N1)-Y(NK)
BZ=Z(N1)-Z(NK)
BB=BX*BX+BY*BY+BZ*BZ
BB=SQRT(BB)
IF (BB.GT.0.0) GO TO 77
CALL ERROR (6,NEL,7HCREAM )
77 CX=CY*BZ-CZ*BY
CY=CZ*BX-CY*BZ
CZ=OX*BY-CY*BX
CX=CY*CX+CY*CY+CZ*CZ
CZ=SQRT(CZ)
BX=BX/BB
BY=BY/BB
BZ=BZ/BB
CX=CX/CC
CY=CY/CC
CZ=CZ/CC
AX=BY*CZ-BZ*CY
AY=BZ*CX-BX*CZ
AZ=BX*CY-BY*CX

C
TI(1,1)=AX
TI(1,2)=AY
TI(1,3)=AZ
TI(2,1)=BX
TI(2,2)=BY
TI(2,3)=BZ
TI(3,1)=CX
TI(3,2)=CY
TI(3,3)=CZ

C
TJ(1,1)=AX*OP-BX*P
TJ(1,2)=AY*OP-BY*P
TJ(1,3)=AZ*OP-BZ*P
TJ(2,1)=AX*P+BX*OP
TJ(2,2)=AY*P+BY*OP
TJ(2,3)=AZ*P+BZ*OP
TJ(3,1)=CX
TJ(3,2)=CY
TJ(3,3)=CZ

C
CHECK IF NEW STIFFNESS NEEDED
IF (NEL.EQ.1) GO TO 80
IF (PH.NE.NR) GO TO 80
IF (ABS(DS-DL)-GT.DL/100.) GO TO 80
IF (PT.NE.MATTYP).CR.(ME.NE.MELTYP)) GO TO 80
IF ((JK(1).NE.NEKC(1)).CR.(JK(2).NE.NEKC(2))) GO TO 80
DO 79 I=1,4
IF (LS(I).NE.LC(I)) GO TO 80
79 CONTINUE
GO TO 100

C
80 DS=DZ

```

```

16.
MT=MATTYP
ME=MELTYP
MR=NR
DO 85 I=1,4
85 LS(I)=LC(I)
JK(1)=NEKODI
JK(2)=NEKOCJ

C
FORM NEW CURVED BEAM STIFFNESS
C
CALL NEWCEM (E,G,RG,COPROP,SFT,RAO,NUMFIX,NUMETP)
C
CALL TRANSFM (RC,COPROP,NUMETP)
C
FORM ELEMENT LOCATION MATRIX
C
DO 170 M=1,6
LM(M)=10(NI,M)
LM(M+12)=0
LM(M+18)=0
170 LM(M+6)=10(NJ,M)
NS=12
NO=12

C
TRANSFORM TO MASTER DEGREES OF FREEDOM
C
CALL SLAVE (X,Y,Z,IC,NUMNP,NI,NJ)
C
WRITE ELEMENT INFORMATION ON TAPE
C
CALL WRITEF (MBANO,NUIF)
C
SET NONLINEAR ELEMENT INDICATOR AND STORE NONLINEAR PARAMETERS
C
NN=NUMEL+NEL
IF (NI.NE.0) GO TO 200
IND(INN)=3
DO 190 I=1,12
190 ENFAP(I)=ENPROP(INC,I)
MTYPE=3
WRITE (3) MTYPE,LM,NC,NS,ASA,SA,S,ENPAR,TTY
GO TO 250
200 IND(INN)=3

C
CHECK FOR LAST ELEMENT
C
250 IF (INCBEAM-NEL) 66,500,60
500 RETURN

C
1000 FORMAT(15,F10.0)
1001 FORMAT(15,F10.0)
1002 FORMAT(15,F10.0)
1005 FORMAT(15,F10.0,F15.0,F10.0)
1006 FORMAT(4F10.0)
1007 FORMAT(15,F10.0,F10.0)
2000 FORMAT(26+1RADII OF CURVED BEAMS.... //

```



```

27H RADIUS /
27H CURVATURE /
27H MATERIAL PROPERTIES..... //
54H MATERIAL YOUNG S POISSON S /
54H NUMBER MDULUS RATIC /
2002 FCRPAT (11, 15, 3X, F12, C, F14, 5, F14, 5)
2003 FCRPAT (30HICURVE BEAM GEOMETRIC PROPERTIES..... //
1 48H ELEMENT AREA AREA AREA
2 60H INERTIA INERTIA INERTIA
3 / 48H TYPE X Y Z
4 30H X Y Z
2004 FCRPAT (11, 15, 2X, 6F12, 3)
2005 FCRPAT (39H1.....TRREE OIM. CLVRD BEAM ELEMENTS...//
36H NUMBER OF CURVEV BEAMS =,15//
36H NUMBER OF SECTIONAL PROPERTY SETS =,15//
36H NUMBER OF FINEC ENC FORCE SETS =,15//
36H NUMBER OF MATERIALS =,15//
36H NUMBER OF RACIT =,15//
36H NUMBER OF N/L PARAMETER SETS =,15//
2006 FCRPAT (///30H ELEMENT LOAC MULTIPLIERS.....//12X,11HA,14X,1HB,14X,
1 1-C,14X,1HD/6H X-CIR 4E15.6/6H Y-OIR 4E15.6/6H Z-CIR 4E15.6/ )
201C FCRPAT (11H
1 30X40H FIXED END FORCES IN LCCAL COORDINATES
2//53H TYPE NCCE 35P MOMENT X FORCE Y FORCE Z
3 35P MOMENT X MOMENT Y MOMENT Z
2011 FCRPAT (11H, 13, 6X, 1H1, 3X, 6F12, 3/1H, 9X, 1HJ, 3X, 6F12, 3// )
2013 FCRPAT (1H0/
1 60H SECTION PROPERTIES OTHER THAN SHEAR AREAS MAY NOT BE SPECIF
2 36HIED AS ZERO. EXECUTION TERMINATED.)
2014 FCRPAT (1H0/
1 60H RADIUS OF CURVATURE MAY NOT BE SPECIFIED
2 36H AS ZERO. EXECUTION TERMINATED.)
2015 FCRPAT (15, F20, 5)
202C FCRPAT (11, 1/30X 40H CURVED BEAM ELEMENT NCALINEAR PARAMETERS //
B NL PAR 4X BPAIAL 4X BHMCPENT 4X BHMOMENT 4X
B ITCRSION 20X 24H YIELD FUNCTION CONSTANTS /
B P NC 6X 2PUC 9X 4HMLU/Y 8X 4HMLU/Z 9X 2HTU 8X 2HAD 6X 2HAI
6X 2HAD 6X 2HAD 6X 2HB0 6X 2HB1 6X 2HB2 6X 2HB3 //
2021 FCRPAT (15, 3X, 4E12, 3, RF8, 3)
30CC FCRPAT (1015, 216, 18, 15)
40CC FCRPAT (30HICURVE BEAM ELEMENT DATA..... //
5HCREAM 5X SHNCOES 5X 5H MATL 5H GEOM 5X 10HELEM LCAUS 4X 10X
12P ENO CODES 3X 6H RADIUS 2X 5H NINO /
4X 1H A 4X 1H E 4X 1H C 4X 1H O 5X 1H I 9X 1H J 4X 1H K 5H NC 5H NC
4001 FCRPAT (1015, 2110, 1110, 18)
4004 FCRPAT (11H, 31HNCCL PCINT NUMBERS FOR ELEMENT, 15, 36HARE ICENTICAL.
1 EXECUTION TERMINATED.)
C
ENC

```

```

C
F11=CCMPZ*(BETA+CC-2.C*8+PHIZ*CC+ZETA*AA)
F12=CCMPZ*(C-EE-PT*IZ+EE*ZETA*EE)
F16=(CCMPZ/RA)*(B-BETA)
F22=CUPMZ*(AA+PT*IZ*AA+ZETA*CC)
F26=(CCMPZ/RA)*(-D)
C
F33=CCMPY*(AA+PT*IV*(BETA+CC-2.C*8)+ZETA*BETA)
F34=(CCMPY/RA)*(AA+PT*IV*(B-CC))
F35=(CCMPY/RA)*(EE+PT*IV*(O-EE))
F44=(CCPMY/RA2)*(AA+PT*IV*CC)
F45=(CCPMY/RA2)*(EE+PT*IV*EE)
F55=(CCPMY/RA2)*(CC+PT*IV*AA)
F66=(CCPMZ/RA2)*BETA
C
U=F11*F22*F66*2.0*F12*F16*F26-F22*F16*F16-F11*F26*F26-F66*F12*F12
W=F33*F44*F55*2.0*F35*F45*F35-F44*F35*F35-F33*F45*F45-F55*F34*F34
C
S(1,1)=(F22*F66-F26*F26)/U
S(1,2)=-(F12*F66-F16*F26)/U
S(1,6)=(F12*F26-F22*F16)/U
S(2,2)=(F11*F66-F16*F16)/U
S(2,6)=-(F11*F26-F12*F16)/U
S(6,6)=(F11*F22-F12*F12)/U
C
S(3,3)=(F44*F55-F45*F45)/W
S(3,4)=-(F34*F55-F35*F45)/W
S(3,5)=(F34*F45-F44*F35)/W
S(4,4)=(F33*F55-F35*F35)/W
S(4,5)=-(F33*F45-F35*F34)/W
S(5,5)=(F33*F44-F34*F34)/W
C
S(1,7)=S(1,1)*OP+S(1,2)*B
S(1,8)=S(1,1)*B-S(1,2)*OP
S(1,12)=S(1,1)*RA*CC+S(1,2)*RA*B-S(1,6)
S(2,7)=S(1,2)*OP+S(2,2)*B
S(2,8)=S(1,2)*B-S(2,2)*OP
S(2,12)=S(1,2)*RA*CC+S(2,2)*RA*B-S(2,6)
S(3,9)=S(3,3)
S(3,10)=S(3,3)*RA*CC-S(3,4)*OP+S(3,5)*B
S(3,11)=S(3,3)*RA*B-S(3,4)*B-S(3,5)*DP
S(4,9)=S(3,4)
S(4,10)=S(3,4)*RA*CC-S(4,4)*OP+S(4,5)*B
S(4,11)=S(3,4)*RA*B-S(4,4)*B-S(4,5)*DP
S(5,9)=S(3,5)
S(5,10)=S(3,5)*RA*CC-S(4,5)*OP+S(5,5)*B
S(5,11)=S(3,5)*RA*B-S(4,5)*B-S(5,5)*DP
S(6,7)=S(1,6)*OP+S(2,6)*B
S(6,8)=S(1,6)*B-S(2,6)*DP
S(6,12)=S(1,6)*RA*CC+S(2,6)*RA*B-S(6,6)
C
S(7,7)=S(1,1)
S(7,8)=S(1,2)
S(7,12)=S(1,6)
S(8,8)=S(2,2)
S(8,12)=S(2,6)

```

```

S(9,9)=S(3,3)
S(9,10)=S(3,4)
S(9,11)=S(3,5)
S(10,10)=S(4,4)
S(10,11)=S(4,5)
S(11,11)=S(5,5)
S(12,12)=S(6,6)
C
DO 106 I=2,12
K=I-1
DO 106 J=1,K
106 S(I,J)=S(J,I)
C
ELEMENT LOCAL FORCES DUE TO GRAVITIES IN 3 DIRECTIONS
C
DO 107 I=1,60
107 EL(I)=0.
RCM=RO(MATTYP)*AX
DO 110 J=1,4
DO 110 I=1,3
XX=0.
DO 109 K=1,3
109 XX=XX+KCM*F(I,K)*EMUL(K,J)
110 EL(I,J)=XX
C
V11=CCPMZ*(12.0*0.0-0.75*B*8-BETA*8+0.5*BETA*8*DP+0.25*BETA*BETA)
+PHIZ*(C.5*BETA*8*DP+0.25*BETA*BETA-0.25*B*8)
V12=CCMPZ*(13.0*0.8-BETA*OP-0.75*8*DP+0.5*BETA*OP*DP-0.75*BETA)
-PHIZ*(O.5*BETA*8*OP-0.25*8*OP)
V21=CCPMZ*(10.25*BETA-0.75*8*DP+0.5*BETA*CP*OP)
-PHIZ*(O.5*BETA*OP-0.25*8*DP-0.5*BETA*OP*OP)
V22=CCPMZ*(10.25*BETA*8-BETA-0.5*BETA*8*OP+C.5*8*8-0.25*OP*OP*OP)
-0.75)*PHIZ*(C.25*BETA*BETA-0.5*BETA*8*OP+0.25*B*8)
V3=CCPMY*(11.0*OP-0.5*8*B)*PT*IV*(C.5*BETA*BETA-BETA*8+0.5*8*8)
V4=(CCPMY/RA)*(11.0*CP-0.5*8*B)-PT*IV*(CP*BETA*8-0.5*8*B-1.0)
V5=(CCPMY/RA)*(B-C.5*BETA-0.5*8*CP)
+PT*IV*(B-C.5*BETA-BETA*CP+0.5*8*OP)
V61=(CCPMZ/RA)*(BETA*8-2.0*2.C*OP)
V62=(CCPMZ/RA)*(BETA*BETA*CP-2.C*8)
C
R71=-RA*BETA*OP
R72=-RA*BETA*B
R81=-R72
R82=-R71
R9=-RA*BETA
R10=-RA2*(BETA-B)
R11=-RA2*C
R121=RA2*(8-BETA*OP)
R122=RA2*(BETA*8*CP-1.0)
C
DO 120 J=1,4
V(1,J)=EL(1,J)*V11+EL(2,J)*V12
V(2,J)=EL(1,J)*V21+EL(2,J)*V22
V(3,J)=EL(3,J)*V3
V(4,J)=EL(3,J)*V4
V(5,J)=EL(3,J)*V5

```

```

C
V(6,J)=FL(1,J)*V61+EL(2,J)*V62
SF( 7,J)=SF( 7,J)+EL(1,J)*R71+EL(2,J)*R72
SF( 8,J)=SF( 8,J)+EL(1,J)*R81+EL(2,J)*R82
SF( 9,J)=SF( 9,J)+EL(1,J)*R9
SF(10,J)=SF(10,J)+EL(3,J)*R10
SF(11,J)=SF(11,J)+EL(3,J)*R11
SF(12,J)=SF(12,J)+EL(1,J)*R121+EL(2,J)*R122
120 CONTINUE
C
DO 124 I=1,12
DO 124 L=1,4
XX=0.
DO 123 K=1,6
123 XX=XX-S(I,K)*V(K,L)
124 SF(1,L)=SF(1,L)+XX
C
MCC(FY STIFFNESS AND FIXED END FORCES FOR ZERO END CONDITIONS
C
IF (JK(1)+JK(2)).EC.D) GO TO 145
DO 140 K=1,2
KK=JK(K)
KO=100000
11=6*(K-1)+1
12=11+5
DO 140 I=1,12
IF (KK.LT.KO) GO TO 140
S11=S(1,I)
DO 125 N=1,12
R(N)=S(1,N)
DO 130 M=1,12
C(P)=S(M,I)/S11
DO 130 N=1,12
S(M,N)=S(M,N)-C(M)*R(N)
DO 135 N=1,4
SF(1,N)=SF(1,N)
DO 135 M=1,12
SF(M,N)=SF(M,N)-C(M)*SF(
135 SF(M,N)=SF(M,N)-C(M)*SF(
136 KK=KK-KO
140 KO=KO/10
145 CONTINUE
C
RETURN
END

```

```

*DECK BOUNC
SUBROUTINE BOUNC
C
COMMON A(1)
COMMON/EPAR/ NPAR(14),NUMP,NELTYP,NUMEL,NUMNEL,NEQ,MBAND,MTOT,
* CCMCN/JUNK/ STR(4),MM,L,K,NTAC,NCYN,SIG(12),EXTRA(184)
C
N7=N6+MPAR(3)*6
N8=N7+MPAR(4)*12
IF (N8.GT.MTOT) CALL ERROR (1,N8-MTOT,7HBOUND )
CALL EIND (NPAR(2),NPAR(3),NPAR(4),A(1),A(2),A(3),A(4),A(5),
* A(6),A(7),NUMP,MBAND,NUMEL)
C
RETURN
END

```

```

*DECK BIND
SUBROUTINE BIND (NBCUNC,NSTIF,NUMNPAR,IC,X,Y,Z,IND,ST(F,ENPROP,
* NUMP,MBAND,NLMEL)
C
CIPENS ICN (U(NUMP,1),X(1),Y(1),Z(1),IND(1),STIF(NSTIF,1),
* CCMCN/EMTX/ LM(24),NCNS,ASAI(24,24),P(24,4),XM(24),SA(12,24),
* SF(12,4),SY(6),EP(6),UE(6),PAR(6),S(12,12),F(48),
* TTT(72)
C
CCMCN/JUNK/ DX,DY,CZ,CD,AX,AY,AZ,AA,BX,BY,BZ,BB,SPRING(6),NN
ECLIVALENCE (ENPAR,SY),(I,TTT)
C
FORM ELEMENT STIFFNESS OF BOUNDARY SPRING ELEMENTS
C
DO 5 I=1,1346
5 LM(I)=0.
NS=6
NE=0
WR(TE(6,2000) NBOUNC,NSTIF,NUMNPAR
C
READ AND PRINT SPRING STIFFNESS SETS
C
REAC (5,1010) (N,(STIF(N,J),J=1,6),N=1,NSTIF)
WRITE(6,2001)
WR(TE(6,2010) (N,(STIF(N,J),J=1,6),N=1,NSTIF)
C
READ AND PRINT NONLINEAR ELEMENT PARAMETERS
C

```





```

180 CONTINUE
MTYPE=4
WRITE (3) MTYPE,L,M,NO,NS,ASA,SAIS,ENPAR,TTT
GC TC 250
200 INC(NN)=-4
C
250 IF (AC,LT,NBUINC) GO TO 10
RETURN
C
1010 FORMAT (15,6F10.0)
1020 FORMAT (15,6F10.0/5X,6F10.0)
1030 FORMAT (6I5)
C
2000 FCPRAT (24I1,.....,BOUNDARY ELEMENTS ///
. 28P NUNPFR OF ELEMENTS =,15//
. 28P NUMBER OF STIFFNESS SETS =,15//
. 28P NUMBER OF N/L PAR. SETS =,15)
2001 FCPRAT (4I15I, 20X 31PSTIFFNESSES OF BOUNARY SPRINGS /
4H NC 4X 2HRI 10X 2HR2 10X 2HR3 10X 2HP1 10X 2HM2 10X 2HM3 /)
2002 FCPRAT (4I15CT 20X 35PYIELDING FCRCES CF BOUNARY SPRINGS /
4H NC 4X 2HRI 10X 2HR2 10X 2HR3 10X 2HP1 10X 2HR2 10X 2HP3 /)
2003 FCPRAT (4I15ET 20X 39HPLASTIC STIFFNESSES CF BOUNARY SPRINGS /
4H NC 4X 2HRI 10X 2HR2 10X 2HR3 10X 2HP1 10X 2HP2 10X 2HP3 /)
2004 FCPRAT (5I1ELE, 5X 5HRCODES 5X 5H MATL 5X 5H NINO /
5H NO 4X 1HI 4X 2HJ 4X 1HK 5H NO 5X 5H NO /)
2010 FORMAT (14,6E12.3)
2040 FCPRAT (5I5,11G)
C
ENC
C
*DECK EXPJT SUPRCUTINE EXPJT
C
CCPCN/EPAR/ NPAR(14),NUNP,NELTYP,NUMEL,NUNP,NEL,NEG,MBANO,PTOT,
N1,N2,N3,N4,N5,N6
CCPCN/JUNK/ STR(4),MP,L,K,NTAG,NCYN,SIG(12),EXRA(164)
CCPCN ALL)
C
N7=N6+NPAR(4)*7
N8=N7+NPAR(4)
N9=N8+NPAR(4)*6
N10=N9+NPAR(3)*6
IF (N10,GT,MTOT) CALL ERROR (1,A(1),A(2),A(3),A(4),A(5),
CALL XPJT (NPAR(2),NPAR(3),NPAR(4),A(1),A(2),A(3),A(4),A(5),
A(6),A(7),A(8),A(9),NUNP,MBANO,NUMEL)
C
RETURN
ENC

```



```

20 SC=0.0
   TSC=0.0
   CSC=1.0
   SSC=0.0
21 DO 25 I=1,6
   DO 25 J=1,6
25 A(I,J)=0.0
C
   A(1,1)=1.0
   A(1,6)=0.5*D
   A(2,2)=1.0
   A(3,3)=1.0
   A(3,4)=-A(1,6)
   A(3,5)=0.5*C*TSQ
   A(4,1)=1.0
   A(4,6)=-A(1,6)
   A(5,5)=1.0/CSQ
   A(6,3)=1.0
   A(6,4)=A(1,6)
   A(6,5)=-A(3,5)
C
FCRM LOCAL TO GLOBAL TRANSFORMATION
C
DX=X(INL)-X(NI)
DY=Y(INL)-Y(NI)
DZ=Z(INL)-Z(NI)
CL=SQRT(DX*DX+DY*DY+DZ*DZ)
IF (CL) 55,55,6C
55 CALL ERROR (5,NF,7*EXPJB )
C
60 AX=X(NK)-X(NI)
   AY=Y(NK)-Y(NI)
   AZ=Z(NK)-Z(NI)
   RX=AY*DZ-AZ*DY
   RY=AX*DZ-AZ*DX
   RZ=AX*DY-AY*DX
   BB=SQRT(RX*RX+RY*RY+RZ*RZ)
   IF (BB) 65,65,70
65 CALL ERROR (6,NE,7*EXPJB )
C
70 T(3,1)=BX/BB
   T(3,2)=BY/BB
   T(3,3)=BZ/BB
   AA=SQRT(AX*AX+AY*AY+AZ*AZ)
   IF (AA) 65,65,80
80 T(2,1)=-AX/AA
   T(2,2)=-AY/AA
   T(2,3)=-AZ/AA
   T(1,1)=T(2,2)*T(3,3)-T(2,3)*T(3,2)
   T(1,2)=T(2,3)*T(3,1)-T(2,1)*T(3,3)
   T(1,3)=T(2,1)*T(3,2)-T(2,2)*T(3,1)
C
FCRM JCINT TO GLOBAL TRANSFORMATION
C
DO 90 I=1,36
90 AT(I)=0.0
C
20 SC=0.0
   LB=LA*2
   CC 100 MA=1,6,3
   MB=MA-1
   DO 100 I=LA,LB
   DO 100 JM=1,3
   J=JM+MB
   XX=0.0
C
   DC 95 K=1,3
   XX=XX+A(I,K+MB)*T(K,JM)
95 CONTINUE
100 AT(I,J)=XX
C
FCRM LOCAL TO EXPANSION JCINT COORDINATE
C
DO 56 I=1,36
56 A(I)=0.0
   A(1,1)=0.5
   A(1,6)=1.0/D
   A(2,2)=1.0
   A(3,3)=0.5
   A(3,4)=-1.0/D
   A(4,1)=0.5
   A(6,6)=-1.0/I)
   A(5,4)=SSC
   A(5,5)=CSQ
   A(6,3)=0.5
   A(6,4)=1.0/D
C
FCRM JCINT STIFFNESS MATRIX IN LOCAL COORDINATE SYSTEM
C
DO 101 I=1,144
101 S(I)=0.0
   DC 110 I=1,6
   J=XD(I)+1
   GC TC (110,111,112) J
111 S(1,1)=TRACE
   S(1+6,I)=-TRACE
   S(1+6,I+6)=TRACE
   GO TC 110
112 S(1,1)=STIF(MS,I)
   S(1+6,1)=-STIF(MS,I)
   S(1,1+6)=-STIF(MS,I)
   S(1+6,1+6)=STIF(MS,I)
11C CONTINUE
C
FCRM JCINT GLOBAL STRESS MATRIX
C
DO 120 I=1,144
120 DA(I)=0.0
   DO 150 LA=1,10,3
   LB=LA*2
   UC 150 MA=1,10,3
   MR=MA-1
   CD 150 I=LA,LB

```

```

DO 150 JM=1,3
J=JM+MB
XX=0.0
DO 151 K=1,3
151 XX=XX+S(I,K+MB)*T(K,JM)
150 DA(I,J)=XX
C
DO 149 I=1,288
149 SA(I)=0.0
DO 130 LA=1,12,6
LB=LA-1
DO 130 MA=1,12,6
MB=MA+5
DO 130 IL=1,6
I=IL+LB
DO 130 J=MA,MB
XX=0.0
DO 135 K=1,6
135 XX=XX+A(IL,K)*OAIK*LB,J)
130 SA(I,J)=XX
C
C FORM JOINT STIFFNESS MATRIX IN GLOBAL COORDINATE
C
DO 161 I=1,576
161 ASAI(I)=0.0
DO 162 LA=1,10,3
LB=LA-1
DO 162 MA=1,10,3
MB=MA+2
DO 162 IL=1,3
I=IL+LB
DO 162 J=MA,MB
XX=0.0
DO 163 K=1,3
163 XX=XX+T(K,IL)*CAIK*LB,J)
162 ASAT(I,J)=XX
C
C FORM ELEMENT LOCATION MATRIX
C
DO 170 I=1,6
LM(I)=ID(NI,I)
LM(I+6)=ID(NJ,I)
LM(I+12)=0
170 LM(I+18)=0
C
C WRITE ELEMENT INFORMATION ON TAPE
C
CALL WRITET (MBAND,NUIF)
C
C SET NONLINEAR ELEMENT INDICATOR AND STORE NONLINEAR PARAMETERS
C
NN=NUREL+NE
IF (INNO.EQ.0) GO TO 200
INC(NN)=5
DO 180 I=1,7
180 ENPAR(I)=ENPROP(INC,I)

```

```

41.
NTIE=NT(MIND)
DO 190 I=1,6
190 XTIE(I)=XT(INNO,I)
UETIE=SYTIE/STIE
SJ=JS
MYPE=5
WRITE (3) MYPE,L,M,ND,NS,ASA,SA,S,ENPAR,TTI
GC TC 250
200 INC(NN)=-5
C
250 IF (NE.LT.NEXPJ) GO TO 10
RETURN
C
1010 FORMAT (15,7F10.0,15/ 6F10.0)
1030 FORMAT (515,4X,611,315,3F10.0)
1040 FORMAT (15,6F10.0)
2000 FORMAT (31H1....EXPANSION JOINT ELEMENTS ///
. 29# NUMBER OF ELEMENTS = 15//
. 29# NUMBER OF STIFFNESS SETS = 15 //
. 29# NUMBER OF N/L PAR. SETS = 15)
2001 FORMAT (53HINCLINE#2 PARAMETERS CF EXPANSION JOINT ELEMENTS....//
. 4#NPAR 8X 8#FRICTION 4X 8#FRICTION 5X 4#SEAT 7X 3#TIE 7X 3#TIE
. 8X 9#TIE YIELD 6X 6#IMPACT / 3#NO. 7X 6#CCEFF. 6X 9#STIFFNESS
. 4X 3#CAP 8X 3#CAP 8X 5#STIFF 6X 5#FRCOE 10X 6#SPRING )
2002 FORMAT (15,7E12.3)
2003 FORMAT (///20H JOINT TIE PARS..... //
. 56# NPAR NUMBER TIE POSITIONS RELATIVE TO JOINT CENTER /
. 59# NO. OF TIES 1 2 3 4 5 6 )
2004 FORMAT (15,15,3X,6F8.3)
2010 FORMAT (///34H EXPANSION JOINT ELEMENT DATA..... //
. 5# ELEM 8X 4#NOCE 11X 6H JOINT 3X 5#JOINT 3X 6#SPRING 2X 3#N/L
. 8# JOINT 8# SKEW 8# JOINT /
. 5# NC. 4X 1#I,4X 1#J 4X 1#K 4X 1#L 3X 5# CODE 5X 4#SIGN 3X
. 4#SET NC 5H INC 8H WICTH 5H ANGLE 2X 9#STIFFNESS /)
2020 FORMAT (515,4X,611,2X,316,2F9.3,6E12.3)
2030 FORMAT (4#ISET 20X 32#STIFFNESSES CF EXPANSION SPRINGS /
. 4# NC 4X 2#R1 10X 2#R2 10X 2#R3 10X 2#M1 10X 2#M2 10X 2#M3 /)
2040 FORMAT (14,6E12.3)
END

```

```

*DECK NEXPJT
SUPRCUTINE NEXPJT (INEL,NIND) 11
C
C C#CN/EMTX/ MTYPE,L,P(24),ND,NS,ASA(24,24),SA(12,24),S(12,12),
. COF,SCF,CAP,TC,STIE,SYTIE,SIMP,NTIE,XTIE(6),TRACF,C,
. UETIE,SJ,NO(6),A(6,6),T(3,3),PTIE,KKO(6),TT(12C),
. ASSA(24,24),SSA(12,24),OF(24),F(6),FT(6),UL(6),
. UPTIE(6)

```



```

*CHECK NKPJT
SUBROUTINE NKPJT (NINC)
C
C CCMPCN/EMTA/ MTYPE,LW(24),NC,NS,ASA(24,24),SA(12,24),S(12,12),
C CDF,SCF,GAP,TC,STIE,SYTIE,SIMP,NTIE,XTIE(6),TRACE,0,
C UETIE,SJ,KROT(6),AIC(6),T(3,3),PTIE,KKROT(6),YIT(2C),
C ASSAI(24,24),SSA(12,24),OF(24),F(6),F(6),U(6),
C UPTIE(6)
C CCMPCN/NEP / EEE(72),DEF(12),CP(12),EXJ(12),EXJ(12),SS(12,12),
C U(6),TK(6)
C CCMPCN/COLB/ USP(10,2),USPF(10,2),KF(6),LPSLIP(2)
C
C DO 10 I=1,6
C FT(I)=0.
C KF(I)=0.
C 10 TK(I)=0.
C
C CHECK JOINT CONDITION
C
C PTIE=1000.
C IF (NTIE.EQ.0) GO TO 25
C DO 20 I=1,NTIE
C IF (PTIE.GT.UPTIE(I)) PTIE=UPTIE(I)
C 20 CONTINUE
C 25 PTIE=PTIE+TC
C
C KK(1)=KX(1)
C KK(4)=KQ(1)
C
C DO 30 I=1,6,3
C I1=I/3+1
C IF (U(I1,LT,-GAP) KK(I1))=-1
C IF (U(I1,GT,PTIE) KK(I1))=1
C UESLIP=COF*ABS((F(1+2))/SCF)
C XX=UPSLIP(I1)*UESLIP
C YY=LPSLIP(I1)-UESLIP
C IF (U(I1,GT,XX) KF(I1))=1
C IF (U(I1,LT,YY) KF(I1))=-1
C 30 CONTINUE
C
C COMPUTE TIE STIFFNESSES
C
C TAA=0.
C TBB=0.
C IF (NTIE.EQ.0) GO TO 60
C DO 50 I=1,NTIE
C XX=U(I1)+C(4)*0.5*XTIE(I1)*(U(I1)-U(4))/C
C XX=XX-TG
C IF (XX.LT.UPTIE(I1)) GO TO 45
C IF (XX-PTIE(I1)-UETIE) 40,40,35
C 35 UPTIE(I1)=XX-UETIE
C TK(I1)=0.
C FT(I1)=SYTIE
C GO TO 50
C 40 TK(I1)=1.0

```

```

FT(I1)=STIE*(XX-UPTIE(I1))
GO TO 50
45 FT(I1)=0.
50 CONTINUE
C
C DO 55 I=1,NTIE
C TK(I1)=STIE
C IF (TKS.EQ.0.) GO TO 55
C TAA=TAA+TKS*(0.5*XTIE(I1))*2/D**2
C TAB=TAB+TKS*(0.5*XTIE(I1))*(C.5*0-XTIE(I1))/D**2
C TBB=TBB+TKS*(0.5*XTIE(I1))*2/D**2
C 55 CONTINUE
C 60 CONTINUE
C
C FCRP NEW NONLINEAR STIFFNESS MATRIX IN JOINT COORDINATE
C
C DO 65 I=1,144
C 65 SS(I)=0.
C
C 1. CONTRIBUTION FROM COULUMB FRICTIONAL FORCE
C
C NINF=0
C IF (COF.LE.0.) GO TO 85
C DO 80 I=1,6,3
C IF (SJ*F(1+2).LE.0.) GO TO 80
C IF (KF(I)) 80,75,8C
C 75 SS(I,1)=SS(I,1)+SCF
C NINF=1
C 80 CONTINUE
C 85 CONTINUE
C
C 2. CONTRIBUTION FROM TIE BAR AND/OR IMPACT SPRING
C
C DO 90 I=1,6,3
C IF (KKU(I).NE.KC(I)) GO TO 10C
C 90 CONTINUE
C NIND=0
C GO TO 130
C 100 K=0
C NIND=1
C DO 120 I=1,6,3
C KK=KK(I)+2
C GO TO (110,120,115,12C) KK
C 110 SS(I,1)=SS(I,1)+SIMP
C GO TO 120
C 115 IF (K.NE.0) GO TO 12C
C K=1
C SS(I,1)=SS(I,1)+TAA
C SS(1,4)=SS(1,4)+TAB
C SS(4,1)=SS(4,1)+TAB
C SS(4,4)=SS(4,4)+TBB
C 120 CONTINUE
C 130 CONTINUE
C
C IF (NIND.EQ.1.OR.NINF.EQ.1) GO TO 200
C DO 150 I=1,576

```

```

150 ASSA(I)=ASA(I)
DD 160 I=1,288
160 SSA(I)=SA(I)
RETURN
200 CONTINUE
C
DD 250 LA=1,2,6
LB=LA+5
DD 250 MA=1,12,6
MB=MA+5
IF (LA.EQ.1.AND.MA.EQ.1) GO TO 250
SIGN=-1.
IF (LA.EQ.7.AND.MA.EQ.7) SIGN=1.
DD 240 I=LA,LB
II=I-LA+1
DD 240 J=MA,MB
JJ=J-MA+1
SS(I,J)=SIGN*SS(II,JJ)
240 CONTINUE
250 CONTINUE
C
TRANSFORM TO GLOBAL COORDINATE SYSTEM
C
DD 310 I=1,288
310 SSA(I)=0.
DD 330 LA=1,12,6
LB=LA+5
DD 330 MA=1,12,6
MB=MA+1
DD 330 I=LA,LH
DD 330 JM=1,6
J=JM+MB
XX=0.
DD 325 K=1,6
IF (SS(I,K+MB).EQ.D..OR.A(K,JM).EQ.0.) GO TO 325
XX=XX+SS(I,K+MB)*A(K,JM)
325 CONTINUE
330 SSA(I,J)=XX
C
DD 351 I=1,576
351 ASSA(I)=0.
DD 360 LA=1,12,6
LB=LA+1
DD 360 MA=1,12,6
MB=MA+5
DD 360 IL=1,6
I=IL+LB
DD 360 J=MA+MB
XX=0.
DD 355 K=1,6
IF (A(K,IL).EQ.0..OR.SSA(K+LB,J).EQ.0.) GO TO 355
XX=XX+A(K,IL)*SSA(K+LB,J)
355 CONTINUE
360 ASSA(I,J)=XX
C
COMBINE LINEAR AND NONLINEAR STIFFNESS MATRIX
C

```







TE 662  
.A3  
no.FHWA-RD-

77-51 BORROWER

*1977-1978*

\_\_\_\_\_  
\_\_\_\_\_  
\_\_\_\_\_  
\_\_\_\_\_  
\_\_\_\_\_  
\_\_\_\_\_  
\_\_\_\_\_

DOT LIBRARY



00055937

